NOTE TO USERS

The original manuscript received by UMI contains pages with indistinct and/or slanted print. Pages were microfilmed as received.

This reproduction is the best copy available

UMI

UNIVERSITY OF ALBERTA

NUMERICAL SIMULATION OF THE ONSET AND PROPAGATION OF SHEAR BAND LOCALIZATION

By

Xingran Wang

A thesis submitted to the Faculty of Graduate Students and Research in partial fulfillment of the requirements for the degree of Doctor of Philosophy

In

Geotechnical Engineering

Department of Civil and Environmental Engineering

Edmonton, Alberta

Fall 1998

National Library of Canada
Acquisitions and Bibliographic Services
395 Wellington Street
Ottawa ON K1A 0N4
Canada

Bibliothèque nationale du Canada
Acquisitions et services bibliographiques
395, rue Wellington
Ottawa ON K1A 0N4
Canada

Your file Votre référence

Our file Notre référence

The author has granted a non-exclusive licence allowing the National Library of Canada to reproduce, loan, distribute or sell copies of this thesis in microform, paper or electronic formats.

L'auteur a accordé une licence non exclusive permettant à la Bibliothèque nationale du Canada de reproduire, prêter, distribuer ou vendre des copies de cette thèse sous la forme de microfiche/film, de reproduction sur papier ou sur format électronique.

The author retains ownership of the copyright in this thesis. Neither the thesis nor substantial extracts from it may be printed or otherwise reproduced without the author's permission.

L'auteur conserve la propriété du droit d'auteur qui protège cette thèse. Ni la thèse ni des extraits substantiels de celle-ci ne doivent être imprimés ou autrement reproduits sans son autorisation.

0-612-34855-5

Canada

University of Alberta

Library Release Form

Name of Author: Xingran Wang

Title of Thesis: Numerical simulation of the onset and propagation of shear band localization

Degree: Doctor of Philosophy

Year this Degree granted: 1998

Permission is hereby granted to the University of Alberta Library to reproduce single copies of this thesis and to lend or sell copies for private, scholarly, or scientific research purpose only.

The author reserves all other publication and rights in association with the copyright in the thesis, and except as hereinbefore provided, neither the thesis nor any substantial portion thereof may be printed or otherwise reproduced in any material form whatever without the author's prior written permission.

Xingran Wang

Date July 7th, 1998

Xintang School
Shilian, Wuhu
Anhui Province, China

University of Alberta

Faculty of Graduate Studies and Research

The undersigned certify that they have read, and recommend to the Faculty of Graduate Studies and Research for acceptance, a thesis entitled ***numerical simulation of the onset and propagation of shear band localization*** by **Xingran Wang** in partial fulfillment of the requirements for the degree of Doctor of Philosophy in Geotechnical Engineering.

Dr. D. Chan
(Supervisor)

Dr. N. R. Morgenstern
(Co-Supervisor)

Dr. P. K. Robertson

Dr. J. Szymanski

Dr. A. W. Lipsett

Dr. R. Wan
(External Examiner)

Date: June 26, 1998

Abstract

It is presently a concern and a challenge to model numerically shear band localization. Many numerical methods have been developed to take into account the strain and displacement discontinuities across a shear band. In these methods, only smeared shear is modeled and only small deformation is treated. The anisotropy and the inhomogeneity of shear band materials induced by the propagation of localization require the introduction of discrete shear band elements.

In this research, a contact band element approach is proposed to model the propagation of shear bands with finite thickness for large shear deformation. The contact band elements are continuously updated based on their current configurations to prevent large distortions of conventional elements, and alleviate band kinking. In order to model material anisotropy of shear band materials, and to prevent element from overlapping each other, a cross-isotropic elastic model with special Mohr-Coulomb yielding criterion is proposed, in which deformation properties along and across a shear band can be different. In this model, yielding and failure always occurs along a preferred shearing orientation.

One of the highlights of this research is the application of the contact band element approach to interfaces and joints subjected to large shear deformations. Special strain expressions are derived with regard to characteristics of shear strain concentration along an interface. Simulation of a pull-out test has shown that very large pullout displacement can be modeled after the ultimate load has been reached and smooth distributions of mobilized shear stress and axial force along the reinforcement can be

obtained.

A framework to incorporate shear band elements automatically and continuously in a finite element scheme is developed. The propagating shear band is modeled with discrete shear band elements which will split up the original finite element mesh. In the original mesh, no shear band element is specified. The use of the proposed empirical bifurcation criterion, location criterion ensure that band propagation is as realistic as possible. Preliminary results from the numerical simulation of biaxial tests and passive earth pressure problems have shown that the discrete band element models closely the actual pattern of shear bands in geomaterials.

To my wife and our daughter and

To my father and mother

Acknowledgments

The author wishes to express his deepest appreciation to his supervisors, Professor D. H. Chan and Professor N. R. Morgenstern, for their guidance and encouragement. Their ideas, consultations and supports were invaluable.

Thanks to all support staff in the Department of Civil and Environmental Engineering, especially those in the Geotechnical Office.

The author also wishes to thank his wife Jenny (Jianhua) Gao and his daughter Louise (Luyang) Wang for their understanding, patience and encouragement during his period of studies.

The author acknowledges the financial support provided by the Natural Science and Engineering Research Council of Canada (NSERC). The computer facilities in the Geotechnical Division of the Department is also acknowledged.

Finally the author extends his deepest gratitude to his father, Kexuan Wang and his mother Jiafeng Mao for their love and patience. The author has guilty conscience over their continuous concerns, anxieties.

Contents

Chapter 1

Introduction 1

1.1 Background 1

1.1.1 The phenomenon of strain localization 1

1.1.2 Overview of previous studies 2

1.2 Objectives and scopes 3

1.3 Organization of the thesis 4

Chapter 2

On development of the study of localization 8

2.1 Introduction 8

2.2 Bifurcation analysis of inelastic stress-strain response 9

2.3 The enhancement of standard continuum theories 12

2.3.1 Cosserat medium theory 13

2.3.2 The non-local concept 15

2.3.3 High-order deformation gradient model 16

2.3.4 Rate-dependent model 17

2.4 Computational simulation of localization 18

2.4.1 The enhancement of displacement interpolation in the localization zones 19

2.4.2 The embedment of the localization zone in an element 21

2.4.3 Adaptive remeshing for shear band localization 23

2.4.4 The simulation of post localization 24

2.5 Concluding remarks 26

Chapter 3

Formation and development of shear band localization in soils 32

3.1 Introduction 32

3.2 Strain localization in clays 33

3.2.1 Inception and evolution of microstructures in Kaolin under direct shear 33

3.2.2 The influence of flaws or discontinuous existing in the materials 34

3.2.3 Dimensions, aspect ratio and end effects 35

3.3 Strain localization in sands 36

3.3.1 The preliminary observations of localization in sands 36

3.3.2 Shear band formation in triaxial and plane strain tests 37

3.3.3 Localization in loose sand under undrained conditions 38

3.3.4 Medium to dense sand behavior under strain path control 40

3.3.5 Localization in reinforced sand 41

3.3.6 The investigation of localization patterns and void ratio by computed tomography 42

3.4 The understanding of strain softening and localization 43

3.4.1 The coupling of strain softening and strain localization at the microscopic level 43

3.4.2 The relationship between strain softening and strain localization at the macroscopic level 44

3.5 Concluding remarks 46

Chapter 4

Characteristics of constitutive responses and localization criteria under bifurcation theories.....53

4.1 Introduction 53

4.2 Material instability and general bifurcation.....58

4.3 Non-uniqueness and limit point.....60

4.4 Discontinuous bifurcation characteristics 62

4.5 The summary of various constitutive responses.....65

4.6 General theories for the bifurcation into a shear band.....66

4.6.1 Elasto-plastic relationships.....66

4.6.2 General localization criteria 67

4.6.3 Plane strain conditions.....71

4.6.4 Plane stress conditions.....73

4.7 Shear band localization under Drucker-Prager criterion.....74

4.7.1 Case of plane stress 76

4.7.2 Case of plane strain 76

4. 8 The comparison of various bifurcation modes 77

4.8.1 Eigensystem and bifurcation modes.....77

4.8.2 Critical hardening moduli under different bifurcation modes.....78

4.9 Concluding remarks 79

Chapter 5

Implementation of the kinematics modeling of shear band propagation.....86

5.1 Introduction 86

5.2 A contact band element approach to model localized deformation 90

5.2.1 An ordinary contact approach for shear bands with zero thickness 91

5.2.2 Remeshing of shear band elements 93

5.2.3 The formation of special shear band elements 95

5.2.4 A judgement of the technique to update shear band elements using error analysis 96

5.3 Formation of shear band element 98

5.3.1 Triangular and quadrilateral element 98

5.3.2 Special shear band element 99

5.3.3 Separation of shear band elements 102

5.3.4 Kink band problems 103

5.4 Numerical examples 105

5.4.1 Direct shear test 105

5.4.2 Plane strain compression test 107

5.4.3 Uniaxial test with two shear bands in the specimen 108

5.4.4 A kink problem with the biaxial test (plane strain) 111

5.5 Concluding remarks 114

Chapter 6

Constitutive modeling of shear band materials 140

6.1 Introduction 140

6.2 Von-Mises model with hyperbolic softening 142

6.2.1 Yielding criterion 142

6.2.2 Hyperbolic stress-strain curves 143
6.2.3 Hardening rule 144
6.3 Cross-isotropic elastic model with Special Mohr-Coulomb yielding criterion 146
6.3.1 Cross-isotropic elastic model 147
6.3.2 Special Mohr-Coulomb yielding criterion 148
6.3.3 Eigenvalue analysis of the constitutive matrix 150
6.4 The application of modified Cam-Clay model 152
6.4.1 The description of yielding function 153
6.4.2 Evaluation of plastic materials 154
6.5 Kinematic treatment of the overlapping problem 157
6.5.1 Direct modification of nodal displacement 159
6.5.2 Application of correctional forces due to the penetration 159
6.6 Concluding remarks 160

Chapter 7

The applications of contact band element to interfaces and joints 174

7.1 Introduction 174
7.2 Special strain description continuous interface elements 177
7.3 Formation of strains of an interface element 180
7.3.1 Triangular interface element 180
7.3.2 Quadrilateral interface element 184
7.4 Elastic-plastic constitutive model for the continuous interface element 185

7.4.1 The elastic constitutive model 186
7.4.2 The plastic constitutive model 187
7.5 A Numerical example----pull-out test 188
7.6 Concluding remarks 191

Chapter 8

The automatic creation of discrete shear band elements 199

8.1 Introduction 199
8.2 The empirical criterion for shear band localization 200
8.3 Framework of formation of shear band elements 202
8.3.1 Techniques to generate shear band elements 203
8.3.1.1 Geometric check of potential band in one element 203
8.3.1.2 Location criterion 204
8.3.1.3 The propagation of old shear bands and the formation of new shear bands 205
8.3.1.4 The creation of new shear band elements 206
8.3.2 The recalculation of stresses for shear band elements and reshaped regular soil elements 208
8.3.3 Numbering of new band elements and remeshed soil elements. 209
8.4 Numerical examples 210
8.4.1 Plain strain biaxial test 210
8.4.1.1 Brief description of the biaxial test 211
8.4.1.2 Shear banding initiation and development 212
8.4.2 A passive earth pressure problem 215

8.4.2.1 Description of the problem 215
8.4.2.2 Results and discussions 217
8.5 Concluding remarks 220

Chapter 9

Conclusions and recommendations 253

9.1 Introduction 253
9.2 Conclusions 254
9.2.1 Contact band element approach 254
9.2.2 Cross-isotropic elastic model with Mohr-Coulomb yielding criterion 255
9.2.3 The application of contact element approach to interfaces and joints using special strain descriptions 255
9.2.4 Kinematics remedy of overlapping problem 255
9.2.5 Automatic creation of discrete shear band elements 256
9.3 Recommendations 257
9.3.1 The study of constitutive response of shear band materials 257
9.3.2 The further study of contact band element approach 258
9.3.2.1 Mesh independent check 258
9.3.2.2 The simulation of closing-opening-reclosing procedures 258
9.3.3 The automatic creation of shear band elements 259
9.3.3.1 An independent shear band isolated in one element 259
9.3.3.2 The improvement of remeshing techniques 259
9.3.3.3 The treatment of shear band conjugate directions 260
9.3.3.4 The improvement of empirical bifurcation

criterion and location criterion 260
9.3.3.5 Renumbering of all the elements 260

References 262

Figure List

Figure 1.1 The gradual development of failures in the SANDNESS slope 7

Figure 2.1 The chart showing the study of localization 27
Figure 2.2 The application of Cosserat continuum for the bar subjected to a dynamic loading conditions a transverse stress σ_{yx} 28
Figure 2.3 The application of gradient plasticity to an one-dimension tension bar ... 29
Figure 2.4 Embedded shear band in a normal element 30
Figure 2.5 Influence of mesh alignment 31

Figure 3.1 Detail of discontinuities S_2 47
Figure 3.2 The propagation of discontinuities of S_3 47
Figure 3.3 Shear band and interaction of two cracks 48
Figure 3.4 Evolution of shear bands as observed in tests named MS1 and 32 49
Figure 3.5 Stress-strain curves 50
Figure 3.6 Tangential displacement vs. axial coordinate and axial displacement vs. axial coordinate, respectively 51
Figure 3.7 Localization patterns in a specimen 52

Figure 4.1 Evolution of stress-strain curves for non-associative and associative flow rules 80
Figure 4.2 Localization modes 81
Figure 4.3 The dimensionless critical hardening modulus when dilation parameter n=-0.3 82
Figure 4.4 The dimensionless critical hardening modulus when dilation parameter n=0.0 83
Figure 4.5 The dimensionless critical hardening modulus when dilation parameter n=0.3 84
Figure 4.6 The dimensionless hardening modulus when associated flow rule is applied (m=n) 85

Figure 5.1 Kinematic problems with existing interface elements 115
Figure 5.2 Illustration of contact band 116
Figure 5.3 Configuration of shear band elements before and after intensive shearing deformation 117-118
Figure 5.4 The application of special shear band elements 119
Figure 5.5 Analysis of shear strains both in normal and parallel directions To the alignment of shear band 120
Figure 5.6 Calculation of stress components at nodes on shear band boundaries 121
Figure 5.7 Special shear band elements 122
Figure 5.8 Handle of shear band elements in tension 123
Figure 5.9 Kink problems in the localization analysis 125
Figure 5.10 Configuration of the shear box before and after loading 126
Figure 5.11 Load-horizontal displacement relationship for the 'shear box' 127
Figure 5.12 Load-apparent shear stress relationship for the 'shear box' 128
Figure 5.13 Configuration of the specimen before and after deformation 129-130
Figure 5.14 Vertical load-tangential displacement relationship 131
Figure 5.15 Relationship between vertical load-apparent shear stress along the shear band 132
Figure 5.16 Uniaxial test of the specimen with kink problem 133
Figure 5.17 Vertical stress contours at p=315 N/mm^2 for the specimen under uniaxial test 134
Figure 5.18 Evolution of shear band elements 135-136
Figure 5.19 Original mesh and prescribed shear bands 137
Figure 5.20 Output of finite element analysis of the kink problem 138
Figure 5.21 The relationship between tangential displacements at points 267 and 145 and vertical pressure acting on the top of the pressure 139

Figure 6.1 Stress-strain relationship for the hyperbolic strain softening model 162
Figure 6.2 Relationship between vertical normal stress and axial strain under Von-Mises yielding criterion with hyperbolic softening 163

Figure 6.3 Cross-anisotropic description for shear band element 164
Figure 6.4 The simple structure for eigenvalue analysis 165
Figure 6.5 Stress state at initial stage of the single element under the specific Mohr-Coulomb yielding criterion 166
Figure 6.6 Mode shapes of a 4-node rectangular element for elastic analysis .. 167-168
Figure 6.7 Mode shapes of a 4-node rectangular element for elasto-plastic stiffness 169-170
Figure 6.8 The relationship between the thickness of a shear band and mean stress P 171
Figure 6.9 Comparison of numerical results and hypothetical data 172
Figure 6.10 Pathological penetration of shear band element 173

Figure 7.1 Continuous interface elements 193
Figure 7.2 The discretization of soils and reinforcements 194
Figure 7.3 Relationship between axial force and applied left end horizontal displacement 195
Figure 7.4 Shear stress distrbution along the interface at different end displacements 196
Figure 7.5 The tensile force distribution along the reinforcement 197
Figure 7.6 Horizontal displacement change of the reinforcement in its longitudinal direction 198

Figure 8.1 An illustration of relationships among yielding, diffuse bifurcation, and shear banding 222
Figure 8.2 Plastic shear strain at the onset of shear band localization 223
Figure 8.3 The geometric check of the potential shear band line 224
Figure 8.4 Location and orientation check for the newly occurring shear band 225
Figure 8.5 Two categories of shear band propagation 226
Figure 8.6 The creation of double shear band elements 227
Figure 8.7 Different cases for the creation of new bands 228
Figure 8.8 Renumbering of regular soil elements and band elements 229

Figure 8.9 Original mesh for the biaxial test....230
Figure 8.10 The structure configuration at axial strain equal to 13.3%....231
Figure 8.11 The structure configuration at axial strain equal to 14.0%....232
Figure 8.12 The structure configuration at axial strain equal to 14.7% (stage 1)....233
Figure 8.13 The structure configuration at axial strain equal to 14.7% (stage 2)....234
Figure 8.14 The structure configuration at axial strain equal to 15.1% (stage 1)....235
Figure 8.15 The structure configuration at axial strain equal to 15.1% (stage 2)....236
Figure 8.16 The structure configuration at axial strain equal to 15.1% (stage 3)....237
Figure 8.17 The relationship between the equivalent vertical pressure and axial load....238
Figure 8.18 The structure configuration at axial strain equal to 14.7% (the weak element placed at left side)....239
Figure 8.19 The structure configuration at axial strain equal to 16.5% (stage1, the weak element placed at left side)....240
Figure 8.20 The structure configuration at axial strain equal to 16.5% (stage2, the weak element placed at left side)....241
Figure 8.21 The structure configuration at axial strain equal to 16.5% (stage3, the weak element placed at left side)....242
Figure 8.22 The relationship between the equivalent vertical pressure and load....243
Figure 8.23 A passive earth problem....244
Figure 8.24 Deformed mesh when horizontal displacement equal to 1.1 mm....245
Figure 8.25 Deformed mesh when horizontal displacement equal to 1.3 mm....245
Figure 8.26 Deformed mesh when horizontal displacement equal to 1.5 mm....246
Figure 8.27 Deformed mesh when horizontal displacement equal to 1.7 mm....246
Figure 8.28 Deformed mesh when horizontal displacement equal to 1.9 mm....247
Figure 8.29 Deformed mesh when horizontal displacement equal to 2.1 mm....247
Figure 8.30 Deformed mesh when horizontal displacement equal to 2.3 mm....248
Figure 8.31 Deformed mesh when horizontal displacement equal to 2.5 mm....248
Figure 8.32 Lateral earth resistant force versus horizontal displacement....249
Figure 8.33 Deformed mesh when horizontal displacement equal to 1.1 mm for the 'rigid' sheet pile wall....250

Figure 8.34 Deformed mesh when horizontal displacement equal to 1.3 mm for the 'rigid' sheet pile wall....250
Figure 8.35 Deformed mesh when horizontal displacement equal to 1.4 mm for the 'rigid' sheet pile wall....251
Figure 8.36 Deformed mesh when horizontal displacement equal to 1.5 mm for the 'rigid' sheet pile wall....251
Figure 8.37 Deformed mesh when horizontal displacement equal to 1.6 mm for the 'rigid' sheet pile wall....252

Table list

Table 5.1 Interface element information at original load step....113
Table 5.2 Updated shear band element information at top pressure p=85 N/mm^2....113
Table 5.3 Updated shear band element information at final load step....113
Table 5.4 Shear band elements in tension at final load step....114

Table 6.1 Eigenvalue analysis for elastic constitutive matrix $[C]_e$ and elastic-plastic matrix $[C]_{ep}$....151

Table 7.1 Material properties of soil, reinforcement and interface....190

Table 8.1 Strength parameters used for the biaxial test....211
Table 8.2 Loading procedures for the biaxial test....211
Table 8.3 The automatic creation of nodal points and shear band elements....214
Table 8.4 The comparison of passive resultant forces using different ways....219

Symbol list

θ ---------- The angle a shear band makes with major principal stress direction

ϕ ---------- Mobilized friction angle

ψ ---------- The value of dilatancy angle at failure

γ ---------- Density of material

Θ ---------- Inertia of micro-rotation per unit volume

γ^p ---------- The internal state variable

σ ---------- Stress variable

ε ---------- Strain variable

$\dot{\gamma}_b$ ---------- Localized mode amplitude

ξ ---------- Functional of field variable

D_{50} ---------- Mean particle diameter

C_u ---------- The coefficient of uniformity

G_s ---------- Specific gravity

[D] ---------- The constitutive matrix

[K] ---------- The structure stiffness matrix

[B] ---------- Matrix which relates the strain rate to the nodal displacement rate

Q_{ij} ---------- The second order acoustic tensor

g ---------- Polarization vector

n ---------- Unit vector normal to the band

Q ---------- Yield surface gradient

P ---------- Plastic potential surface gradient

θ_{cr} ---------- The angle between the shear band inclination and major principal stress

e_{ij}^{s} ---------- stress errors

e_{ij}^{d} ---------- Displacement errors

M ---------- Collection of nodal points on upper surface of a shear band

N ---------- Collection of nodal points on lower surface of a shear band

J_2 ---------- Second stress invariant of the stress deviatoric tensor

Chapter 1

Introduction

1.1 Background

1.1.1 The phenomenon of strain localization

Strain localization is a common phenomenon seen in a wide variety of solid structures such as ductile single crystals, polycrystalline structure metals, rocks, concrete and soils. Its occurrence refers to the emergence of localized bands of intense straining in a structure where inelastic deformation tends to concentrate. The remaining parts of the structure are probably still in an elastic state. The localization zone where shear strains concentrate is called a shear band. Strain localization manifests itself through the concentration of deformation into one or more narrow bands. The physical mechanisms responsible for triggering localization vary widely. The imperfections and stress concentrations in a soil structure are most frequently observed before the initiation of localization. The localization can be considered to be a material instability in which non-homogeneous deformation is developed. In this case, the constitutive relation of the material determines the inception of shear banding and the subsequent propagation.

It is well known that shear band localization is a precursor to progressive failure in geotechnical analysis. As illustrated in figure 1.1 (Bjerrum, 1967), a slide occurred at Sandnes, Norway in 1963. The slide was initiated by a passive shear failure (shear band

localization) below the bottom of an excavation, and then the shear band propagated gradually upward. Simultaneously, some new shear bands were initiated at other location. The bands kept developing and joining together, and eventually, a general slip channel was formed. These events are shown in figure 1.1.

1.1.2 Overview of previous studies

From the case of the landslide, one may conclude that computational prediction is indispensable in understanding the final failure of structures. For the past few decades, localization of shear zone deformation has been the object of intense studies. A lot of researchers carried out investigations of the inception, inclination and development of the localization into shear bands based on the consideration of plasticity theory in localization studies.

Since the late 1950s, researchers have analyzed shear banding as a bifurcation problem in continuum mechanics. They considered localization of deformation into a shear band as a result of an instability in the constitutive description of homogeneous deformation. They proposed a general condition for bifurcation, and provided details in the formulation for the onset of shear banding and its inclination.

In the last decade, modelling localized deformation in computational geomechanics has become a major concern and challenge. Some attention has been given to the kinematic aspect of shear banding which basically involves the discretization of a discontinuous field. The enhanced finite element method (Ortiz et al., 1987), the smeared approach (Pietruszczak and Mroz, 1981), the adaptive remeshing (Pastor et al., 1991), discontinuous displacement approach (Wan, 1990, Wan et al., 1992), and the element-

embedded localization band approach (Larsson et al., 1996a, Larsson and Runesson, 1996b) have successively been proposed. However, there are still some drawbacks relevant to these approaches. For instance, the strong mesh sensitivity based on classical continuum in modeling shear banding affects the final result of computation. The above approaches are incapable of capturing the actual width of a shear band. In particular, the finite element solutions from these methods can not easily be related to physical reality. The discrete band zone has never been specified in the solutions. They can not be applied to model large slip, non-homogeneity, and anisotropy. Those phenomena arise due to localization factors, such as shear band inception and propagation, which always occur in the post-localization stage.

1.2 Objectives and scopes

The issue of how to model localized material failure in a realistic fashion has been the subject of considerable interest. To model the problem realistically, it is necessary to take into account the important characterization of localization from physical observations in numerical simulation, such as the development of inhomogeneous deformation, large shearing along the shear zone, and material anisotropy due to strong orientation and breaking of soil particles. An efficient finite element scheme is to place elements with different constitutive relations to capture the evolving localization, and to keep updating the elements to simulate the kinematic propagation of shear bands at the post-localization stage. The new scheme will be described in different chapters in this thesis.

In this thesis, the existing theories about the study of localization are extensively and systematically reviewed and discussed. The research will then focus on the simulation of the kinematics of post-localization. Endeavors are made to develop a realistic numerical model to effectively simulate the initiation and propagation of shear bands at the post-localization stage. Some highlights of the research are stated as:

A. A new strategy is proposed to simulate large shearing in shear band propagation.

B. The numerical and physical issues are identified which are accompanied by the newly proposed numerical model with a specific constitutive relationship.

C. Some attention is paid to capture automatically the inception and propagation of shear band localization. Once a bifurcation point is detected within an element, the affected soil elements are remeshed. New nodes and new shear band elements are employed to model the occurrence of non-homogeneous deformation.

D. The contact band element is successfully applied to model interfaces and joints. A new strain description is given.

E. The proposed models are implemented in a finite element program, and the corresponding numerical examples are performed.

1.3 Organization of the thesis

This dissertation has been organized into nine chapters.

In chapter two, a review of localization studies is presented. Classical discontinuous bifurcation theories are briefly described. The different types of enhancements of standard continuum mechanics are also discussed. The development of computational simulation of localization is emphasized in the chapter. Various numerical methods and their deficiencies and strengths are outlined and discussed.

In order to thoroughly understand the mechanism of inception and propagation of shear band localization, experimental observations are important. In chapter three, the experimental results addressing the phenomenon of shear banding in clays and sands are presented. These are obtained under different loading conditions and stress paths by virtue of visual observation and special techniques. Different localization patterns, orientations, locations, thickness and corresponding triggering mechanisms from experimental observations are fundamental characteristics which must be captured in numerical modeling.

In chapter four, characteristics of constitutive responses are discussed. Material instability, limit point, general bifurcation, diffuse bifurcation, and discontinuous bifurcation are defined individually. The critical conditions for them to occur, such as loss of ellipticity, loss of positive definiteness, and non-uniqueness of equations governing incremental equilibrium, are stated. Eventually, the general critical condition for strain localized (discontinuous) bifurcation is described. The specific criteria for localized bifurcation for different constitutive equations are also derived.

The contact band element approach is proposed in chapter five to model the kinematics of shear bands at the post-localization stage. The mathematical and mechanical problems occurring in the simulation of kinematic propagation, such as shear

band kinking, virtual overlapping, large distortion and opening of band elements, are illustrated and properly treated. The method has been implemented in a finite element program. Numerical examples are given to illustrate the techniques.

In chapter six, the constitutive response of post-localization is investigated. An anisotropic model with a specific Mohr-Coloumb yielding criterion is suggested. Some other constitutive laws used in the analysis are also discussed. At the end of the chapter, the scheme to treat the kinematic overlapping problem is presented.

The application of the contact band element approach to interfaces and joints with large shear deformations is given in chapter seven. With the particular deformation mode in interfaces and joints, a specific strain description is proposed and implemented, one that may also be used in modeling the kinematics of shear band development. Several examples, including a pull-out test, are analyzed.

In chapter eight, the approach to generate discrete shear band elements is developed. The new discrete shear elements are continuously created in the propagation of shear bands. The evolution of shear bands is realistically simulated. The results from the modeling of biaxial tests and the passive earth pressure problems have shown the efficiency and practicality of the proposed scheme.

In chapter nine, conclusions and recommendations for further research are presented.

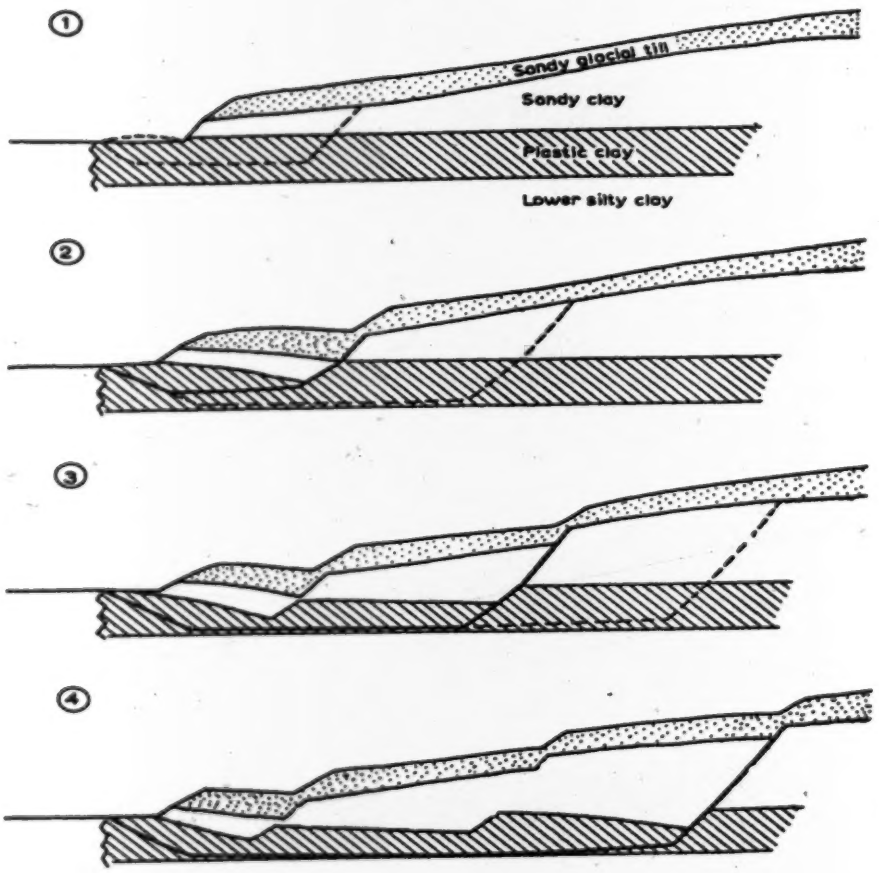

Figure 1.1 The gradual development of failures in the SANDNES slope (after Bjerrum, 1967)

Chapter 2

On development of the study of localization

2.1 Introduction

Two theories are traditionally authoritative in soil mechanics to calculate the inclination of a shear band in two dimensional (2-D) plain strain problems. They are the Mohr-Coulomb theory and the Roscoe theory. The Mohr-Coulomb theory states that shear bands are parallel to the surfaces which are subjected to the stresses of the failure envelope of Mohr-Coulomb. The shear band makes an angle θ with the major principal stress direction (Bardet, 1990), $\theta = \frac{\pi}{4} - \frac{\phi}{2}$, where ϕ is the value of mobilized friction angle at failure. Roscoe theory emphasizes the importance of strain on failure. It states that the shear bands are parallel to the line of no-extension. They make an angle θ with the major principal strain increment, $\theta = \frac{\pi}{4} - \frac{\psi}{2}$, where ψ is the value of dilatancy angle at failure. In view of the poor performance of the classical theories in explaining the shear band orientation in their experiments, Arthur and Dustan. (1982) summarized experimental results and proposed an empirical relation for θ, $\theta = \frac{\pi}{4} - \frac{\phi}{4} - \frac{\psi}{4}$. All the three theories have been widely applied in solving practical engineering problems. In addition to these three theories, great achievements have been made in the study of shear band localization, which is illustrated in figure 2.1.

Some decades ago, it was recognized that shear band localization could be considered as a bifurcation problem (Rice, 1976). Within this framework it proved possible to derive analytically formulae for the critical hardening modulus at which the bifurcation into a localized deformation band becomes possible. A major motivation to determine analytically the critical bifurcation directions is another interest in the context of localization studies. In contrast to the classical failure theories, the bifurcation analyses incorporate the elastoplastic models to determine the shear band orientations. The general shear band directions are derived for various elastoplastic models. The substitution of the Mohr-Coulomb yield criterion with associated and non-associated flow rules would give the shear band the same directions as those given respectively by the Mohr-Coulomb and Arthur theories.

2.2 Bifurcation analysis of inelastic stress-strain response

The theoretical study of localization with continuum mechanics in elastic-plastic solids was initiated in the late 1950's. Hill (1962) connected localization with the special case of a stationary acceleration wave, and analyzed the shear band as a bifurcation problem in continuum mechanics. The proposed linear bifurcation theory which is still the basis of localization analysis now states that a shear band is considered as a thin material layer, and that a shear band is bounded by two material discontinuity surfaces of velocity gradient. Rudnicki and Rice (1975) considered the localization of deformation into a shear band that results from an instability in the constitutive description of homogeneous deformation, proposed conditions for the bifurcation, distinguished between continuous and discontinuous bifurcation, and gave in detail the formulations for

the onset and inclination of the shear band for general constitutive models. On the other hand, they derived the formulations for the localization of deformation in pressure-sensitive dilatant materials yielding to the Drucker-Prager criterion. Palmer and Rice (1973) formulated the formation of a shear band in overconsolidated clays. Then Rice (1976) presented a very general criterion for the localization into a shear band, in which the critical hardening modulus and the inclination of the shear band are coupled. He also carried out specific calculations of localization conditions for a variety of material models.

Based on Hill's and Rice's theories, Vardoulakis and Aifanties (1980), Vardoulakis et al. (1978) elaborated the calculation of shear band initiation and inclination in sand bodies which were described by the Mohr-Coulomb model with non associated flow rules. They pointed out that both Coulomb's and Roscoe's classical solutions of the inclination of a shear band coincide with different bifurcation modes which were determined by material response and configuration-dependent loading. Needleman and Tvergaard (1983) developed a criterion for the inception of localization for some constitutive models like the J_2 corner theory, single-crystal plasticity, and the continuum model of a ductile porous material. Vermeer (1982) described the inception of a shear band using compliance. The particular shear band direction $\theta = \frac{\pi}{4} - \frac{\phi_h}{4} - \frac{\psi_h}{4}$ (ϕ_h, ψ_h are the mobilized friction angle and dilation angle, respectively, which depend on the degree of hardening) corresponds to the lowest bifurcation point in the stress-strain curve

which will tend to be raised by external constraints. Orientations of shear bands are generally expected in the range between $\theta = \frac{\pi}{4} - \frac{\psi}{2}$ and $\theta = \frac{\pi}{4} - \frac{\phi}{2}$.

Pietruszczak and Stolle (1987) related mobilized friction to the amount of dilation at any stress level based on Rowe's stress dilatancy theory, and proposed an expression which describes the locus of stress points which satisfy bifurcation in the stress space. The resulting surface is similar to the yield surface. They viewed the inception of softening as a bifurcation problem, and described the post bifurcation behavior. Strain softening was regarded as a local phenomenon which occurs only in a shear band. But the induced plastic strains are averaged over the whole area of an element. Two approaches were proposed for incorporating strain softening response into a phenomenological framework. Bigoni and Hueckel (1991), and de Borst (1994) investigated the relationship between the localization into a shear band, material instability, the loss of positiveness of the second order work density, etc.. The sufficient criterion for uniqueness of the incremental elasto-plastic response of a homogeneous, homogeneously strained body is never violated if the second order work density is positive. Neilssen and Schreyer (1993) performed an intensive study on eigensystem of elastic-plastic constitutive matrix. They defined the limit point as the point where the tangent modulus tensor obtains a zero eigenvalue, a general bifurcation wherein the occurrence of a zero eigenvalue of the symmetric part of the tangent modulus tensor is a necessary condition for any type of bifurcation and loss of uniqueness (Hill, 1958). Classical discontinuous bifurcation is related to the inception of localized deformation. It

is denoted as the loss of ellipticity of the differential equations governing the incremental equilibrium. Discontinuous bifurcation may not occur until the advent of a zero eigenvalue from the acoustic tensor. The loss of strong ellipticity of the differential equations governing the incremental equalibrium occurs when there is a zero eigenvalue of the symmetric part of the acoustic tensor. It may indicate the occurrence of diffuse or discontinuous bifurcation. The loss of strong ellipticity can precede the satisfying of the necessary condition for a classical discontinuous bifurcation.

2.3 The enhancement of standard continuum theories

All of the analyses mentioned above, that are concerned with modeling the behavior of geologic materials, do not account for changes in microstructure which predominantly control the onset and the evolution of shear band localization. Subsequently, these theories cannot model the localization of deformation precisely. In particular, they cannot predict theoretically the thickness of a shear band. To be able to predict theoretically the size of a shear band, the constitutive description should include the grain size or higher-order deformation gradients, beside the first-order gradient (Muhlhaus and Vardoulakis, 1987). The mathematical structure of such generalized continuum models is equipped with the necessary ingredients to prevent the change of the type of governing differential equations in the post localization regime. So, the introduction of higher order gradients or additional degrees of freedom within a polar continuum will make the mathematical problem well-posed and remove spurious mesh size dependence in the numerical analysis. A most prominent feature of higher-order continuum models lies in the presence of an internal length scale. Accordingly, this

internal length scale causes the localization zone to have a finite width and to not collapse into genuine discontinuities. On the other hand, it introduces a structural size effect to remove the spurious mesh-sensitivity problem. The width of the shear band and spacing emerges as a natural result of the analysis in the post localization regime (de Borst et al., 1993).

2.3.1 Cosserat medium theory

Within the continuum mechanics, the grain size as an internal length scale is introduced into the constitutive model by means of the Cosserat theory, which is suitable to model changes in microstructures of granular material. Brown and Evans (1972) and Bogdanova-Bontcheva and Lippman (1988) described the behavior of granular media by utilizing the concept of a Cosserat continuum. Muhlhaus (1986) suggested a different approach in which the kinematics of slip and rotation between individual grains are emphasized. Muhlhaus and Vardoulakis (1987) recognized that the Cosserat approach introduces a length scale in the continuum description and that the rate boundary value problem remains elliptic with the development of a shear band. In the Cosserat theories, the additional static and kinematic quantities, namely, the couple-stress and the micro-curvatures, are introduced. A micro-rotation, the third independent kinematic component, appears in the planar Cosserat theory in addition to the two displacement quantities. The conventional Young's modulus has the dimension of length. An internal length scale is quoted even in the elastic regime, which is not the case for non-local and high-order gradient continuum models. If the invariants on which the yield function depends are redefined, the theory can be extended to account for plastic flow (de Borst et al., 1991).

So far, some theoretical work for the bifurcation problem of a shear band, which is referenced within the framework of the simplest possible generalization of the deformation theory for granular materials that contains microstructures, has revealed that the Cosserat effect is observable only beyond the bifurcation state since its microstructures govern the organization of the grains into the shear band. The prediction of the shear band thickness in granular materials shows a remarkably good agreement with experimental findings (Muhlhaus and Vardoulakis, 1987). de Borst and Sluys (1991) investigated a bar in pure shear which was subjected to the dynamic loading condition of a transverse stress σ_{yx}, as shown in figure 2.2 (a). The material properties of the bar for a softening Cosserat plasticity with Von-Mises yield model is as follows: classical shear modulus G=3500 MPa, rotational shear modulus G_c=100 MPa, density ρ=500 kg/m^3, and inertia of micro-rotation per unit volume Θ=1.786X10^{-8} MPaS^2, virgin yield strength $\sigma(0)$=100 MPa, softening modulus h=-0.4762. Figure 2.2 (b) shows strongly that numerical solutions are in agreement with general physical observation. Different discretization almost give exactly the same results. Apparently, the rotations emerge as additional degrees-of-freedom at the global level which inevitably increase the computational effort. Furthermore, in pure tension, rotational degrees-of- freedom do not become active where micro-curvatures are zero and the couple-stresses are zero. It has been confirmed by numerical experiment that the Cosserat effect is generally too weak to preserve ellipticity of the boundary value problem if tension is the predominant failure mode rather than frictional slip. Therefore, Cosserat medium is not so effective for structural failures where tension plays dominant roles.

2.3.2 The non-local concept

Coleman and Hodgdon (1985) and Triantafyllidis and Aifantis (1986) used constitutive equations that involve second-order deformation gradients when studying shear band formation in ductile rigid-plastic and hyperelastic materials respectively. Bazant and Lin (1988) have suggested to calculate average internal variables within an area when evaluating yielding surface in lieu of evaluating them at one point. For instance, for the sake of simplicity, the yield function is generally expressed as:

$$f = f(\sigma, \gamma^p) \tag{2-1}$$

whereas, γ^p, the internal state variable, is $\gamma^p = \int \dot{\gamma}^p dt$, $\dot{\gamma}^p = \sqrt{\frac{2}{3}\left(\dot{\varepsilon}^p\right)^T\left(\dot{\varepsilon}^p\right)}$, where $\dot{\varepsilon}_p$ is plastic strain increment. The average $\dot{\gamma}^p$ at location $\mathbf{x}$ is obtained as:

$$\bar{\dot{\gamma}}^p = \frac{1}{V_\gamma(\mathbf{x})} \int_v g(\mathbf{s})\dot{\gamma}(\mathbf{x}+\mathbf{s})dv \tag{2-2}$$

where, $V_r(\mathbf{x}) = \int g(\mathbf{s}-\mathbf{x})dv$, V_r is the domain over which the integration is taken. Its size was given by Kroner (1967) and Krumhansl (1968). $g(\mathbf{s})$ is a weighting function, and $\mathbf{x}$ is a position vector indicating the point around which the average shear strain is calculated. Then yield function is dependent on $\bar{\gamma}^p$ instead of on γ^p itself:

$$f = f\left(\sigma, \bar{\gamma}^p\right) \tag{2-3}$$

This non-local plasticity theory can lead to a set of integral-differential rate equations instead of algebraic equations that remain elliptic after the onset of localization. The non-local approach is generally effective in numerical simulations for the development of both shear bands and crack bands which will be differentiated in chapter 4.

In the case of tensile loading, where cohesion-loss is the main cause of structural failure, non-local formulations are very effective in keeping the boundary value problem elliptic (Bazant et al., 1984). However, the non-local formulations suffer a definite disadvantage in that they are not consistent with existing numerical strategies (Simo, 1989). The important issue for non-local application is how to properly formulate the additional boundary conditions which have not yet been well addressed (de Borst et al., 1993).

2.3.3 High-order deformation gradient model

To eliminate or alleviate the issues mentioned above, higher order terms are added to the inelastic strain expressions. For gradient plasticity, the yield function is:

$$f=f(\sigma, \gamma^p, \nabla^2\gamma^p), \qquad (2\text{-}4)$$

where ∇^2 is the second order derivatives. This regularization can be derived from full non-local models by first expanding the weight function g(s) introduced in (2-2) in a Taylor series about s=0 and then carrying out the integration (Muhlhaus and Aifantis, 1991). The gradient terms reflect the fact that the microstructures below a certain size scale interact non-locally (Kubin and Lepinoux, 1988). They act as a stabilizer and guarantee ellipticity of the governing equations after the onset of localization. In the

gradient model, the plastic multiplier is considered as a fundamental unknown and has a role similar to that of the displacements. The gradient plasticity theories have a distinct advantage in that the consistency condition results in a partial differential equation instead of an integral-differential equation in non-local models. In gradient models, the additional boundary conditions on the inelastic strains can be solved uniquely and elegantly (de Borst and Mulhaus, 1992). However, an ensuing disadvantage is the introduction of an additional variable at the global level in addition to the conventional displacement.

An example of a one-dimensional imperfect bar was given by de Borst et al. (1993) to illustrate the good performance of the high-order gradient model. The loading configuration is shown in figure 2.3 (a), where h, the softening modulus, is equal to -200MPa, σ_t is the tensile strength, whose value is equal to 2 MPa, and l, the internal length scale, is equal to 5 mm. The conventional elastic modulus is 20000 MPa. The results in figures 2.3 (b), 2.3 (c) illustrate that different mesh discretization almost results in the same width of localization zone, but the ratio of internal length scale l over L , the length of the bar, greatly influences stresses in the softening stage. This implies that the length scale has a large influence on the final results.

2.3.4 Rate dependent model

Throughout the works mentioned above, attention is confined to rate-independent constitutive relations. But the inelastic response of materials is perhaps inevitably rate dependent (Needleman, 1988). Similarly, once material's rate dependence is taken into account, there is no loss of ellipticity in quasi-static problems, and wave speeds remain

real, as long as stress levels remain small compared to the elastic stiffness. In effect, material rate dependence introduces a length scale into the boundary value problem, even though the constitutive law does not contain a material parameter with dimension of length. However, its applicability is obviously limited to transient loading conditions. For slow loading rates, the rate-dependent effect rapidly decreases.

It is noteworthy that for all the enhanced continuum models the additional model parameters are not easily determined. They are not directly derivable from laboratory tests such as uniaxial or triaxial tests.

2.4 Computational simulation of localization

During the past decade, the numerical simulation of the development of localization received more and more attention. Modeling localized deformation in computational geomechanics has become a major concern. It is known that, in geomaterials, failure occurs in resulting phenomenological responses such as micro-cracking, discrete cracks, void formation and rupture/shear bands, which are characterized by strain softening or softening damage of the local material. The description of strain softening will pose severe mathematical difficulties, for instance, the numerical instability triggered by the loss of positive definiteness of the tangent modulus. Subsequently, great importance is placed on modeling numerically the localization of deformation with bifurcation theories and special finite element techniques.

Finite element method is a very robust numerical method in solving various engineering problems. It is based on continuum mechanics, but it can still handle

macroscopic discontinuities which occur in some local areas. Finite element method has been proved to be the most effective numerical method to model the shear band localization. Changes in microstructures always precede macro shear banding i.e. shear band localization. They involve the discontinuities such as nucleation, growth and coalescence of microvoids. They take place on a very small length scale. However, in many circumstances the key processes for determining the mechanical performance of engineering materials take place on a much larger length scale. The use of a continuum approach is justified. The changes in microstructures can be incorporated into the material's constitutive description. Macro shear banding stemming from the changes in microstructures can be simulated by placing independent shear band elements in the original element mesh. This is cannot be done using other numerical methods such as boundary element method.

2.4.1 The enhancement of displacement interpolation in the localization zones

Localization is related to a concentration of deformations with high gradients that are within a narrow zone. The actual experimental width of localization bands is far smaller than the practical mesh size. Conventional finite elements perform poorly in problems involving strain localization in frictional materials. It inhibits the occurrence of localization and yields no solution other than uniform state at the hardening stage. Furthermore, the minimum band thickness is set in terms of mesh size. Attention has been drawn to the kinematic aspect of localization modeling which basically involves the discretization of a discontinuous field. Some methods such as strain field enrichment, mesh refinement, or remeshing have been suggested.

Ortiz et al. (1987) proposed a method to enhance the performance of conventional isoparametric elements for the problems involving strain localization in which a discontinuous bifurcation analysis is carried out to determine the geometry of the localized deformation modes. Once the onset of localization is detected, suitable shape function terms are added to the original interpolation to reproduce the localized deformations. With **n** being the normal to the discontinuity surface passing through the element, the local displacement field is expressed as:

$$\mathbf{u}(x) = \sum_{a=1}^{N} \mathbf{u}_a N_a(x) + \sum_{b=1}^{NL} \dot{\gamma}_b \mathbf{M}_b(x), \qquad (2\text{-}5)$$

in which the first term indicates C^o finite element interpolation, and the second term stands for the incompatible term expressed by the localized mode amplitude $\dot{\gamma}_b$, b implies the b^{th} localized mode, and $\mathbf{M}_b(x)$ is called unit polarization vector. Note that the enhanced element would be a non-conforming element. The strain rate fields exhibit a jump across the discontinuity surface:

$$\left[\left[\dot{\varepsilon}_{ij}(x)\right]\right] = \frac{1}{2}\dot{\gamma}_b\left(m_{ib}n_{jb} + m_{jb}n_{ib}\right) \ (i,j=1,2). \qquad (2\text{-}6)$$

The unit vectors $\mathbf{m}_b$ and $\mathbf{n}_b$ can be estimated by employing localization analysis. Their relationship will be shown in chapter 4. Since the localization modes represent internal degrees of freedom within the element, $\dot{\gamma}_b$ is eliminated by static condensation. The shear band width is dependent on the element size, and it is of the same order as the element size. Leroy and Ortiz (1989) studied the method in the context of strain

localization in frictional materials. To reduce the mesh dependence of strain localization, Nacar et al. (1989) generalized the method to account for finite deformations and material rate dependence, and revealed that all the calculations, including the orientation of the enhanced modes are remarkably insensitive to details of the mesh design.

As another way to enhance displacement interpolation for the localized elements, Wan (1990) and Wan et al. (1992) added a discontinuous interpolation term for the onset of localization with zero thickness. The displacement function reads:

$$\mathbf{u}(x) = \sum_{a=1}^{N} N_a(x)\mathbf{u}_a + \sum_{b=1}^{NL} N_b(x)\mathbf{g}_b , \qquad (2\text{-}7)$$

N_a and N_b are continuous and discontinuous interpolation polynomials for $\mathbf{u}_a$ and $\mathbf{g}_b$, which are the conventional nodal displacement and the displacement jump, respectively. $\mathbf{g}_b$ is an independent variable which represents displacement slip in the localization analysis. Due to the presence of discontinuous surfaces (discontinuous displacements, discontinuous strains), shear bands within an element have been modeled. The enhanced formulation is conducive to capture a localized mode, which is different from the method proposed by Ortiz et al. (1987) in that the localized zone is not smeared, and the exact band configuration through an element is given. The framework provides a viable tool to model both inception and development of the kinematic discontinuity surface.

2.4.2 The embedment of the localization zone in an element

As stated previously, the thickness of a shear band is significantly smaller than the normal size of an element. Some researchers embedded a band into an element. As an effective method to embed a localization band, Pietruszczak and Mroz (1981) proposed a

smeared shear band approach, in which the shear band with a prescribed thickness is assumed within a conventional element once localization is detected. The alignment of the band is given by using classical theories. The plastic strains only occur in the localization zone, which are averaged in terms of the ratio of the band area to the element area. As a consequence, the average mechanical properties of an initially homogeneous element that is intercepted by the shear band which occurs afterwards are estimated. In this method, no strain or displacement discontinuities are accounted for in the element where the shear band occurs. However, due to the presence of the localization band that has a defined thickness in the element, the results such as the load-displacement curves for different mesh discretization are almost identical.

The shear band with a defined thickness is bounded by two discontinuous surfaces across which local strains have jumps. However, in the framework of Ortiz's or Wan's research, only one discontinuity surface is accounted for. Belytschko et al. (1988) suggested another way to embed the localization band. The methodology is based on the introduction of a special strain field in the localization band. The strains in the localized zone differ substantially from the remainder of the element. The strain rates are discontinuous across the two interfaces between the localization zone and the remainder of the element. The strain discontinuity can be derived by incorporating the local equilibrium equation, the strain-displacement relation, and the constitutive law. This embedding material significantly reduces the spurious mesh dependency of the calculation. This method was then used by Fish and Belytschko (1990) for the problem of shear banding in visco-plastic solids, in which rate-dependency is incorporated into the

computational model to restore well-posedness. The regularized discontinuous fields were proposed by Simo et al. (1993), Larsson and Runesson (1996a, 1996b) for the embedded localized zone. In addition to the presence of a localized strain rate $\dot{\varepsilon}$ in the element, the displacement rate field is smooth except that it has a constant jump $[\dot{\mathbf{u}}]$ across the internal surface Γ_s, as shown in figure 2.4. In the localization zone, strain rate is written as:

$$\dot{\varepsilon}_s = \dot{\varepsilon}_c + \frac{1}{2t}\left(\mathbf{n}\left[\dot{\mathbf{u}}\right] + \left[\dot{\mathbf{u}}\right]\mathbf{n}\right), \tag{2-8}$$

where, $\dot{\varepsilon}_c$ is the normal strain tensor in the non-localization zone, n is a unit vector indicating the normal direction of the shear band, and t is the thickness of the band.

2.4.3 Adaptive remeshing for shear band localization

Adaptive remeshing is one of several computational schemes which have been suggested to solve strain localization problems. Adaptive mesh refinement is technically applied to produce an optimal finite element grid for a given problem to keep the discrepancy between theoretical and numerical results constant over the computational domain. The element meshes are produced with the element aligned along the shear band orientation, presenting a small spacing in the band region. The grid size is much bigger in the zone that is far from the localization zone (Pastor et al., 1991, 1992). For two-dimensional problems, at any nodal point in principal directions X_1 and X_2, the mesh is fully characterized by:

$$\delta_1^2\left|\frac{\partial^2\xi}{\partial X_1^2}\right| = C_1, \tag{2-9}$$

$$\delta_2^2\left|\frac{\partial^2\xi}{\partial X_2^2}\right| = C_2, \tag{2-10}$$

where, δ_1, and δ_2 denote the sizes of the element in X_1 and X_2 directions, respectively. C_1 and C_2 are constants which define the degree of refinement. ξ is a functional of field variables. Here, it is given as:

$$\xi = \int\left(\frac{1}{2}de_{ij}^p de_{ij}^p\right)^{\frac{1}{2}}, \tag{2-11}$$

where, de_{ij}^p is the increment of plastic derivative strain. Alternatively, ξ can also be expressed as:

$$\xi = \min\left[\det\left(n_i D_{ijkl}^{ep} n_l\right)\right]. \tag{2-12}$$

Some investigators (Pastor et al., 1992) have shown that the orientation of the original mesh used may influence the results to the extent that the method may fail (see figure 2.5). These failures may be avoided or alleviated by using a mixed triangular element form (displacement and pressure are independent variables) and suitable error measures that locate more efficiently the localization regions in the adaptive process (Zinkiewicz and Huang, 1995).

2.4.4 The simulation of post localization

In the previous sections, many numerical methods have been analyzed and discussed, and many achievements have been outlined. Nevertheless, shear bands have never been treated as independent elements. They are embedded in the normal elements. The kinematic evolution of a shear band, like slipping, kinking, and separation, which all lead to significant changes in the structure configuration, is hard to trace after the occurrence of localization. Therefore, it is necessary to handle shear bands as independent elements in order to simulate numerically post localization deformation, namely, the development of shear bands with large shear deformations. In the simulation of post-localization deformation, there are other pressing issues which should be addressed. Due to sharp gradients of large deformation problems across a shear band, the local region will be skewed, and the highly distorted mesh will degrade all numerical solutions. After the onset of the shear band, especially when the failure load is approached, conventional elements close to the intersections of two shear bands will be locked, which is referenced to as the kinking problem. In the special finite elements with discontinuous shape functions (Wan, 1990), kink problems will arise in relation to the development of localization.

In this thesis, attention will be focused on the numerical model of post-localization, and on the rediscretization of shear band elements. A contact band element approach is proposed in which finite thickness of a shear band is defined. The thickness of the shear band is determined physically prior to the numerical analysis. The stick, slide, and opening modes of the band elements will be considered using various

techniques in relation to contact problems. The onset and the propagation of the shear band will be simulated through each load step by successively generating independent shear band elements based on the previous shear band elements.

2.5 Concluding remarks

In this chapter, an overview of classical theories and current developments in localization analyses has been presented within the framework of standard continuum mechanics and enhanced continuum mechanics. Analytical bifurcation criteria for onset of localization are discussed. Some numerical methods are described, such as the strain enhanced model, the band embedded method, and the adaptive remeshing technique. Contact band elements for post-localization deformation are mentioned. Some outstanding problems with respect to the simulation of the post-localization deformation are illustrated, which hamper the effective and accurate numerical predictions of the onset and the propagation of shear band localization. The pathological mesh-dependence of numerical results with rate-independent continuum mechanics is caused by the loss of ellipticity of incremental governing equations. The Cosserat medium, non-local or high order plasticity, and rate-dependent theory might be efficient ways to solve the above-mentioned problem. However, they suffer from being short of experimental results to determine material parameters, difficulties in handling the mathematics of some equations, boundary conditions, etc. It is concluded that effectiveness and deficiency are inherent to each method. So far, no completeness is claimed for studies of both constitutive and computational aspects.

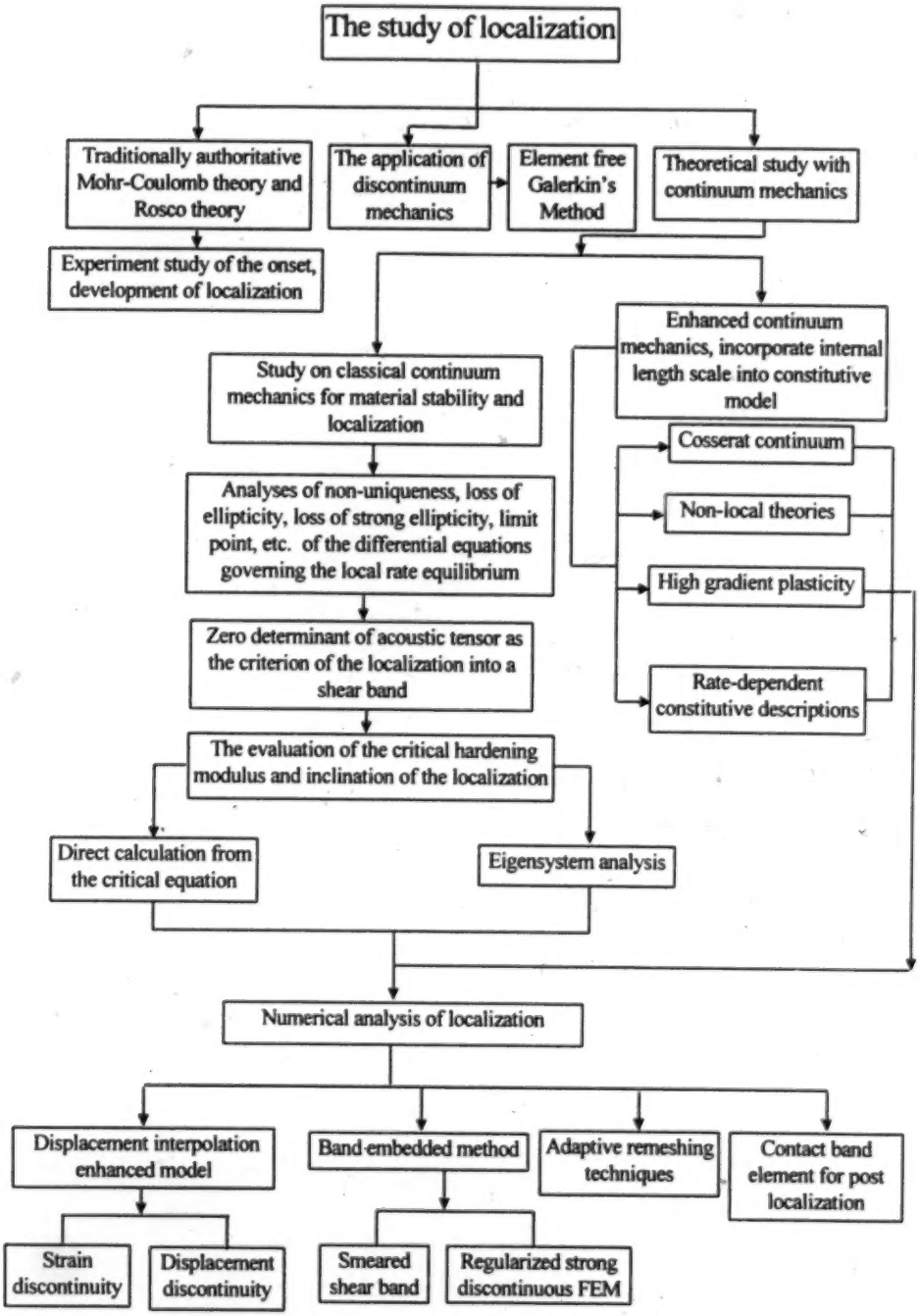
The study of localization
Traditionally authoritative Mohr-Coulomb theory and Rosco theory
The application of discontinuum mechanics
Element free Galerkin's Method
Theoretical study with continuum mechanics
Experiment study of the onset, development of localization
Study on classical continuum mechanics for material stability and localization
Enhanced continuum mechanics, incorporate internal length scale into constitutive model
Cosserat continuum
Non-local theories
High gradient plasticity
Rate-dependent constitutive descriptions
Analyses of non-uniqueness, loss of ellipticity, loss of strong ellipticity, limit point, etc. of the differential equations governing the local rate equilibrium
Zero determinant of acoustic tensor as the criterion of the localization into a shear band
The evaluation of the critical hardening modulus and inclination of the localization
Direct calculation from the critical equation
Eigensystem analysis
Numerical analysis of localization
Displacement interpolation enhanced model
Band-embedded method
Adaptive remeshing techniques
Contact band element for post localization
Strain discontinuity
Displacement discontinuity
Smeared shear band
Regularized strong discontinuous FEM

Figure 2.1 The chart showing the study of localization

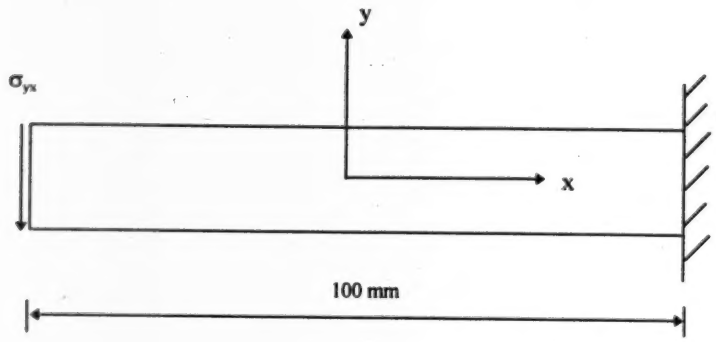

Figure 2.2 (a)

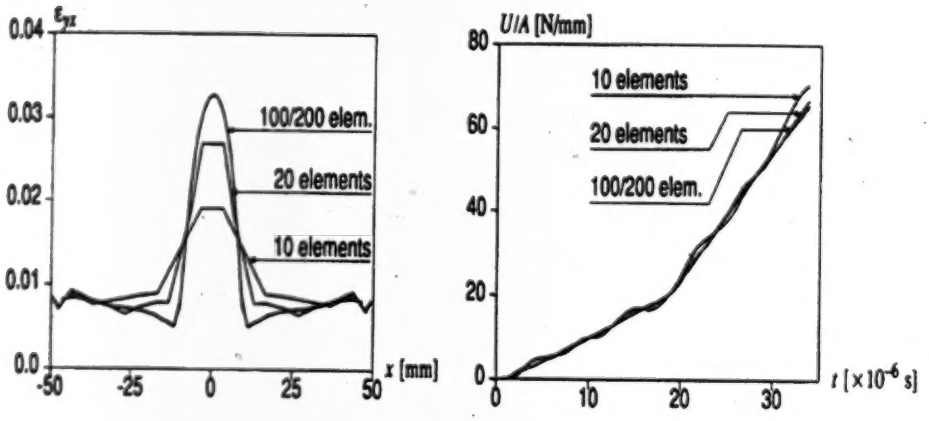

Figure 2.2 (b)

Figure 2.2 The application of Cosserat continuum for the bar subjected to a dynamic loading conditions of a transverse stress σ_{yx}, (a) the bar with a length L=100 mm, (b) strain distributions and energy dissipation for different meshes. (after de Borst et al., 1992)

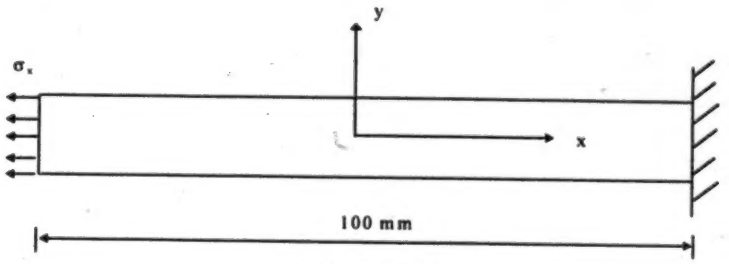

Figure 2.3 (a)

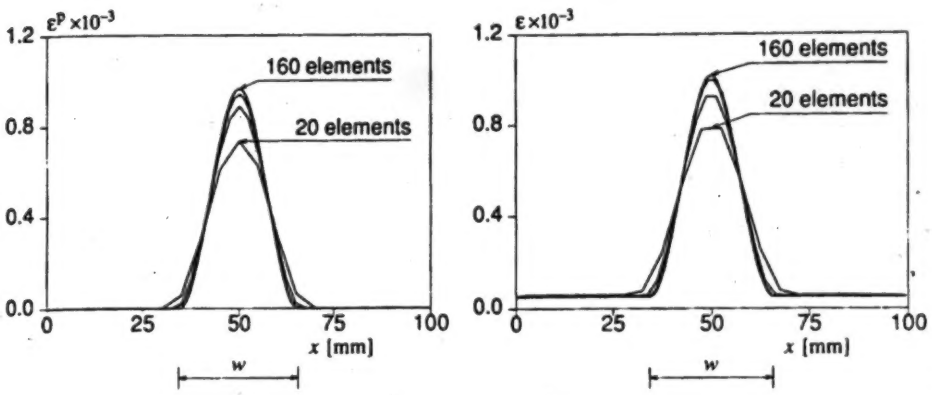

Figure 2.3 (b)

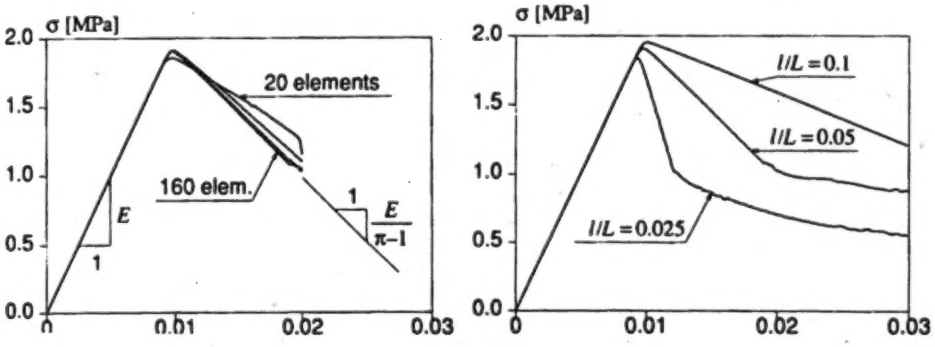

Figure 2.3 (c)

Figure 2.3 The application of gradient plasticity to an one-dimension tension bar, (a) One-dimension imperfect bar with a length L=100 mm, (b) plastic (left) and total (right) strain distribution , (c) axial stress vs. axial displacement under different discretization (left) and different ratios of l/L (right) (after de Borst et al., 1992)

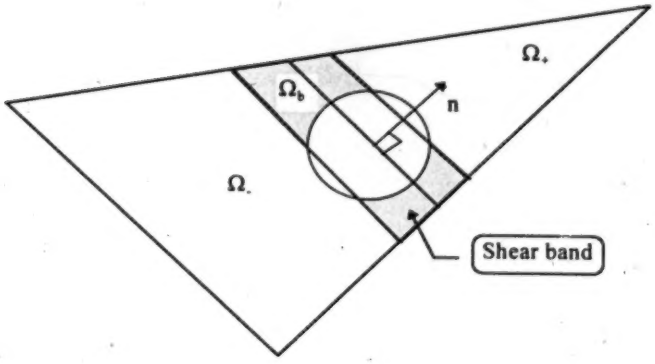

Figure 2.4 (a)

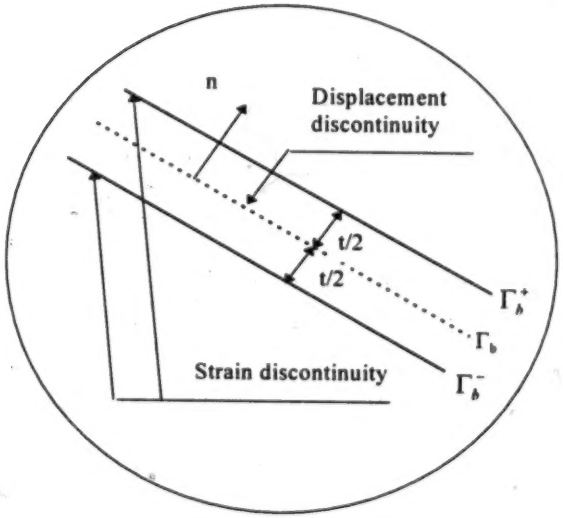

Figure 2.4 (b)

Figure 2.4 Embedded shear band in a normal element, (a) regularized displacement discontinuity, (b) details of the shear band

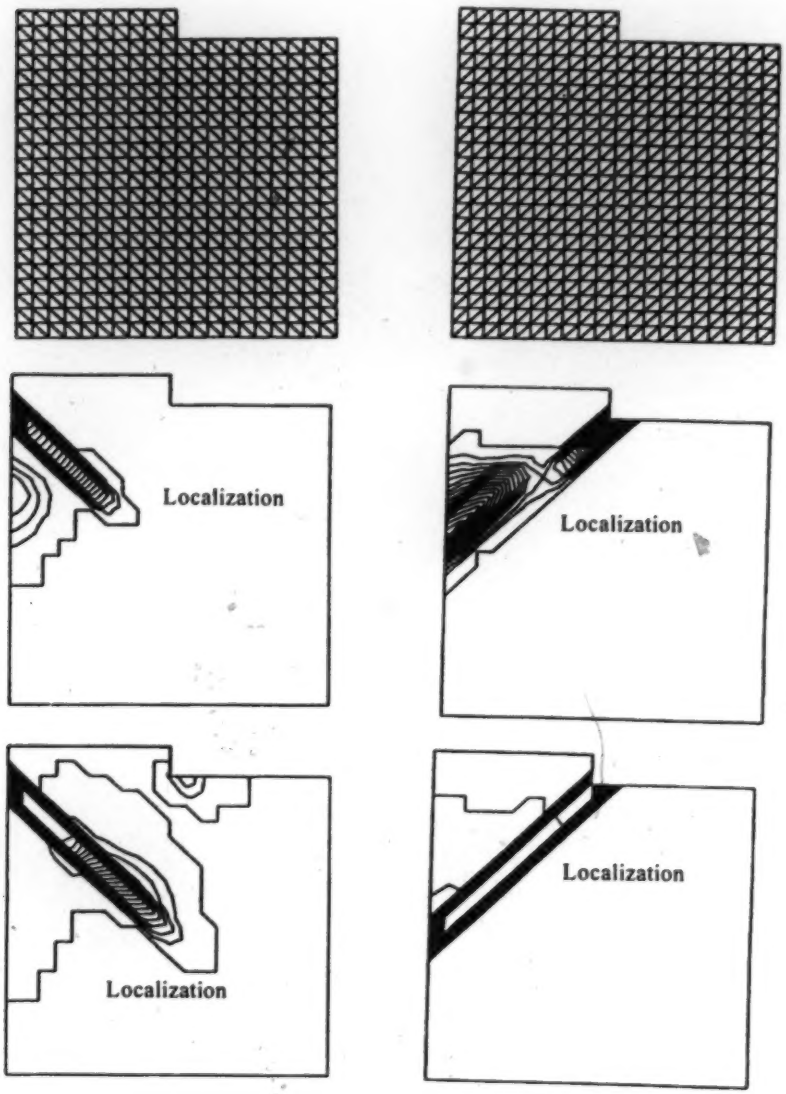

Figure 2.5 Influence of mesh alignment (after Pastor et al., 1992)

Chapter 3

Shear band localization in soils

3.1 Introduction

The failure phenomena of soil structures are often accompanied by the occurrence of shear band localization. Shear bands have been observed frequently in geotechnical structures and laboratory-tested soil specimens. Whether the developed theoretical and numerical methods are able to take into account strain localization largely depends on the precise characterization of the physical localization mechanisms. Since the 1960s, systematic studies have been undertaken to analyze and describe experimental observations of strain localization within a soil specimen subjected to shearing. Much has been published about experimental results which address the phenomenon of shear banding in clays, sands, and rocks. These scientific contributions were related to the studies of conditions for creating shear bands. The orientations and thickness of these bands in connection with the size of grains, local measurements of void ratio for sands, and even the void ratio evolution inside shear bands were determined. Scientists performed these studies through visual observations and other special graphic techniques such as use of radiographs (Alsiny, et al., 1992), X-ray scanning (Hicher, et al., 1994), stererophotogrammetry (Harris, 1995), and computed tomography (Desrues, 1996). Due

to the fact that the size of clayey particles makes observations of the shear bands more difficult, most of the experimental investigations were devoted to granular soils.

3.2 Strain localization in clays

3.2.1 Evolution of microstructures in Kaolin under direct shear

Morgenstern and Tchalenko (1969) observed the consecutive changes in microscopic structures in Kaolin subjected to direct shear. They studied the influence of a known original fabric on the strength of Kaolin and described in detail the features of the shear-induced fabric as the Kaolin was deformed to its residual shearing resistance. The earliest observed manifestation of shear was a rotation of the average particle orientation with respect to the original S_1 (original bedding) direction in terms of the relative displacement of the two halves of the shear box. The rotation was most intense near the edges of the box. The amount of rotation depended on the initial orientation of S_1. During stable yielding to peak strength, no discontinuities appeared. If specimens were sheared in a direction perpendicular to the original fabric, and at or immediately after peak strength, the specimen was penetrated by kinematic discontinuities denoted by S_2, which were inclined at about 12° to the horizontal and had a spacing of 10~50 μ. The central portion of the specimen was in simple shear. As motion proceeded further, kinematic discontinuities within the S_2 zone consisted of a family of displacement discontinuities lying 12°-14° to S_2 denoted by S_{2b}, then followed by small displacement discontinuities S_{2c} which interconnected S_{2b} and ultimately resulted in the formation of the continuous displacement discontinuity S_{2d} aligned in the S_2 direction. Subsequent

motion induced new discontinuities S_3 beyond the peak strength, interconnecting pre-existing structures S_2, bounded by strain and displacement discontinuities which were inclined at about -15° and 12° to the horizontal, respectively. With further rotation of S_1, the penetrative discontinuities S_{3a} appeared. Then an increased local rotation of S_1 and S_{3a} resulted in the development of displacement discontinuities S_{3b} which were parallel to S_2 and had a spacing of 2mm. The next stage in the development of S_3 was the formation of a family of sub-horizontal displacement discontinuities. All the structures can be seen in figures 3.1 and 3.2. Towards the end of the travel of the shear box, the residual strength was approached. In the meanwhile, a displacement discontinuities S_4 appeared, which was a distinctly wavy surface formed by the active parts S_3 and the portion of S_2. The rotation of S_1 between two strain discontinuities(S_2) had resulted in a kink band. It has been revealed that kinking is the dominant mode of deformation, which is comparable to full-scale geological structures.

3.2.2 The influence of flaws or discontinuities existing in the materials

In most of the overconsolidated clays, mechanical responses are dictated not only by their fabric, but by flaws or discontinuities which may exist in the materials. These flaws or discontinuities were often in the form of cracks or fissures, and inclusions. Saada et al. (1994) observed and described the initiation and propagation of shear bands with and without the presence of discontinuities by using controlled-stress and controlled-rotation devices to apply combinations of axial, torsional and spherical stresses at pre-determined ratios. A shear band started in the vicinity of a crack. It developed near the peak of the stress-strain curve in an unnotched specimen or at 80% of the peak, which

was triggered by the presence of a crack. Its experimental inclination agreed well with the Coulomb theory. They showed that the influence of the crack is minimal despite its size. The deformation is completely controlled by the plastic behavior of the material. Although cracks create local stress concentration, which controls the moment of initiation and the initial direction of the shear band, their influence quickly vanishes. The shear band eventually takes the same direction, which is fixed with respect to the direction of the major principal stress. For example, plasticity of the materials will be in control of the kinematics of the specimen, as shown in figure 3.3.

In the absence of cracks there are a very large number of diffuse shear lines all around the specimen, but in the presence of cracks, the number is limited to two or three. The overall strength of a specimen is not substantially affected by the presence of a small crack (or notch) in the specimen. Stress-strain curves, for specimens with or without cracks, differ very little, even though the observed pattern of displacement differed markedly.

3.2.3 Dimension, aspect ratio, and end effects

Hicher and Wahyudi (1994) performed a series of conventional triaxial tests to study the influence of sample dimensions, specifically the aspect ratio between the length L, the diameter D, and the friction of end restrain on the development of shear bands. The limiting of the shear band phenomenon can be achieved by reducing the friction at the cap and the base. The other effective way is to reduce the ratio L/D. For $L/D<0.5$, no localization pattern was observed. Similar results were illustrated by Read and Hegemier (1984), and by Lade and Tsai (1985). They also confirmed that there is a strong

correspondence between the calculated critical orientation obtained by using the Coulomb criterion, and the measured one, which is constant for a given clay. The orientation is independent of the size of the samples, of the end condition and of the overconsolidation ratio. The examination of a normally consolidated Kaolinite sample under a scanning electron microscope and through transmission electron microscopy has shown that the orientation of the particles next to the failure surface is parallel to the direction of the shear band. In comparison with the other parts of the samples, the mean size of the particles in the zone of failure is smaller and the size of the particles is less variable. Their shapes are more angular. As a consequence of a significant breakage of the aggregates and of the particles themselves, the thickness of this zone varies from 2 mm up to 7 mm according to the amount of sliding which is generated along the failure surface.

3.3 Strain localization in sands

3.3.1 The preliminary observations of localization in sands

In the study of the phenomenon of shear banding in soils, strain localization in sands has received particular attention. Although a number of experimental studies have been performed, the findings on the subject of shear banding in sand are still inconclusive.

Vardoulakis et al. (1978) conducted biaxial experiments with lubricated plates and a roller bearing. The homogeneous cubical samples kept the same shape during the pre-failure deformation, and the stress-strain behavior for these rectangular specimens

depended only on the initial void ratio. Shear bands were spontaneously formed at peak in both initially loose and dense samples. In all the experiments, shear band orientations were sensitive to boundary condition. The orientations of loose samples were more sensitive than those of dense ones. For the failure mode of plane shearing between two rigid bodies, the thickness of the shear band varied between about 3 mm and 5 mm.

The thick walled hollow cylinder inflation experiment was performed by Alsiny et al. (1984). Experimental observations revealed the development of localized and diffused deformation modes. The localized deformation mode was seen as a curvilinear shear band extending from the cavity to the outer surface of the specimen, and whose occurrence was preceded by the diffuse deformation which manifested itself as a surface rumpling. The shear banding took place slightly beyond the peak in the differential cavity pressure against cavity volume change curve.

Some investigators have performed extension tests in the past. Yamamuro and Lade (1995) presented an experimental study on granular materials in triaxial extension at different confining pressures. Strain localization was repeatedly encountered in the form of specimen necking, which was initiated very early in the test. Failure was generally precipitated by strain localization in all conventional extension tests in which volumetric dilation appeared to exacerbate strain-localization effects.

3.3.2 Shear band formation in triaxial and plane strain tests

Peters et al. (1988) performed three series of tests under the conditions of triaxial compression, triaxial extension, and plane strain, using dense sand specimens with relative density of 90%. For both triaxial compression tests, the formation of shear bands

were far beyond the peak point on the stress-strain curve. The rates of dilation in the area where shear bands are to form in dense sand reduced substantially right before the visible shear bands. It might be said that the onsets of shear bands in the triaxial extension test in dense sand would diminish dramatically the soil's dilation. In the triaxial extension test, shear bands initiate closely after the peak point, with a sudden and considerable drop in sustained stress difference σ_1-σ_3 and with an almost complete termination of dilation. In plane strain tests, the initiation of shear bands is very difficult to detect visibly. The visible shear bands are not apparently reflected by the stress-strain curves, which indicate that the shear band development is gradual.

3.3.3 Localization in loose sand under undrained conditions

Localization in loose sand sheared under undrained conditions is an important issue which has practical implications related to liquefaction. The nature of this issue is still in question. The experimental results presented by Han and Vardoulakis (1992) show that strain localization does not develop in undrained compression of loose sand, whereas data provided by Mokni (1992) indicated the contrary. Recently, more and more sophisticated techniques and instruments are being used by investigators to analyze the development of shear bands in sands. The questions mentioned in the last sub-section are explored further.

Harris and other researchers (1995) obtained a number of experimental results that characterized the behavior of a loose, fine-grained, water-saturated sand tested under globally undrained and drained conditions in a plane-strain compression (biaxial) apparatus in which the sterophotogrammetric method was used. All these tests were

conducted on masonry sand. Its mean particle diameter D_{50} was 0.32 mm, and the coefficient of uniformity ($C_u=D_{60}/D_{10}$) was 1.3. The conventional minimum and maximum void ratios are 0.6 and 0.875, and the specific gravity, G_s, was 2.677. Researchers found that in the early stages of undrained tests, soon after the peak of the shear stress was reached, a periodic pattern of parallel and at times crossing bands was formed at global axial strain equal to around 4%. These bands generally disappeared as the deformation process progressed. As these diffuse shear bands were observed, the overall deformation patterns were macroscopically 'uniform', and no changes in the overall shape of the specimen were observed. Eventually, at, or shortly before the maximal effective stress ratio, a single persistent shear band was formed. Then, overall deformations were concentrated in this single band, and the macroscopic deformations became non-uniform as this band progresses. The evolution of localization is shown in figure 3.4. Prior to localization of shear strains in the region where the final band eventually formed, the soil had contracted. For the test where the deviatoric stress response is that of a sudden peak followed by a monotonic decrease to a final plateau, in the region outside the band, the average response was moderately contractive with ε_{vol} less than 2 %. The material inside the shear band showed a stronger contraction at 3% global axial strain as soon as the band was fully formed. For continuing shear, the shear strains gradually localized in the shear band, and the soil inside the band either did or did not exhibit dilatant behavior. The localized shear strain in the band could arrive at as high as 65% at 12% global axial strain, whereas the maximum shear strain outside the band was approximately 7%. It has been confirmed that the orientation of the shear band

varies between the limits of β_c and β_r with respect to the major principal stress direction. β_c and β_r are given by well-known Coulomb and Roscoe expressions. Experimental data report thickness ranging from 4 to 6 mm, which is 12 to 17 times the mean particle diameter. The thickness generally increases as the deformation progresses.

3.3.4 Medium to dense sand behavior under strain path control

Recently, Chu et al. (1992, 1996) have undertaken a series of conventional triaxial compression tests or multiaxial tests under the condition of independent σ_1, σ_2, σ_3 by using Sydney sand with an average grain size of 0.3 mm, and which was reconstituted into a saturated dense state. Its void ratio ranged from 0.6 to 0.618. They investigated strain softening and shear banding behavior along different strain paths (strain increment ratio $d\varepsilon_v/d\varepsilon_1$ was kept to a specified value, i.e. fixed dilatancy). The specific definition of strain softening ($d\varepsilon_{ij}d\sigma_{ij}<0$) in their studies was classified into three types: shear band mode I, shear band mode II (banding softening), and material softening. Shear band mode I was mainly due to boundary imperfection in the form of end restrains, such as platen restrains, which led to non-uniformity in stress and strain before the occurrence of any true strain softening. Shear band II (banding softening) was always associated with shearing in the post-failure regime, an association which was similar to that observed by Vardoulakis (1979,1983) and Drescher et al. (1990) in a special biaxial apparatus. It was not due to boundary imperfection but to an inevitable response to the stress path and stress state. Hence, its initiation was a material property, but the process after the shear band formation could not be regarded as a true material property of a soil element. Failure could be taken as a necessary condition for the onset of shear band II. Material

softening occurred without loss of homogeneity. Both its initiation and the process were true material properties of the soil. The occurrence of material softening in the pre-failure strain softening regime was dependent on both the strain increment ratio ($d\varepsilon_v/d\varepsilon_1$) and the initial stress state from which strain path control commenced. Material softening would occur provided the imposed strain increment ratio was adequately dilative. Here, Lade's failure criterion, expressed as $\eta=\eta_{max}$, is adopted, where,

$$\eta = \left(I_1^3/I_3 - 27\right)\left(I_1/P_a\right)^m,$$

p_a is the standard atmospheric pressure in consistent units, and m and η_{max} are constants established experimentally to be 0.183 and 65 respectively. I_1 and I_3 are first and third stress invariant. In the tests where σ_2 was kept equal to σ_3, no shear band occurred in the post-failure regime. Thus, true soil behavior could be obtained in the large strain domain (Uchida and Vaid, 1994).

3.3.5 Localization in reinforced sand

A number of investigators (Waldron 1977; Juran and Chen 1989; Shewbridge and Sitar 1989, 1990) have presented the results of studies of the shear zone development and shear zone deformation patterns for reinforced sands in large direct shear devices. Shear displacement of the soil across the shear zone resulted in the reorientation of the reinforcements. Then, tensile and bending stresses developed in the reinforcements, and this in turn induced increased resistance to the displacement. The results of the studies show that the mobilization of tension in the reinforcement is a function of the reinforcement properties and deformation characteristics of the reinforced soil.

The simplicity of direct shear devices makes them widely used. However, unlike the conditions in a reinforced soil structure, deformation in a direct shear device is forced to occur in a shear zone that is constrained by the configuration and dimensions of the device. Shewbridge and Nicholas (1996) conducted tests in a plane-strain hollow cylindrical testing device which can test the reinforced soils under conditions that more closely approximate the field conditions. The reinforced sand samples developed wider shear zones than the unreinforced samples, as shown in figure 3.6. Shear zone width increased with increasing reinforcement concentration, reinforcement stiffness, and reinforcement-soil bond strength. In other words, dense, dilatant unreinforced sand samples formed narrow shear zones with large strains (up to 200%), whereas the reinforced samples had smaller but more uniform strains distributed throughout the samples. Therefore, narrow shear zone formation should not be assumed when analyzing the stability of reinforced soil structures (Shewbridge and Sitar, 1996).

3.3.6 The investigation of localization patterns and void ratio evolution by computed tomography

With the use of computed tomography, Desrues et al. (1996) detected and described, both qualitatively and quantitatively, different localization patterns depending on test conditions in conventional triaxial dense sand specimens. All these results were based on tomograms taken perpendicular to the axis of the specimen at different heights or taken parallel to the axis and containing it.

In the tests performed on a non-lubricated specimen, a single shear plane, which was not perfectly planar, appeared and retained the unique localization structure until larger strain. For the short but non-lubricated specimen, the localization pattern looked

like a rigid cone, which was attached to the end platen. This cone was delimited by a circular shear surface which was a locus of a large dilatancy. When short lubricated specimens were tested, the onset of localization was significantly delayed. The localized deformation was organized with a single rigid cone attached to one of the platens, while the other platen did not generate any cone. The localized strains were developed mainly on one side of the specimen. The upper platen had a severe rotation. If the specimen was slightly perturbed (soft inclusion) , then the localization pattern in this specimen involved two kinds of structures. One was a cone centered on the axis of the specimen, with its tip outside the specimen and its contour matching exactly the specimen's bottom section. The other one was a pair of planes, each pair of which crossed on a line that was the diameter of the top section. The numerical images of the cross-sections recorded during the CT also gave quantitative information which could be used to monitor the evolution of the global and local densities. From these results, an important conclusion is drawn: a void ratio limit is reached in the shear zones. This void ratio is significantly different from the final void ratio as defined by the global measurements.

3.4 The understanding of strain softening and strain localization

3.4.1 The coupling of strain softening and strain localization at the microscopic level

So far, the inception, and the development of localization have been characterized in different soils under various circumstances. From the viewpoint of bifurcation, localization arises as a result of an instability in the inelastic behavior of the solid. It can

take place even under hardening condition, and can result in the overall softening of the specimen. Thus, some researchers have not taken strain softening to be a true material property (Leroy and Ortiz 1989, Read and Hegemier, 1984). As a matter of fact, the appearance of localization is frequently accompanied by the strain softening. The occurrence of softening is due to the nucleation and progressive growth of microscopic voids, cracks, which could be viewed as the inceptions, and propagation of localization. In the local area where strain softening occurs, the stress and strain deviate significantly from homogeneity with the strain softening. The strain softening in geological materials inevitably generates material inhomogeneities as well. Theoretically, changes in micro-structure of the damaged material should be taken into account in the mathematical description. A solution to this problem is the introduction of additional terms in the continuum mechanics. It will reflect the changes in micro-structure which occur step by step during loading progress. The available theories are non-local, micro-polar continuum theories, continuous damage mechanics, and so forth, which have been briefly summarized in chapter two. In these cases, we do not need to view softening as a material property, or no special localization theories are necessary. What we need to do is to keep track of changes in micro-structures of the material.

3.4.2 The relationship between strain softening and strain localization at the macroscopic level

Generally, standard continuum mechanics is still used for the study of localization. Although changes in microstructures can not be directly and consecutively accounted for, their macroscopic responses can be feasibly described as material property, instead the changes are incorporated into a constitutive model. This treatment infers that

softening materials are homogeneously strained. In practical engineering or conventional laboratory tests, the material inhomogeneities due to the accumulation of changes in microstructures are very often localized. In other words, strain softening occurs only within the localized shear zone. In engineering practice, it seldom extends to the whole area of a structure. If the response of a structure subjected to a variety of loads needs to be truly described, the macroscopic inhomogeneities at different loading steps should be kinematically determined. On the other hand, it is necessary to have the softening properties of the material within the localization. The analysis of inception of inhomogeneities (localization) can be referred to bifurcation theories which are based on standard continuum mechanics. The effort to describe the kinematics is in progress (Wang et al., 1995).

Strain softening as a material property is an abstract concept. It is characterized by a constitutive response in which stresses at one point decrease monotonically with further increases in strains at that point. However, this constitutive response is obtained from tests performed on finite-sized specimens. In conventional triaxial compression tests for materials such as heavily over-consolidated clay, the localization (i.e. material inhomogeneity) always forms in the specimens. Obviously, softening only happens in the shear band zone along the shear band direction. The conventional constitutive description is obtained by mapping the vertical force-displacement relationship onto the stress-strain curves. This is done without accounting for the localized material inhomogeneities in the specimens. Therefore, the measured stress-strain relationship at the softening stage, to be strict, does not stand for the real material behavior, but for the structure response. The structure response is always dependent on boundary conditions,

sizes and shapes of the specimens etc.. These are reasons why the stress-strain curves at post-peak stage for the same material in different tests are always variable. In addition, we should be careful in which direction the strain softening occurs. Frequently, softening does not occur in the direction along which stress and strain are measured. Sometimes, there is even no softening stage in the measured stress-strain curve for a specimen which normally fails in a test. This phenomenon provided the researchers a good excuse to argue that the strain softening is not a true material property.

As mentioned previously, using conventional continuum mechanics to obtain real softening response of a structure, non-homogeneous localization should be taken into account. In addition, the real softening property of the material in the shear zone should be available.

3.5 Concluding remarks

The phenomena of shear band localization in laboratory experiments are described in details which are categorized in soil types, test types, and stress paths. The influences of flaws or discontinuities, which exist in the materials, dimensions, aspect ratios, and boundary conditions of specimens on the inception and the propagation of localization, are discussed. In the precise observations of changes in microstructures, localization patterns are fundamental to a true understanding of localization. These will also provide an important starting point for theoretical studies. All the experiments have shown that strain softening as material property is accompanied by localization in many cases.

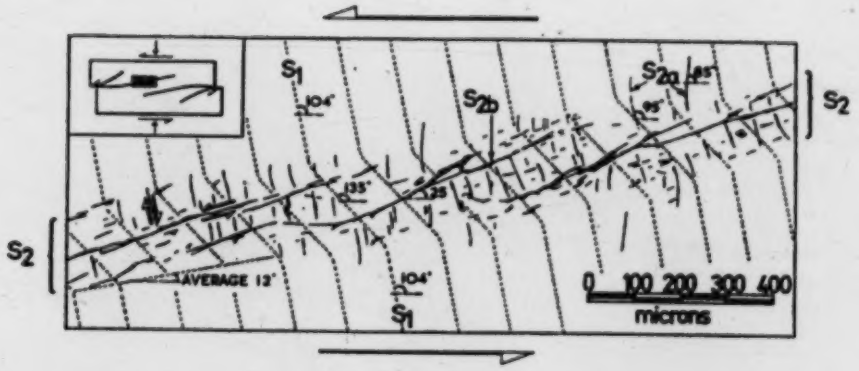

Figure 3.1 Detail of discontinuities S_2 (after Morgenstern and Tchalenko, 1967).

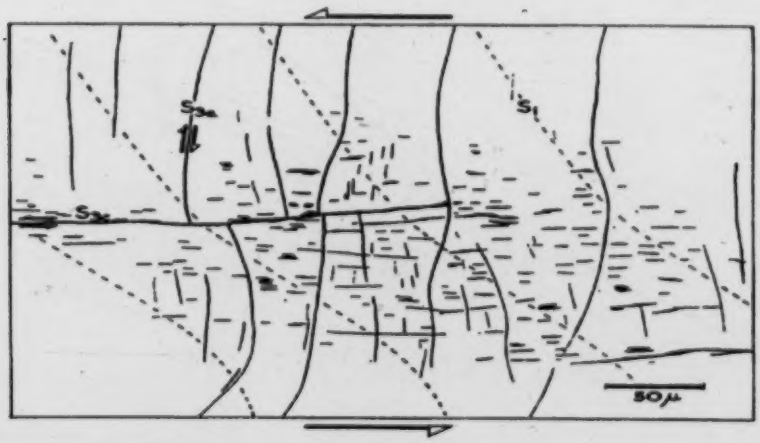

Figure 3.2 The propagation of discontinuities of S_3
(after Morgenstern and Tchalenko, 1967)

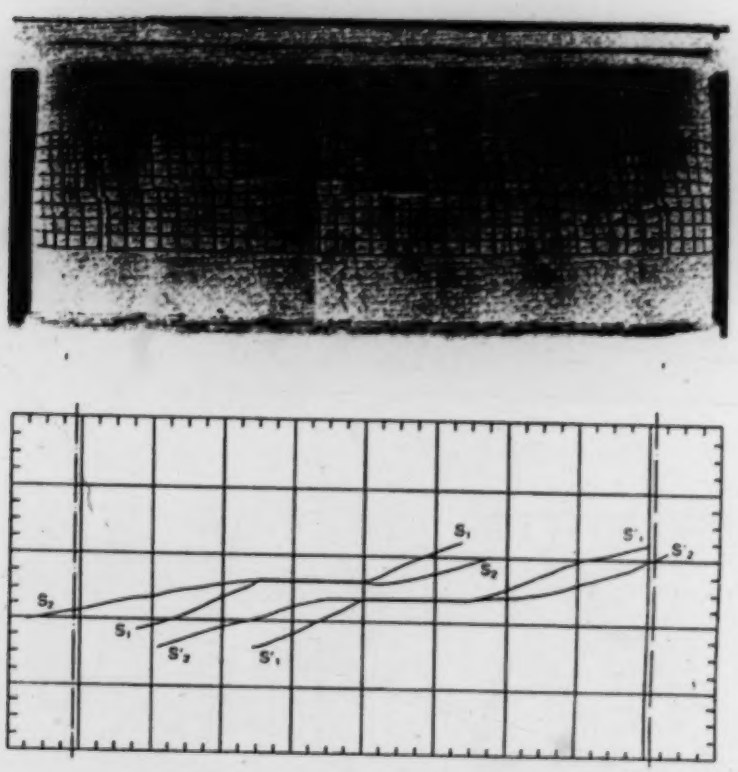

Figure 3.3 Shear bands and interaction of two cracks
(after Saada, Bianchini and Liang, 1994)

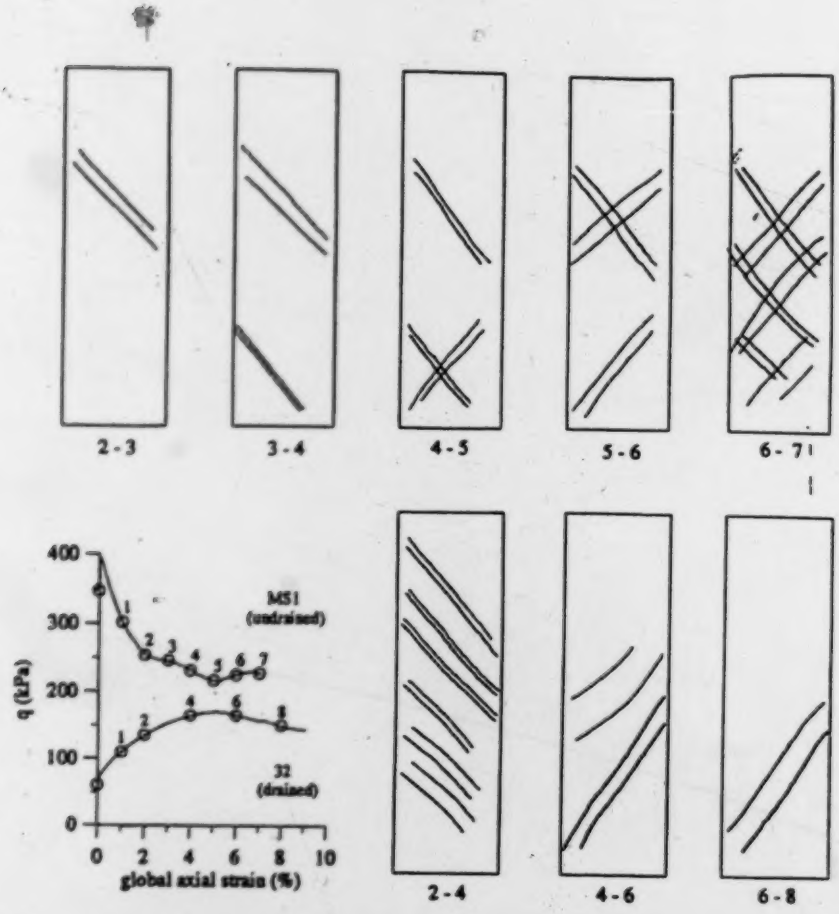

Figure 3.4 Evolution of shear bands as observed in tests named MS1 and 32 (After Harris et al., 1995)

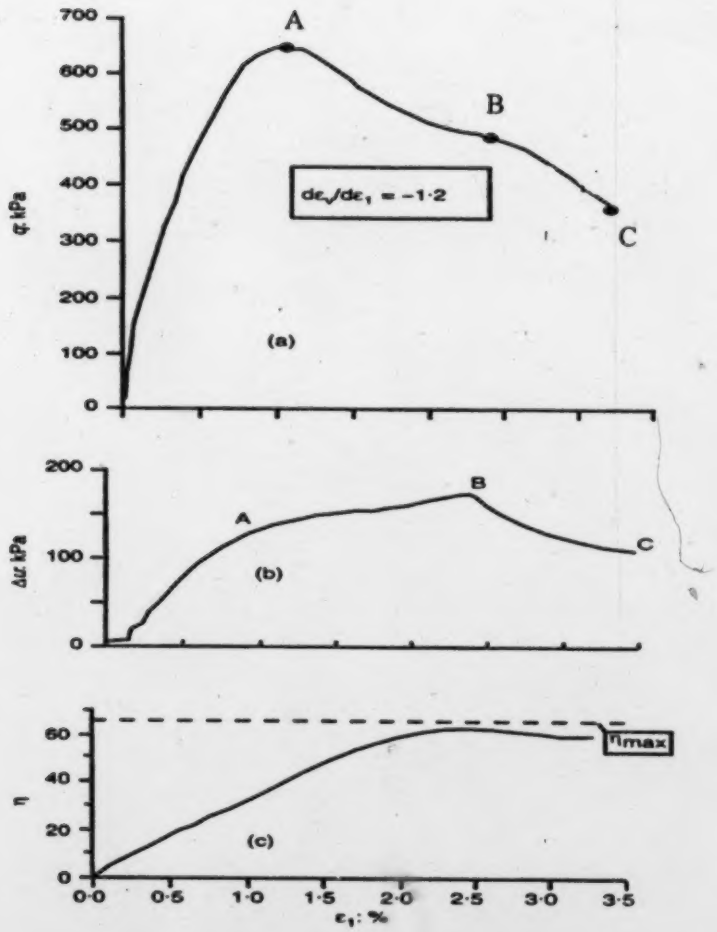

Figure 3.5 Stress-strain curves: (a) Deviatoric stress q vs. axial strain ε_1; excess pore pressure vs. axial strain ε_1; (c) failure parameter η vs. axial strain ε_1 (after Chu et al., 1996)

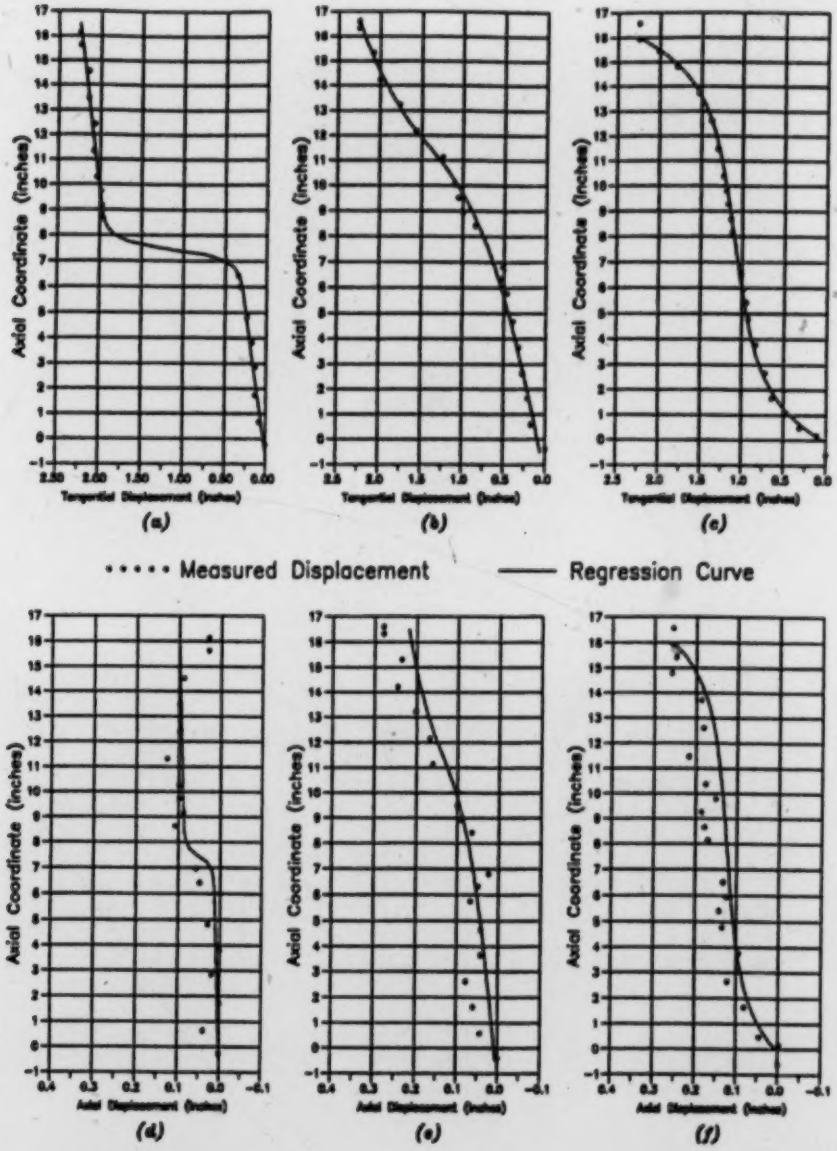

Figure 3.6 Tangential displacement vs. axial coordinate and axial displacement vs. axial coordinate, respectively. (a,d) sample with no reinforcement; (b,c,e,f) sample with reinforcements. (after Shewbridge and Nicholas, 1996)

Figure 3.7 (a)

Figure 3. 7 (b)

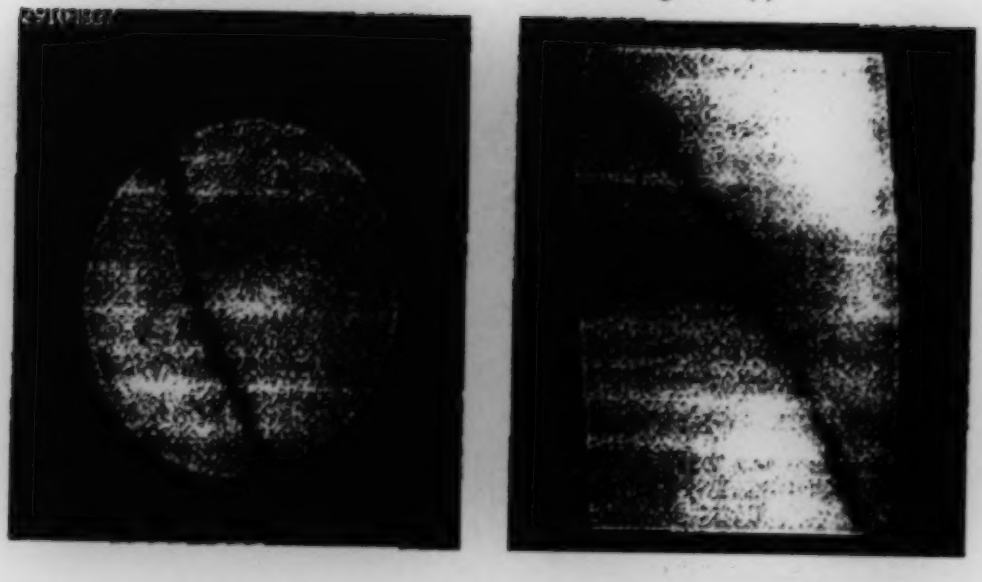

Figure 3.7 Localization patterns in a specimen (a) trace of the section zone in a section perpendicular to the axis in a cross-section (b) trace of the shear zone in the section parallel and containing the axis of the specimen. (after Desrues et al., 1996)

Chapter 4

Characteristics of constitutive responses and localization criteria under bifurcation theories

4.1 Introduction

As mentioned in the foregoing chapter, the physical mechanisms responsible for triggering shear band localization are mainly the boundary imperfections in the form of any restraints, material weaknesses, or stress concentrations. Shear band localization is often a direct precursor to ductile failure. If a solid can be modeled as rate and time independent, a theoretical framework developed by Hadamard (1903), Thomas (1961), and Hill (1962) is available for analyzing the onset of shear band formation. The analyses determine the state at which bifurcation from homogeneous or smoothly varying deformation into the shear band mode is first possible. In this framework, localization is associated with a material instability and bifurcation coincides with loss of ellipticity of the equations governing incremental equilibrium (Hill, 1962; Rice, 1976). Specifically, instability is understood in the sense that the constitutive relations may allow the homogeneous deformation of an initially uniform material leading to a bifurcation point, at which non-uniform deformation could be incipient in a planar band under continuing equilibrium and continuing homogeneous deformation outside the zone of localization (Rudinicki and Rice, 1975). Localization is associated with a strain rate jump within the

band over the strain rate in the surrounding material. This mode is called a classical discontinuous bifurcation.

Bigoni and Hueckel (1991) pointed out that localization implies a specific non-uniqueness in the incremental elastoplastic response of a homogeneous, homogeneously strained body. In principle, any sufficient condition for uniqueness is lost in the deformation process before the condition for a particular form of non-uniqueness, such as a localization, is met. Therefore, other forms of non-uniqueness, like diffuse bifurcation, may occur before the condition of localized strain is reached. Hill and Hutchinson (1959) and Needleman (1979) found that shear band localization may be incipient when the system of differential equations governing incremental equilibrium is hyperbolic, whereas a variety of diffuse bifurcation may precede the localization when the system is still elliptic.

Drucker (1950) and Hill (1958) stated that a necessary condition for the loss of material stability, that is a loss of uniqueness which is called general bifurcation criterion, is the loss of positive definiteness of the rate of second order work. Neilsen and Schreyer (1993) expressed this general bifurcation criterion as a loss of positive definiteness of the symmetric part of the tangent modulus tensor. Valanis (1989) indicated that loss of material stability should be associated with the limit point where the tangent modulus tensor obtains a zero eigenvalue. It is also associated with a loss of positive-definiteness of the tangent modulus tensor (de Borst, et al., 1993). For materials with associated flow rule, the Valanis' or de Borst's interpretation, and Drucker's general bifurcation criterion, both identify the limit point as the point at which necessary conditions for the loss of material stability are first satisfied. For materials with non-associated flow rule, loss of

positive definiteness of the symmetric part of the tangent modulus tensor, namely, the satisfaction of the necessary condition for a general bifurcation, can occur prior to the limit point.

Ottosen and Runesson (1991) indicated the implication of loss of ellipticity of the differential rate equilibrium equations to discontinuous bifurcation. They stated that the loss of strong ellipticity of the governing differential equations occurs whenever positive definiteness of the symmetric part of the acoustic tensor is lost. If the acoustic tensor and the tangent modulus tensor are symmetric, the loss of strong ellipticity and the satisfaction of the classical necessary condition for a discontinuous bifurcation will first occur at the same point. However, if the acoustic tensors are non-symmetric, the loss of strong ellipticity will precede the satisfaction of the necessary condition for a classical discontinuous bifurcation.

In an eigenanalysis of the symmetric part of the tangent modulus tensor $\mathbf{D}^s$, the necessary condition for a general bifurcation (diffuse and classical discontinuous bifurcation) is first satisfied if the fundamental eigenvalue of the tangent modulus tensor obtains a value of zero. The deformation mode associated with this bifurcation is characterized by the fundamental eigenvectors $\mathbf{x}_i$. The basic eigenvalue problem is described as $\mathbf{D}^s:\mathbf{x}_i=\omega_i\mathbf{x}_i$, here ω_i denotes the i^{th} eigenvalue, : represents the multiplication between two matrices . Discontinuous bifurcation is detected by choosing a deformation mode which satisfies the general bifurcation criterion and is restricted to being of a form normally associated with a discontinuous bifurcation. The corresponding mode is

expressed as a linear combination of the eigentensors which are related to the symmetric part of the tangent modulus tensor.

The condition for emergence of strain localization into a shear band, as a particular type of non-uniqueness (classical discontinuous bifurcation point), is attained when the system of differential equations governing the local rate equilibrium suffers a loss of ellipticity. Presently, it is comprehensively applied to various types of elastic-plastic soils to predict the existence and orientation of the emerging shear band. The implicit expression for the critical orientation of the shear band and the corresponding hardening modulus was genetically given by Rice (1976). It was then directly adopted for specific elastic-plastic models by Bardet (1990) and Wan (1990). Ottosen and Runesson (1991), Runesson et al. (1991) performed eigenvalue analysis for the acoustic tensor to give explicit expressions of critical inclination and hardening modulus of the shear band for the special cases of plane stress and plane strain. Furthermore, different criteria were achieved for a series of common elastic-plastic models. Similar explicit expressions were obtained by Bigoni and Hueckel (1991) by virtue of the Largrangian multiplier method. For materials with different elastic-plastic models, the shear band bifurcation might occur at different stages of the stress-strain curves. The bifurcation into a shear band always occurs on softening branch or at peak point of the stress-strain curve for materials yielding according to the associated flow rule. If materials obey the non-associated flow rule, the bifurcation can occur on the hardening branch. Bifurcation points also depend on loading configurations. In other words, the same material will have been bifurcated at different points on the stress-strain curve under triaxial compression, triaxial extension, and plane strain conditions (Peters et al., 1988).

In the analyses of soil structures, some models like the Mohr-Coulomb criterion and the Drucker-Prager criterion are widely applied to geological materials due to their simplicity. However, it is necessary to mention that all the directions that these simple criteria predict using bifurcation theories do not always account for the physical directions of shear bands in all circumstances. The discrepancies originate from several sources (Bardet, 1990): 1, The dilantancy and mobilized friction angles vary within the soil structure. 2. The shear band orientation depends not only on the mobilized friction angle ϕ and dilatancy angle ψ, but also on the other constitutive parameters and state variables (Molenkamp, 1985). 3. The strain localization theory provides only a necessary but not sufficient condition for inceptions of shear bands. Some experimental observations of Chambon and Desrus (1985) revealed that the real shear band emerges after the predicted critical point passes. This delayed strain localization may enhance the disagreement between the experiment observations and theoretical predictions of shear band inclinations.

In this chapter, material instability, general non-uniqueness, limit point, losses of ellipticity and strong ellipticity of the governing incremental equilibrium equations are precisely defined. Their relationships are discussed in detail. Lastly, the general criterion for discontinuous bifurcation into a narrow band is attained. Thereafter, specific criteria for different yielding equations and different stress paths are derived. Some explicit expressions are highlighted for critical hardening modulus and shear band orientation.

4.2 Material instability and general bifurcation

A sufficient criterion for a material stability is that the inner product of the stress rate and the strain rate be positive (Drucker, 1956):

$$\left\{\dot{\varepsilon}\right\}^{T}\left\{\dot{\sigma}\right\} > 0. \tag{4-1}$$

In a uniaxial tension or compression test, when this inner product becomes negative, it coincides with the negative slope of the homogenized axial stress-axial strain curve, a process which is called 'strain softening'. Substitute the relationship between stress and strain rates:

$$\left\{\dot{\sigma}\right\} = [D]\left\{\dot{\varepsilon}\right\}, \tag{4-2}$$

into (4-1) , and an equivalent condition of positive definiteness of the constitutive tensor D is obtained:

$$\left\{\dot{\varepsilon}\right\}^{T}[D]\left\{\dot{\varepsilon}\right\} > 0. \tag{4-3}$$

Mathematically, the critical condition for the loss of the positive definiteness could be expressed as:

$$\det([D]+[D]^{T}) = 0, \tag{4-4}$$

where the $[D]^T$ is the transpose of [D]. This is used as the criterion for material instability. It may also be used as a general bifurcation criterion. The material instability can lead to structural instability. The term 'structural instability' here is different from the same one defined as 'buckling' in structural mechanics. For a structure over a volume of V, the sufficient criterion for its stability is written as:

$$\int_V \left\{\dot{\varepsilon}\right\}^T \left\{\dot{\sigma}\right\} dV > 0. \qquad (4\text{-}5)$$

The limiting case of neutrally stable equilibrium is attained for a discretized structural system if:

$$\det([K]+[K]^T) = 0, \qquad (4\text{-}6)$$

where [K], the structural stiffness matrix, is:

$$[K] = \int_V [B]^T [D][B] dV. \qquad (4\text{-}7)$$

In the finite element method, [B] matrix relates the strain rate to the nodal displacement rate $\left\{\dot{x}\right\}$:

$$\left\{\dot{\varepsilon}\right\} = [B]\left\{\dot{x}\right\}. \qquad (4\text{-}8)$$

Although Drucker's postulate and Hill's stability condition are sufficient to guarantee stability, theoretical considerations have suggested that they are not necessary conditions for granular materials (Mroz, 1963; Lade, 1989). Stability may be obtained even if inequality (4-1) is violated. Lade (1988, 1989) performed two series of triaxial compression tests designed to expose the type of behavior exhibited by granular materials. When the sand dilated during shear, it exhibited non-associated flow. When it is exposed to stress paths in the region of potential instability where Drucker's postulate has been violated, no material instability was observed. When the sand tended to compress during shear, it exhibited non-associated flow, too. Instability was observed along stress paths in the region of potential instability. The type of volume change (dilation or compression) is of great importance for stability in granular materials.

4.3 Non-uniqueness and limit point

The question of non-uniqueness of the elasto-plastic incremental response is addressed in the context of boundary value problem. In other words, there must be a uniqueness of the solution of the incremental boundary value problem. Suppose now that the uniqueness of the solution is violated. Then there must be two different stress rates, $\left\{\dot{\sigma}_1\right\}$ and $\left\{\dot{\sigma}_2\right\}$, that both satisfy incremental equilibrium (de Borst et al., 1993). To derive the non-uniqueness criterion, the virtual work principle is simply written as:

$$\int_V \left\{\delta\dot{\varepsilon}\right\}^T \left\{\dot{\sigma}\right\} dV = \left\{\delta x\right\}^T \left\{\dot{f}\right\}, \qquad (4\text{-}9)$$

where, δ denotes the variation of a quantity and f the external load increments. Equation (4-9) is applicable to both $\left\{\dot{\sigma}_1\right\}$ and $\left\{\dot{\sigma}_2\right\}$. If the two stress rates are related to the strain rates by the same material tangential stiffness matrix, subtraction of both equilibrium equations for $\left\{\dot{\sigma}_1\right\}$ and $\left\{\dot{\sigma}_2\right\}$ results in:

$$\int_V \left\{\delta\dot{\varepsilon}\right\}^T \left\{\Delta\dot{\sigma}\right\} dV = 0, \qquad (4\text{-}10)$$

Δ denotes the difference between two quantities. The two stress rates correspond to two different displacement rates $\left\{\dot{a}_1\right\}$ and $\left\{\dot{a}_2\right\}$. Under the framework of finite element analysis, (4-10) is rewritten as:

$$[K]\left\{\dot{\Delta a}\right\} = 0. \tag{4-11}$$

Expression (4-11) is satisfied non-trivially if and only if:

$$\det([K]) = 0. \tag{4-12}$$

The criterion (4-6) for loss of stability and the criterion (4-12) for loss of uniqueness only coincide with each other for a symmetric material tangential matrix [D], which is related to associated flow. For non-symmetric [D], this is not true. The loss of stability may precede loss of uniqueness.

If a much more restrictive condition holds for the uniqueness, it is required that the rate of second order work , which is expressed as:

$$\dot{W} = \frac{1}{2}\left\{\dot{\sigma}\right\}^T\left\{\dot{\varepsilon}\right\} > 0, \tag{4-13}$$

should be always positive at every point of the body for every strain rate and corresponding stress rate. Bigoni and Hueckel (1991) referred to (4-13) as the local criterion for uniqueness, which will be quoted thereafter. In a common sense, the loss of this uniqueness is equivalent to the concept of general bifurcation, and also consistent with the material stability mentioned before.

Limit point is defined as a point on stress-strain curve where strain rate $\dot{\varepsilon}_{ij}$ corresponds to a null stress rate. Mathematically, the criterion for limit point is written as:

$$\dot{\sigma}_{ij} = D_{ijkl}\,\dot{\varepsilon}_{kl} = 0 \text{ or } \det(D_{ijkl}) = 0. \tag{4-14}$$

In other words, when the tangent modulus tensor D_{ijkl} has a zero eigenvalue, limit point is reached (Neilsen and Schreyer, 1993).

4.4 Discontinuous bifurcation characteristics

In this section, some of the basic principles of the general theory of localization of inelastic deformations, as developed by Hadamard (1903), Thomas (1961) and Hill (1962), will be referred to. For the sake of simplicity, attention is confined to infinitesimal deformations, rate-independent material behavior, and local strain descriptions. No rotational degrees of freedom are added.

Assume that the current state of static equilibrium is characterized by continuous displacements u_i, stresses σ_{ij} and strains ε_{ij}. With an increased loading, discontinuous bifurcation (Ottosen and Runesson, 1991) of the displacement rate $\dot{u}_i$ and the rate of the corresponding displacement gradient $\dot{u}_{i,j}$ may occur across a plane of orientation n_i. Displacement field u_i would still be continuous even after the inception of the discontinuous bifurcation, i.e. the occurrence of localization. The displacement gradient $\dot{u}_{i,j}$ would exhibit a jump across the discontinuity plane S. It is written as:

$$[[\dot{u}_{i,j}]] = \dot{u}^{u}_{i,j} - \dot{u}^{l}_{i,j}, \qquad (4\text{-}15)$$

where superscript u denotes the upper side of the discontinuity plane, and l the lower side of the discontinuity plane. Maxwell's theorem gives the form of the discontinuity of the deformation gradient:

$$[[\dot{u}_{i,j}]] = g_i n_j, \qquad (4\text{-}16)$$

where g_i is the component of a polarization vector **g**, which depends only on the distance across the band and vanishes outside the band. Take the expressions for small strain $\varepsilon_{ij} = \frac{1}{2}(u_{i,j} + u_{j,i})$ into (4-16), and it follows that:

$$[[\varepsilon_{ij}]] = \frac{1}{2}(g_i n_j + g_j n_i). \tag{4-17}$$

Assuming that the solid is at the onset of localization, the tangent stiffness tensor D_{ijkl} takes the same value of either side of the singularity surface. Accordingly, the incremental stress-strain relations throughout the body still take the form:

$$\dot{\sigma}_{ij} = D_{ijkl}\dot{\varepsilon}_{kl}. \tag{4-18}$$

From equilibrium consideration across the discontinuity plane, the traction t_i must be continuous, i. e.:

$$[[\dot{t}_j]] = [[n_i \dot{\sigma}_{ij}]] = n_i[[\dot{\sigma}_{ij}]] = 0. \tag{4-19}$$

Combining (4-17),(4-18), and (4-19) yields:

$$\left(n_i D_{ijkl} n_j\right)\dot{g}_k = 0. \tag{4-20}$$

The second order acoustic tensor Q_{kl} is defined as:

$$Q_{kl} = \left(n_i D_{ijkl} n_j\right). \tag{4-21}$$

It is also called the characteristic tangent stiffness modulus tensor. If non-trivial solution of $\dot{g}_k$ is obtained, the following equation must exist:

$$\det\left(n_i D_{ijkl} n_j\right) = 0. \tag{4-22}$$

The basic requisite for the existence of discontinuous bifurcation is that real solutions must be obtained from the above equation. Bardet (1990) underlined that this localization theory has the following limitations:

a. The onset instead of the propagation of localization is analyzed.

b. Equation (4-22) is only a necessary, not the sufficient condition for the emergence. In other words, it does not guarantee that localization actually occurs.

After the emergence of localization, at further deformation, equilibrium can be maintained only if the material outside the band responds elastically, whereas the material inside the band is conditioned to respond plastically, corresponding to 'softening' behavior (Larsson et al., 1993).

To get a better understanding of equation (4-22), Bigoni and Hueckel (1991) proposed a weaker condition with respect to the criterion for uniqueness: they specialized strain rate $\dot{\varepsilon}_{ij}$, a particular rate deformation mode defined as the cross product of direction vector n_i normal to discontinuity plane and polarization vector g_j. Equation (4-3) becomes:

$$\dot{g}_j(n_i D_{ijkl} n_l)\dot{g}_k > 0. \qquad (4\text{-}23)$$

(4-23) is equivalent to the requirement of positive definiteness of every acoustic tensor $n_i D_{ijkl} n_l$. (4-23) is also the condition to keep the strong ellipticity of the system of differential equations governing the local incremental equilibrium. The criterion for the loss of strong ellipticity of the system is:

$$\dot{g}_j(n_i D_{ijkl} n_l)\dot{g}_k = 0. \tag{4-24}$$

Whereas, the criterion for the loss of ellipticity of the system is different. It reads:

$$\det\left(n_i D_{ijkl} n_l\right) = 0. \tag{4-25}$$

This is viewed as a particular type of non-uniqueness into the form of strain localization.

4.5 The summary of various constitutive responses

As mentioned previously, inequality (4-3) is a sufficient condition for material stability, uniqueness (general bifurcation) for arbitrary $\dot{\varepsilon}_{ij}$ irrespective of $\dot{\varepsilon}_{ij}$ being continuous or discontinuous (Ottosen and Renesson, 1991). Assume that $\dot{\varepsilon}_{ij} = g_i n_j$ is a particular solution to make (4-3) violated, which leads to a discontinuous deformation gradient. The discontinuous deformation gradient corresponds to the hardening modulus H_{db}. Suppose that equation (4-3) is firstly violated when the hardening modulus reaches a value of H_{gb}. Subscripts db and gb denote discontinuous bifurcation and general bifurcation, respectively. Obviously, discontinuous bifurcation must occur after general bifurcation, or coincide with general bifurcation, i.e.:

$$H_{gb} \geq H_{db}. \tag{4-26}$$

As mentioned in section (4.3), limit points occur when D_{ijkl} becomes singular. Let H_l denote the corresponding value of the hardening modulus. Runesson and Mroz (1989) showed that H_l=0 holds for limit points irrespective of the amount of non-associativeness involved. Furthermore, λ_1, the smallest eigenvalue of D_{ijkl}, is always increasing with H,

and must be greater than λ_1^s, which is the smallest eigenvalue of the symmetric part of D_{ijkl}. When (4-4) is satisfied, only λ_1^s is equal to zero, and λ_1 still greater than zero. But, when (4-14) is satisfied, λ_1 is equal to zero. So, it follows immediately that:

$$H_{gb} \geq H_1 = 0. \tag{4-27}$$

Let H_{se} denote the critical hardening modulus for the loss of strong ellipticity, which corresponds to $g_i Q_{ij} g_j = 0$. The loss of ellipticity is equivalent to det(Q_{ij})=0, and corresponds to the discontinuous bifurcation. Obviously, the arguments relating H_{se} and H_{db} to Q_{ij} are similar to those relating H_{gb} and H_1 to D_{ij}. Therefore, it is concluded that $H_{se} \geq H_{db}$. On the other hand, mathematically, if eqn (4-3) is satisfied, strong ellipticity holds true but the converse does not. It is possible that loss of general bifurcation would occur before the occurrence of loss of strong ellipticity, i.e.:

$$H_{gb} \geq H_{se} \geq H_{db}. \tag{4-28}$$

In the special case of associated flow rule, both D_{ijkl} and Q_{ij} are symmetric. General bifurcation coincides with limit point, and loss of strong ellipticity with loss of ellipticity. Therefore, it is concluded that:

$$H_{db} = H_{se} \leq H_{gb} = H_1 = 0. \tag{4-29}$$

The conclusion may be reached that the discontinuous bifurcation can never occur in the hardening regime. All these analyses are illustrated in figure 4.1.

4.6 General theories for the bifurcation into a shear band

4.6.1 Elasto-plastic relationships

The constitutive matrix of the incremental flow theory of plasticity is expressed as:

$$[C_{ep}]=[C_e]-\frac{[C_e]\left\{\frac{\partial G}{\partial \sigma}\right\}\left\{\frac{\partial F}{\partial \sigma}\right\}^T[C_e]}{\left\{\frac{\partial F}{\partial \sigma}\right\}[C_e]\left\{\frac{\partial G}{\partial \sigma}\right\}^T+H}, \tag{4-30}$$

where $[C_e]$ is elastic matrix, F and G are yield function and plastic potential function, respectively. H represents plastic hardening modulus. In the analyses hereafter, **P** and **Q** are used to indicate $\left\{\frac{\partial G}{\partial \sigma}\right\}$ and $\left\{\frac{\partial F}{\partial \sigma}\right\}$, respectively. **C** represents $[C_e]$. Equation (4-30) is rewritten to fit the bifurcation criterion. It is classically expressed as:

$$\mathbf{D}=\mathbf{C}-\frac{(\mathbf{P}:\mathbf{C})\otimes(\mathbf{Q}:\mathbf{C})}{H+\mathbf{P}:\mathbf{C}:\mathbf{Q}}, \tag{4-31}$$

where : and $\otimes$ indicate inner and outer products of tensors respectively. H, the plastic hardening modulus, is :

$$H=-\frac{\partial F}{\partial \varepsilon^p}:\mathbf{P}. \tag{4-32}$$

When H is positive, strain hardening occurs while the material exhibits softening if H is negative. If H is zero, the case of perfect plasticity is recovered.

4.6.2 General localization criteria

Rice (1976) specified the plastic hardening modulus at which localization into a shear band takes place in the direction **n** which is orthogonal to the band. It is given as:

$$H(\mathbf{n})=2G\left[2\mathbf{n}\cdot\mathbf{P}\cdot\mathbf{Q}\cdot\mathbf{n}-(\mathbf{n}\cdot\mathbf{P}\cdot\mathbf{n})(\mathbf{n}\cdot\mathbf{Q}\cdot\mathbf{n})\right.$$

$$-\mathbf{P}:\mathbf{Q}-\frac{1-\upsilon}{\upsilon}(\mathbf{n}\cdot\mathbf{P}\cdot\mathbf{Q}-\mathrm{tr}\,\mathbf{P})(\mathbf{n}\cdot\mathbf{Q}\cdot\mathbf{n}-\mathrm{tr}\,\mathbf{Q})\Big], \qquad (4\text{-}33)$$

where G is the elastic shear modulus, ν is Poisson's ratio and tr indicates the trace of a tensor: **n** is the unit vector normal to the band; $\cdot$ denotes the cross product between matrices. Maxwell's compatibility conditions (Thomas, 1961) require that the strain rate discontinuity must be of the form:

$$\left[\left[\dot{\varepsilon}\right]\right]=\frac{1}{2}(\mathbf{g}\otimes\mathbf{n}+\mathbf{n}\otimes\mathbf{g}), \qquad (4\text{-}34)$$

in which **g** is termed as polarization vector, and will give the strain rate discontinuity. At shear band inception, the constitutive behavior of material inside the shear band is the same as that of material outside the shear band. This implies that there is an infinite number of nontrivial solution for **g**. However, from the viewpoint of eigenvalue analyses, the strain rate discontinuity **g** is a right eigenvector of the acoustic tensor $\mathbf{n}\cdot\mathbf{D}\cdot\mathbf{n}$, and corresponds to a null eigenvalue, at a given **n** (Bigoni and Hueckel, 1991). It is written as:

$$\mathbf{g}=2\mathbf{n}\cdot\mathbf{n}\cdot\mathbf{P}+\frac{1}{1-\upsilon}(\upsilon\mathrm{tr}\,\mathbf{P}-\mathbf{n}\cdot\mathbf{P}\cdot\mathbf{n})\mathbf{n}. \qquad (4\text{-}35)$$

Depending on the directions of the vectors **n** and **g**, there are three localization modes which are noteworthy to indicate:

A. If **g** is parallel to **n**, the band is referred to as a split failure mode which undergoes extension or compression normal to the planes of discontinuity.

B. If **g** is orthogonal to **n**, the material in the band deforms in a simple shear, a pure shear band develops, which is characteristic of materials exhibiting isochoric plasticity.

C. If **g** is neither parallel nor orthogonal to **n**, general shear banding occurs.

The three cases are shown in figure 4.2. Based on a number of experimental results, some investigators (Harris, et al., 1995) have confirmed that materials inside the band dilate around the inception of shear band localization, and remain at constant volume at the range of post-localization, which are close to the pure shear band mode.

Once **n** and **g** are available, the principal components of the principal strain rate jump can be calculated:

$$\begin{cases} \left[\left[\dot{\varepsilon}_1\right]\right] = \dfrac{\left(|\mathbf{g}| + \mathbf{g}\cdot\mathbf{n}\right)}{2}, \\ \left[\left[\dot{\varepsilon}_2\right]\right] = 0, \\ \left[\left[\dot{\varepsilon}_3\right]\right] = \dfrac{\left(-|\mathbf{g}| + \mathbf{g}\cdot\mathbf{n}\right)}{2}, \end{cases} \tag{4-36}$$

subjected to $\dot{\varepsilon}_1 \geq \dot{\varepsilon}_2 \geq \dot{\varepsilon}_3$. The magnitude of **g** is equal to $|\mathbf{g}| = \sqrt{g_1^{\,2} + g_2^{\,2} + g_3^{\,2}}$. Theoretically, in order to obtain the critical hardening modulus H_{cr}, we have to perform a constrained maximization of (4-33) over all possible directions **n**:

$$H_{cr} = \max H(\mathbf{n}) \text{ , subject to } |\mathbf{n}|=1. \tag{4-37}$$

In (4-37) , H_{cr} is coupled with the vector **n**. A numerical algorithm should be developed to reach the value of the critical hardening modulus (Ortiz et al., 1987). Bigoni and Hueckel (1991) derived an explicit expression for the critical hardening modulus. Using

Largrangian multiplier method, the constrained maximization problem(4-34) could be changed into an unconstrained maximization problem:

$$L(\mathbf{n},\beta) = 2G\Big[2\mathbf{n}\cdot\mathbf{P}\cdot\mathbf{Q}\cdot\mathbf{n} - (\mathbf{n}\cdot\mathbf{P}\cdot\mathbf{n})(\mathbf{n}\cdot\mathbf{Q}\cdot\mathbf{n})$$

$$-\mathbf{P}:\mathbf{Q} - \frac{\upsilon}{1-\upsilon}(\mathbf{n}\cdot\mathbf{P}\cdot\mathbf{n} - \mathrm{tr}\mathbf{P})(\mathbf{n}\cdot\mathbf{Q}\cdot\mathbf{n} - \mathrm{tr}\mathbf{Q}) - \beta(\mathbf{n}\cdot\mathbf{n} - 1)\Big], \qquad (4\text{-}38)$$

where β is the Lagrangian multiplier. By taking derivatives of $L(\mathbf{n}, \beta)$ with respect to $\mathbf{n}$ and β, we could characterize the extrema of equation (4-38):

$$\frac{\partial L}{\partial \mathbf{n}} = 0, \text{ and } \frac{\partial L}{\partial \beta} = 0, \qquad (4\text{-}39)$$

which leads to:

$$2\mathbf{n}\cdot\mathbf{P}\cdot\mathbf{Q} - \frac{1}{1-\upsilon}\Big[(\mathbf{n}\cdot\mathbf{Q}\cdot\mathbf{n})\mathbf{n}\cdot\mathbf{P} + (\mathbf{n}\cdot\mathbf{P}\cdot\mathbf{n})\mathbf{n}\cdot\mathbf{Q}\Big]$$

$$+2\mathbf{n}\cdot\mathbf{P}\cdot\mathbf{Q} - \frac{\upsilon}{1-\upsilon}\Big[(\mathrm{tr}\mathbf{Q})\mathbf{n}\cdot\mathbf{P} + (\mathrm{tr}\mathbf{P})\mathbf{n}\cdot\mathbf{Q}\Big] = \frac{\beta}{2G}\mathbf{n}. \qquad (4\text{-}40)$$

Choose the axes of the coordinate system consistent with the directions of principal stresses and strains, then we have the yield surface gradient $\mathbf{Q}$ and plastic potential surface gradient $\mathbf{P}$ expressed as:

$$\mathbf{Q} = \begin{bmatrix} Q_1 & 0 & 0 \\ 0 & Q_2 & 0 \\ 0 & 0 & Q_3 \end{bmatrix}, \quad \mathbf{P} = \begin{bmatrix} P_1 & 0 & 0 \\ 0 & P_2 & 0 \\ 0 & 0 & P_3 \end{bmatrix}. \qquad (4\text{-}41)$$

Then, equations (4-37) may be written explicitly in the following form:

$$2n_iP_iQ_i - \frac{1}{1-\upsilon}\Big[(\mathbf{n}\cdot\mathbf{Q}\cdot\mathbf{n})P_i + (\mathbf{n}\cdot\mathbf{P}\cdot\mathbf{n})Q_i\Big]n_i$$

$$+\frac{\upsilon}{1-\upsilon}\Big[(\mathrm{tr}\,\mathbf{Q})P_i + (\mathrm{tr}\,\mathbf{P})Q_i\Big]n_i = \frac{\beta}{2G}n_i. \qquad (4\text{-}42)$$

(i=1, 2, 3 not summed)

4.6.3 Plane strain condition

In the case of plane strain condition, the band lies in one plane formed by two of the principal axes of stresses, namely, the band that is always normal to the other axis. One component of direction vector **n**, say n_3, is equal to zero. Therefore, the system is reduced to three equations for n_1, n_2, and β. They are:

$$2n_1P_1Q_1-\frac{1}{1-\upsilon}\left[\left(n_1^2Q_1+n_2^2Q_2\right)P_1+\left(n_1^2P_1+n_2^2P_2\right)Q_1\right]n_1$$

$$+\frac{\upsilon}{1-\upsilon}\left[(\mathrm{tr}\,\mathbf{Q})P_1+(\mathrm{tr}\,\mathbf{P})Q_1\right]n_1=\frac{\beta}{2G}n_1, \tag{4-43}$$

$$2n_2P_2Q_2-\frac{1}{1-\upsilon}\left[\left(n_1^2Q_1+n_2^2Q_2\right)P_2+\left(n_1^2P_1+n_2^2P_2\right)Q_2\right]n_2$$

$$+\frac{\upsilon}{1-\upsilon}\left[(\mathrm{tr}\,\mathbf{Q})P_2+(\mathrm{tr}\,\mathbf{P})Q_2\right]n_2=\frac{\beta}{2G}n_2, \tag{4-44}$$

$$n_2^2=1-n_1^2, \tag{4-45}$$

$n_1=\cos\theta$, $n_2=\sin\theta$. Here, θ is the angle between the shear band inclination and the major principal stress. Combining (4-40), (4-41) and (4-42), the result is:

$$n_1^2=(1-\upsilon)\frac{P_1Q_1-P_2Q_2}{(P_1-P_2)(Q_1-Q_2)}-\frac{Q_2}{2(Q_1-Q_2)}-\frac{P_2}{2(P_1-P_2)}$$

$$+\frac{\upsilon(Q_1+Q_2+Q_3)}{2(Q_1-Q_2)}+\frac{\upsilon(P_1+P_2+P_3)}{2(P_1-P_2)}\quad (Q_1\neq Q_2,\ P_1\neq P_2), \tag{4-46}$$

$$n_2^2=1-n_1^2,\quad n_3=0. \tag{4-47}$$

If $Q_1=Q_2$, $P_1=P_2$, equation (4-43) is not applicable. The localization mode for this special case is a splitting discontinuity, which will not be discussed further. The corresponding critical hardening modulus is found as:

$$\begin{aligned} H_{cr}/2G = n_1^2\Big\{&2(P_1Q_1-P_2Q_2)-\frac{1}{1-\upsilon}\big[(P_1-P_2)Q_2+(Q_1-Q_2)P_2\big]\\ &+\frac{\upsilon}{1-\upsilon}\big[(\mathrm{tr}\,\mathbf{Q})(P_1-P_2)+(\mathrm{tr}\,\mathbf{P})(Q_1-Q_2)\big]\Big\}\\ &-n_1^4\frac{1}{1-\upsilon}(P_1-P_2)(Q_1-Q_2)-P_1Q_1-P_3Q_3\\ &-\frac{\upsilon}{1-\upsilon}(Q_1+Q_3)(P_1+P_3). \end{aligned} \tag{4-48}$$

The polarization vector **g** is given by the expressions:

$$\begin{cases} g_2=\left\{2P_1-\dfrac{1}{1-\upsilon}\left(n_1^2(P_1-P_2)+P_2\right)+\dfrac{\upsilon}{1-\upsilon}\mathrm{tr}\,\mathbf{P}\right\}n_1,\\ g_2=\left\{2P_2-\dfrac{1}{1-\upsilon}\left(n_1^2(P_1-P_2)+P_2\right)+\dfrac{\upsilon}{1-\upsilon}\mathrm{tr}\,\mathbf{P}\right\}n_2,\\ g_3=0. \end{cases} \tag{4-49}$$

For associative flow rule, **P**=**Q**, equations (4-46) and (4-47) reduces to:

$$\begin{cases} n_1^2=\dfrac{Q_1+\upsilon Q_3}{Q_1-Q_2},\\ n_2^2=1-n_1^2, \end{cases} \tag{4-50}$$

The corresponding critical hardening modulus is:

$$H_{cr}=-2G(1+\upsilon)Q_3^2. \tag{4-51}$$

Polarization vector **g** is given as:

$$\begin{cases} g_1 = (Q_1 - Q_2)n_1, \\ g_2 = (Q_2 - Q_1)n_2, \\ g_3 = 0. \end{cases} \tag{4-52}$$

Equation (4-51) shows that the critical hardening modulus for strain localization in the case of associative flow rule is never positive; the bifurcation point always lies either on the softening branch or at the peak of the stress-strain curve, no matter what yield model is used.

4.6.4 Plane stress conditions

Under plane stress conditions, above all, the solid is considered as two-dimensional. **P** and **Q** have only two components. Moreover, the constitutive matrix takes on a particular form. Therefore, equation (4-37) reduces to the following form:

$$H_{cr} = \max\left\{2G\left[2\mathbf{n}\cdot\mathbf{P}\cdot\mathbf{Q}\cdot\mathbf{n} - (\mathbf{n}\cdot\mathbf{P}\cdot\mathbf{n})(\mathbf{n}\cdot\mathbf{Q}\cdot\mathbf{n}) - \mathbf{P}:\mathbf{Q} - \upsilon(\mathbf{n}\cdot\mathbf{Q}\cdot\mathbf{n} - \mathrm{tr}\,\mathbf{Q})(\mathbf{n}\cdot\mathbf{P}\cdot\mathbf{n} - \mathrm{tr}\,\mathbf{P})\right]\right\}, \tag{4-53}$$

subjected to $|\mathbf{n}|=1$. The corresponding polarization vector **g** is expressed by:

$$\mathbf{g} = 2\mathbf{n}\cdot\mathbf{P} - (1+\upsilon)(\mathbf{n}\cdot\mathbf{P}\cdot\mathbf{n})\mathbf{n} + \upsilon(\mathrm{tr}\,\mathbf{P})\mathbf{n}. \tag{4-54}$$

Take $\mathbf{n}=[n_1, n_2, 0]^T$, $\mathbf{P}=[P_1, P_2, 0]^T$ and $\mathbf{Q}=[Q_1, Q_2, 0]^T$ into (4-53), and the solution becomes:

$$H_{cr} = 2G(1+\upsilon)\max\left\{\frac{(P_1Q_2 - P_2Q_1)^2}{4(P_1 - P_2)(Q_1 - Q_2)},\ -P_1Q_1,\ -P_2Q_2\right\}. \tag{4-55}$$

$$(P_1 \neq P_2,\ Q_1 \neq Q_2)$$

If the first term in (4-55) gives the maximum, then the components of **n** and **g** are:

$$\begin{cases} n_1^{\,2} = \dfrac{P_1}{2(P_1 - P_2)} + \dfrac{Q_1}{2(Q_1 - Q_2)}, \\ n_2^{\,2} = 1 - n_1^{\,2}. \end{cases} \tag{4-56}$$

$$\begin{cases} g_1 = 2P_1 - (1+\upsilon)\left[n_1^{\,2}(P_1 - P_2) + P_2\right] + \upsilon(P_1 + P_2)n_1, \\ g_2 = 2P_2 - (1+\upsilon)\left[n_1^{\,2}(P_1 - P_2) + P_2\right] + \upsilon(P1 + P2)n_2. \end{cases} \tag{4-57}$$

If the second or third term gives the maximum H_{cr}, **n** and **g** will be co-axial. Therefore, the corresponding localization mode will be a split mode discontinuity, which is excluded from discussion here. If associative plasticity is applied, (4-52) reduces to:

$$H_{cr} = \max\left(0,\ -2G(1+\upsilon)Q_1^{\,2},\ -2G(1+\upsilon)Q_2^{\,2}\right), \tag{4-58}$$

The corresponding band inclination is expressed as:

$$n_1^{\,2} = \frac{Q_1}{Q_1 - Q_2},\quad n_2^{\,2} = 1 - n_1^{\,2}. \tag{4-59}$$

From (4-58), we know that the maximum hardening modulus is zero. This implies that the strain localization into a shear band always occurs at the peak of the stress-strain curve.

4.7 Shear band localization under Drucker-Prager criterion

As an example, the Drucker-Prager yield criterion is applied to localization analysis to show how to obtain the critical hardening modulus and shear band orientation. Explicit analytical expressions for the critical bifurcation direction and corresponding hardening modulus have been established for quite a broad class of elastic-plastic models. From all the results for cases of plane stress, it may be concluded that the critical inclinations are

always independent of the elastic properties. However, they are dependent on Poisson's ratio in the case of plane strain. The localization into a shear band may occur prior to, at, or beyond the peak of the stress-strain curves which is completely subjected to the elastic-plastic models and loading configurations for the case.

Drucker-Prager's yield criterion and plastic potential function are defined by Runesson (1991) as:

$$F = \left(\frac{3}{2}s_{ij}s_{ij}\right)^{1/2} + \frac{m}{3}\sigma_{kk} - \kappa^2 = 0, \tag{4-60}$$

$$G = \left(\frac{3}{2}s_{ij}s_{ij}\right)^{1/2} + \frac{n}{3}\sigma_{kk} = 0, \tag{4-61}$$

where $m \geq 0$ and $n \geq 0$ are expressed in terms of the internal friction angle and dilatancy angle, respectively, while κ is the yield stress, $s_{ij} = \sigma_{ij} - \frac{1}{3}\delta_{ij}\sigma_{kk}$. If the uniaxial compressive strength values represented by Drucker-Prager's criterion are taken to be equal to the corresponding strength values according to the Mohr-Coulomb criterion, we obtain:

$$m = \frac{6\sin\phi}{3-\sin\phi}, \qquad n = \frac{6\sin\phi}{3+\sin\phi}. \tag{4-62}$$

From equations (4-60) and (4-61), it is not hard to discover that only the volumetric behavior is non-associated, while the deviatoric portion of the flow rule is associated. The gradients **P** and **Q** are given as:

$$P_{ij} = \frac{3}{2}\frac{s_{ij}}{q} + \frac{n}{3}\delta_{ij}, \tag{4-63}$$

$$Q_{ij} = \frac{3}{2}\frac{s_{ij}}{q} + \frac{m}{3}\delta_{ij}. \tag{4-64}$$

The reference system is still taken to be co-axial with principal stresses.

4.7.1 Case of plane stress

$$s_1 = \frac{1}{3}(2\sigma_1 - \sigma_2), \quad s_2 = -\frac{1}{3}(\sigma_1 - 2\sigma_2). \tag{4-65}$$

$$P_1 = \frac{3}{2}\frac{s_1}{q} + \frac{n}{3}, \qquad P_2 = \frac{3}{2}\frac{s_2}{q} + \frac{n}{3}. \tag{4-66}$$

$$Q_1 = \frac{3}{2}\frac{s_1}{q} + \frac{m}{3}, \qquad Q_2 = \frac{3}{2}\frac{s_2}{q} + \frac{m}{3}. \tag{4-67}$$

Substitute (4-66), (4-67) into (4-55) and (4-56) , and the result is :

$$\cos^2\theta_{cr} = \frac{3s_1 + \frac{1}{3}(m+n)q}{3(s_1 - s_2)}, \tag{4-68}$$

$$H_{cr} = \frac{2G(1+\upsilon)}{36}(m-n)^2. \tag{4-69}$$

From equation (4-69), for Drucker-Prager materials with non-associated plasticity under plane stress conditions, the strain localization always occurs at the hardening branch.

4.7.2 Case of plane strain

Under plane strain condition, take $s_3 = \frac{1}{3}(2\sigma_3 - (\sigma_1 + \sigma_2))$, and **P** and **Q** to (4-46) and (4-48), the inclination of localization and critical hardening modulus would be:

$$\cos^2\theta_{cr} = \frac{9(2-\upsilon)s_1 + 9(1-\upsilon)s_2 - (1+\upsilon)q(m+n)}{9(s_1 - s_2)}, \tag{4-70}$$

$$H_{cr} = \frac{(1+\upsilon)G}{18}\left[2(m-n)^2 - (1-\upsilon)\left(\frac{9s_3}{q} + m + n\right)^2\right]. \qquad (4\text{-}71)$$

4.8 The comparison of various bifurcation modes

In the first part of this chapter, much attention has been devoted to differentiating various bifurcation modes and their criteria. Classical discontinuous bifurcation corresponds to the localization into a shear band. The loss of strong ellipticity prior to or at the same time as the classical discontinuous bifurcation will first occur if the determinant of the symmetrical part of acoustic tensor is zero, i.e. det ($\mathbf{Q}_s$)=0. The occurrence of limit point is consistent with det ($\mathbf{D}$)=0. The prerequisite to all types of bifurcation is the occurrence of general bifurcation, the criterion of which is det ($\mathbf{D}_s$)=0.

4.8.1 Eigensystem and bifurcation modes

The relationship between the bifurcation criteria and the eigensystem has been much investigated. The eigenvalue problem with $\mathbf{D}_s$ is expressed as:

$$\mathbf{D}_s : \mathbf{x}_i = \omega_i \mathbf{x}_i, \qquad (4\text{-}72)$$

in which, $\mathbf{x}_i$ denotes the i^{th} normalized eigentensor for $\mathbf{D}_s$, and ω_i is the corresponding eigenvalue. The necessary condition for a general bifurcation is initially satisfied when the fundamental eigentensor associated with the zero eigenvalue. The critical hardening modulus:

$$H_{cr}^{gb} = \frac{1}{2}\left(\sqrt{\mathbf{Q}:\mathbf{C}_e:\mathbf{Q}}\sqrt{\mathbf{P}:\mathbf{C}_e\,\mathbf{P}} - \mathbf{Q}:\mathbf{C}_e:\mathbf{P}\right), \qquad (4\text{-}73)$$

Similarly, we can obtain values for the critical hardening moduli for various bifurcation criteria.

4.8.2 Critical hardening moduli under different bifurcation modes

In this section, the uniaxial tension test is taken as an example to illustrate the relationship between the various critical hardening moduli. The specimen material yields to non-associated Drucker-Prager yield criterion. The critical hardening modulus associated with a classical discontinuous bifurcation is (Rudinicki and Rice, 1975):

$$\frac{H_{cr}^{db}}{G}=\frac{1+\mu}{9(1-\mu)}(m-n)^2-\frac{1+\mu}{2}\left(-\frac{1}{\sqrt{3}}+\frac{m+n}{3}\right)^2, \qquad (4\text{-}74)$$

where ν is the poisson ratio, m and n are the internal frictional and dilation parameters, respectively. While the critical hardening modulus corresponding to general bifurcation reads:

$$H_{cr}^{gb}=\frac{1}{2}\sqrt{(G+m^2K)(G+n^2K)}-\frac{1}{2}(G+mnK), \qquad (4\text{-}75)$$

where K denotes elastic volumetric modulus and G is shear modulus. In the same way, the critical moduli for the limit point and loss of strong ellipticity are easily obtained. The critical hardening moduli for uniaxial tension by various criteria are plotted in terms of the internal frictional parameter m for different values of dilation parameter n. In figures 4.3, 4.4 and 4.5, critical values of the dimensionless hardening modulus, H/E, are shown as the ordinate. The abscissa represents the internal frictional parameter. Along one curve, the dilation parameter n keeps constant. Poisson ratio ν is taken to be 0.3. In all the plots, the important points stated previously are confirmed, namely, that the general bifurcation is always reached first, and that the strong ellipticity condition is

always attained prior to the classical discontinuous bifurcation condition if m is not equal to n. If m is equal to n, which implies associated flow rule, the general bifurcation condition is equivalent to the limit point condition. Likewise, the classical discontinuous bifurcation and the loss of strong discontinuity are identified, as depicted in figure 4.6. In the special case that materials yield to elastic-perfectly plastic model with associated flow rule, all the four bifurcation conditions would be identified to the same point. On the other hand, it has been seen that the first general bifurcation is reached at the hardening stage of the stress-strain curve if non associated flow rule is used.

4.9 Concluding remarks

The characteristics of different constitutive responses are described which includes material stability, limit point, general bifurcation and discontinuous bifurcation, etc. It is pointed out that a smoothly varying deformation field into a number of highly localized shear bands corresponds to the loss of ellipticity of the equations governing incremental equilibrium. In other words, it coincides with the discontinuous bifurcation. In this chapter, the criterion for general localization is derived. With different yielding criteria and different stress states (plane strain, plane stress), the discontinuous bifurcation criterion is degraded to various specific criteria to calculate critical state moduli, inclinations of shear bands.

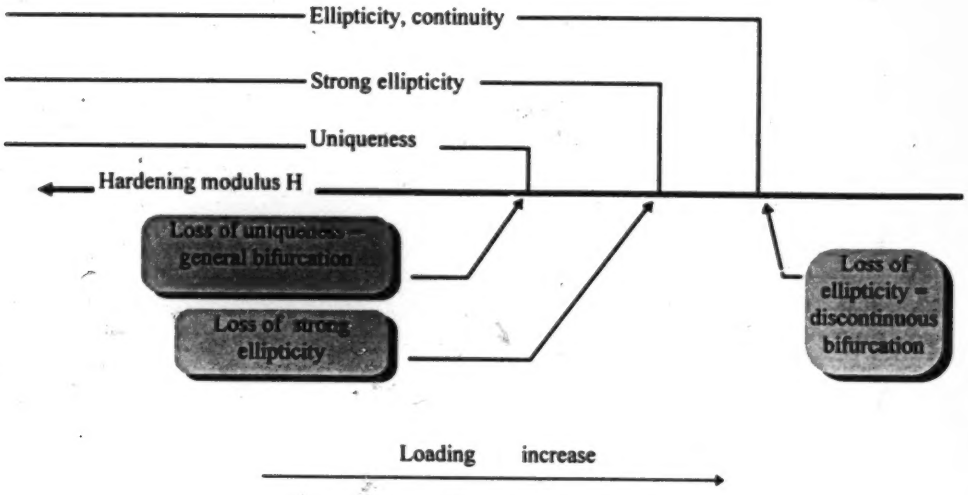

Figure 4.1 (a)

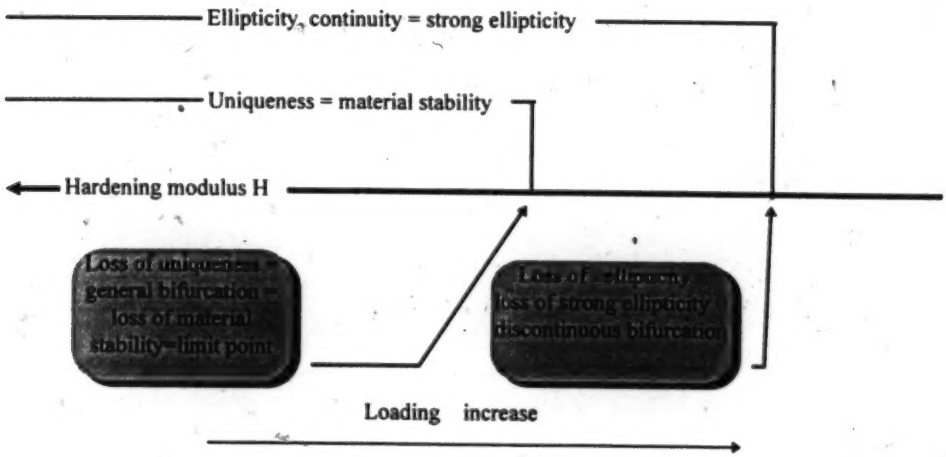
Ellipticity, continuity = strong ellipticity
Uniqueness = material stability
Hardening modulus H
Loss of uniqueness = general bifurcation = loss of material stability = limit point
Loss of ellipticity = loss of strong ellipticity = discontinuous bifurcation
Loading increase

Figure 4.1 (b)

Figure 4.1 Evolution of stress-strain curves for (a) non-associative flow rule, (b) associative flow rule

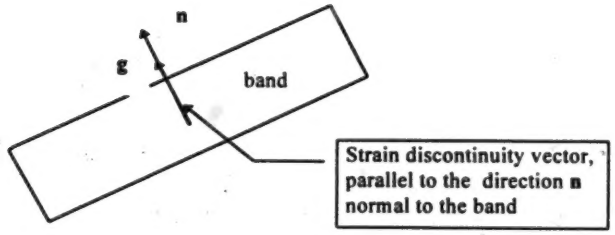

Figure 4.2 (a)

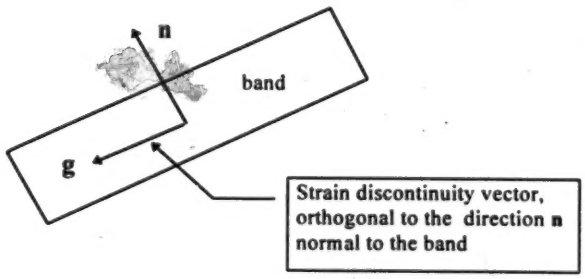

Figure 4.2 (b)

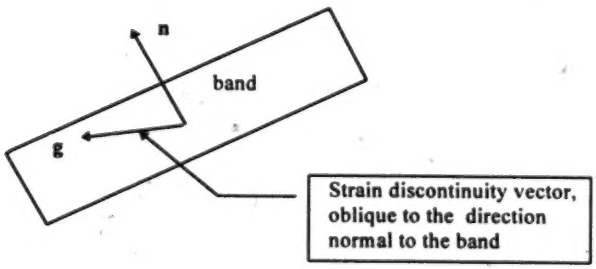

Figure 4.2 (c)

Figure 4.2 localization modes, (a) splitting mode, (b) pure shear mode (c) general shear mode

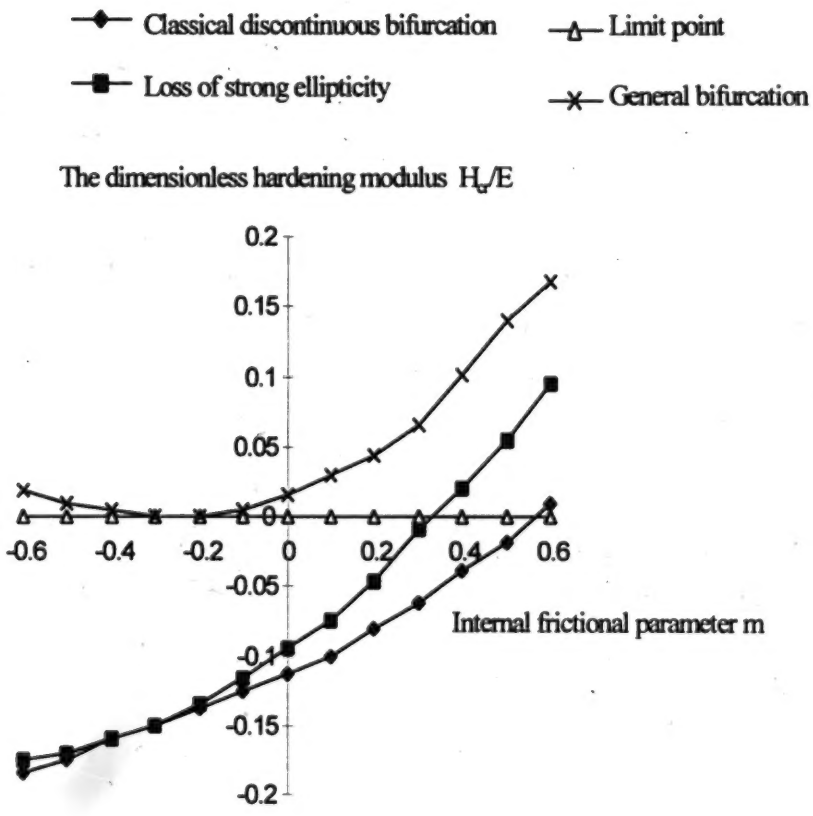

Figure 4.3 The dimensionless critical hardening modulus when dilation parameter n=-0.3

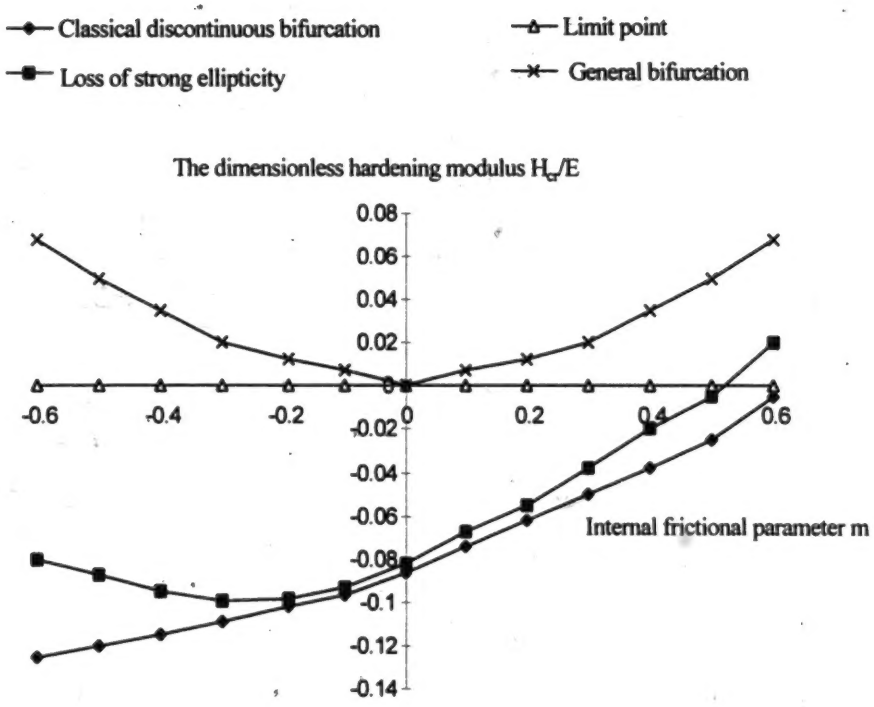

Figure 4.4 The dimensionless critical hardening modulus when dilation parameter n=0.0

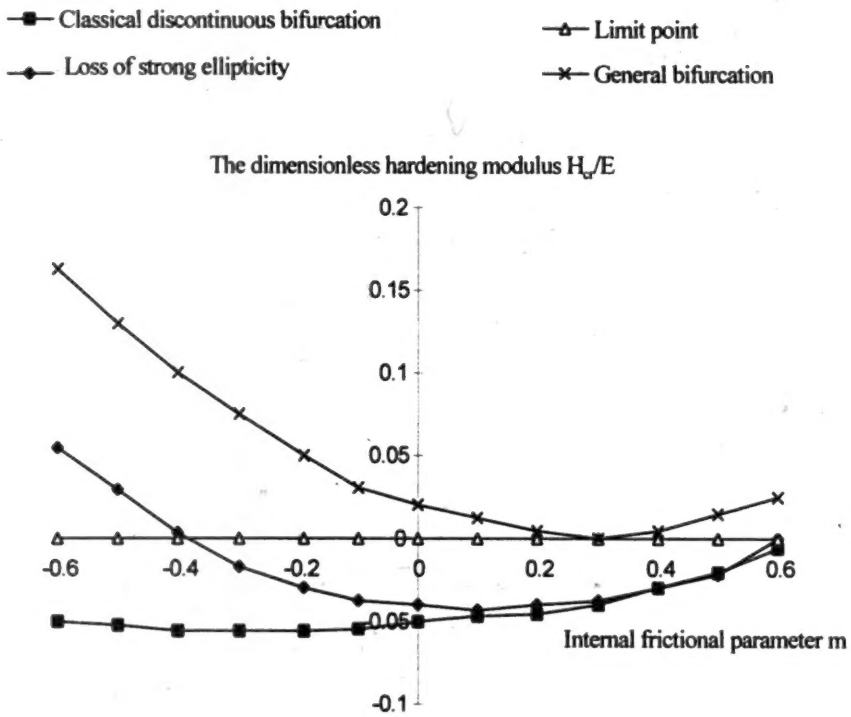

Figure 4.5 The dimensionless critical hardening modulus when dilation parameter n=0.3

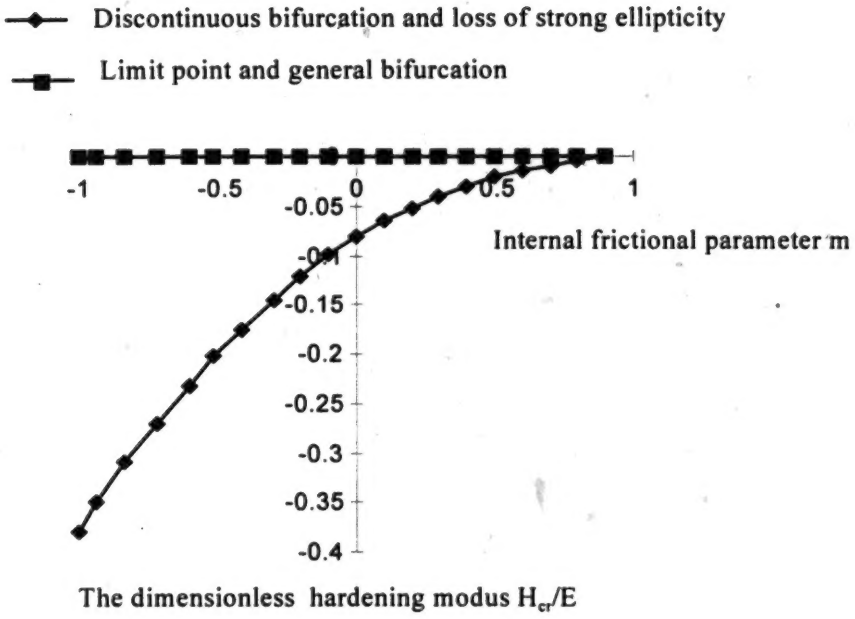

Figure 4.6 The dimensionless hardening modulus when associated flow rule is applied (m=n)

Chapter 5

Implementation of kinematics modeling of shear band propagation

5.1 Introduction

Before a numerical simulation of localization can be carried out, it is necessary to have a thorough understanding of the physical phenomenon of localization based on material characterization as well as kinematics of localized deformation patterns. In geomaterials, localization occurs as a result of changes in material micro-structures: micro-cracking, discrete cracks, void formation and rupture/shear banding, all of which lead to the macroscopic inhomogeneities of the materials. Theoretically, changes in micro-structures of the damaged material should be taken into account in the mathematical description to simulate the inhomogeneities. A solution to this problem is the introduction of additional physical parameter termed as an internal length scale, such as grain size, in the enhanced continuum mechanics which will reflect the changes in the micro-structure that occur during the step by step loading process. The size, location, and properties of the subsequent shear band can be automatically determined. Non-local (Bazant, 1992), rate-dependency (Needleman, 1988), micro-polar continuum theories (de Borst et al., 1993), and continuous damage mechanics (Frantziskonis and Desai, 1987) illustrate some good examples due to the fact that all these treatments are associated with

well-posed mathematical problems. To simulate the development of localization, it is necessary to keep track of changes in the micro-structures of the material.

In the analysis of strain localization, standard continuum mechanics is still used. Some attention has been given to the kinematic aspect of shear banding which basically involves the discretization of a discontinuous field. Such models have been briefly described in chapter 2. But, so far, most localization theories have only described the inception of discontinuous bifurcation, rather than the kinematic transformation of a continuum into a discontinuum because of progressive failure. They cannot directly handle the material inhomogeneities due to localization development. No finite zone or thickness for a shear band can be considered. The development of inhomogeneities of geological materials, the changes in location, size and material properties of the shear band, to be exact, are very hard to reflect in these research endeavors. As a result, the displacement, stress and stress-displacement suffer from highly pathological mesh dependence. No exact solution can be worked out. The essence of the whole problem of spurious mesh-sensitivity comes from the fact that the force-displacement relations which are measured in laboratory and field tests are simply mapped onto the stress-strain curves by dividing the force and elongation by the original load-carrying area and the original length of the specimen respectively. This is done without accounting for any changes in the micro-structure when the material is so heavily damaged. Mathematically, it is associated with loss of ellipticity in equations governing incremental equilibrium.

With standard continuum mechanics, although gradual changes in microstructures of the material may not be considered, it is possible to detect the initiation of localization, with the help of some criteria like the Mohr-Columb theory, the Roscoe theory or

bifurcation theories. Then, the inhomogeneity of the material due to localization in the structure is kept specified in the loading process by using independent shear band elements. The material and geometric behaviors of localization are obtained physically and experimentally. Once the orientation, location, size and material properties of the inhomogeneity are set up, the energy consumed in the localization is determined. Pietruszczak and Mroz (1981) proposed a smeared shear band approach by defining the average plastic strain for an element, which contains part of the shear band, to avoid introducing an independent shear band element. In a way, the thickness effect is accounted for in the analysis. However, the location effect of the shear band is not included, and kinematics can not be simulated at all.

In this study, the inhomogeneity of a shear band is described using an independent shear band element. In the specific finite element method developed, a finite domain and location of the shear band are specified. They reflect macroscopically the changes in microstructures of the material. The effect of thickness is automatically accounted for numerically in the finite element calculations. The thickness is an analogy for internal length scale like grain size built in the constitutive model in enhanced continuum mechanics, namely, the mechanics for a semi-discontinuum.

With the thickness of a shear band introduced into the analysis, the spurious mesh dependence is eliminated in the standard continuum models. Different mesh discretization will lead to almost the same result. But, if the thickness of the shear band is not properly identified, the softening response of the structure, and even the calculated limit load, will be quite different (Pietruszczak and Mroz, 1981). In the enhanced continuum theories, similarly, different internal length scale will result in different

softening responses, even though the mesh discretizations are unchanged (de Borst, et al., 1993). Accordingly, the determination of the thickness is of great significance since it reflects the macroscopic inhomogeneity that is due to progressive change in the microstructure of materials.

As to the modeling of the shear band propagation, there are still some major limitations. Kinematically, due to the large gradient of deformation in a shear band, the finite elements are highly distorted and lead to degradation of the solution scheme. After the onset of shear banding, especially when approaching the failure load, shear band elements will lock up due to the near incompressibility of the materials around the kinks and will prevent kinematic propagation of the band. This is referred to as the kink problem. The thickness of a band is small compared with typical element sizes. So, in numerical modeling, solid elements on either side of the shear band are easily penetrated into each other. The penetrations are called overlapping problems. With a small shear band thickness and large shear strains, elastic and plastic behavior of the shear band would inevitably exhibit its specialty which leads to some specific mathematical descriptions.

Special interface elements allow some researchers to avoid mesh dependency and mesh degradation (Charlier, 1992a, Charlier and Wang, 1992b). The shear band is modeled as an interface without any thickness between two parts of a body. After the onset of localization, an ill-posed problem can be avoided to some extent using remeshing technique in order to obtain a numerical solution. In this chapter, a methodology called the contact band element approach is proposed to enhance modeling large slipping of a shear band at the post localization stage, through which a finite zone of

the shear band is described. Numerical ill conditioning, such as element distortion and kinematic incompatibility, and mesh locking due to kinks, are eliminated or alleviated. Triangular and quadrilateral elements are used to accommodate the deformed configuration of the shear band. The element interpolation and integration schemes are correspondingly revised to track the development of local shear stresses and strains. Numerical examples have demonstrated the capability and effectiveness of the methods to model a discontinuity with large shear deformation leading to progressive failure. The focus here will be on the simulation of post localization behavior. The contact approach generally deals with the contact between two objects. By incorporating a finite thickness into the analysis, the thickness of a band being determined physically prior to the numerical analysis, a contact band element approach with a new computational scheme is proposed. Large deformation of a band element is handled by updating the coordinates of each nodal point.

5.2 A contact band element approach to model localized deformation

With the onset and the development of a shear band, large shear deformation and large shear strain will unavoidably arise along the band. As shown in figure 5.1, a shear band channel which contains two shear bands with different orientations virtually occurs abruptly at a certain axial load state. Generally speaking, a shear band channel is composed of one or more than one shear band with different directions. As depicted in figure 5.1 (a), in a shear band channel, the shear bands are connected to each other. The nodal points on boundaries of different shear bands along one channel can be re-

combined to form new shear band elements. In figure 5.1 (b)), if the ordinary finite elements are used, the elements will be highly distorted. This will lead to poor performance of finite element techniques if the original mesh in the shear band is unchanged, as shown in figure 5.1 (c). On the other hand, the thickness of the localized band is very small which can be vanishing; moreover, normal stiffness for the shear band can be quite soft relatively to the stiffness of the material outside the band, which can result in kinematic incompatibility (an overlapping at the shear zone) as shown in figure 5.1 (d). With the development of large deformation along a slip surface which is composed of shear bands at different orientations, and with the band thicknesses approaching a constant value, the materials close to a kink would become incompressible or near incompressible. Some shear band elements, especially those around kinks (see figure 5.1 (b)) will be in a locking position, which is similar to the mesh locking associated with internal constraints in the elasto-plastic finite element approach (Nagtegaal et al., 1974). The occurrence of mesh locking will result in an unrealistic resistance to the slipping of shear bands. As such, it is necessary to develop a specific scheme to run finite element analysis in this simulation of shear band propagation.

5.2.1 An ordinary contact approach for shear bands with zero thickness

A contact approach has been adopted by many researchers for large deformation problems (Bathe, 1985; Hughes, 1977). The sequence of motion and displacement field of the moving objects must be tracked during the course of deformation. However, in modeling shear band deformation, the stiffness of shear band materials must also be taken into account. The presence of highly sheared materials requires stresses and strains to be

calculated and updated. Therefore, there are more than the displacements to be considered in the contact band element approach.

Referring to figure 5.2, consider a shear band which undergoes intensive shearing between two parts of a deforming body. Stresses are developed on the upper and lower surfaces of the band. In finite element modeling, it is required to calculate the nodal forces on the surfaces of the band. If there is no material in the band, the thickness of the element KAB is zero. Lengths L_{AB} and L_{KB} are defined by:

$$L_{AB} = (\mathbf{X}_A - \mathbf{X}_B) \cdot \mathbf{t}, \qquad L_{KB} = (\mathbf{X}_K - \mathbf{X}_B) \cdot \mathbf{t}, \tag{5-1}$$

where $\mathbf{X}_A$, $\mathbf{X}_B$ and $\mathbf{X}_K$ are position vectors for points A, B and K respectively. $\mathbf{t}$ is the orientation vector of the shear band. In the general analysis of a contact problem, the contact forces at each nodal points are independent variables. Assume that point K penetrates into the segment AB. The relationship between contact forces at points A, B and K can be written as (Bathe and Chaudhary, 1985):

$$\mathbf{F}_A = -(1-\beta)\mathbf{F}_K, \quad \mathbf{F}_B = -\beta\mathbf{F}_K, \quad \text{and } \beta = L_{AB}/L_{KB}. \tag{5-2}$$

The forces calculated will be applied on both sides of the shear band which results in parting of the bodies. By successive applications of the contact forces, the overlapping displacements between two surfaces can be eliminated. During numerical iterations, sticking, sliding, and separation processes of the band elements can be simulated.

If the thickness of a shear band is not zero, the stiffness of the band should be incorporated in the finite element formulation. The real band material property has to be used when the overlapping problem and separation are treated, rather than applying contact forces. During the propagation of the band, the band elements should be updated

continuously to avoid numerical ill-conditioning. Owing to the band element distortion, an important question in the contact band element approach is how to rediscretize the elements in the band to minimize element distortion. For different cases, two types of band elements are suggested. The selection of any type of element depends on the kinematics of the band element.

5.2.2 Remeshing of shear band elements

First, the technique of rediscretization of shear band elements to eliminate mesh distortion is illustrated, which is an important concept in the contact band element approach. In subsequent loading steps, different elements (3-node, 4-node elements) will be used. To demonstrate the procedures, the formulation of a 3-node triangular element is shown here in detail. The scheme is also applicable to quadrilateral elements.

As shown in figure 5.3, with an increase in the applied load, the configuration of the band elements changes from that shown in figure 5.3 (a) to that in figure 5.3 (b). Obviously, in the conventional finite element approach, the old mesh is highly distorted (e.g. element 321, element 342, etc.). If the original discretization remains unchanged during the course of the analysis, numerical ill conditioning will eventually arise. At this point, the numerical solution will be drastically degraded. This conclusion can be easily deduced from the error analysis. The dispiacement and stress errors were formulated by Xu (1977):

$$e_{ij}^{s} = \left\| \sigma_{ij} - \sigma_{ij}^{h} \right\| \propto \frac{c_1}{\sin(\alpha)}, \qquad (5\text{-}3)$$

$$e_i^d = \left\| u_i - u_i^h \right\| \propto \frac{c_2}{\sin(\alpha)}, \qquad (5\text{-}4)$$

where, u_i, σ_{ij} are exact solutions, u_i^h, σ_{ij}^h are numerical solutions from finite element analysis; α is the minimum angle within the element; c_1 and c_2 are positive constants. It is not hard to see that, the more distorted are the band elements the smaller are the minimum angles, and, therefore, the higher are the displacement and stress errors. If the coordinates of the nodal points along the band boundaries are updated, they will be reorganized to produce new band elements. New shear band elements have much better configurations, as illustrated in figure 5.3 (c). These band elements are kinematically compatible with the soil mass elements. It turns out that they can give a more accurate description of displacements and strains in the band. In the following, the scheme for rediscretization of the shear band elements is described.

Let **M** be the collection of nodal points of one upper surface of a shear band, and **N** be the collection of nodal points of the opposite surface:

$$\begin{aligned} &\mathbf{M}:= \{\eta \in \text{nodal points of upper surface}\}, \\ &\mathbf{N}:= \{\xi \in \text{nodal points of lower surface}\}. \end{aligned} \qquad (5\text{-}5)$$

From collection **M**, select any point η_i, then pick up two points ξ_j, ξ_k from **N** to satisfy the following conditions:

$$\alpha = \cos^{-1}\left[\frac{\left(\mathbf{X}_{\eta_i} - \mathbf{X}_{\xi_j}\right) \bullet \left(\mathbf{X}_{\xi_k} - \mathbf{X}_{\xi_j}\right)}{\left|\mathbf{X}_{\eta_i} - \mathbf{X}_{\xi_j}\right| \bullet \left|\mathbf{X}_{\xi_k} - \mathbf{X}_{\xi_j}\right|}\right] < \frac{\pi}{2}, \qquad (5\text{-}6)$$

$$\beta = \cos^{-1}\left[\frac{\left(\mathbf{X}_{\eta_i} - \mathbf{X}_{\xi_k}\right)\bullet\left(\mathbf{X}_{\xi_k} - \mathbf{X}_{\xi_j}\right)}{\left|\mathbf{X}_{\eta_i} - \mathbf{X}_{\xi_k}\right|\bullet\left|\mathbf{X}_{\xi_k} - \mathbf{X}_{\xi_j}\right|}\right] < \frac{\pi}{2}, \tag{5-7}$$

where, **X** denotes the position vector of any point in the global coordinate system; α and β are shown in figure 5.3(c). $\bullet$ is the sign of dot product, and $|\ |$ indicates the length of a line section. Furthermore,

$$\left|\mathbf{X}_{\eta_i} - \mathbf{X}_{\xi_k}\right|, \left|\mathbf{X}_{\eta_i} - \mathbf{X}_{\xi_j}\right| = \min\left|\mathbf{X}_{\eta} - \mathbf{X}_{\xi}\right|. \tag{5-8}$$

In other words, ξ_k, and ξ_j are the two closest points to point η_i on the opposite boundary which locate at left and right sides, respectively. Then, points ξ_k, ξ_j and η_i will form a shear band element. There is no doubt that this element would give the largest minimum angle. Any upper and lower surface points which satisfy conditions (5-6), (5-7) and (5-8) will form a new band element. The number of nodal points for an element is a variable and is dependent on the locations of the points. Points η_i, ξ_j and ξ_k form a new 3-node triangular band element. If points η_i, η_k, ξ_j, ξ_k satisfy the conditions above, a 4-node quadrilateral band element will be created as shown in figure 5.3 (c). Generally, these two types of elements are joined together to model the kinematics of a shear band. Of course, the 4-node quadrilateral band element can be broken into two triangular band elements. The triangular elements also have good shapes.

5.2.3 Special shear band elements

During the propagation of a shear band, it is possible that a shear band element has more than 4 nodes due to large movement and difference in mesh density in the domain. As shown in figure 5.4, along the surface IJ, three points M, L and K on the opposite boundary lie between two points I and J. All these points should be included in

constructing a new band element. Because of the arbitrary number and locations of nodal points, it is very difficult to generate an interpolation function to describe the displacement distribution within this element. Special shear band elements and its numerical treatment are the important issues in the contact band element approach. The following is a special strategy.

At first, two temporary points are added to surface IJ, following the scheme which will be described in section 5.3.2. The element is then divided into subelements (element I1M, 1LM, etc.). The newly added nodal points 1 and 2, which may disappear in the next load step, are related to nodal points I and J. The corresponding nodal variables are interpolated from the shape functions of nodal points I and J. No new degree of freedom is introduced by using static condensation technique for the temporary nodal points 1 and 2. Finally, only the independent boundary points are involved in stiffness and load formulations. In one special element, the more nodal points appear on the opposing surface, the more temporary points are needed (Wang et al., 1995), but, the same rule is abided by for the analysis of the special element no matter how many temporary nodal points are added.

5.2.4 A judgment of the technique to update shear band elements using error analysis

Owing to the small thickness of the shear band and typical element size along the band, shear band elements may have very large aspect ratios. It may be necessary to decrease the mesh spacing of band elements along the band. For the shear band zone, the high gradients of shear deformation present themselves only across the shear band. In the direction parallel to the shear band, shear strains do not manifest intense variations.

Shear strain is normally expressed as $\left(\frac{\partial u}{\partial n}+\frac{\partial v}{\partial t}\right)$ in continuum mechanics and finite element analysis, here n denotes the direction normal to a shear band, and t, the direction parallel to the shear band, u and v are displacements parallel and normal to the shear band respectively. u has a much higher gradient in the normal direction than v has in the tangent direction. That implies that $\left|\frac{\partial u}{\partial n}\right| >> \left|\frac{\partial v}{\partial t}\right|$. Therefore, the shear strain can be approximately simplified as $\frac{\partial u}{\partial n}$. It implies that the refinement of shear band elements is not needed in the direction parallel to the shear band.

It is well known that the differential equation governing the incremental equilibrium tends to be hyperbolic at localized zones (Zienkiewicz et al., 1995). The local error is defined as:

$$e = \|\mathbf{u}\| - \|\mathbf{u}\|^h, \tag{5-9}$$

where, $\mathbf{u}$ is the exact displacement vector, and $\mathbf{u}^h$ is the finite element solution, $\|\mathbf{u}\| = \left(\mathbf{u}^T\mathbf{u}\right)^{1/2}$. In the localization zone, errors can be estimated (Zienkiewicz and Huang, 1995) using:

$$e \le ch\left|\frac{\partial\|\mathbf{u}\|}{\partial \mathbf{n}}\right| \tag{5-10}$$

h denotes element size, $\mathbf{n}$ represents the shear band direction and c is a positive constant. The elongation ratio of shear band elements can still be specified by the following equation to produce an optimal finite element grid in order to keep the error constant in directions normal and parallel to the shear band:

$$s = \frac{h_t}{h_n} = \frac{h_{max}}{h_{min}} = \left(\frac{\left| \frac{\partial^2 \|\mathbf{u}\|^h}{\partial n^2} \right|}{\left| \frac{\partial^2 \|\mathbf{u}\|^h}{\partial t^2} \right|} \right). \qquad (5\text{-}11)$$

h_t represents the element size along the shear band that the band elements can retain; h_n is the element size normal to the shear band the band elements can retain, i.e. the thickness of the shear band. Obviously, $\left| \frac{\partial^2 \|\mathbf{u}\|^h}{\partial n^2} \right| >> \left| \frac{\partial^2 \|\mathbf{u}\|^h}{\partial t^2} \right|$. Therefore, h_t is much greater than h_n. From this result, it is not difficult to reach the conclusion that when a shear band is initiated, shear band elements with small thickness should be incorporated into the solid structure, but the length of the element along the shear band may have the same dimension as the adjacent solid elements. The length can be much larger than the thickness without degrading the numerical solutions. Considering numerical stability, the appropriate aspect ratio of the shear band elements should be kept to prevent the stresses along the shear band from fluctuating (Day and Potts, 1994).

5.3 Formulation of contact band elements

5.3.1 Triangular and quadrilateral Element

The stiffness formulation of the triangular and quadrilateral element follows the conventional approach. However, with the progressive development of a shear band, the nodal points along the band boundaries will be rearranged to update band elements from time to time. The displacement and stresses at each nodal point could be tracked, but old Gaussian integration points would disappear when the band elements are updated.

Subsequently it is not possible to keep stresses at the traditional Gaussian points. Therefore, it is necessary to keep stresses and strains at nodal points which are obtained by taking an average of all the values for the same nodal point which is involved in some particular band elements. Mathematically, it is expressed as:

$$\sigma_{ij}^{k} = \sum_{e=1}^{m} (\sigma_{ij}^{k})_e / m, \qquad (i, j = 1, 2, 3) \qquad (5\text{-}12)$$

in which σ_{ij}^{k} represents stress components at nodal point k. $(\sigma_{ij}^{k})_e$ is the stress components at nodal point k of individual element e; m is the number of shear band elements around point k. As shown in figure 5.6, in order to calculate stress components at point k, band elements I, II, and III are involved. Once a new band element is created, stresses and strains at the Gauss integration points can be interpolated from the nodal values by using polynomial interpolation functions, which are given by:

$$\sigma_{ij}^{g} = \sum_{k} N_k(\xi_g, \eta_g)\sigma_{ij}^{k}, \qquad (k=1, 2, 3, 4) \qquad (5\text{-}13)$$

where g denotes Gaussian points, and k nodal points; σ_{ij}^{g} denotes the stresses at Gaussian points of new band elements. (ξ_k, η_k) are local coordinates under the master reference system. Shape function $N_k(\xi, \eta)$ reads:

$$N_k(\xi, \eta) = \frac{1}{4}(1 + \xi_k \xi)(1 + \eta_k \eta), \qquad (k=1, 2, 3, 4) \qquad (5\text{-}14)$$

where ξ_k=1, -1, -1, 1; η_k=1, 1, -1, -1.

5.3.2 Special shear band element

As stated previously, special shear band elements will form when more than two nodal points along a band boundary lie between two nodal points on the opposite

boundary. As illustrated in figure 5.7, a special band element is generated with permanent nodal points 1, 3, 4, 5, 7, 6, and 2. It is difficult to formulate this element only using conventional interpolation functions. Therefore, temporary nodal points 8 and 9 are added. The displacements, stresses, and some mobilized material parameters of the temporary nodes are obtained from the permanent nodal points by linear interpolation.

The coordinates of the temporary nodal points 8 and 9 are interpolated from points 3, 4, and 5. They are considered to lie on the bisecting lines of boundary edges 3-4 and 4-5, respectively. Approximately, due to very small thickness, the local coordinates of points 8 and 9 can be obtained from:

$$\begin{aligned} X_n^8 &= \frac{1}{2}(X_n^3 + X_n^4), \quad X_t^8 = \frac{1}{2}(X_t^3 + X_t^4) - d \\ X_n^9 &= \frac{1}{2}(X_n^4 + X_n^5), \quad X_t^9 = \frac{1}{2}(X_t^4 + X_t^5) - d \end{aligned} \qquad (5\text{-}15)$$

where d is the band thickness. Because the displacement increments of points 8 and 9 are dependent on those of points 2 and 6 , they are shown here as:

$$\dot{U}_i = N_2 \dot{U}_2 + N_6 \dot{U}_6 \ , \ \dot{V}_i = N_2 \dot{V}_2 + N_6 \dot{V}_6 , \quad (i=8, 9) \qquad (5\text{-}16)$$

the displacement rates of the temporary points are replaced by those of permanent points. For linear interpolation, N_2=1-r, N_6= r. The local coordinate r can be back calculated from the concept of an isoparamatric element based on the global coordinates which are obtained by transferring local coordinates given in equations (5-15).

$$X_i = N_2 X_2 + N_6 X_6 , \ Y_i = N_2 Y_2 + N_6 Y_6 . \ (i=8,9) \qquad (5\text{-}17)$$

As an illustration, take element II in figure 5.7 in which permanent nodes 3 and 2 and temporary node 8 are involved. The incremental equilibrium equation can be written as:

$$[K]^e_{II}\begin{Bmatrix}\dot{U}_2\\ \dot{V}_2\\ \dot{U}_3\\ \dot{V}_3\\ \dot{U}_8\\ \dot{V}_8\end{Bmatrix}=\begin{Bmatrix}\dot{P}^2_x\\ \dot{P}^2_y\\ \dot{P}^3_x\\ \dot{P}^3_y\\ \dot{P}^8_x\\ \dot{P}^8_y\end{Bmatrix} \tag{5-18}$$

The left side of equation (5-18) becomes:

$$[K]^e_{II}\begin{Bmatrix}\dot{U}_2\\ \dot{V}_2\\ \dot{U}_3\\ \dot{V}_3\\ N_2\dot{U}_2+N_6\dot{U}_6\\ N_2\dot{V}_2+N_6\dot{V}_6\end{Bmatrix}=[K]^e_{II}\begin{bmatrix}1&0&0&0&0&0\\0&1&0&0&0&0\\0&0&1&0&0&0\\0&0&0&1&0&0\\N_2&0&0&0&N_6&0\\0&N_2&0&0&0&N_6\end{bmatrix}\begin{Bmatrix}\dot{U}_2\\ \dot{V}_2\\ \dot{U}_3\\ \dot{V}_3\\ \dot{U}_6\\ \dot{V}_6\end{Bmatrix} \tag{5-19}$$

$$=[K]^e_{II}[L]^e\{\dot{U}\},$$

The external forces acting on point 8 are also converted to points 2 and 6:

$$\begin{Bmatrix}\dot{P}^2_x\\ \dot{P}^2_y\end{Bmatrix}=\begin{bmatrix}N_2&0\\0&N_2\end{bmatrix}\begin{Bmatrix}\dot{P}^8_x\\ \dot{P}^8_y\end{Bmatrix},\quad \begin{Bmatrix}\dot{P}^6_x\\ \dot{P}^6_y\end{Bmatrix}=\begin{bmatrix}N_6&0\\0&N_6\end{bmatrix}\begin{Bmatrix}\dot{P}^8_x\\ \dot{P}^8_y\end{Bmatrix}. \tag{5-20}$$

From equations (5-19) and (5-20) , the local stiffness matrix for element 238 is finally related to permanent nodes 2, 3 and 6. The stiffness matrix of the elements in global coordinate system reads:

$$[K]_{II}=[Q]^T[K]^e_{II}[L]^e[Q]. \tag{5-21}$$

For a triangular element, $[\mathbf{Q}]=\begin{bmatrix}[\mathbf{a}] & 0 & 0\\ 0 & [\mathbf{a}] & 0\\ 0 & 0 & [\mathbf{a}]\end{bmatrix}$, $[\mathbf{a}]=\begin{bmatrix}\cos\beta & \sin\beta\\ -\sin\beta & \cos\beta\end{bmatrix}$,

where [**a**] denotes the orientation matrix of the shear band; β is the inclination of the band with respect to the X axis. Similarly, the stiffness matrices are formed for elements I, and III to VII by transferring the corresponding stiffness to permanent points 2 to 6. Finally, the stiffness matrix for the special band element is given by

$$[\mathbf{K}]=[\mathbf{K}]_{\mathrm{I}}+[\mathbf{K}]_{\mathrm{II}}+[\mathbf{K}]_{\mathrm{III}}+[\mathbf{K}]_{\mathrm{IV}}+[\mathbf{K}]_{\mathrm{V}}+[\mathbf{K}]_{\mathrm{VI}}+[\mathbf{K}]_{\mathrm{VII}}\ . \qquad (5\text{-}22)$$

5.3.3 Separation of the shear band elements

With the development of a shear band, some local regions within the shear band may be separated because of tension. The decision on whether a nodal point is or is not in a separating condition is perhaps most quickly made based on the normal traction at that point. However, whether a shear band element is in tension, the judgment should be more appropriately based on the average normal traction acting on the boundary segment of the element instead of on the actual distributed traction to reduce the iteration sensitivity due to the release of tension. Assume that the traction (stress normal to the shear band boundary) at each point has been evaluated. The average traction $\bar{s}$ on segment Γ_{JK} (figure 5.8) will be:

$$\bar{s}=\frac{\int_{\Gamma_{JK}}[N]^{T}\{s\}\,dt}{\int_{\Gamma_{JK}}dt}\ ,\quad s=\sigma_{ij}n_{j}n_{i}\ . \qquad (5\text{-}24)$$

$[N]^T$ is the transpose of the shape function on boundary segment JK. The direction cosine of the normal of the shear band is determined as:

$$\mathbf{n} = \begin{Bmatrix} \dfrac{\partial X}{\partial t} \\ \dfrac{\partial Y}{\partial t} \\ 0 \end{Bmatrix} \mathbf{x} \begin{Bmatrix} 0 \\ 0 \\ 1 \end{Bmatrix} = \begin{vmatrix} \mathbf{i} & \mathbf{j} & \mathbf{k} \\ \dfrac{\partial X}{\partial t} & \dfrac{\partial Y}{\partial t} & 0 \\ 0 & 0 & 1 \end{vmatrix}$$

$$= \frac{\partial Y}{\partial t}\mathbf{i} - \frac{\partial X}{\partial t}\mathbf{j}, \qquad (5\text{-}25)$$

where, **x** is the cross product symbol, X and Y are the axes of global coordinate system. If $\bar{s}$ is greater than the tension strength s_0, then, this element is in tension. The normal stresses will be reduced to zero at the nodal points of the shear band segment Γ_{JK}. Note that at points J and K, the part of the normal stresses contributed only by element OJK are reduced to zero. The unbalanced forces are applied on the relevant nodes. The iterations will proceed until the iteration tolerance is satisfied. While the parts from the other band elements remain unchanged. Also, the resultant normal stresses at points J and K will be changed. For many geomaterials, the tensile strength can be considered to be zero. Hence, if $\bar{s}$ is greater than zero, its stiffness contribution is set to be zero. All the stresses at the Gaussian points and the nodal points for this element will disappear. The element should be released as well.

5.3.4 Kink band problems

There has been a long history of attempts to solve the kink problem in numerical analyses of geotechnical stability problems. As shown in figure 5.9 (a), the slip surface contains several kink shear bands. With the increase of passive pressure on a retaining wall, the materials around the kinks are subjected to intense compression, which finally becomes nearly incompressible. In finite element analysis, the incompressibility will

impose large resistance to shearing of the slip surface, which in turn will lead to a higher limit passive pressure.

Some successful finite element formulations have been developed to alleviate mesh locking for incompressible and nearly-incompressible media, which is similar to the kink problem. Two popular techniques are the reduced/selective integration procedures and the mean-dilation formulation which are also applicable to the kink problem. Hughes (1980) presented a new procedure which generalizes both the selective integration and mean-dilation techniques. The new procedure involves only a modification of the usual strain-displacement matrix. In shear band analysis, However, incompressibility only occurs around the kinks. The use of the above techniques would engender a large amount of numerical calculations. The geometrical approximation from shear band element will show its validity.

As shown in figure 5.9 (b), in normal finite element analysis, the band elements are never updated. With increase in shearing of the band, elements around point C will become stiffer and stiffer which will restrict kinematic movements of the band, and eventually leads to locking. The incompressibility or near incompressibility around point C will make only pure shear. Eventually, the movements of local points around point C will be parallel either to boundary L_1 or to boundary L_2. Since nodal point c is involved in both shear bands. kinematically, on one hand, the movement of point C should be parallel to boundary L_2 (assuming no change in band thickness during shearing), on the other hand, the movement of point C should be parallel to boundary L_1. So, there is a paradox. This called singularity in mathematics. There will be actually no movement at point C. However, with the application of techniques of contact band element, geometry

of shear band elements around the kink will keep changing. In figure 5.9 (c), at the preliminary stage of shearing, nodal point C has moved to the domain of band S_2. The singularity phenomenon has been removed. From then on, point C is only with S_2, and can be used to form new shear band elements within the domain of S_2. The direction of motion of point C is defined. The 'locking' phenomenon is drastically alleviated. The scheme is well illustrated in figure 5.9 (c).

5.4 Numerical examples

To validate the applicability of the contact band element approach in modeling kinematic propagation of a shear band, four examples are performed under plane strain condition to illustrate the proposed method, in which potential shear bands are specialized.

5.4.1 Direct shear test

First of all, the mechanical and geometric responses of the direct shear test are examined to test the effectiveness of the method in modeling localization. As shown in figure 5.10 (a), a potential shear band with a thickness of 0.5 mm is assumed to lie horizontally between two halves of the shear box. The soil sample is represented by 144 soil elements and 16 prescribed undeformed shear band elements. In order to compare the finite element result with analytical solution for the problem, only elastic analyses were carried out. Since we are mainly concerned with shear band kinematics, elastic models are powerful enough to illustrate the effectiveness of the scheme. However, the method can be applied to plastic analysis using elasto-plastic constitutive model. The

material parameters used in the analysis are $E_{soil}=5x10^6$ N/mm^2, ν_{soil}= 0.35, E_{band}=10.0 N/mm^2, and ν_{band}=0.35, where E and ν are Young's modulus and Poisson's Ratio, respectively. Compared with the shear band, the upper half of the soil mass is assumed to be almost rigid. The top boundary points of the soil are constrained in the vertical direction. Along the bottom boundary, the first node at the left end is fixed in two directions and all the other nodal points are fixed in horizontal direction. Due to the fact that the shear band area is eliminating with the increase of horizontal load, this question will be geometrically non-linear although the materials are always constitutively linear. The load is divided into 12 steps in total. With an increase of the horizontal load, large shear strains are induced in the band. During the loading process, the shear band elements are updated from time to time. Some are eliminated automatically. Quadrilateral, triangular and special band elements are introduced simultaneously. The shear stress along the shear band is uniformly distributed because the upper and bottom parts of the shear box are almost rigid. A plot of the computed horizontal displacement versus horizontal force corresponding to the conventional finite element approach (no shear band element is updated) for the contact band element approach and the analytical solution is shown in figure 5.11. The analytical solution is based on uniform shearing of an elastic material in which the diminishing effective length of the band is taken into account. Apparent shear stresses corresponding to all three methods stated above are also plotted with respect to the applied load in figure 5.12. The apparent shear stresses are obtained by dividing the shear force by the current area of the shearing zone. As shown in the figures, results from the contact band element approach agrees well with the analytical

solution, but the conventional finite element method exhibits considerable discrepancy due to the presence of highly distorted elements which are eliminated in the present contact band element approach, and no band elements are eliminated with the increase of the load to reflect the diminishing shearing area. Hence, the calculated displacements are smaller than the analytical solution. The calculation was completed on the basis of keep updating coordinates of each nodal point. In each load step, the analysis is performed on the current configuration. The large shear strain at the last stage cannot be calculated directly from the shear stress and shear modulus G using small deformation theories.

It is seen that the contact band element approach can effectively model the kinematic propagation of the shear band. By contrast, the displacements and stresses along the shear band from the conventional isoparametric element method differ from the actual physical response of the shear band, especially under high loading.

5.4.2 Plan strain compression test

The second example is to simulate a uniaxial compression test. The test specimen is shown in figure 5.13 (a). The shear band is oriented at an angle of 62.8° with respect to the X-axis with a thickness of 0.889 mm. As mentioned previously, for the sake of simplicity, all the materials, as assumed to be elastic, obey elastic constitutive relations with the modulus of soil mass much greater than that of the shear band. Therefore, the deformation is mainly due to the propagation of the shear band. The material parameters are $E_{soil}=5x10^{6}$ N/mm^{2}, $\nu_{soil}=0.35$, $E_{band}=15.0$ N/mm^{2}, $\nu_{band}=0.35$. With an increase of vertical load on the top of the specimen, the normal stress on the shear band will increase accordingly. The tangential deformation increment of the band tends to become

infinitesimally small due to the rapid decrease in the band thickness, which eventually results in displacement incompatibility, namely, element penetration or overlapping. An effective amendment for this pathological decrease in the band thickness is to prescribe a minimum band thickness by dramatically increasing the normal stiffness of the band material. This can be achieved numerically by imposing the same normal movement on both sides of the shear band at each iterative step to eliminate the penetration and maintain a minimum thickness. In addition, appropriate constitutive models could be selected for an efficient alleviation. The algorithm will be presented in chapter 6.

Figure 5.13 (b) displays the deformed configuration at one stage of deformation and illustrates the changes in the band elements. Vertical load versus tangential displacement and apparent shear stress curves are plotted in figures 5.14 and 5.15. respectively. The final tangential displacement at step 13 is equal to 53.66 mm, almost two thirds of the initial length of the shear band. Displacement and stress calculations from the proposed strategy and analytical method agree remarkably well, which shows once again that the numerical simulation can effectively capture the kinematic propagation of the shear band.

5.4.3 Uniaxial test with two shear bands in the specimen

The third example is still the uniaxial test model. It is different from the second example 5.4.2 in that the slip channel (shear band channel) is composed of two shear bands at different orientations. The upper shear band is oriented at an angle of 62.8° with respect to the X-axis, whereas the lower one has an angle of 34° with respect to the horizontal direction, as shown in figure 5.16 (a). The initial thickness for steep band and

gentle band are 2.40 mm and 1.35 mm, respectively. A vertical load was applied on the top of the sample, which is increased by 45 N/mm^2 to 315N/mm^2 in 7 steps. The soil parameters used are E_{soil} =5x10^6 N/mm^2, ν_{soil}=0.35. Tensile strength of the shear band is assumed to be zero.

The deformed mesh and vertical stress contours for the last loading step are given in figures 5.16 (b), and 5.17 respectively. The maximum tangential displacement at p=315 N/mm^2 was calculated to be 7.22 mm at the left end of the upper bound, and a maximum vertical stress of 604 N/mm^2 at the right side of the gentler shear band close to the kink location. Four shear band elements were in tension state around the kink. The indications of stress concentration and stress release along the shear band from the stress contours are consistent with the deformed configuration of the specimen. The results have shown that the method to eliminate tension materials is effective. An effective way is obtained to overcome the overlapping problem, which happens frequently in the simulation of kinematic development of the shear bands. The test illustrates the success of the contact band element approach for shear band development.

To alleviate the overlapping problem, the concept of a thin-layer element is utilized, which was put forward by Desai et al. (1984). The key point is that there are three independent parameters E, ν and G for shear band materials. In this approach, the band is assumed to be in an elastic state. Here, E is the elastic modulus across the shear band. G is the shear modulus along the shear band, which is independent of E. Later, in chapter 6, a cross-isotropic model with special Mohr-Coulomb criterion is developed. It takes the same form of general elastic constitutive matrix, but the relationship between E

and G of general isotropic model doesn't apply to it. It is assumed that shearing property along the shear band is independent of compression or tension properties of the material. It is a special case of the cross-isotropic model. Satisfactory results can be obtained by assigning the shear band material a large normal stiffness, and keeping a very small shearing stiffness along the shear band. This model is more complicated than the isotropic model, but simpler than the cross-isotropic model. In this test, the values are given as: E=90 N/mm^2, G=30 N/mm^2 and v=0.35, respectively. In effect, the normal deformation properties of the shear band vary with changes of the stresses within the shear band and thickness, which will be taken into account using modified Cam-Clay model presented in chapter 6.

In the first two examples, the shear band elements are updated from time to time by referring to the relative location of points on the upper and lower surfaces in each shear band, because there are only one shear band in the shear band channel. In this example, the scheme to update the band elements for shear bands connecting each other with different orientations should be established. The revision makes a difference in that the nodal points belonging to different shear bands can still make a new shear band element, as long as all these shear bands are in one shear band channel. In other words, all the nodal points along the boundaries of one shear band channel can form shear band elements The element will be filled with material properties of the previous element which has a majority of nodal points in the new element. The evolution of shear band elements are shown in figure 5.18. It is seen that kink locking of the shear band elements is greatly alleviated due to the re-combination of nodal points from the deformed mesh

(figure 5.16 (b)). To illustrate the effect, another example will be given for the limit load analysis.

5.4.4 A kink problem with the biaxial test (plane strain)

The original configuration of the specimen is shown in figure 5.19. The prescribed slip channel is composed of two bands with different directions. In this example, shear bands are considered as interfaces with a minimal thickness of 0.5 mm, which would be modeled using the continuous interface element. The upper one is oriented at an angle of 62.8° with respect to X-axis, whereas the lower one has an angle of 34°. Their initial thickness for steep one and gentle one are 2.40 mm and 1.35 mm, respectively, which is measured in each normal direction of the shear bands. The shear band materials are handled with associated Von-Mises yielding criterion. Young's modulus is taken as 90 N/mm^2, Poisson's ratio as 0.35. Yield parameter at peak and residual κ=60 N/mm^2. Soils outside the shear band are still looked upon as elastic materials. $E=5x10^4$ N/mm^2, ν=0.35. The load is applied by 15 steps. The confining pressure 10 N/mm^2 is applied at the first two steps, respectively. Then, pressure increment is only applied vertically on the top of the specimen. As it is expected physically, the top part of the specimen slips and tilts, and gets large shear deformation (maximum tangential slip displacement at the tip point 145: 10 mm). The ultimate load 105 N/mm^2 for this test is obtained from figure 5.21.

Originally, soil and shear bands are discretized with 4-node rectangular elements as shown in figure 5.19. From the shear band element information given in tables 5.1, 5.2, and 5.3, it has been explicitly seen that continuous interface elements consecutively

evolved in terms of updated nodal coordinates with the kinematic development of shear bands. In the meantime, some nodal points (e. g. point 145 at the left side of the specimen) will not be involved in the rediscretizations due to tensile normal stresses at the tip of the interface. The corresponding nodal forces are released by iterating. At the limit load, all the shear band elements are either at yielding or in a tensile state. The stiffness and stresses of the continuous interface elements in tension state are both eliminated. The vertical stress contours, as illustrated in figure 5.20 (b), show the locations where stresses concentrate or are greatly released are consistent with the current specimen configuration. Please note that vertical stress contours are obtained from the analyses based on the current configuration of the structure, but they are plotted on its original configuration. Owing to the consecutive evolution of continuous interface elements, it is impossible to draw automatically the contours within the shear bands using available software. All the results demonstrate that analyses are carried out effectively.

In the traditional finite element analysis with regular isoparametric elements, virtually high limit load can be obtained with the kink interlocking in the specimen. The finite element solution often exhibits no limit load at all, but rather a steadily rising load-displacement curve due to the kinematic constraints (Nagtegaal et al., 1974). However, here, the displacement versus load curve shows a very flat line at the last stage of loading. It implies that the limit load has been reached, and strongly indicates that the interlocking phenomenon has at least been alleviated with the successful update of the shear band elements, which also displays Von-Mises criterion has been perfectly tracked.

Table 5.1 Interface element information at original load step

Element	Node No.	Element	Node No.
1	131 144 147 145	9	198 212 218 203
2	144 146 158 147	10	212 226 229 218
3	146 150 162 158	11	226 240 253 229
4	150 161 164 162	12	240 254 267 253
5	161 163 176 164		
6	163 169 183 176		
7	169 184 190 183		
8	184 198 203 190		

Table 5.2 Updated shear band element information at top pressure p=85 N/mm^2

Elemen	Node No.	Element	Node No.	Element	Node No.
1	131 144 145	9	198 212 203	17	176 164 163
2	144 146 147	10	212 226 218	18	183 176 169
3	146 150 158	11	226 240 229	19	190 183 184
4	150 161 162	12	240 254 253	20	203 190 198
5	161 163 164	13	147 145 144	21	218 203 212
6	163 169 176	14	158 147 146	22	229 218 226
7	169 184 183	15	162 158 150	23	253 229 240
8	184 198 190	16	164 162 161	24	267 253 254

Table 5.3 Updated shear band element information at final load step

Elemen	Node No.	Elemen	Node No.		Node No.
1	131 144 158	9	212 226 229	17	190 183 169
2	144 146 162	10	226 240 253	18	203 190 184
3	146 150 164	11	240 254 267	19	218 203 198
4	161 163 176	12	158 147 131	20	229 218 212
5	163 169 183	13	162 158 144	21	253 229 226
6	169 184 190	14	164 162 146	22	267 253 240
7	184 198 203	15	176 164 150 161		
8	198 212 218	16	183 176 163		

Table 5.4 Shear band elements in tension at final load step

Element	Node No.	Element	Node No.	Element	Node No.
7	184 198 203	8	198 212 218	18	203 190 184

5.5 Concluding remarks

A new strategy called the contact band element approach for modeling the kinematics of a shear band with a finite thickness is presented. The shear band element is formed by referring to the relative locations of points on the upper and lower surfaces of the shear band. Contact band elements can be in continuous link or separation with bulk materials. Band elements are updated from time to time, which ensures the aspect ratio of the 3-node triangular elements, and the 4-node quadrilateral elements to lie within acceptable ranges values. The technique of adaptive remeshing is justified by the error analysis in section 5.2.4. A new technique is developed to judge the release of shear band elements. The stiffness of the special band elements with more than 4-nodes is derived.

In this scheme, the distortion of band elements is eliminated. The problems of shear band kinking and soil element overlapping are greatly alleviated. Three numerical examples have shown that the present formulation can effectively capture the kinematics of shear banding even when large deformation arises. The present approach, which is applicable to other contact problems, can also provide an efficient way to solve the interlocking phenomenon of deforming meshes. It is predicted that similar mesh dependence which occurs in conventional isoparamatric element can be avoided, or at least alleviated with the application of this method. However, many numerical tests should be conducted.

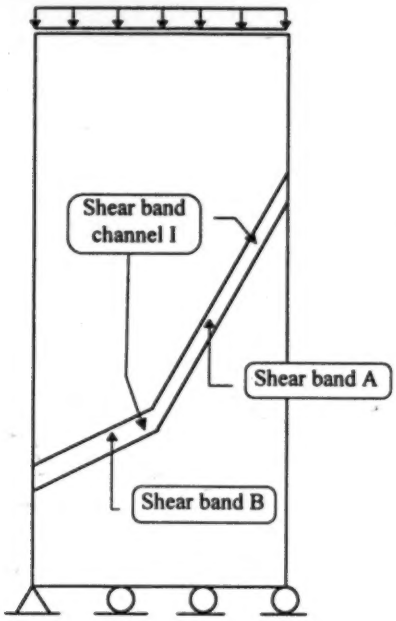

Figure 5.1 (a)

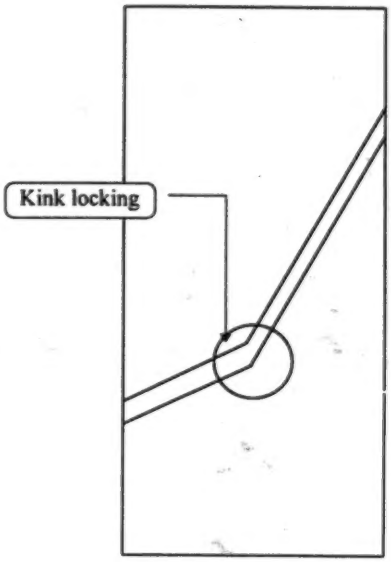

Figure 5.1 (b)

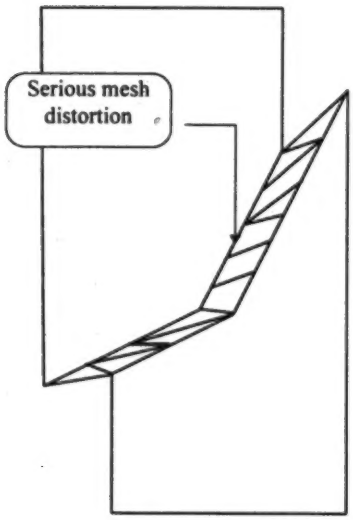

Figure 5.1 (c)

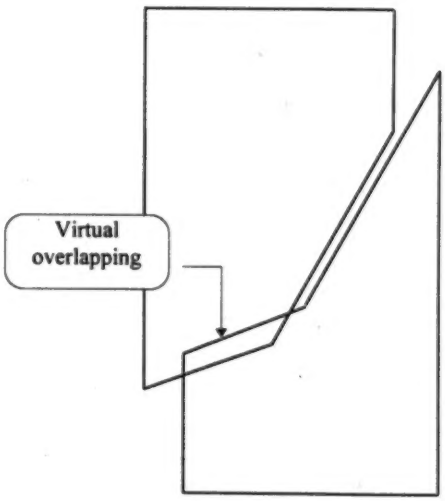

Figure 5.1 (d)

Figure 5.1 kinematic problems with existing interface elements, (a) uniaxial test, (b) kink problem, (c) mesh distortion, (d) mesh overlapping

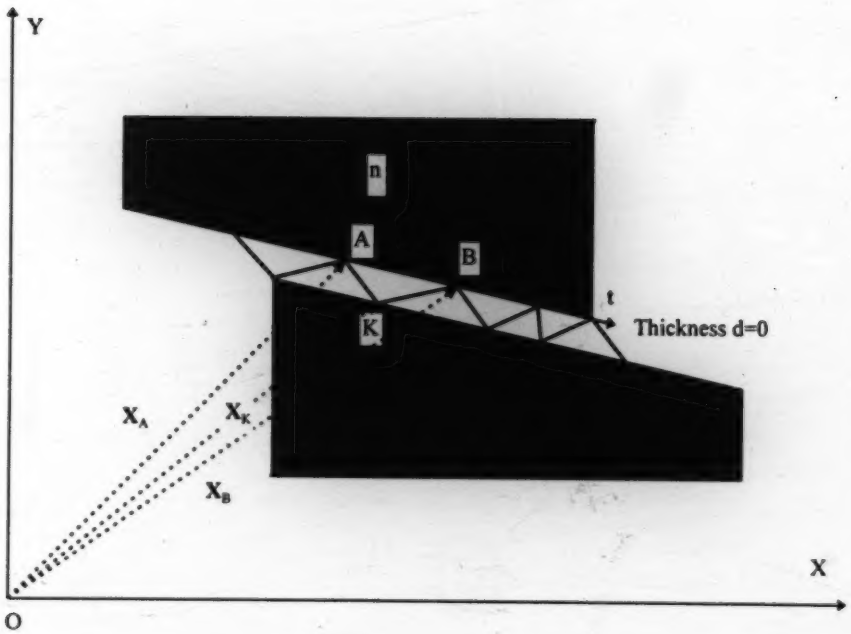

Figure 5.2 An illustration of the contact band

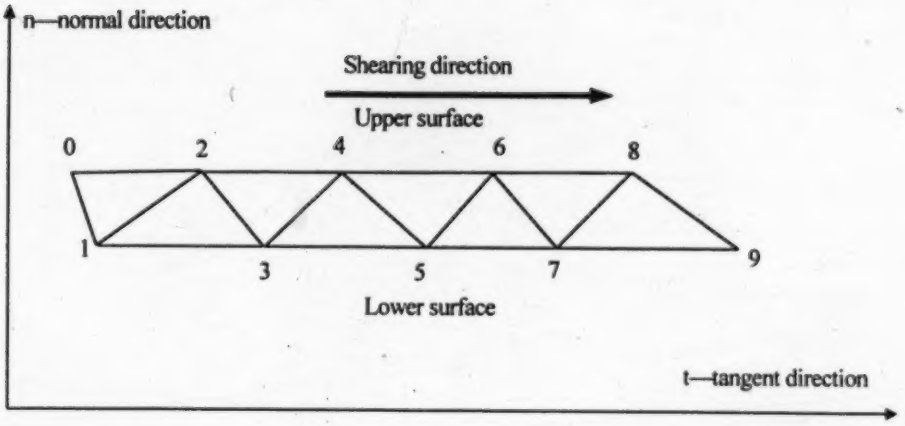

Figure 5.3 (a)

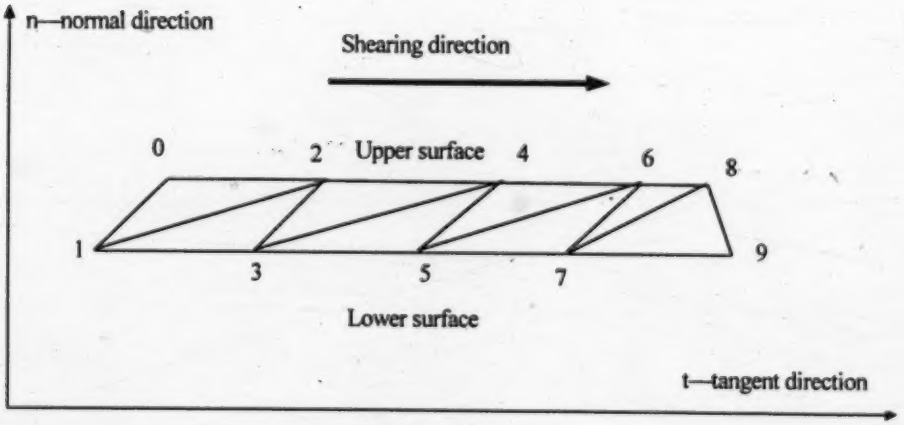

Figure 5.3 (b)

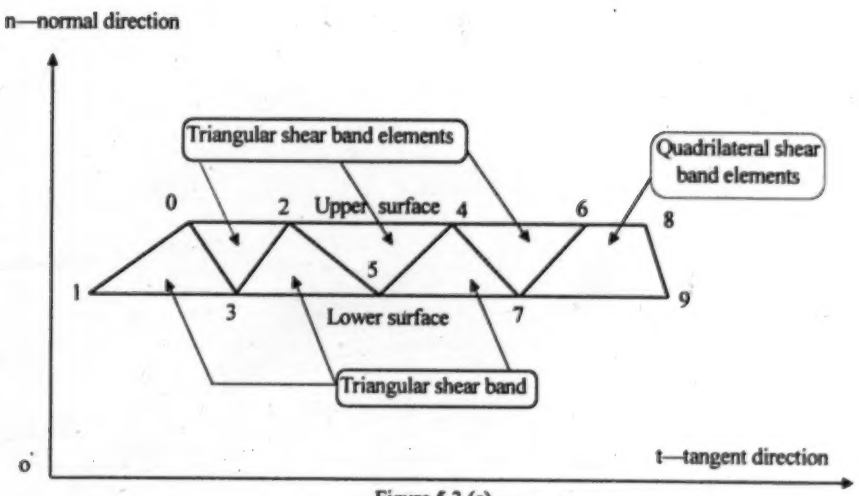

Figure 5.3 (c)

Figure 5.3 Configuration of shear band elements before and after intensive shearing deformation. (a) Band discretization before deformation, (b) Mesh configuration after deformation in conventional finite element method, (c) Mesh configuration after deformation in shear band approach

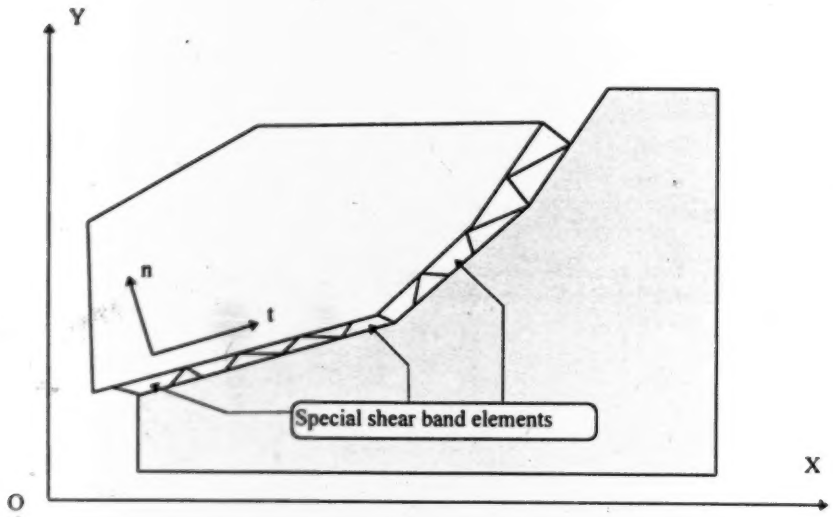

Figure. 5.4 (a)

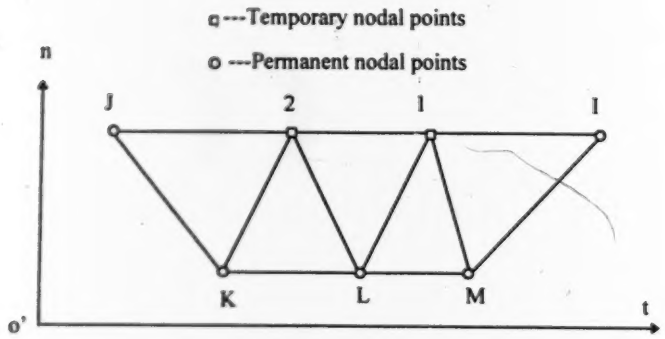

Figure 5.4 (b)

Figure 5.4 The application of special shear band elements, (a) illustration of shear band elements along a slip surface, (b) a special band element with five nodal points

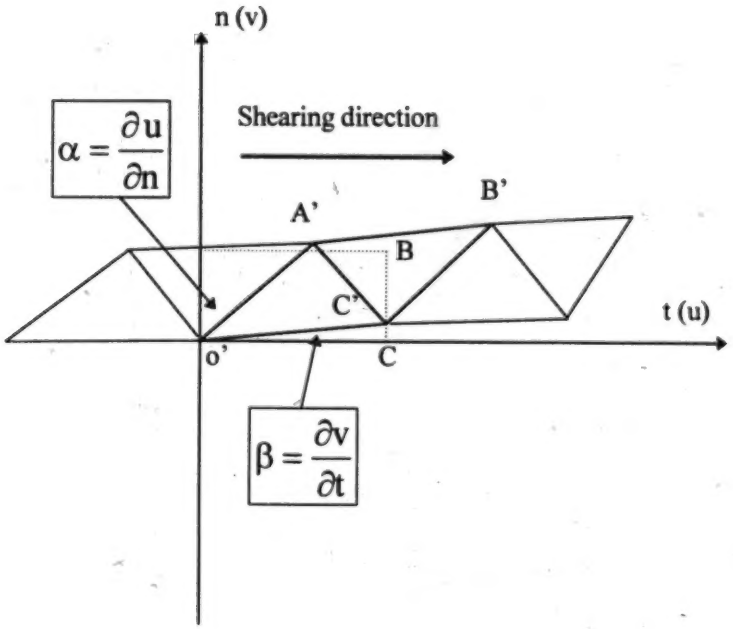

Figure 5.5 Analysis of shear strains both in normal and parallel directions to the alignment of shear band

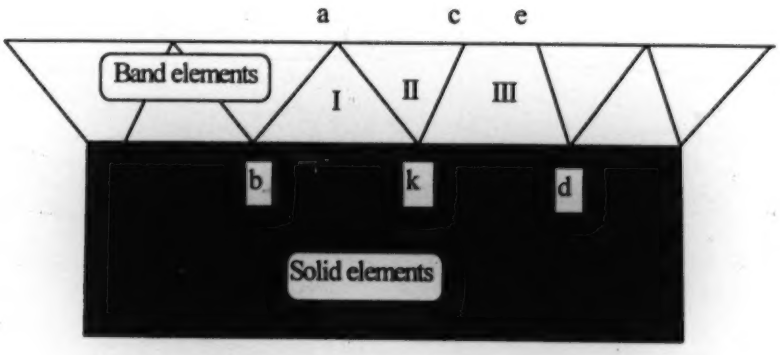

Figure 5.6 Calculation of stress components at nodes on shear band boundaries (not to scale)

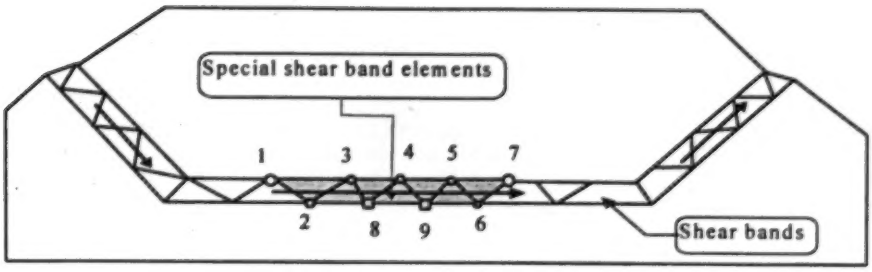

Figure 5.7 (a)

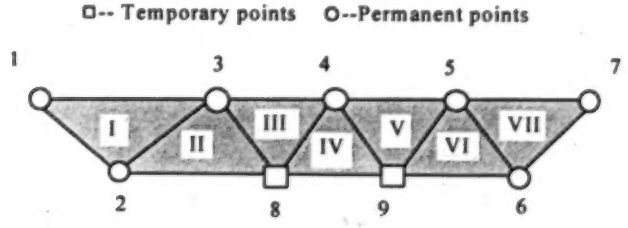

Figure 5.7 (b)

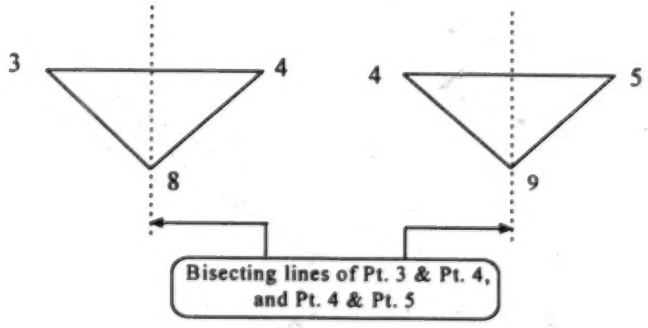

Figure 5.7 (c)

Figure 5.7 Special shear band elements, (a) application of special band elements, (b) formulation of special band elements, (c) determination of temporary nodal points

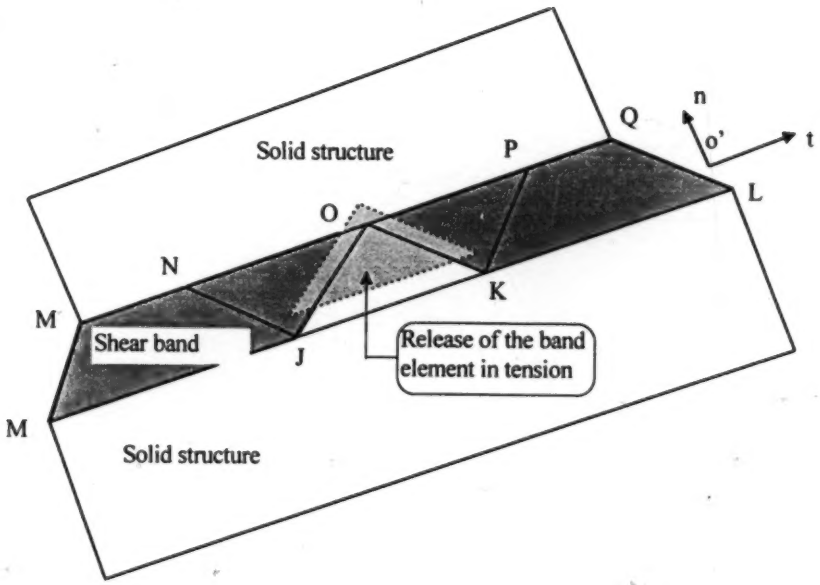

Figure 5.8 Handle of shear band elements in tension

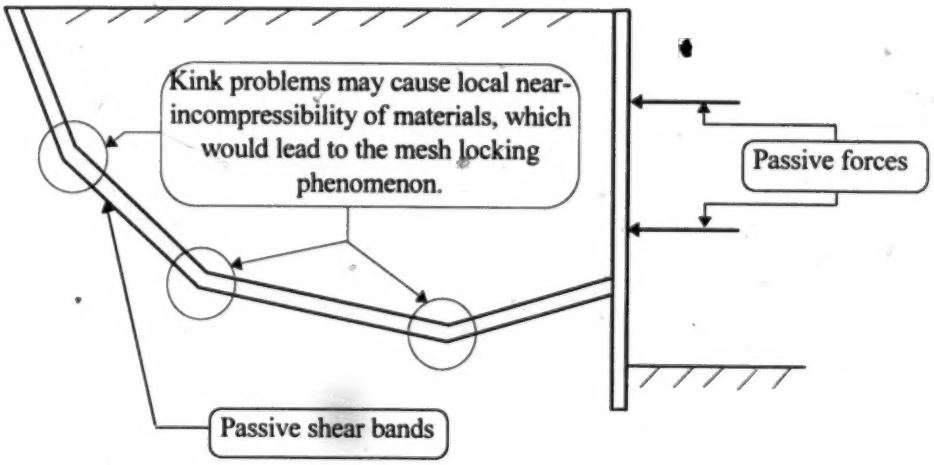
Kink problems may cause local near-incompressibility of materials, which would lead to the mesh locking phenomenon.
Passive forces
Passive shear bands

Figure 5.9 (a)

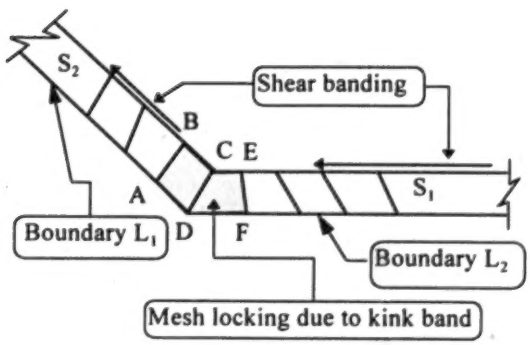

Figure 5.9 (b)

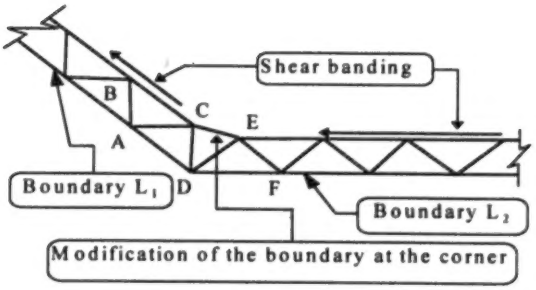

Figure 5.9 (c)

Figure 5.9 Kink problems in the localization analysis, (a) kink bands in the sheet pile wall analysis, (b) mesh locking in the general FEM, (c) The disposal of mesh locking in the shear band element method

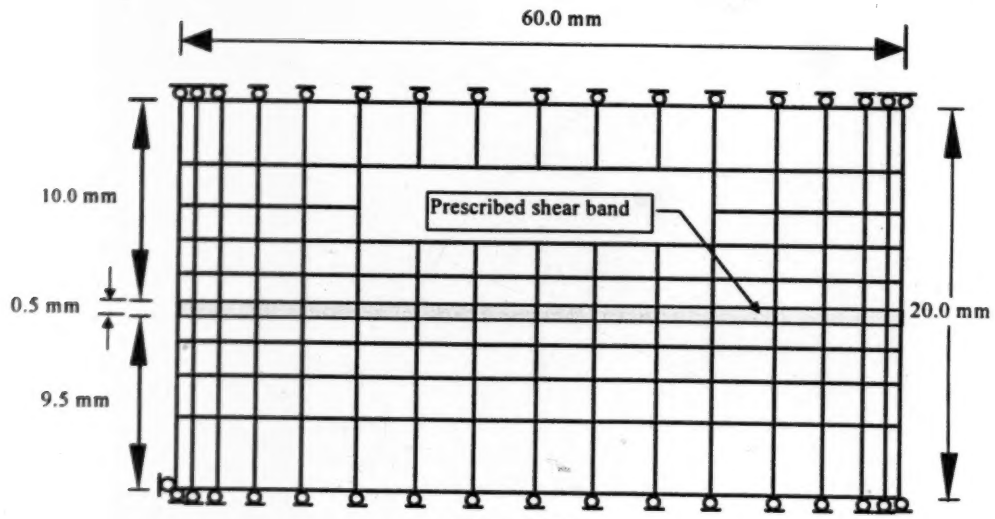

Figure 5.10 (a)

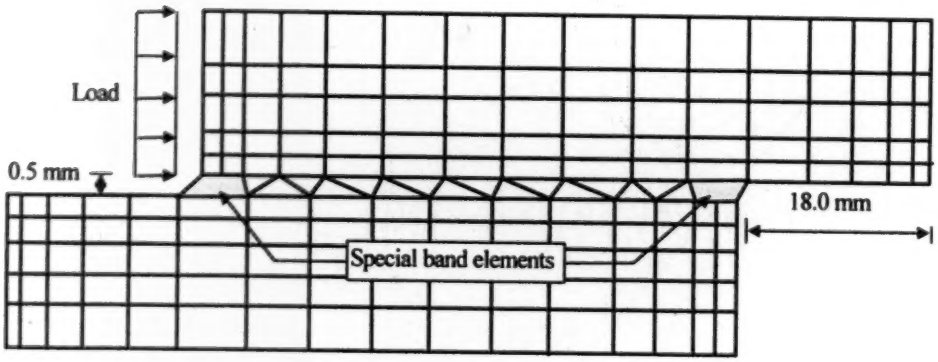

Figure 5. 10 (b)

Figure 5.10 (b)

Figure 5.10 Configuration of the shear box before and after loading, (a) undeformed 'shear box ' specimen, (b) updated mesh after large deformation

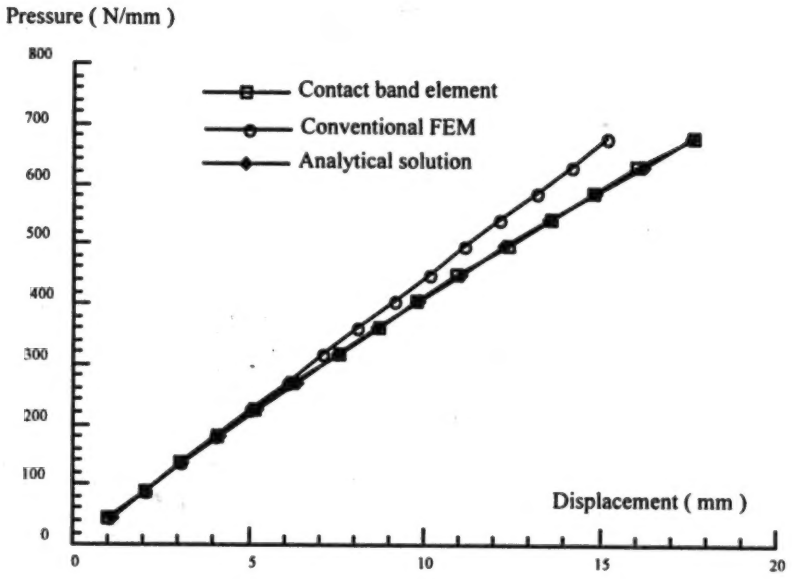

Figure 5.11 Load-horizontal displacement relationship for the 'shear box'

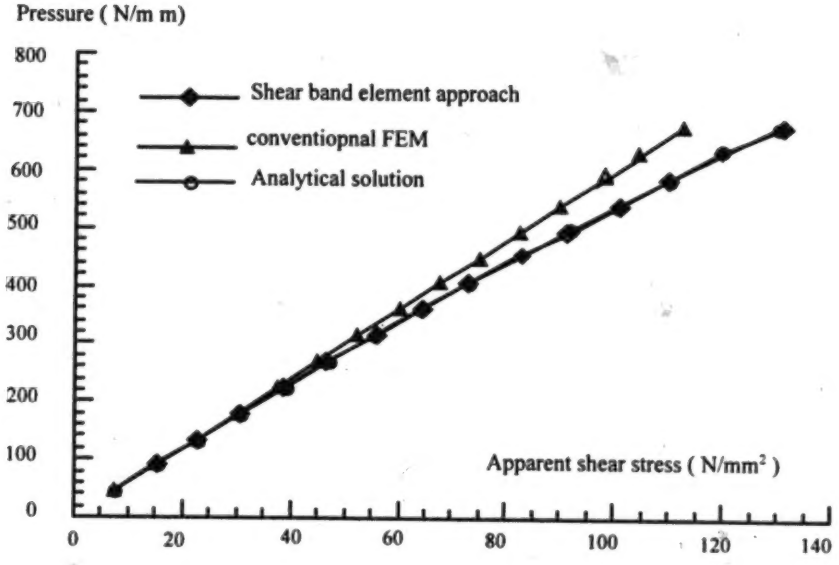

Figure 5.12 Load-apparent shear stress relationship for the 'shear box'

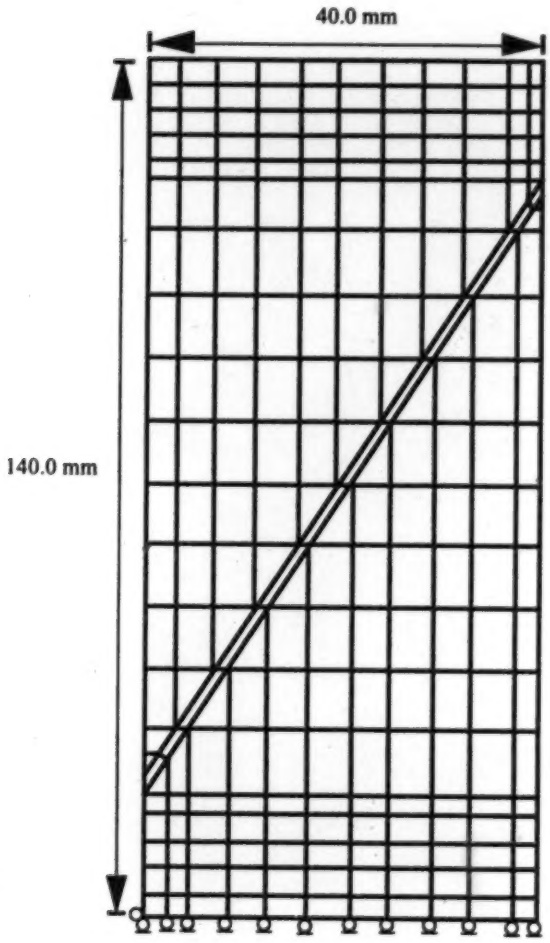

Figure 5.13 (a)

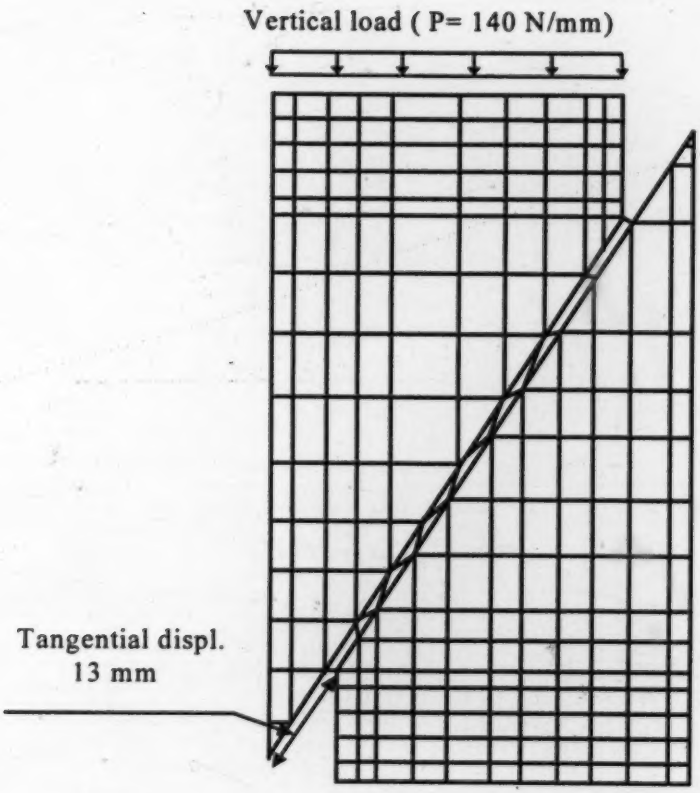

Figure 5. 13 (b)

Figure 5.13 Configuration of the specimen before and after the large deformation, (a) initial meshes before loading , (b) deformed configuration when p=140 (N/mm^2)

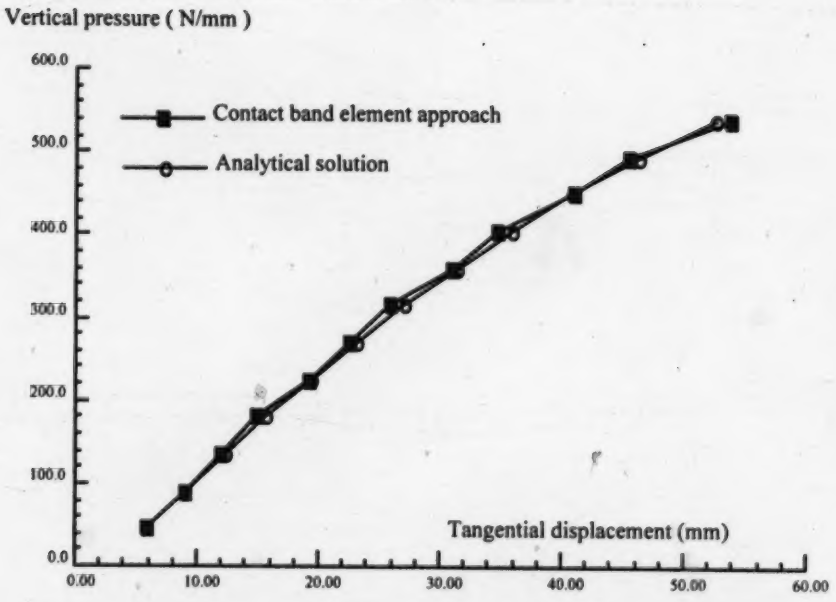

Figure 5.14 Vertical load—tangential displacement relationship

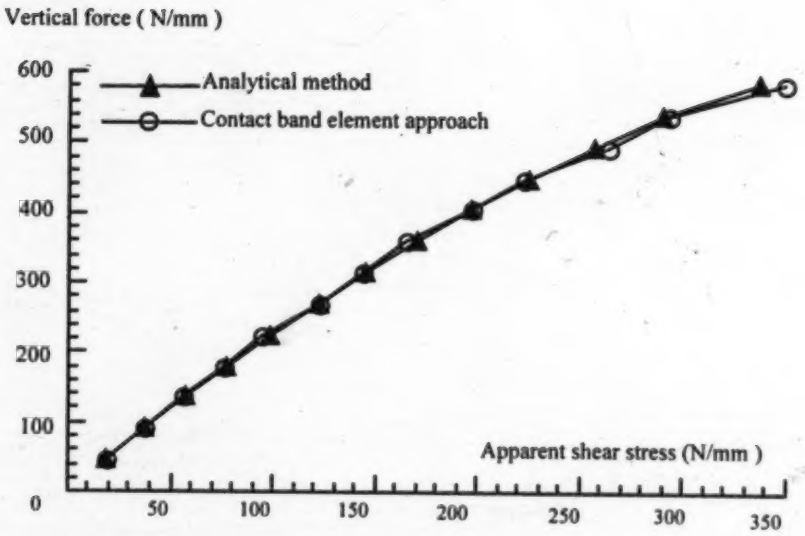

Figure 5.15 Relationship between vertical load – apparent shear stress along the shear band

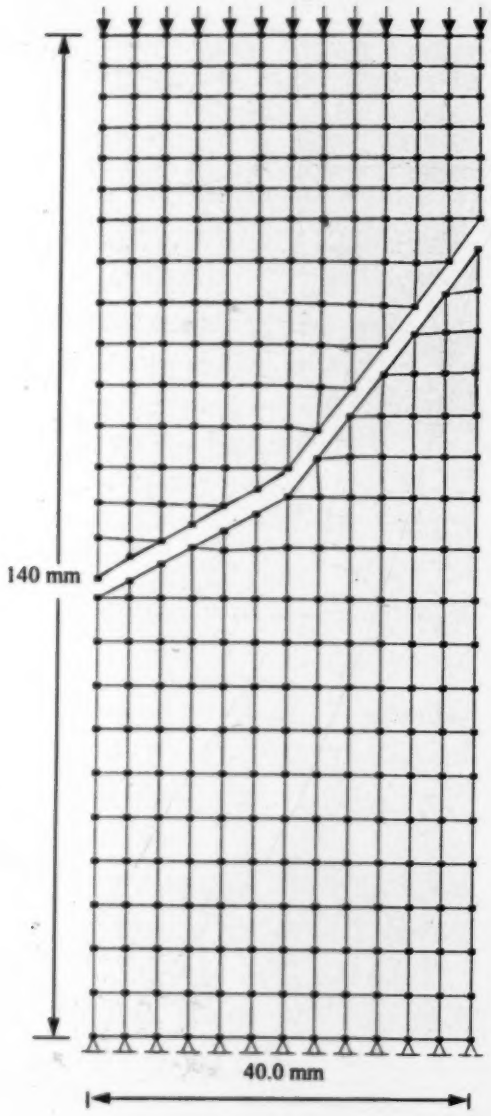

Figure 5.16 (a)

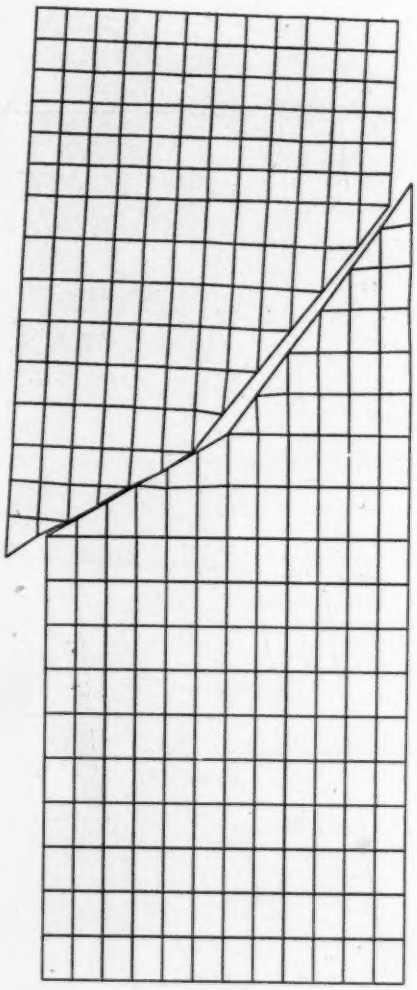

Figure 5.16 (b)

Figure 5.16 Uniaxial test of the specimen with kink problem, (a) original mesh discretization, (b) deformed mesh at p=315 N/mm^2

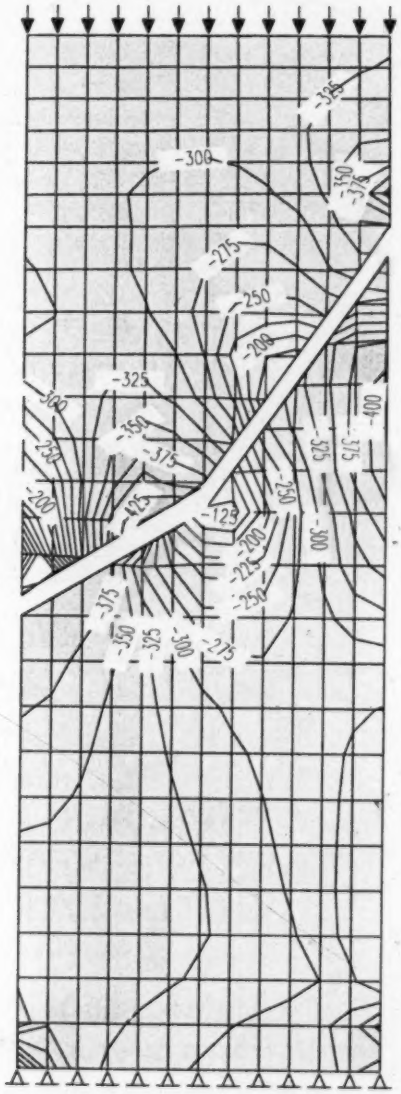

Figure 5.17 Vertical stress contours at p=315 N/mm^2 for the specimen under uniaxial test (unit: N/mm^2)

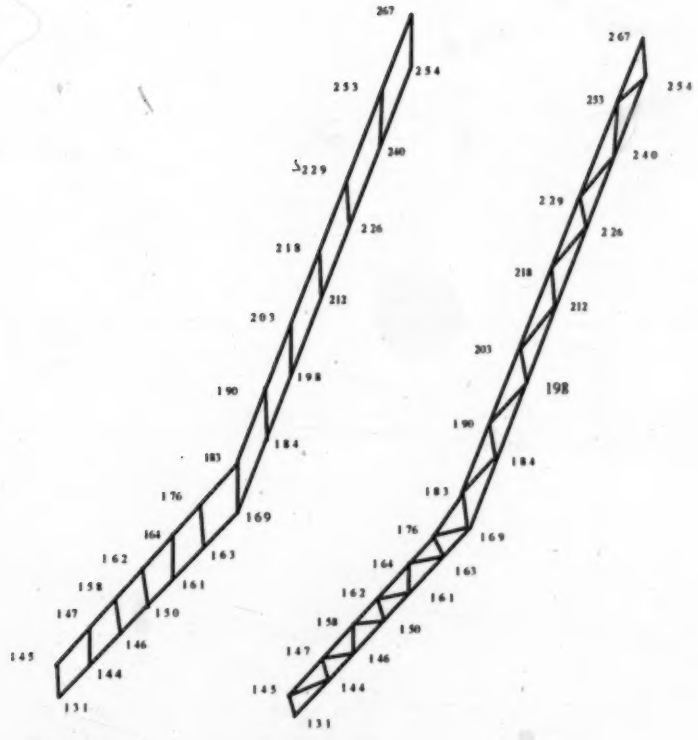

Original mesh P=45 N/mm²

Figure5.18 (a)

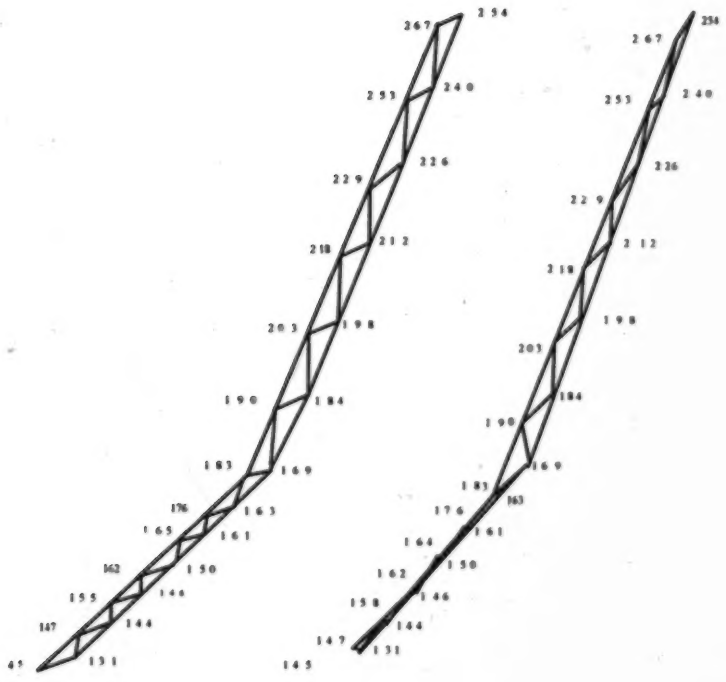

Figure 5.18 (b)

Figure 5.18 Evolution of shear band elements, (a) Original elements and elements at p=45 N/mm², (b) Elements at p=225 N/mm² and p=315 N/mm², respectively

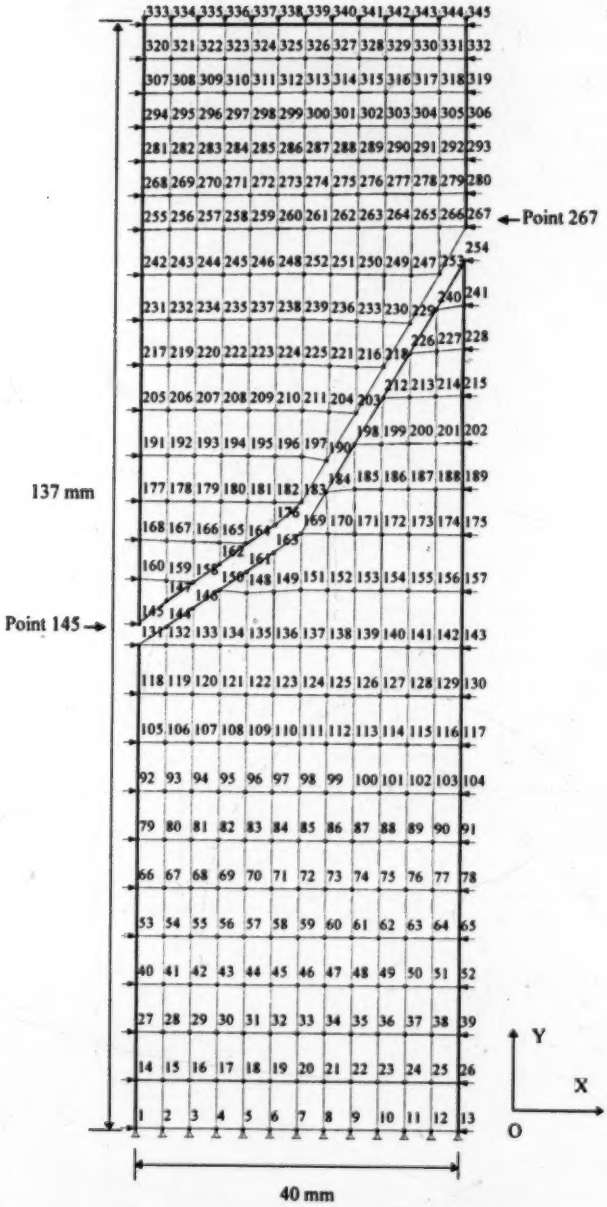

Figure 5.19 Original mesh and prescribed shear bands

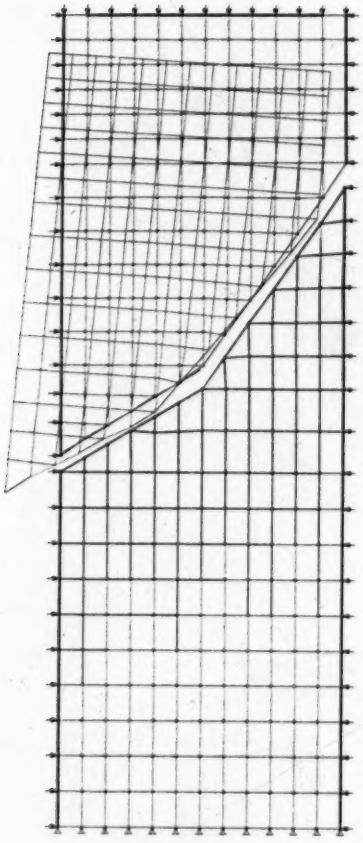

Figure 5.20 (a) (mm)

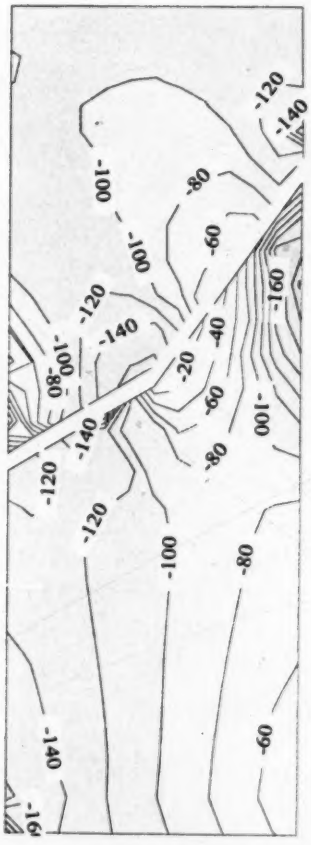

Figure 5.20 (b) (N/mm^2)

Figure 5.20 Output of finite element analysis of the kink problem, (a) final configuration of the specimen , (b) vertical stress contours at final load step

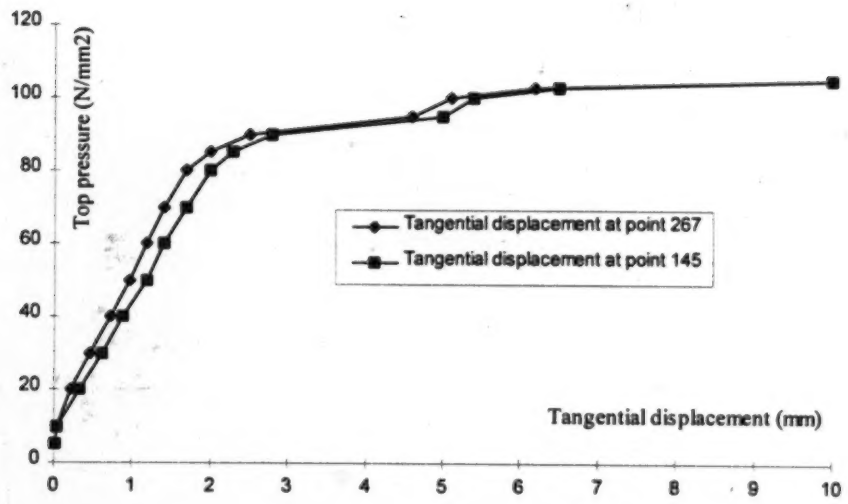

Figure 5.21 The relationship between tangential displacements at points 267 and 145 and vertical pressure acting on the top of the specimen

Chapter 6

Constitutive models for shear band materials

6.1 Introduction

Many investigators (Skempton, 1964; Morgenstern and Tchalenko, 1967; Vardoulakis and Graf, 1985) have conducted laboratory tests which consistently showed that upon the emergence of a shear band, the materials inside the band are either in the softening stage, or are prior but close to the softening stage. Large shear deformation usually occurs at the post-localization stage. Recently, systematic studies (Harris, 1995) on granular materials have indicated that the soil inside the band either dilates or remain at a constant volume. Desrus and Chambon (1983) showed that the local dilatancy angle within the shear band is twice as large as the global dilatancy angle calculated from the total volume change measurements under some circumstances. Dilation in the band will result in an increase of the mean stress P. In turn, it increases the bulk modulus, which would increasingly resist the normal deformation across the shear band. The way shear band localization will propagate with further loading largely depends on the post-peak behavior of the soil. If there is no post-peak shear strength degradation, the propagation will slowly proceed as mobilized shear stresses in the adjoining regions around the shear band tips reach the available ultimate strength. The shear band will propagate in a diffuse manner (Lo, 1972). On the contrary, if the soils exhibit strain softening behavior,

materials inside the band, but far from the band tip, would have been sheared well beyond its peak strength with further propagation of the shear band. The shear band will undergo dramatic strength degradation leading to the residual strength. However, for the materials close to the band tip, which are subjected to a localized strain discontinuity, the stresses are either at or near the peak strength. Therefore, shear bands introduce non-uniform spatial shear strains. Accordingly, large post-localization movements are created. The strong strain softening and the non-uniform straining along the shear band are basically two necessary conditions based on the foregoing conditions to trigger progressive failure.

The continuous shear band propagation definitely induces material anisotropy due to the intensive shearing. Shearing normally proceeds in preferred directions.

The ultimate objective to simulate shear band propagation at large deformation in the post localization stage is to model progressive failure. Therefore, it is necessary to simulate the constitutive behavior of the soil inside the shear band as strain softening. Shear dilation is also an important behavior to account for under certain circumstances. Moreover, due to induced anisotropy, it is also necessary to develop a pressure sensitive frictional model with preferred direction of shearing for shear band materials. The model must be anisotropic, and takes into account changes in material characteristics as a result of intense shearing within the band.

In this context, a general continuum plasticity model is still employed for shear band materials. After applying the flow rule and consistency equation dF=0, the generic incremental stress-strain equation reads as follows:

$$\{d\sigma\} = \left[C_{ep}\right]\{d\varepsilon\}, \qquad (6\text{-}1)$$

where

$$[C_{ep}]=[C_e]-\frac{[C_e]\left\{\frac{\partial G}{\partial \sigma}\right\}\left\{\frac{\partial F}{\partial \sigma}\right\}^T[C_e]}{\left\{\frac{\partial F}{\partial \sigma}\right\}^T[C_e]\left\{\frac{\partial G}{\partial \sigma}\right\}^T-\left\{\frac{\partial F}{\partial \bar{\varepsilon}_p}\right\}^T\left\{\frac{\partial G}{\partial \sigma}\right\}}, \qquad (6\text{-}2)$$

in which $[C]_e$ is the elastic constitutive matrix, and F and G denote the yield function and plastic potential function, respectively. $\bar{\varepsilon}_p$ is called the effective plastic strain. Hereafter, several elastic-plastic constitutive models characterizing shear band deformation at post-peak stage with different F and G, and different hardening rule will be described one by one.

6.2 Von-Mises model with hyperbolic softening

In some cases, for the sake of simplicity, the Von-Mises yielding criterion with constant undrained shear strength is still applied for 'short term' failure under undrained condition.

6.2.1 Yielding criterion

The conventional Von-Mises yielding criterion is written as:

$$F = q - \kappa = 0, \qquad (6\text{-}3)$$

where, $q = \sqrt{3J_2}$, $\kappa = \kappa_p$, J_2 is the second stress invariant of the stress deviatoric tensor, which is dominated by the shear stress along the shear band, and κ_p is uniaxial compressive peak strength. The foregoing consideration is frequently in use in limit equilibrium analysis of slope stability under undrained conditions.

6.2.2 Hyperbolic stress-strain curves

Based on two series of consolidated drained tests done at different consolidation pressures on specimens trimmed from stiff fissured clay, Lo (1972) pointed out that a progressive failure plane develops at or around the peak strength. The post-peak stress-strain curve is purely nominal and is a reflection of the localized shear stress-strain behavior of the failure zone. It was seen that the post-peak stress-strain curve decreases in strength much more, and converges to the residual strength at larger deformations. The extrapolation of test results shows that the post-peak nominal stress-strain curves are generally of the hyperbolic type. If the origin is now moved to peak point, the post-peak stress and strain refers to this new origin. It is mathematically given by:

$$S' = \frac{\varepsilon'}{a + b\varepsilon'}, \tag{6-4}$$

in which $S'=S/S_f$, S is shear stress at any instant. S_f is shear strength at peak point. $\varepsilon'=\varepsilon/\varepsilon_f$, ε denotes the shear strain corresponding to S. ε_f represents shear strain at peak point. a and b are material parameters. The yielding function of this hyperbolic strain softening model takes the same form of Von-Mises yielding model, as equation (6-3), but κ takes the form:

$$\kappa = \kappa_p\left(1 - \frac{\bar{\varepsilon}_p}{a + b\bar{\varepsilon}_p}\right), \tag{6-5}$$

where, $\bar{\varepsilon}_p$ is termed effective plastic strain, $\bar{\varepsilon}_p = \int d\bar{\varepsilon}_p$, $d\bar{\varepsilon}_p = \left(\frac{2}{3} de_{ij}^p de_{ij}^p\right)^{\frac{1}{2}}$, deviatoric plastic strain increment $de_{ij}^p = d\varepsilon_{ij}^p - d\varepsilon_{kk}^p \delta_{ij}/3$, $d\varepsilon_{ij}^p$ is plastic strain increment. Assume the following:

$$\bar{\varepsilon}^p|_{\kappa=\kappa_p} = 0, \quad \kappa|_{\bar{\varepsilon}_p=\infty} = \kappa_r, \tag{6-6}$$

and κ_r is uniaxial compressive residual strength. Parameters a, b in equation (6-5) could be derived by making use of above assumptions. They are:

$$b = \frac{1}{(1-\kappa_r/\kappa_p)}, \quad a = -\kappa_p / \left.\frac{\partial\kappa}{\partial\bar{\varepsilon}_p}\right|_{\bar{\varepsilon}_p=0}. \tag{6-7}$$

As illustrated in figure 6.1, $\frac{\kappa_p}{a}$ is the tangent of the initial slope of stress-strain curve at post-peak stage.

6.2.3 Hardening rule

Consistency condition is expressed as:

$$dF = \left\{\frac{\partial F}{\partial\sigma}\right\}^T \{d\sigma\} + \frac{\partial F}{\partial\kappa}\frac{\partial\kappa}{\partial\bar{\varepsilon}_p} d\bar{\varepsilon}_p = 0. \tag{6-8}$$

In this equation, the effective plastic strain increment, $d\bar{\varepsilon}_p$, needs to be calculated. The plastic deviatoric strain de_{ij}^p is:

$$de_{ij}^p = d\varepsilon_{ij}^p - d\varepsilon_{kk}^p \delta_{ij}/3$$

$$= \lambda\left(\frac{\partial G}{\partial\sigma_{ij}} - \frac{\partial G}{\partial\sigma_{kk}}\delta_{ij}/3\right), \tag{6-9}$$

$$de_{ij}^p \cdot de_{ij}^p = \lambda^2\left(\frac{\partial G}{\partial\sigma_{ij}}\frac{\partial G}{\partial\sigma_{ij}} - \frac{\partial G}{\partial\sigma_{kk}}\frac{\partial G}{\partial\sigma_{pp}}\frac{1}{3}\right). \tag{6-10}$$

Here, $d\bar{\varepsilon}_p$ is defined as:

$$d\bar{\varepsilon}_p = \sqrt{\frac{2}{3} de_{ij}^p \cdot de_{ij}^p} = \lambda\sqrt{\frac{2}{3}}\left(\frac{\partial G}{\partial\sigma_{ij}}\frac{\partial G}{\partial\sigma_{ij}} - \frac{\partial G}{\partial\sigma_{kk}}\frac{\partial G}{\partial\sigma_{pp}}\frac{1}{3}\right)^{\frac{1}{2}}$$

$$= \lambda \overline{Q}, \tag{6-11}$$

where, $\overline{Q} = \sqrt{\frac{2}{3}}\left(\frac{\partial G}{\partial \sigma_{ij}}\frac{\partial G}{\partial \sigma_{ij}} - \frac{\partial G}{\partial \sigma_{kk}}\frac{\partial G}{\partial \sigma_{pp}}\right)^{\frac{1}{2}}$.

$$\lambda = \frac{1}{H'}\left\{\frac{\partial F}{\partial \sigma}\right\}^T \{d\sigma\}, \quad d\bar{\varepsilon}_p = \lambda \overline{Q} \tag{6-12}$$

Substitute (6-12) into (6-8), and the result is:

$$H'\lambda + \frac{\partial F}{\partial \kappa}\frac{\partial \kappa}{\partial \bar{\varepsilon}_p}\overline{Q}\lambda = 0. \tag{6-13}$$

Then, H', the hardening modulus, is expressed as:

$$H' = -\frac{\partial F}{\partial \kappa}\frac{\partial \kappa}{\partial \bar{\varepsilon}_p}\overline{Q}. \tag{6-14}$$

Here, H' is equivalent to $-\left\{\frac{\partial F}{\partial \bar{\varepsilon}_p}\right\}^T \left\{\frac{\partial G}{\partial \sigma}\right\}$. Therefore:

$$\left\{\frac{\partial F}{\partial \bar{\varepsilon}_p}\right\}^T \left\{\frac{\partial G}{\partial \sigma}\right\} = \frac{\partial F}{\partial \kappa}\frac{\partial \kappa}{\partial \bar{\varepsilon}_p}\overline{Q}. \tag{6-15}$$

From the yielding function (6-3) and the expression for the yield stress after peak (6-5), the following results can be obtained:

$$\frac{\partial F}{\partial \kappa} = -1, \qquad \frac{\partial \kappa}{\partial \bar{\varepsilon}_p} = -a\kappa_p / (a + b\bar{\varepsilon}_p)^2. \tag{6-16}$$

Parameters a and b are determined from triaxial test results which are detailed by Chan (1986). In order to test the model, a triaxial test was analyzed, with E=3500 N/mm^2, ν=0.35, uniaxial compressive peak strength κ=60 N/mm^2, and a=10, b=2, which corresponds to the same load procedures as those in laboratory tests. Finally, the numerical solutions were compared with the analytical one which is based on uniformly

distributed stresses throughout the triaxial test. The curve of vertical normal stress versus axial strains from numerical analysis fits very well with the analytical solution (figure 6.2) except the deviation occurring at the end part of the curves. The reason is that much larger calculation steps for analytical method were used, which gave less accurate results. The very good fit verifies the correction of the coding work. Although this model is deduced from consolidated drained tests, it was successfully applied under undrained conditions (Alencar et al., 1988; Chen et al., 1990).

6.3 Cross-isotropic elastic model with special Mohr-Coulomb yielding criterion

The conventional Mohr-Coulomb model is still one of the most popular models for geological materials. In this study, it is also utilized to describe yielding and failure of shear band materials. However, in general, the deformation properties of the materials inside the shear band at post-localization stages are different from those of the same material. The validity of the conventional Mohr-Coulomb model might need analysis and investigation when it is specialized for shear band behavior. Upon the inception of shear band localization, high strain gradients would occur across the shear band which is bounded by two discontinuity surfaces based on the bifurcation theories. The discontinuity surfaces are consistent with shear band orientation. Yielding and failure would only occur along the direction parallel to the shear band orientation (Chan et al., 1997).

In the numerical simulation of the propagation of shear bands, one important issue has emerged. With the large shear deformation, large shear strains and relatively small

normal strains along the shear band would develop. Roscoe (1970) proposed that in the directions parallel to the shear band, there is no extension of the shear band material. Furthermore, the deformation properties along the shear band are physically altered due to further compression of the materials within the band in the direction normal to the band. As a consequence, shear bands would exhibit different deformation properties in these two directions. The normal stresses along the shear band should be dramatically smaller than the normal stresses across the band.

6.3.1 Cross-isotropic elastic model

As the first step of the research, an elastic cross-isotropic model is used to simulate shear band deformation. The usual situation calls for the x-o-t plane of isotropy to be "horizontal" and the n axis of the anisotropic direction to be "vertical" under local coordinate system x-o-t-n, as shown in figure 6.3. The n axis refers to the direction normal to the shear band, and the t axis refers to the tangential direction of the shear band. For plane strain problems, there is no deformation in the x direction. For the cross-isotropic elastic model, the stress-strain relationship is given by Desai and Christian (1977) as:

$$\begin{Bmatrix} \sigma_{n} \\ \sigma_{nn} \\ \tau_{tn} \\ \sigma_{xx} \\ \tau_{xn} \\ \tau_{xt} \end{Bmatrix} = [C] \begin{Bmatrix} \varepsilon_{n} \\ \varepsilon_{nn} \\ \gamma_{tn} \\ \varepsilon_{xx} \\ \gamma_{xn} \\ \gamma_{xt} \end{Bmatrix}, \qquad (6\text{-}17)$$

[C] is a 6x6 constitutive matrix whose components are given by:

$$C_{11} = C_{44} = A(\frac{E_{tt}}{E_{nn}} - \nu_{nt}^2);$$

$$C_{22} = A(1 - \nu_{nt}^2);$$

$$C_{14} = C_{41} = C_{11} - C_{66};$$

$$C_{12} = C_{21} = C_{42} = C_{24} = A\nu_{nt}(1 + \nu_{tt});$$

$$C_{33} = C_{55} = 2G_{nt};$$

$$C_{66} = \frac{E_{tt}}{1 + \nu_{tt}} = 2G_{tt};$$

$$\text{where, } A = \frac{E_{tt}}{(1 + \nu_{tt})[E_{tt} / E_{nn}(1 - \nu_{tt}) - 2\nu_{nt}^2]};$$

$$\text{All other } C_{ij} = 0;$$

E_{tt} and E_{nn} are interpreted as the Young's moduli for loading in the tangential plane (xot) and along the normal axis n, respectively. ν_{tt} is the Poisson's ratio relating loading along one axis in the tangential plane to strains along the other axis in the plane. The relationship between extensional strains in the tangential plane and normal loading, or between normal extensional strains and tangential loading is controlled by the other Poisson's Ratios ν_{tn} or ν_{nt}. G_{nt} relates shear stresses out of the tangential plane to shear strains out of the tangential plane (Desai and Christian, 1977).

6.3.2 Special Mohr-Coulomb model

As described in the beginning of this section, tangential shearing along the shear band is the preferred direction of yielding due to induced anisotropy. This implies that the general Mohr-Coulomb criterion is not applicable to shear band modeling. Yielding along the tangent direction of shear bands should be prescribed in the yielding criterion. Based on the phenomena noted above, a special Mohr-Coulomb yielding criterion is stated as follows:

$$f = |\tau_n| + \sigma_n \tan\phi - c \tag{6-18}$$

This is really the same expression as the normal Mohr-Coulomb model except that it is applied along the band. Where τ_n is the shear stress along the preferred shearing direction, i.e. tangent direction of a shear band; σ_n is the normal stress across the shear band, whereas ϕ is the friction angle of the soil inside the band along the band. The corresponding derivatives with respect to the stress components σ_{ij} under the XYZ coordinate system are:

$$\left\{ \frac{\partial f}{\partial \sigma_{ij}} \right\} = \begin{Bmatrix} \tan\phi \dfrac{\partial}{\partial \sigma_{ij}} \\ \dfrac{\partial}{\partial \sigma_{ij}} \end{Bmatrix}^T \begin{Bmatrix} \sigma_n \\ |\tau_n| \end{Bmatrix}. \tag{6-19}$$

For plane problems, the derivatives are expressed as:

$$\begin{Bmatrix} \dfrac{\partial f}{\partial \sigma_x} \\ \dfrac{\partial f}{\partial \sigma_y} \\ \dfrac{\partial f}{\partial \tau_{xy}} \end{Bmatrix} = \begin{Bmatrix} \sin\alpha\cos\alpha + \sin^2\alpha\tan\phi \\ -\sin\alpha\cos\alpha + \cos^2\alpha\tan\phi \\ \cos^2\alpha - \sin^2\alpha - 2\sin\alpha\cos\alpha\tan\phi \end{Bmatrix} \quad \text{when } \tau_n > 0, \tag{6-20}$$

or as:

$$\begin{Bmatrix} \dfrac{\partial f}{\partial \sigma_x} \\ \dfrac{\partial f}{\partial \sigma_y} \\ \dfrac{\partial f}{\partial \tau_{xy}} \end{Bmatrix} = \begin{Bmatrix} -\sin\alpha\cos\alpha + \sin^2\alpha\tan\phi \\ \sin\alpha\cos\alpha + \cos^2\alpha\tan\phi \\ -\cos^2\alpha + \sin^2\alpha - 2\sin\alpha\cos\alpha\tan\phi \end{Bmatrix} \quad \text{when } \tau_n < 0. \tag{6-21}$$

Here, α is the orientation of a shear band to the horizontal direction, and ϕ is the frictional angle of band material.

6.3.3 Eigenvalue analysis of the constitutive matrix

In order to check the validity of the cross-isotropic elastic model with special Mohr-Coulomb yielding criterion, an eigenvalue analysis is employed to give a measure of the strain energy contents associated with various deformation modes. The number of rigid body modes of an element is equal to the number of element degrees of freedom minus the number of element straining modes (e.g. a four-noded plane strain element has 3 straining modes). For 2-D problems, the number of rigid body modes is equal to 3. The individual straining modes, rigid body modes for more complex elements can be studied effectively by solving eigenproblem $[K]\{\phi_i\}=\lambda_i\{\phi_i\}$ (Bathe, 1982), where [K] is the stiffness matrix of an element, $\{\phi_i\}$ is the ith eigenvector, while λ_i is the corresponding eigenvalue, λ_i is directly related to the energy of deformation of the element for the corresponding displacement mode. The first analysis is performed on a single element with a side length of 5 unit under plane strain condition for elastic and plastic cases, as shown in figure 6.4 (b). To obtain the results from the cross isotropic model which can be compared with isotropic model, the deformation parameters E_n, E_s and ν_n, ν_s are set to be the same values, respectively, i.e. $E_n=E_s=10$, $\nu_n=\nu_s=0.3$, $G=E/(1+\nu)/2=3.846$, $\phi=30^\circ$ and $c=0$. The bedding angle which is the preferred direction for yielding is taken to be 50° with respect to the horizontal direction. The yielding and failure will occur along the bedding plane. In step one, the element were subjected to confining pressure of p=5 units. Between step two and ten, vertical displacement increments of $\Delta v=2$ were applied at the top surface. In step 7, all the Gaussian points of the 4 elements went into a yielding state, at a vertical normal stress of 16.37 units, which

was exactly the same as the analytical calculation using Mohr circle as shown in figure 6.5. The elastic eigenmodes have shown explicitly the three rigid body modes with zero eigenvalues, two 'shear' and one 'volumetric' modes as shown in figure 6.6.

Table 6.1 (a) Eigenvalue analysis for elastic constitutive matrix $[C]_e$ and elastic- plastic matrix $[C]_{ep}$ for $\alpha=50°$

State	Eigenvalue	Eigenvectors		
		ε_x	ε_y	γ_{xy}
Elastic (step 1)	3.85	0.000	0.000	1.000
	7.69	-0.707	0.707	0.000
Plastic (step 10)	19.20	0.707	0.707	0.000
	5.17 e-13	-0. 871	0.266	0.414
	4.24	-0.371	0.197	-0.907
	14.70	0.323	0.944	0.0730

Table 6.1 (b) Eigenvalue analysis for elastic constitutive matrix $[C]_e$ and elastic- plastic matrix $[C]_{ep}$ for $\alpha=0°$

State	Eigenvalue	Eigenvectors		
		ε_x	ε_y	γ_{xy}
Elastic (step 1)	3.85	0.000	0.000	1.000
	7.69	-0.707	0.707	0.000
Plastic (step 10)	19.20	0.707	0.707	0.000
	2.89 e-13	0.431e-06	0.0872	0.996
	0.766	-0.701	0.710	-0.062
	18.9	0.713	0.699	-0.061

For plastic analysis, there are four eigenmodes with zero eigenvalue values. Three of them are rigid body modes, and one is a 'shear' mode. All the eigenmodes for constitutive matrices and stiffness matrices for a single element are tabled and depicted in table 6.1 (a), as shown in figures 6.6 and 6.7. For comparison, a second eigenvalue analysis was carried out as shown in figure 6.4 (b). In this case, vertical pressure was

applied at the top of the structure with weak directions lying horizontally (α=0°). Boundary conditions are shown in figure 6.4 (b). From step 2 to step 10, the top surface is subjected to horizontal shear displacements. The loading condition is used to simulate a pure shear state. Material parameters are taken to be the same as those in the first analysis except that the friction angle is equal to 5°. The eigenvalue analyses have shown that the proposed model is reasonable and is able to meet theoretical and practical requirements. The eigenmodes and eigenvalues obtained from the analyses have shown that the cross isotropic elastic model with special Mohr-Coulomb yielding criterion is an acceptable model in terms of continuum mechanics. It correctly reflect all the deformation modes every constitutive model should have.

6.4 Application of Modified Cam-Clay model

Kinematic propagation of a shear band at the post-localization stage causes variations of normal stresses and mobilization of shear strengths along a shear band. The propagation would lead to a change in shear band thickness. The decrease in thickness unavoidably brings about an increase in the modulus of deformation, especially in the direction normal to the band. In this study, by referring to the behavior of joints under a normal load (Goodman and John, 1977, Carol et al., 1986), deformation modulus across the band is assumed to increase exponentially to an infinite value with a decrease in its thickness to a minimum value t_{min} as depicted in figure 6.8. As such, the overlapping problems of the shear band never physically occur. The increase in stiffness can be approximately characterized by using the Modified Cam-Clay model in which an increase in mean stress results in an increase in bulk modulus regardless whether the material is in

an elastic or a plastic state. Therefore, the simulation of the kinematic development of a shear band can be improved using the Modified Cam-Clay model to alleviate the overlapping problems discussed earlier.

In this model, bulk modulus K increases with mean stress P. Since the shear modulus can be deduced from the bulk modulus with an assumed value of Poisson's ratio, this would result in the same functional dependent on the shear modulus as the bulk modulus. Alternatively, shear modulus can be specified independently.

6.4.1 Description of the yielding function

The modified Cam-clay yield locus can be expressed in the following form:

$$q^2 + M^2 P'^2 = M^2 P' P'_c, \tag{6-22}$$

which can be rewritten as:

$$\frac{q^2}{M^2} + P'^2 = P' P'_c, \tag{6-23}$$

where, P' is mean stress, which equals to $P'=(\sigma'_x + \sigma'_y + \sigma'_z)/3$, P'_c is mean stress to indicate the size of the yielding surface, $q = \sqrt{3J_2}$, J_2 is the second stress invariant; M is a material parameter which is equal to the slope of the critical state line in P'-q plane. Equation 6-23 can be normalized is normalized by dividing q, P' and P'_c by $\frac{1}{2}P'_c$. The result is:

$$\frac{4q^2}{M^2 P'^2_c} + \frac{4P'^2}{P'^2_c} = \frac{4P'}{P'_c}. \tag{6-24}$$

So, the yielding function can be defined as:

$$f = \frac{4}{M^2 P'^2_c} + \frac{4P'^2}{P'^2_c} - \frac{4P'}{P'_c} = 0. \qquad (6\text{-}25)$$

In Cam-Clay models, it is always assumed that the soil obeys the normality condition. Therefore, the plastic potential is automatically given by the same family of yield loci, i.e. f≡g.

6.4.2 Evaluation of plastic deformation

In the discussion of the MCC model, the consistency condition is rewritten as:

$$df = \left\{\frac{\partial f}{\partial \sigma}\right\}^T \{d\sigma\} + \frac{\partial f}{\partial p'_c}\frac{\partial p'_c}{\partial \varepsilon^p_v} d\varepsilon^p_v = 0, \qquad (6\text{-}26)$$

where, ε^p_v is plastic volumetric strain. Based on the flow rule, $d\varepsilon^p_v$ is expressed as:

$$d\varepsilon^p_v = \lambda \frac{\partial g}{\partial \sigma'_{ii}} = \lambda\left(\frac{\partial f}{\partial p'}\left(\frac{\partial p'}{\partial \sigma'_{ii}}\right) + \frac{\partial f}{\partial q}\left(\frac{\partial q}{\partial \sigma'_{ii}}\right)\right) = \lambda A_{ii}, \qquad (6\text{-}27)$$

in which, λ is a positive scalar of proportionality, $A_{ii} = \frac{\partial f}{\partial \sigma'_x} + \frac{\partial f}{\partial \sigma'_y} + \frac{\partial f}{\partial \sigma'_z}$. Then, the plastic matrix is written as follows:

$$[C]_p = \frac{[C_e]\left\{\frac{\partial f}{\partial \sigma}\right\}\left\{\frac{\partial f}{\partial \sigma}\right\}^T [C_e]}{\left\{\frac{\partial f}{\partial \sigma}\right\}^T [C_e]\left\{\frac{\partial f}{\partial \sigma}\right\} - \frac{\partial f}{\partial p'_c}\frac{\partial p'_c}{\partial \varepsilon^p_v} A_{ii}}. \qquad (6\text{-}28)$$

For the convenience of simplicity, all the derivatives involved in the evaluation of $[C_p]$ are derived and listed as follows:

$$\frac{\partial f}{\partial P'} = \frac{8P'}{P'^2_c} - \frac{4}{P'_c}, \quad \frac{\partial f}{\partial q} = \frac{8q}{M^2 P'^2_c}. \qquad (6\text{-}29)$$

$$\frac{\partial q}{\partial \sigma'_x} = \frac{1}{2q}(2\sigma'_x - \sigma'_y - \sigma'_z), \tag{6-30}$$

$$\frac{\partial q}{\partial \sigma'_y} = \frac{1}{2q}(2\sigma'_y - \sigma'_x - \sigma'_z), \tag{6-31}$$

$$\frac{\partial q}{\partial \sigma'_z} = \frac{1}{2q}(2\sigma'_z - \sigma'_x - \sigma'_y). \tag{6-32}$$

$$\frac{\partial f}{\partial \sigma'_x} = \frac{\partial f}{\partial P'}\frac{\partial P'}{\partial \sigma'_x} + \frac{\partial f}{\partial q}\frac{\partial q}{\partial \sigma'_x}$$

$$= -\frac{1}{3}\left(\frac{8P'}{P'^2_c} - \frac{4}{P'_c}\right) + \frac{12}{M^2 P'^2_c}(\sigma'_x - P'), \tag{6-33}$$

$$\frac{\partial f}{\partial \sigma'_y} = -\frac{1}{3}\left(\frac{8P'}{P'^2_c} - \frac{4}{P'_c}\right) + \frac{12}{M^2 P'^2_c}(\sigma'_y - P'), \tag{6-34}$$

$$\frac{\partial f}{\partial \sigma'_z} = -\frac{1}{3}\left(\frac{8P'}{P'^2_c} - \frac{4}{P'_c}\right) + \frac{12}{M^2 P'^2_c}(\sigma'_z - P'). \tag{6-35}$$

$$\frac{\partial q}{\partial \tau_{xy}} = \frac{3}{q}\tau_{xy}. \tag{6-36}$$

$$\frac{\partial f}{\partial P'_c} = -\frac{8q^2}{M^2 P'^3_c} - \frac{8P'^2}{P'^3_c} + \frac{4P'}{P'^2_c}. \tag{6-37}$$

$$\frac{\partial P'_c}{\partial \varepsilon^p_v} = \frac{P'_c(1+e)}{\lambda - \kappa}. \tag{6-38}$$

$$\frac{\partial f}{\partial \varepsilon^p_v} = \frac{\partial f}{\partial P'_c}\frac{\partial P'_c}{\partial \varepsilon^p_v} = \left(-\frac{8q^2}{M^2 P'^3_c} - \frac{8P'^2}{P'^3_c} + \frac{4P'}{P'^2_c}\right)\frac{P'_c(1+e)}{\lambda - \kappa}. \tag{6-39}$$

In above, e is the void ratio of the soil, λ and κ are the compression and swelling indexes, respectively. Suppose that a shear band lies along a line of zero extension. Then, the change in shear band thickness under plane strain condition would be:

$$\Delta t = -\Delta\varepsilon_v t, \tag{6-40}$$

where volume strain increment $\Delta\varepsilon_v$ is expressed as:

$$\Delta\varepsilon_v = \kappa\frac{\delta p'}{(1+e)p'} + (\lambda-\kappa)\frac{\delta p_c'}{(1+e)p_c'}. \tag{6-41}$$

Therefore, the thickness at the current load step is :

$$t_{cur} = \left(1-\kappa\frac{\delta p'}{(1+e)p'} - (\lambda-\kappa)\frac{\delta p_c'}{(1+e)p_c'}\right)t, \tag{6-42}$$

in which t denotes the thickness at the last load step, $\delta p'$ and $\delta p_c'$ represent changes of p' and p_c' between the current load step and the last load step. The relationship between the thickness and the mean stress p' in terms of equation (6-42) is illustrated in figure 6.8 (b). To check if MCC model is loaded properly, the program was used to analyze a triaxial test of a normally consolidated clay using the following parameters: M=1.0; compression index λ=0.174; unloading index κ=0.026; initial void ratio=1.221; initial yielding locus P_0=5 N/mm^2; initial Young's modulus E_0=369.0 N/mm^2; initial Poisson ratio ν=0.3. During the first 30 steps, confining pressure was applied until p=30 N/mm^2, then vertical displacement was applied on the top surface until step 90, with displacement increments of 0.5 mm per step. The results of the computer simulation and analytical calculation are shown in figure 6.9. It is seen that the numerical results agree well with the analytical calculation which verified that MCC model has been implemented correctly. Here, MCC model is used for the homogeneous material. However, the parameters are hard to select for shear band materials if MCC is used. If the parameters are not properly determined, the results for shear band analysis are reliable. This is the point some unsuccessful examples in this research have verified.

6.5 Kinematics treatment of the overlapping problem

The application of the Modified Cam-Clay model implies that physically there should be no overlapping problems because the deformation properties of the shear band materials changes with the band thickness. However, in the finite element analyses, deformation properties may not be updated frequently enough. Sometimes, the global stiffness matrix is not changed in every load step. As such, numerically, the overlapping problems (penetration) might still occur when the thickness is very small. On the other hand, there are still some possibilities that shear band elements can penetrate the soil elements even though the stiffness of shear bands is recalculated during iterations. As shown in figure 6.10, in the triangular shear band element, nodal point M on one side of the shear band goes over boundary segment PQ on the other side to point M'. This means that penetration occurs. Points M, P and Q can be separated by applying displacements on these three points to allow element MPQ to maintain a minimum thickness t_{min}. Take this element as an example to illustrate the scheme. First, the penetration index I_p is defined as A/t_{min} and A is the penetration value. At the end of load step (i+1), penetration value A is calculated. For the quadrilateral element, say element PRXY in figure 6.10, the penetration values for nodal points R and X should be calculated. In triangular element PMQ, the penetration value A is calculated by:

$$A = \left[\left(u_n^i\right)_M + \left(\Delta u_n^{i+1}\right)_M + t - \left(N_P\left(u_n^i\right)_P + N_Q\left(u_n^i\right)_Q\right) - \left(N_P\left(\Delta u_n^{i+1}\right)_P + N_Q\left(\Delta u_n^{i+1}\right)_Q\right)\right], \qquad (6\text{-}43)$$

where $\left(u_n^i\right)_M$ denotes the displacement normal to the shear band of node M at load step i, and $\left(\Delta u_n^{i+1}\right)_M$ is the normal displacement increment of node M from step i to (i+1) before penetration occurs. Here t represents the thickness of the shear band; N_p=1-β, N_q=β, and β=L_{M_1P}/L_{PQ}, L_{M_1P} is the length of boundary segment M_1P, etc.. If I_p is less than 1, a kinematic separation will be performed on point M from P and Q. Assume $\alpha\left(\Delta u_n^{i+1}\right)_M$, $\alpha\left(\Delta u_n^{i+1}\right)_P$, and $\alpha\left(\Delta u_n^{i+1}\right)_Q$ are displacement increments to be restored for step (i+1). From compatibility consideration, we know that:

$$\left(\left(u_n\right)_M^i+\left(\Delta u_n^{i+1}\right)_M-\alpha\left(\Delta u_n^{i+1}\right)_M\right)+t-\left(N_P\left(u_n^i\right)_P+N_p\left(\Delta u_n^{i+1}\right)_P+\right.$$

$$\left.+N_Q\left(u_n^i\right)_Q+N_Q\left(\Delta u_n^{i+1}\right)_Q-\alpha\left(N_P\left(\Delta u_n^{i+1}\right)_P+N_Q\left(\Delta u_n^{i+1}\right)_Q\right)\right)=t_{min}. \quad (6\text{-}44)$$

Rearrange the above equation, the following is obtained:

$$\alpha=1-\frac{t_{min}-t-\left\{\left(u_n\right)_M^i-\left(N_P\left(u_n^i\right)_P+N_Q\left(u_n^i\right)_Q\right)\right\}}{\left(\Delta u_n^{i+1}\right)_M-\left(N_P\left(\Delta u_n^{i+1}\right)_P+N_Q\left(\Delta u_n^{i+1}\right)_Q\right)}. \quad (6\text{-}45)$$

Then, it is possible to evaluate the amount by which the computed penetration is suppressed to establish the minimum thickness h_{min}:

Nodal point M $\alpha\left(\Delta u_n^{i+1}\right)_M$, (6-46)

Nodal point P $\alpha N_P\left(N_P\left(\Delta u_n^{i+1}\right)_P+N_Q\left(\Delta u_n^{i+1}\right)_Q\right)$. (6-47)

Nodal point Q $\alpha N_Q\left(N_P\left(\Delta u_n^{i+1}\right)_P+N_Q\left(\Delta u_n^{i+1}\right)_Q\right)$. (6-48)

In numerical analysis, there are two ways to eliminate the penetration, which are described below.

6.5.1 Direct modification of nodal displacements

Once penetration is detected in one element after displacements calculation, the displacements for the element will be applied to maintain a minimum thickness h_{min} in stresses calculating. From equation (6-43), the displacement increments on nodal points M, P and Q should be:

Nodal point M $$\left(\Delta u_n^{i+1}\right)_M - \alpha\left(\Delta u_n^{i+1}\right)_M, \qquad (6\text{-}49)$$

Nodal point P $$\left(\Delta u_n^{i+1}\right)_P - \alpha\left(\Delta u_n^{i+1}\right)_P, \qquad (6\text{-}50)$$

Nodal point Q $$\left(\Delta u_n^{i+1}\right)_Q - \alpha\left(\Delta u_n^{i+1}\right)_Q. \qquad (6\text{-}51)$$

The stiffness of the element would be updated based on the new stress state. Then new iteration would be carried out with the unbalanced forces caused by the new displacement increment shown above. The iteration process continues until the unbalanced forces become very small. Furthermore, the penetration index I_p will be calculated if it is still less than 1. The above procedures will be repeated until the penetration index is greater than or close to 1.

6.5.2 Application of correctional forces due to the penetration

With the restored displacement increments (equations 6-49, 6-50 and 6-51), an equivalent correction load vector $\{\Delta R\}$ can be calculated as follows:

$$\{\Delta R\} = \int_{\Delta MPQ} [B]^T [C^i]_{ep} [B] \{\Delta u_n^{res}\} dV. \qquad (6\text{-}52)$$

{ΔR} is applied on the element. Application of {ΔR} is repeated for all band elements in which penetrations occur. Then iterations are performed with the corrected load, which is called the "first layer" iteration. It is then followed by updating local stiffness based on new stress state, especially for the shear band elements in which penetrations occur. After that, the virtual correction loads are removed. Sequentially, a "second layer" iterative analysis is carried out for the unbalanced nodal forces due to the removal of correction loads. These two layers of iterations are alternately conducted until the two types of loads converge to within the tolerable limits. In the biaxial test in which two shear bands at different orientations were specified, the second method was used. It played a great role in the prevention of penetrations. Since cross-isotropic elastic model with special Mohr-Coulomb yielding criterion was used, no penetration has occurred.

6.6 Concluding remarks

Different constitutive relations, such as Von-Mises with hyperbolic softening model, the Modified Cam-Clay models are used to simulate the mechanical properties of the materials inside the shear band. To reflect the induced anisotropy and non-homogeneity of the shear band materials, a cross-isotropic elastic model with special Mohr-Coulomb yielding criterion is proposed. In this model, different deformation properties along and across the shear band are taken into account. Yielding only occurs along a prescribed direction, specifically, along the shear band. This model has been used in several examples. The cross isotropic elastic model with special Mohr-Coulomb yielding criterion has significantly alleviated the numerical overlapping problem. Cam-

clay model is also a good model to alleviate the overlapping problem, but the corresponding parameters are hard to determine for shear band materials. In the end of this chapter, a kinematics treatment has been proposed to eliminates the overlapping problem.

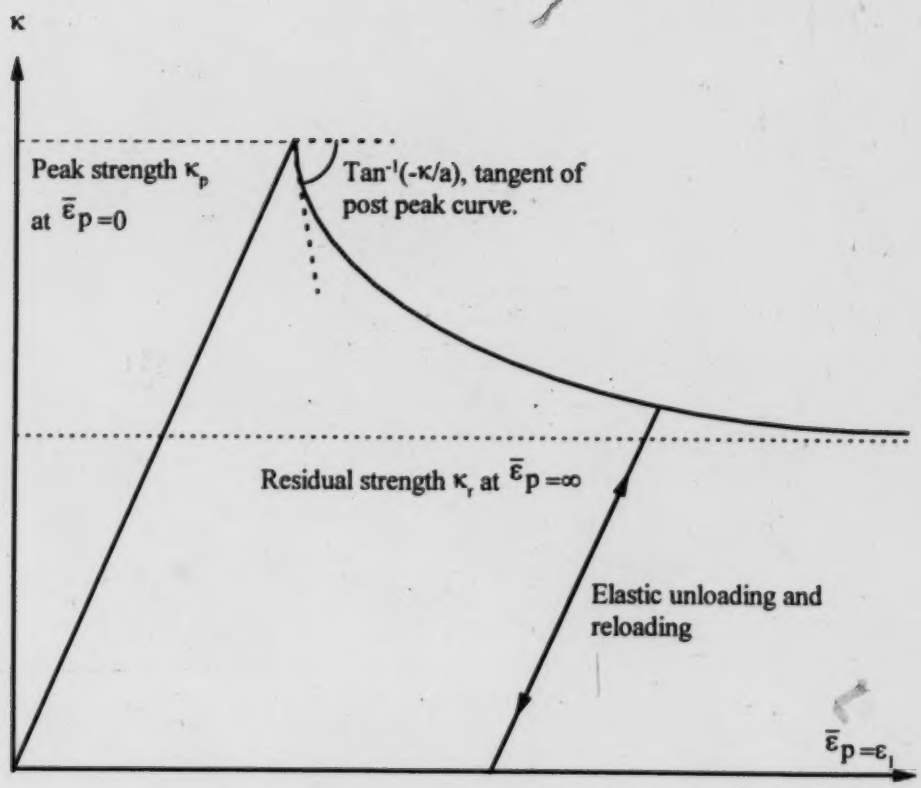

Figure 6.1 Stress-strain relationship for the hyperbolic strain softening model

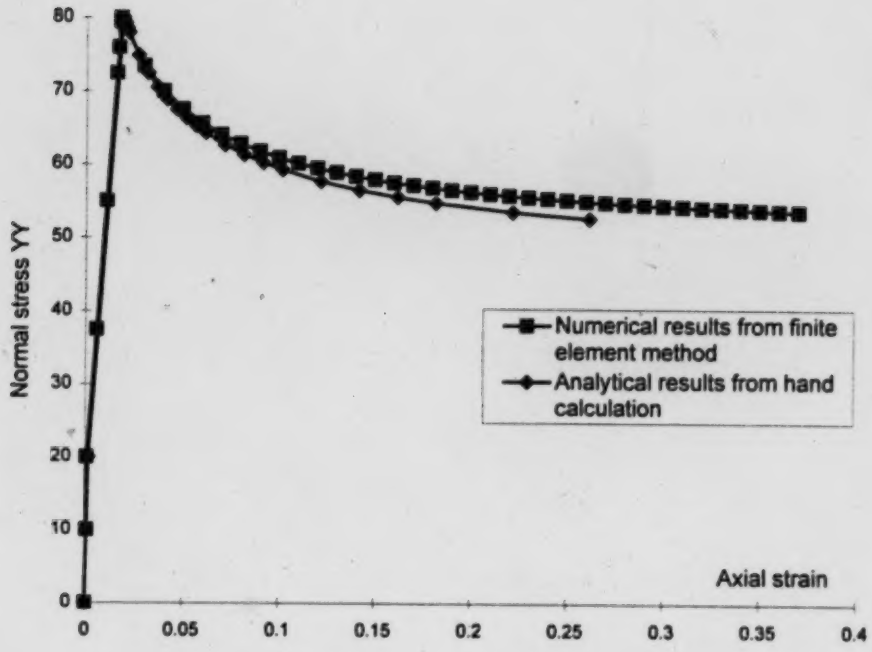

Figure 6.2 Relationship between vertical normal stress and axial strain under Von-Mises yielding criterion with hyperbolic softening

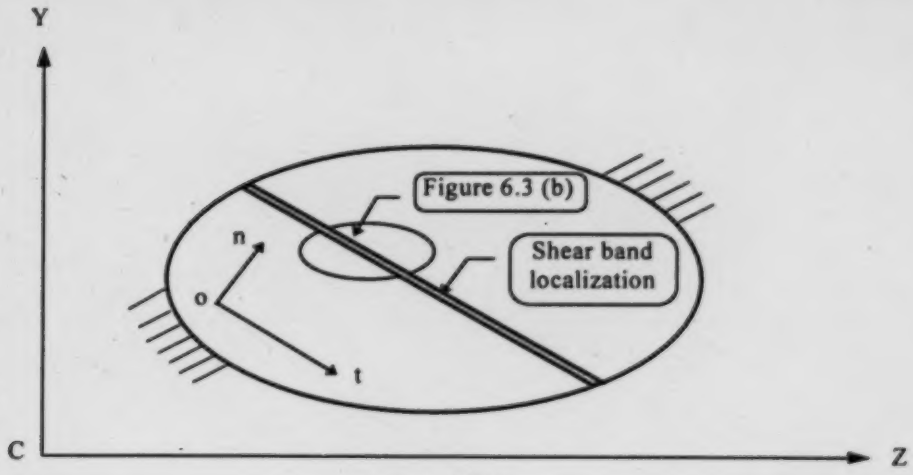

Figure 6.3 (a)

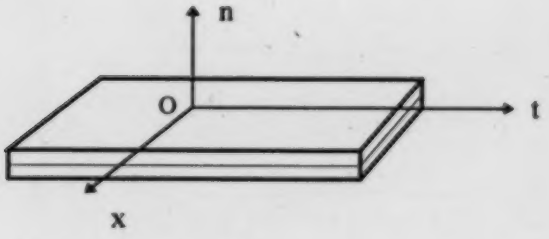

Figure 6.3 (b)

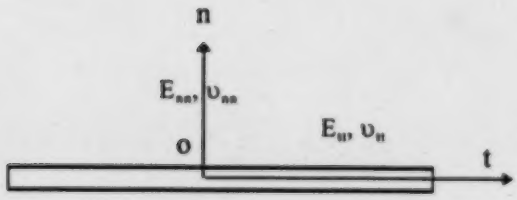

Figure 6.3 (c)

Figure 6.3 Cross-isotropic description for shear band element, (a) shear band under global coordinate system, (b) shear band under local 3-D coordinate system, (c) different deformation properties in the cross directions

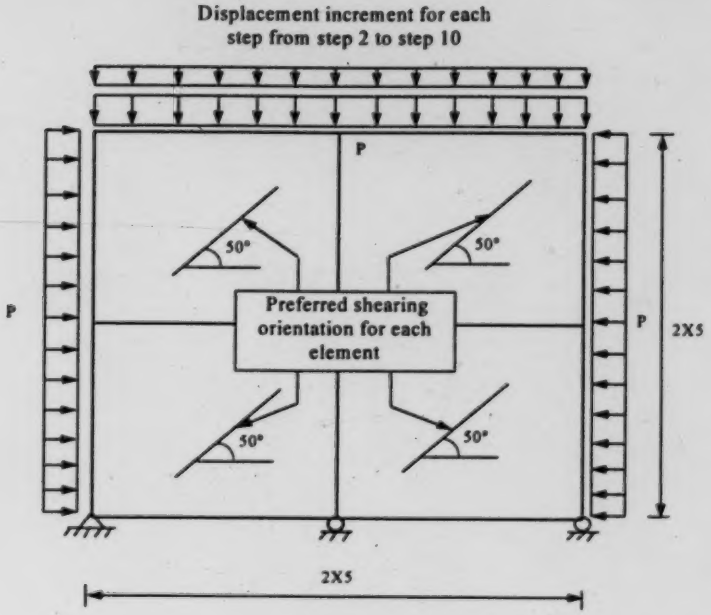

Figure 6.4 (a)

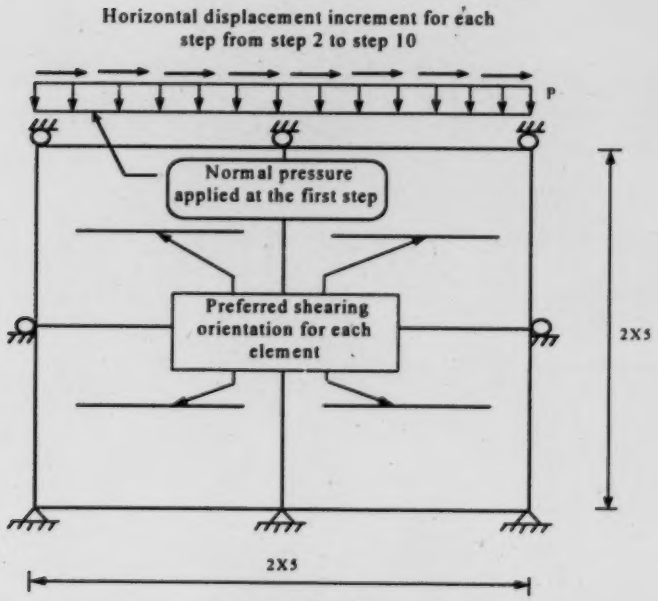

Figure 6.4 (b)

Figure 6.4 (a) The structure for eigenvalue analysis with bending angle of 50°, (b) the simple structure for eigenvalue analysis with bedding angle of 0°

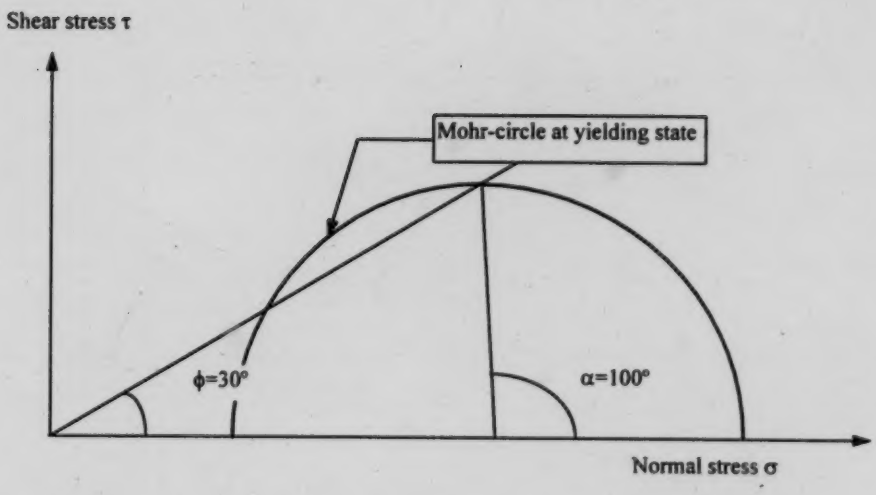

Figure 6.5 Stress state at initial stage of the single element under the specific Mohr-Coulomb yielding criterion

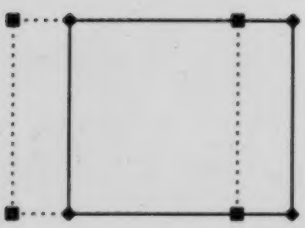

$\lambda_1=0$

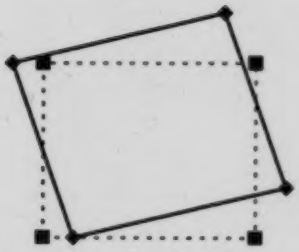

$\lambda_2=0$

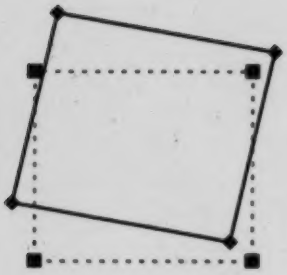

$\lambda_3=0$

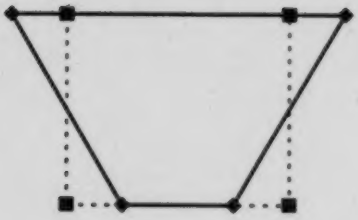

$\lambda_4=5.77$

Figure 6.6 (a)

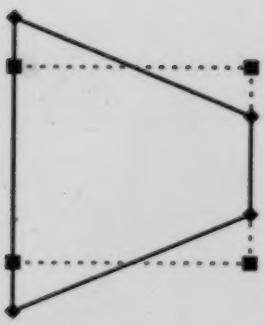

λ_5=5.77

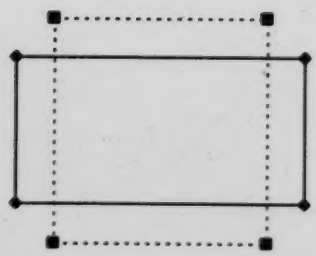

λ_6=7.69

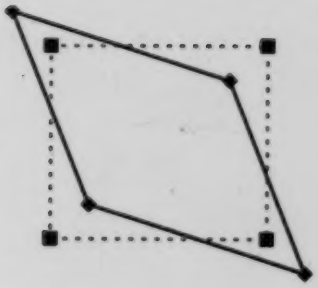

λ_7=7.69

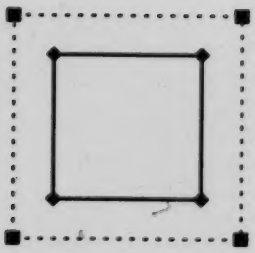

λ_8=19.2

Figure 6.6 (b)

Figure 6.6 (a) and (b) Mode shapes of 4-node rectangular elements for elastic analysis with bedding angle equal to 50°

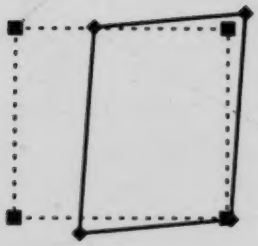

$\lambda_1=0$

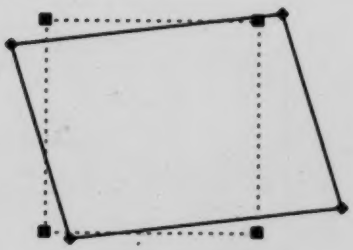

$\lambda_2=0$

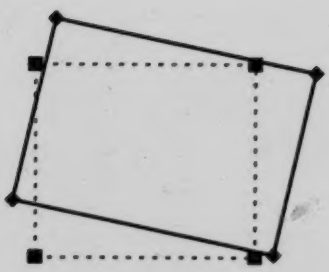

$\lambda_3=0$

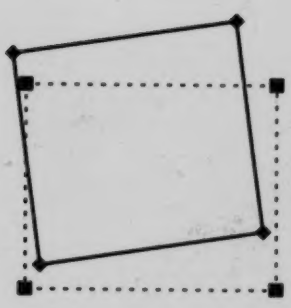

$\lambda_4=0$

Figure 6.7 (a)

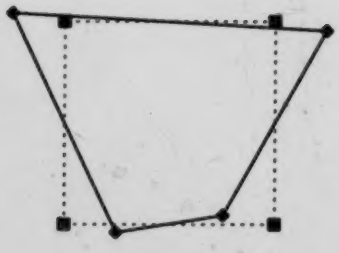

λ_5=1.78

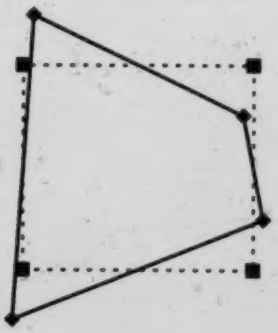

λ_6=5.72

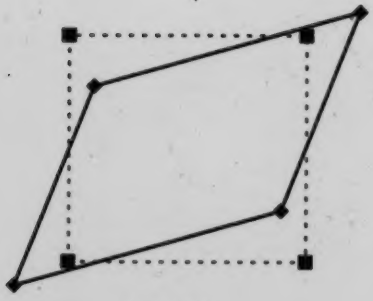

λ_7=7.69

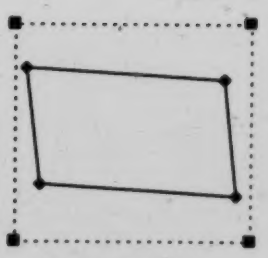

λ_8=14.8

Figure 6.7 (b)

Figure 6.7 (a) and (b) Mode shapes of a 4-node rectangular element for elasto-plastic stiffness with bedding angle equal to 50°

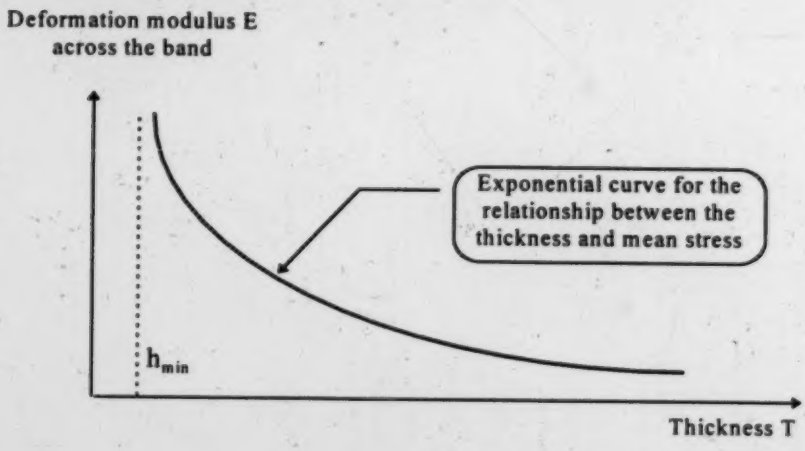

Figure 6.8 (a)

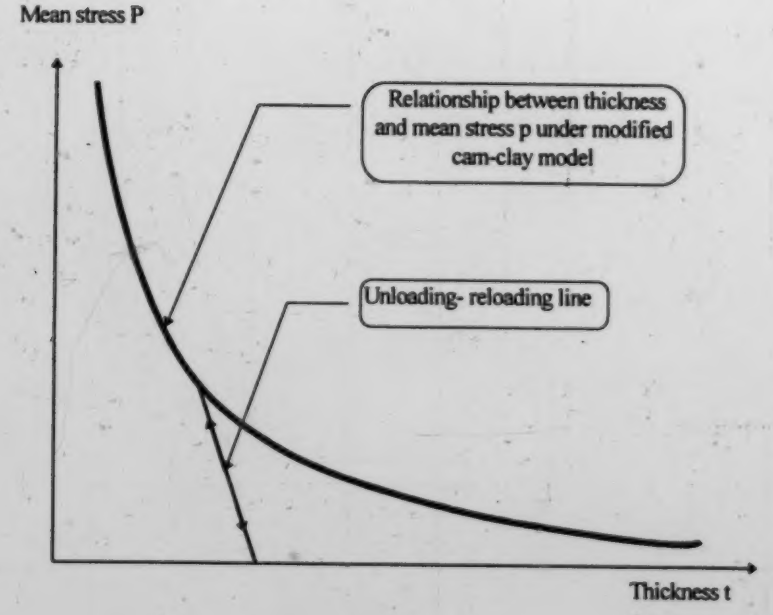

Figure 6.8 (b)

Figure 6.8 The relationship between the thickness of a shear band and mean stress P, (a) assumed mean stress vs. thickness t curve based on the existing results on rock joints, (b) mean stress vs. thickness curve under modified cam-clay model

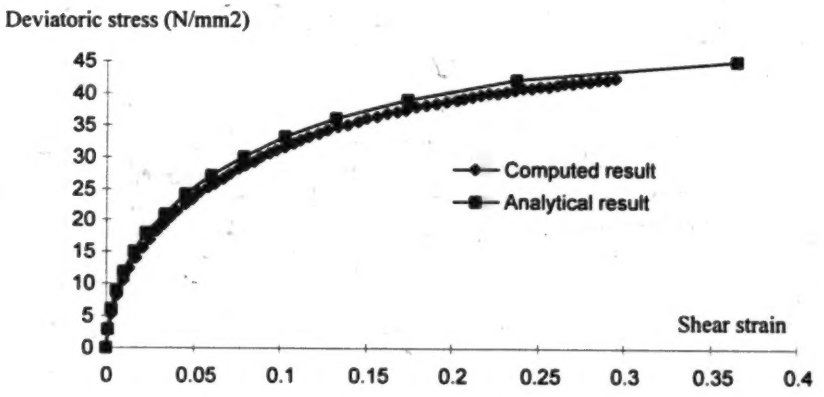

Figure 6. 9 (a)

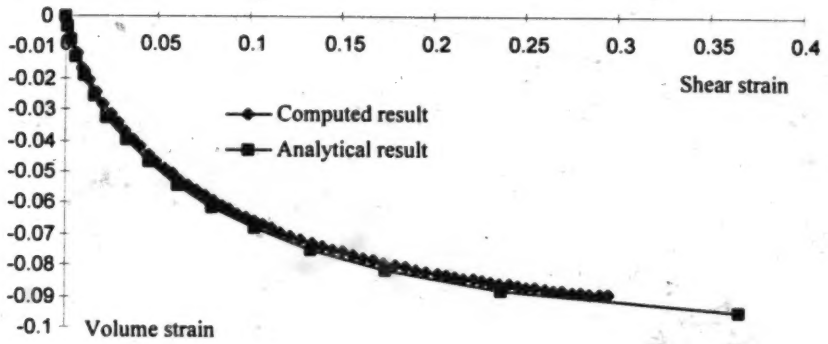

Figure 6. 9 (b)

Figure 6. 9 Comparison of numerical results and hypothetical data, (a) deviatoric stress versus shear strain, (b) volumetric strain versus shear strain

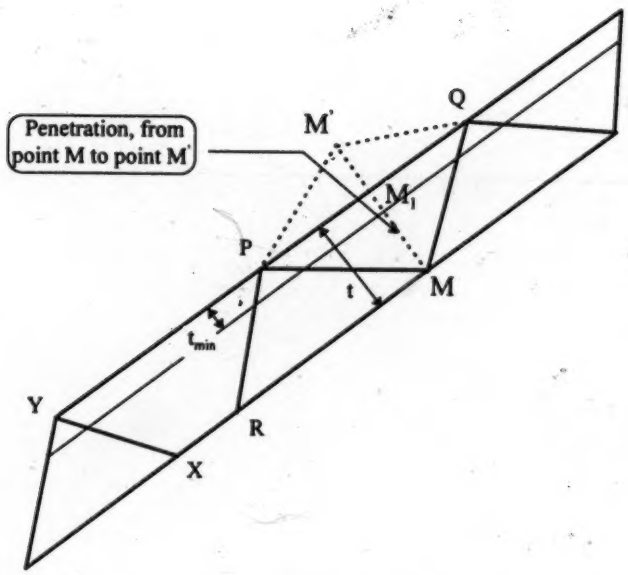

Figure 6.10 Pathological penetration of shear band element

Chapter 7

The applications of contact band element approach to interfaces and joints with large shear deformations

7.1 Introduction

Various finite element techniques for analyzing an interface have been proposed. They can be basically divided into two main categories. The first category contains the nodal or point interface elements that connect the normal solid elements with each other using discrete springs (Beer, 1985), such as the special joint finite elements developed by Goodman (1968). The second category models the joint/interface using a quasi-continuum element with small thickness, i.e. by using, for example, the continuous interface element with a defined thickness. Zienkiewicz et al. (1970) proposed a solid element used as an interface element. The concept of a thin element was developed by Desai et al. (1984). Many analysts reported numerical problems with zero thickness interfaces, and joint elements, both of which frequently lead to a fluctuation of stresses along the discontinuity surface. It is hard to get constant and stable stresses in the interface elements (Day and Potts, 1994). Ill-conditioning of interface element stiffness matrix due to large off-diagonal terms causes a loss of accuracy (Wilson, 1977). The idea of using continuous interface elements with a certain thickness based on continuum mechanics appears more logical. Pande and Sharma (1979) found that little ill-conditioning is experienced with the application of a very thin 2D element. It is argued

that a thin element is numerically more reliable than an element with zero thickness (Day and Potts, 1994).

A special interface constitutive law is generally used to model the principal deformation mode of shearing and opening of an interface. The shear behavior of the interface material can be obtained from laboratory tests. However, it is difficult to perform tests to determine the deformation behavior perpendicular to the interface. Usually, the normal stiffness is chosen arbitrarily to avoid overlapping of elements (Desai et al., 1984). So far, no constitutive description is available for the deformation behavior of an interface in the normal direction. Only a few normal responses are adopted, such as the normal relative displacement versus normal stress relationship in which the structural behavior of the interface is incorporated(Carol, 1986). This representation is used in the modeling of a nodal interface element with zero thickness. Even though shear strains of the interface can be obtained from direct shear tests, they are usually simply defined as the relative displacements divided by the thickness of the interface (Yin and Zhu, 1995). From the consideration of consistency, it is theoretically more appropriate that strains in the continuous interface elements are described with respect to the relative displacements across the interface.

Frequently, the shear strains are concentrated along those interfaces within geological materials which leads to large shear deformations. The large deformation phenomenon is often simulated by updating the nodal coordinates of the finite elements (Bergado et al., 1995). Obviously, the localized shear strains along the interfaces will inevitably lead the original interface element to a dramatic distortion. This distortion will cause poor element configuration if the mesh is kept unchanged, a situation which is very

likely to result in incorrect stress calculations in these elements. In these cases, it is necessary to update the interface elements. On the other hand, large shear deformation must contain sliding deformation which may take place close to the interface (Yin and Zhu, 1995). Conventional finite element analysis is unable to take into account this sliding deformation which causes the reduction of the interface area that is subjected to shearing.

It is not enough to use the conventional 4-node or 8-node rectangular interface (or thin) elements to update the interface elements because of large shear deformation. The 3-node or 6-node triangular interface elements need to be applied to maintain a good configuration for all interface elements to model sliding. The first issue is to generate the elements automatically. The second issue deals with the normal strain across the interface and the shear strain along the interface which must fit the experimental relationship between stresses and relative displacements for the interface, instead of the traditional stress-strain description for a solid. So far, systematic studies and implementations of these concepts are not available in the published literature.

In this study, the interfaces are treated as large deformation problems with a finite thickness to which the continuum finite element analysis might be applied. The finite element mesh (continuous interface element) will be updated and reconstructed from time to time based on the concept of the contact band element approach (Wang et al., 1995). The strains in 3-node/4-node interface elements are newly described. Triangular and quadrilateral elements are used to model the consecutive deformation of the interface. The reduction of the interface area is automatically simulated. As such, the sliding deformation is roughly estimated. In the following continuum finite element analysis,

there are only two experimental relationships available: the normal stress and relative normal displacement across the interface; the shear stress and relative tangential displacement between the upper and lower surfaces. In this research, the relationship between normal stress and normal strain in tangential direction of the interface is assumed to be obtained by carrying out experiments on remolded filling material of interfaces or joints. Whereas the curves of relative tangential displacement versus shear stress and the relative normal displacements versus normal stress across the interface are used by referring to the concepts of nodal interface element.

7.2 Special strain description for continuous interface elements

The occurrence of localized strains along an interface means the concentration of deformation with high gradients within the narrow zone. As stated in chapter 5, the high gradients occur only in the direction normal to the interface. In the direction parallel to the interface, shear strains do not vary significantly. In general, in the displacement-based finite element formulation, with a linear interpolation of displacement **u**, the error in **u** will be of the order $O(h^2)$. The strains, which are given by 1st order derivatives of displacement, have error of the order O(h) (Zienkiewicz and Taylor, 1989). Therefore, the strain discrepancy is directly proportional to the size of an element according to theoretical analysis. For 2-D analysis, to better simulate strain distribution, mesh refinements should be used for the elements within the interface zone in the t and n directions, but for this special interface 2-D problem, mesh refinements are not necessarily implemented in both t and n directions.

In ordinary finite element analysis, the strain-displacement relations are written as:

$$\begin{Bmatrix} \gamma_{nt} \\ \varepsilon_{nn} \\ \varepsilon_{tt} \end{Bmatrix} = \begin{Bmatrix} \dfrac{\partial u}{\partial n} + \dfrac{\partial v}{\partial t} \\ \dfrac{\partial v}{\partial n} \\ \dfrac{\partial u}{\partial t} \end{Bmatrix} \qquad (7\text{-}1)$$

Here, n denotes the direction normal to the interface, and t the direction parallel to the interface. Displacements u and v are parallel and normal to the interface, respectively. u has a much higher gradient in the n direction than v has in the t direction, which is mathematically expressed as $\left|\frac{\partial u}{\partial n}\right| >> \left|\frac{\partial v}{\partial t}\right|$. So, it is accurate enough to write γ_{tn} as $\frac{\partial u}{\partial n}$. Further, it is approximately expressed as $\frac{\Delta u}{\Delta n}$, due to the interface being very thin. Δu and Δv are tangential and normal relative displacements across the interface. In the same way, normal strain across the interface is expressed as $\frac{\Delta v}{\Delta n}$. Here, Δn is the shear band thickness d. In this case, the strains are described in line with the general expressions of interface strains in terms of relative displacements, which read:

$$\begin{Bmatrix} \gamma \\ \varepsilon_n \end{Bmatrix} = \begin{Bmatrix} \dfrac{\Delta u}{d} \\ \dfrac{\Delta v}{d} \end{Bmatrix}. \qquad (7\text{-}2)$$

That is to say, the strains in the continuous interface element are set equal to the interface strains, i.e. $\gamma_{nt} = \gamma$, $\varepsilon_{nn} = \varepsilon_n$. The expression for normal strain along the interface in this continuous interface elements is the same as that in regular soil elements. Therefore, the mathematical expression for the strain in ordinary isotropic finite element analysis still

remains in the continuous interface element. Until now, the strains in the interface are basically characterized with several special expressions.

There are two advantages from the specific strain description. Firstly, the experimental relationship between stresses and relative displacements across the interface for the joint or interface element can be used directly, even though continuum finite element analysis is used for the interface with a finite thickness. Secondly, it provides fundamental approach to describe the strains in 3-node triangular and 4-node quadrilateral elements using relative displacements by reference to the analyses in chapter 5. Those 3-node triangular and 4-node quadrilateral elements with special strain descriptions are necessary in the analyses of interfaces and joints with large shear deformation. We may see that the high gradients in the interface element may be simulated with high accuracy, even interface elements can keep a normal size along the interface which is much longer than its thickness, i.e. continuous interface elements do not need to be well refined in the direction parallel to interfaces.

With the new scheme of continuous interface elements, it is not possible to keep the stresses and strains at traditional Gaussian points. Therefore, it is necessary to calculate and keep the stresses and strains at nodal points. At every loading step, stresses and strains at Gaussian points are interpolated from nodal values. The opening of interface elements will be evaluated based on the magnitudes of normal forces acting on element boundaries. The stiffness of the elements, stresses, strains at corresponding nodal points will be released if they are in tension. The constitutive models developed for shear band elements might be also applied for continuous interface elements.

7.3 Formulation of strains in an interface element

As mentioned previously, with the emergence of large shear deformation from the kinematics of interfaces, the distortion of original interface elements is most likely to occur. The triangular and quadrilateral interface elements will be automatically generated to avoid the element distortion. The strains will be formulated for triangular and rectangular elements, respectively. Shear strain and normal strain across the band are related to relative displacements between upper and lower surfaces. The strains stated above are assumed to be uniform in the normal direction of the interface.

7.3.1 Triangular interface element

As shown in figure 7.1 (a), at a certain load step, points K, A, and B form a new triangular element. The relative displacement rate of point K to segment AB is defined as:

$$\begin{Bmatrix} \dot{\Delta W}_t \\ \dot{\Delta W}_n \end{Bmatrix} = \begin{Bmatrix} \dot{U}_K \\ \dot{V}_K \end{Bmatrix} - \begin{bmatrix} N_A^C & 0 & N_B^C & 0 \\ 0 & N_A^C & 0 & N_B^C \end{bmatrix} \begin{Bmatrix} \dot{U}_A \\ \dot{V}_A \\ \dot{U}_B \\ \dot{V}_B \end{Bmatrix}$$

$$= \begin{bmatrix} -N_A^C & 0 & -N_B^C & 0 & 1 & 0 \\ 0 & -N_A^C & 0 & -N_B^C & 0 & 1 \end{bmatrix} \begin{bmatrix} \dot{U}_A \\ \dot{V}_A \\ \dot{U}_B \\ \dot{V}_B \\ \dot{U}_K \\ \dot{V}_K \end{bmatrix} = [N_\Delta] \{\dot{U}\}, \qquad (7\text{-}4)$$

where Δ denotes the difference of the upper and lower surface quantities, • denotes the rate of quantities, $\dot{U}$ and $\dot{V}$ are the tangential and normal displacement rates under coordinate system to'n, $\Delta\dot{W}_t$, $\Delta\dot{W}_n$ are the relative tangential are normal displacement rates, and $N_A^C = 1 - r_c$, $N_B^C = r_c$, in which r_c is the local coordinate of point C under local coordinate system so'r, It is simply obtained from the ratio of length AC to length AB. Here, point C is the image of point K on boundary AB. As to the location of point C, it is assumed that KC and AB in figure 7.1 (a) are intersected at a right angle. The relative coordinate r (s=0) of point C is calculated based on the direction vector normal to AB which is parallel to the interface direction. The corresponding strain rates in the element still takes the form:

$$\begin{Bmatrix} \dot{\varepsilon}_{nt} \\ \dot{\varepsilon}_{nn} \end{Bmatrix} = \frac{1}{d}[N_\Delta]\{\dot{U}\}, \tag{7-4}$$

where d denotes the thickness of the interface, which is calculated from the current coordinates of points K and C, and which will be updated continuously. For the reason mentioned before, normal strain expression along the interface is taken as :

$$\dot{\varepsilon}_s = \begin{bmatrix} \frac{\partial N_A}{\partial t} & 0 & \frac{\partial N_B}{\partial t} & 0 & \frac{\partial N_K}{\partial t} & 0 \end{bmatrix}\{\dot{U}\}. \tag{7-5}$$

Here, N_A, N_B and N_K are different from N_A^C or N_B^C. They vary through the element, and read:

$$\begin{aligned} N_A &= L_1 - 2*(L_3L_1 + L_1L_2) \\ N_B &= L_2 - 2*(L_1L_2 + L_2L_3) \\ N_K &= L_3 - 2*(L_2L_3 + L_3L_1) \\ L_1 + L_2 + L_3 &= 1 \end{aligned}, \tag{7-6}$$

where , L_1, L_2, L_3 are area coordinates of any point in one element as shown in figure 7.1 (b). Therefore, for the triangular element, the strain rates are:

$$\begin{Bmatrix} \dot{\varepsilon}_{nt} \\ \dot{\varepsilon}_{nn} \\ \dot{\varepsilon}_{n} \end{Bmatrix} = \frac{1}{d}\begin{bmatrix} -N_A^C & 0 & -N_B^C & 0 & 1 & 0 \\ 0 & -N_A^C & 0 & -N_B^C & 0 & 1 \\ d\left(\frac{\partial N_A}{\partial t}\right) & 0 & d\left(\frac{\partial N_B}{\partial t}\right) & 0 & d\left(\frac{\partial N_K}{\partial t}\right) & 0 \end{bmatrix} \begin{Bmatrix} \dot{U}_A \\ \dot{V}_A \\ \dot{U}_B \\ \dot{V}_B \\ \dot{U}_K \\ \dot{V}_K \end{Bmatrix}$$

$$= \frac{1}{d}[N']\{\dot{U}\}, \tag{7-7}$$

where

$$\frac{\partial}{\partial t} = [J]^{-1}\begin{bmatrix} \frac{\partial}{\partial L_1} & \frac{\partial}{\partial L_2} \end{bmatrix}^T, \tag{7-8}$$

and

$$[J] = \begin{bmatrix} \frac{\partial N_A}{\partial L_1} & \frac{\partial N_B}{\partial L_1} & \frac{\partial N_K}{\partial L_1} \\ \frac{\partial N_A}{\partial L_2} & \frac{\partial N_B}{\partial L_2} & \frac{\partial N_K}{\partial L_2} \end{bmatrix} \begin{bmatrix} x_A^{nt} & y_A^{nt} \\ x_B^{nt} & y_B^{nt} \\ x_K^{nt} & y_K^{nt} \end{bmatrix}, \tag{7-9}$$

where,

$$\begin{aligned}
&\frac{\partial N_A}{\partial L_1} = -1 + 4L_1, && \frac{\partial N_A}{\partial L_2} = -2 + 4L_2,\\
&\frac{\partial N_B}{\partial L_1} = -2 + 4L_2, && \frac{\partial N_B}{\partial L_2} = -1 + 4L_1,\\
&\frac{\partial N_K}{\partial L_1} = -3 + 4(L_1 + L_2), && \frac{\partial N_K}{\partial L_2} = -3 + 4(L_1 + L_2),
\end{aligned} \tag{7-10}$$

It is noted that x^{nt}, y^{nt} are the coordinates of nodal points under systems t-o'-n. Here, o' is taken to be consistent with O. The orientation of the shear band is obtained by taking an average of direction angles from all the band elements along this shear band. The calculation of the direction angle for each element is based on the average of the direction angles of the upper and lower boundaries of the band element if applicable.

For large deformation analysis, triangular interface elements are necessary which are not available in the existing finite element analyses of discontinuities. However, the continuous triangular interface elements used in this study can be easily degenerated to triangular interface elements with zero thickness. 'Strain rates' of the element are directly defined as relative displacement rates which are similar to those for general interface element with zero thickness:

$$\begin{Bmatrix} \dot{\varepsilon}_{nt} \\ \dot{\varepsilon}_{nn} \end{Bmatrix} = \begin{bmatrix} -N_A^C & 0 & -N_B^C & 0 & 1 & 0 \\ 0 & -N_A^C & 0 & -N_B^C & 0 & 1 \end{bmatrix} \begin{Bmatrix} \dot{U}_A \\ \dot{V}_A \\ \dot{U}_B \\ \dot{V}_B \\ \dot{U}_K \\ \dot{V}_K \end{Bmatrix}. \tag{7-11}$$

Normal strain rate $\dot{\varepsilon}_{tt}$ is set to be zero. Then, the complete strain expression in one interface element with zero thickness becomes:

$$\begin{Bmatrix} \dot{\varepsilon}_{nt} \\ \dot{\varepsilon}_{nn} \\ \dot{\varepsilon}_{tt} \end{Bmatrix} = \begin{bmatrix} -N_A^C & 0 & -N_B^C & 0 & 1 & 0 \\ 0 & -N_A^C & 0 & -N_B^C & 0 & 1 \\ 0 & 0 & 0 & 0 & 0 & 0 \end{bmatrix} \begin{Bmatrix} \dot{U}_A \\ \dot{V}_A \\ \dot{U}_B \\ \dot{V}_B \\ \dot{U}_K \\ \dot{V}_K \end{Bmatrix}. \qquad (7\text{-}12)$$

7.3.2 Quadrilateral interface element

In the kinematic movement of interfaces, it would be necessary to use quadrilateral elements to accommodate their current configurations. As shown in figure 7.1 (c), the relative displacement between upper and lower surfaces at any point in the element is only the function of local coordinate r, and is irrelevant to the other local coordinate s. They can be written as:

$$\begin{Bmatrix} \Delta w_{nt} \\ \Delta w_{nn} \end{Bmatrix} = \begin{bmatrix} N_3 & 0 & N_4 & 0 & -N_1 & 0 & -N_2 & 0 \\ 0 & N_3 & 0 & N_4 & 0 & -N_1 & 0 & -N_2 \end{bmatrix} \begin{Bmatrix} \dot{U}_3 \\ \dot{V}_3 \\ \dot{U}_4 \\ \dot{V}_4 \\ \dot{U}_1 \\ \dot{V}_1 \\ \dot{U}_2 \\ \dot{V}_2 \end{Bmatrix}. \qquad (7\text{-}13)$$

If $\left\{\dot{U}\right\} = \left\{\dot{U}_3 \quad \dot{V}_3 \quad \dot{U}_4 \quad \dot{V}_4 \quad \dot{U}_1 \quad \dot{V}_1 \quad \dot{U}_2 \quad \dot{V}_2\right\}^T$ is taken, the corresponding strains would read :

$$\begin{Bmatrix} \dot{\varepsilon}_{tn} \\ \dot{\varepsilon}_{nn} \end{Bmatrix} = \frac{1}{d} \begin{bmatrix} N_3 & 0 & N_4 & 0 & -N_1 & 0 & -N_2 & 0 \\ 0 & N_3 & 0 & N_4 & 0 & -N_1 & 0 & -N_2 \end{bmatrix} \left\{\dot{U}\right\} \qquad (7\text{-}14)$$

On the upper and lower boundaries of the band element, local coordinates s are equal to 1 and -1, respectively. Hence,

$$N_1 = \frac{1+r}{2} = N_4;\ N_2 = \frac{1-r}{2} = N_3. \qquad (7\text{-}15)$$

We still take the normal strain along the interface as an ordinary one. Its expression in the isotropic finite element method is retained. Therefore, the total strains in quadrilateral elements are described as:

$$\begin{Bmatrix} \dot{\varepsilon}_m \\ \dot{\varepsilon}_{nn} \\ \dot{\varepsilon}_n \end{Bmatrix} = \frac{1}{d}\begin{bmatrix} N_1 & 0 & N_2 & 0 & -N_4 & 0 & -N_5 & 0 \\ 0 & N_1 & 0 & N_2 & 0 & -N_4 & 0 & -N_5 \\ d\frac{\partial N_3}{\partial t} & 0 & d\frac{\partial N_4}{\partial t} & 0 & -d\frac{\partial N_1}{\partial t} & 0 & -d\frac{\partial N_2}{\partial t} & 0 \end{bmatrix}\begin{Bmatrix} \dot{U} \end{Bmatrix}$$

$$= \frac{1}{d}[N']\begin{Bmatrix} \dot{U} \end{Bmatrix} \qquad (7\text{-}16)$$

$\frac{\partial}{\partial t}$ can also be treated in the same way as used for a triangular element, but natural coordinate system instead of area coordinate system is used to describe the element coordinates and displacements. Similarly, a quadrilateral interface element with a finite thickness is easily transformed to an ordinary interface element with zero thickness.

7.4 Elastic-plastic constitutive model for the continuous interface element

In the continuous interface element, the corresponding stress rate $\begin{Bmatrix} \dot{\sigma} \end{Bmatrix}$ is written as:

$$\left\{\dot{\sigma}\right\} = \begin{Bmatrix} \dot{\tau}_{nt} \\ \dot{\sigma}_{nn} \\ \dot{\sigma}_{tt} \end{Bmatrix} = \left[D_{ep}\right]\left\{\dot{\varepsilon}\right\} = \frac{1}{d}\left[D_{ep}\right]\left[N'\right]\left\{\dot{U}\right\}. \qquad (7\text{-}17)$$

The stress response of an interface is always expressed as (σ_n, τ) in laboratory tests, where σ_n and τ are normal and shear stresses, respectively. They are obtained by dividing the applied forces by the area subjected to the forces. For the same reason as stated in strain discussion, we must have $\dot{\tau}_{nt} = \dot{\tau}$, $\dot{\sigma}_{nn} = \dot{\sigma}_n$.

Here, the physical explanation of $[D_{ep}]$ is different from the normal elastic-plastic matrix in continuum element. Its elastic part should be set to coincide with the stress-strain response:

$$\begin{Bmatrix} \dot{\tau} \\ \dot{\sigma}_n \end{Bmatrix} = \begin{bmatrix} k_t & 0 \\ 0 & k_n \end{bmatrix} \begin{Bmatrix} \Delta\dot{u} \\ \Delta\dot{v} \end{Bmatrix}, \qquad (7\text{-}18)$$

where, $\Delta\dot{u}$ and $\Delta\dot{v}$ are relative tangential and normal displacement increments, respectively. k_n and k_t are the shear and normal stiffnesses of the interface. Also, in the general interface analysis, the normal stress-strain response along the interface is always neglected regardless of the response across the interface. In view of all these facts in the experimental analysis of interfaces, the anisotropic model can be applied for the continuous interface element.

7.4.1 The elastic constitutive model

The components of the anisotropic model is expressed as:

$$[D_e]=\begin{bmatrix} D_{11} & 0 & 0 \\ 0 & D_{22} & D_{23} \\ 0 & D_{32} & D_{33} \end{bmatrix}. \qquad (7\text{-}19)$$

The components of $[D_e]$ matrix are:

$$\begin{aligned} D_{11} &= 2G_{nt}, \\ D_{22} &= A(1-\nu_{nt}^2), \\ D_{23} &= D_{32} = A\nu_{nt}(1+\nu_{tt}), \\ D_{33} &= A(\frac{E_{tt}}{E_{nn}}-\nu_{nt}^2), \end{aligned} \qquad (7\text{-}20)$$

where $A=\dfrac{E_{tt}}{(1+\nu_{tt})[E_{tt}/E_{nn}(1-\nu_{tt})-2\nu_{nt}]}$. The physical meanings of all the parameters are stated in chapter 6, E_{tt} and ν_{tt} can be obtained from conventional laboratory test using the remolded joint or fault materials. E_{nn} and G_{nt} are calculated approximately from the relations (Sharma and Desai, 1992):

$$E_{nt}=k_n d, G_{nt}=k_t d, \qquad (7\text{-}21)$$

where, k_n and k_t are normal and shear stiffnesses of the interface, respectively. The contribution to in-plane stress σ_{tt} from normal strain ε_{nn} is often neglected (Sharma and Desai, 1992), therefore, ν_{nt} is set to be zero.

7.4.2 The plastic constitutive model

Apparently, the yielding and failure of the interface always occur in the plane parallel to the interface direction. All the general yielding models are not applicable for this case. The special Mohr-Coulomb model developed in chapter 6 is the only choice. The yield function f and the gradients of the plastic potential function G are defined as:

$$f = |\tau_{nt}| + \sigma_{nn} \tan\phi - c,$$
$$\frac{\partial G}{\partial \sigma_{nn}} = \tan\psi, \quad \frac{\partial G}{\partial \tau_{nt}} = \pm 1. \tag{7-22}$$

Here, ϕ is the friction angle, and ψ the dilation angle. The dilation of the interface can be represented by a negative value of ψ (Day and Potts, 1994).

7.5 A numerical example---- Pull-out test

In view of both the performance of continuous interface elements on multiple shear band channels and the potential applications to soil reinforcement and pile analyses, the example of the pull-out test demonstrates the continuous interface elements in a problem controlled by the sliding mode of deformation. There are two shear band channels in this example, one is located on the top of the reinforcement, the other one is at the bottom of the reinforcement. This 2-D problem consists of 180 soil elements and 18 reinforcement elements. The interfaces between the reinforcement and the soil on the top and bottom are modeled by 36 continuous interface elements with a thickness of 5mm, as shown in figure 7.2. Originally, all these elements are 4-noded rectangles. With the pulling-out of the reinforcement, large shear strains are localized between the reinforcement and the soil. As a result, the interface elements will be updated. The selection of 3-node triangular or 4-node rectangular elements is subjected to the configuration change, mainly to relative locations of reinforcement nodes to soil nodes. Initially, a uniformly distributed vertical pressure of 51 kPa is applied on the top of the test box. At the same time, self weight was applied on the soil with unit weight of 17.66 kN/m^3. Then, from step 2 to step 46, the left end of the reinforcement was dragged

horizontally out of the soil mass under displacement control in the direction shown in figure 7.2. The soil mass was restrained at the boundaries. The horizontal displacement which was applied on the reinforcement was increased by 2 mm in each step from steps 2 to step 46. This problem involves a sliding front that moves progressively from the point of load application (left end) towards the other end of the reinforcement. Since the analysis was used to test the effectiveness of the continuous interface element, both soil and reinforcement are treated as linear elastic materials. Based on the discussions in section 7.4, the interface material should be simulated using the cross-isotropic elastic model with special Mohr-Coulomb yielding criterion. The Poisson ratios ν_{nt} and ν_{tn} are taken to be zero, which relate extensional strains in the tangential plane and normal loading or normal extensional strains and tangential loading. All the material properties are presented in table 7.1. In the analysis of conventional interface elements, a large value of normal stiffness must be adopted to prevent the overlapping of the interface elements. A large normal stiffness is likely to cause the divergence of the analysis and oscillation of shear stress and axial force in the reinforcement (Day and Potts, 1994). Here, the results have shown that it is not necessary to have a large value of the normal modulus for the continuous interface elements.

Previously, many investigators have proposed a series of well-established methods for the pull out test, which includes a thin strip of 2D elements that represent the reinforcement. The contact between the reinforcement and the soil is conventionally modeled by interface elements with zero thickness. As some researchers (Day and Potts, 1994; Sharma and Desai, 1992) pointed out, sometimes the behavior of the interface

element was not satisfactory. It has been observed that the distributions exhibit large oscillations which should not be part of any meaningful solution to the problem. On the other hand, the existing interface element can hardly handle the large deformation of the pull-out test.

Table 7.1 Material properties in the pullout test

Material	Model	Parameters
Soil	Elastic	Unit weight γ=17.86 kN/m^3 E=3600 kPa, ν=0.36
Interface	Cross-isotropic elastic model with special Mohr Coulomb yielding criterion	E_n=104.4 kPa, E_t=17.4 kPa, G=6.2 kPa, ν_{nt}=0, ν_{tt}=0.30, ϕ=14°, c (cohesion)=0
Reinforcement	Elastic	E=5x10^4 kPa, ν=0.25

The results for different steps are presented below, from figure 7.3 to figure 7.6, and they characterize the behavior of continuous interface elements on the pull-out test. The distributions of mobilized shear stresses and axial forces in the reinforcement along the interfaces have not shown any oscillations. They are smooth and consistent. There is a shear stress concentration at the left end of the reinforcement for the reason that the configuration around this end has been dramatically changed due to pulling-out of a part of the reinforcement. This could be viewed as a slide deformation termed by Yin and Zhu (1995), and is roughly modeled by virtue of a continuous interface element, but can not be obtained by the conventional interface element. The results are not obtained based on the refinement of elements. Compared with results provided by Yi et al. (1995), this analysis with continuous interface element has a real ultimate load (31.4 kN/m) in which

large deformation has developed well after ultimate load is reached (Maximum deformation: 92 mm). Furthermore, the reduction of the load after the peak value is simulated to some extent because of the decrease of the contact area of the interfaces. On the other hand, with the reinforcement pulled out, on its left end, the shear stress, and the vertical normal stress should be reduced to zero as shown in figure 7.4, a reduction which could not be reflected in the normal interface element analysis. Therefore, the application of the continuous interface element is obviously more effective in modeling the pull-out test. The mobilization of axial force of the reinforcement implies that the computed ultimate load corresponds to the theoretical one, assuming full sliding of the reinforcement. Apparently, the normal stresses along the interface should be much smaller than those across the interface, and the failure surface must be parallel to the interface . All the results have shown that the continuous interface element with cross-isotropic elastic model with special Mohr-Coulomb yielding criterion simulate the pullout test more realistically than other methods.

7.6 Concluding remarks

The contact band element approach, with specific strain description, is applied in the simulation of the interfaces for large deformation problems. The new strain descriptions, corresponding to a special constitutive model, are made of 3-node or 4-node band elements, which are proven to be theoretically feasible. It is important that these expressions be consistent with the experimental analyses. The consecutive updating of band elements always keep a good configuration for all the band elements, and this

updating avoids their distortions in conventional finite element analysis. Significantly, this updating provides an efficient way to analyze the soil structures with interfaces along which large shear deformations arise. With the proposed strategy, the analysis of pull-out test, in which considerable displacements occur, has given us satisfactory stress, displacement results with consistency and with no oscillation. These results are not available in the conventional interface analyses. It has been shown that the newly recommended method is more effective for practical use.

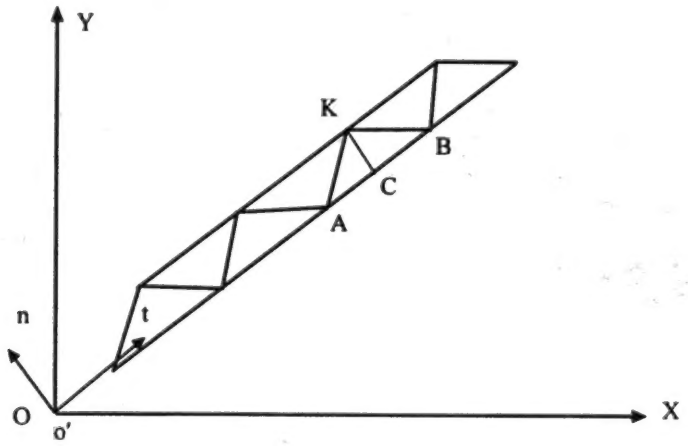

Figure 7.1 (a)

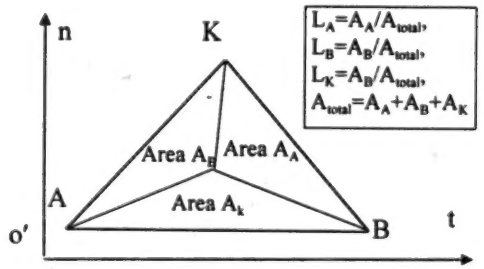

Figure 7.1 (b)

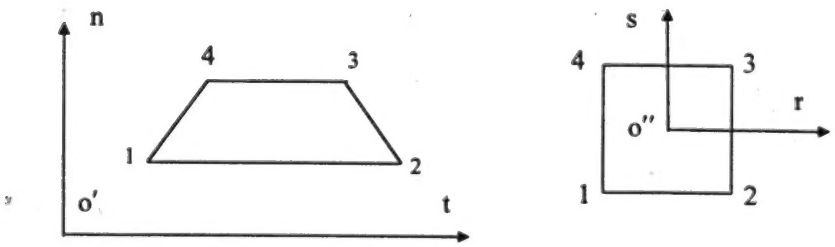

Figure 7.1 (c)

Figure 7.1 Continuous interface elements, (a) triangular elements under different coordinate systems, (b) area coordinate system for a triangular element, (c) rectangular elements under different coordinate system

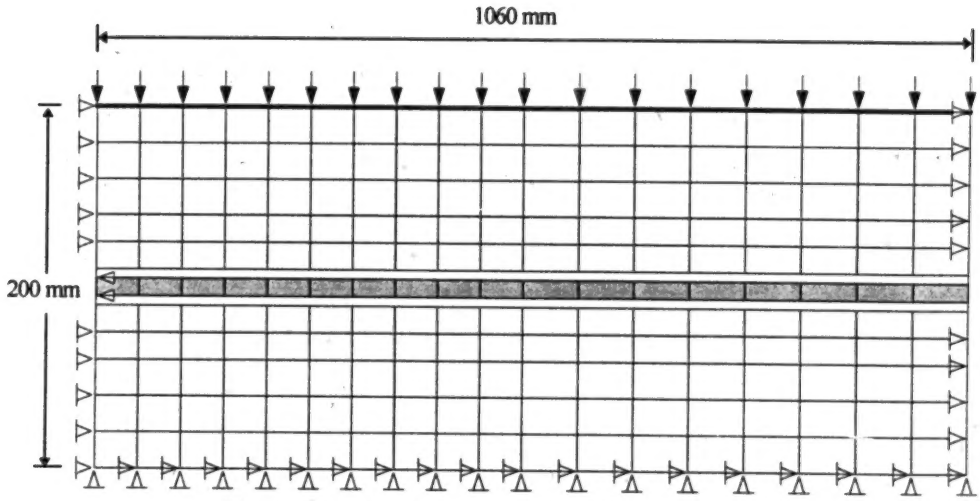

Figure 7.2 The discretization of soils and reinforcement

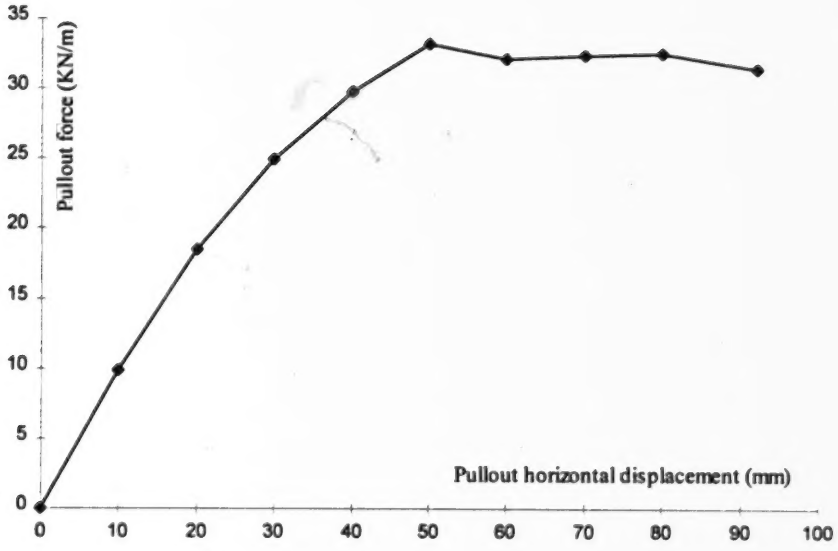

Figure 7.3 Relationship between axial force and applied left end horizontal displacement

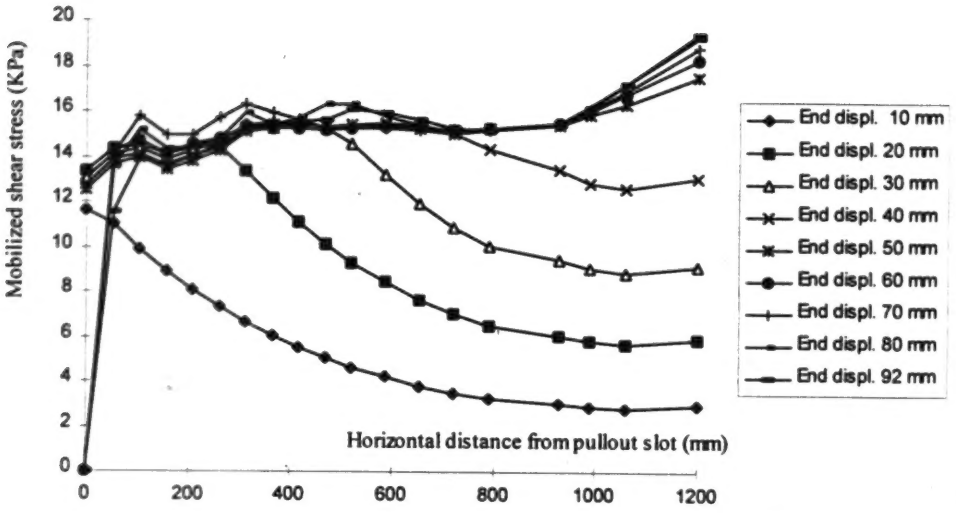

Figure 7.4 Shear stress distribution along the interface at different end displacements

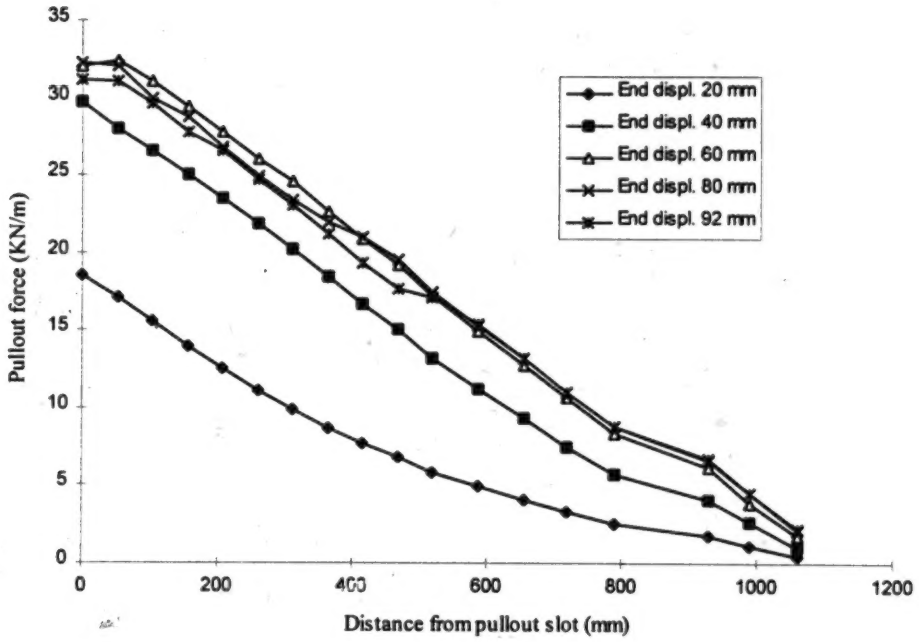

Figure 7.5 The tensile force distribution along the reinforcement

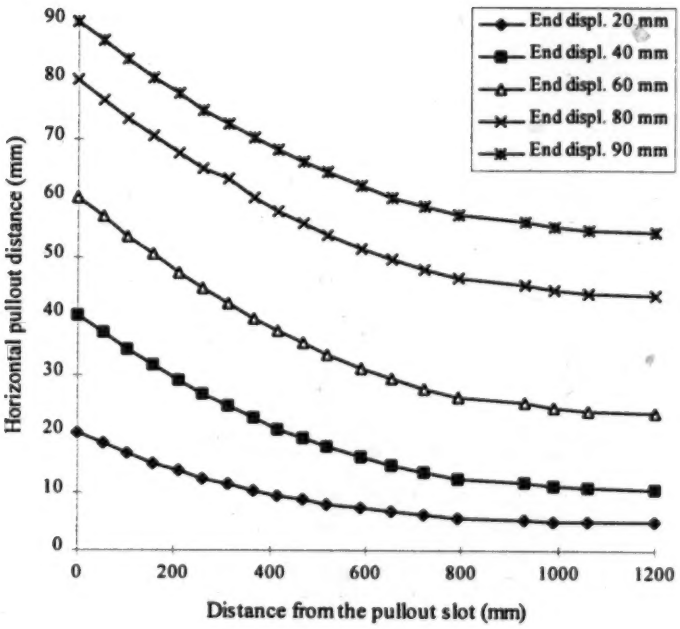

Figure 7.6 Horizontal displacement distribution of the reinforcement in its longitudinal direction

Chapter 8

The automatic creation of discrete shear band elements

8.1 Introduction

As mentioned previously, the failure of soil structures is preceded by the presence of fissures and discontinuities. They scatter randomly in some areas with different alignments. During the failure process, these fissures and discontinuities will develop and join together to form a shear band, i.e. shear band localization, which results in intensive shear strains along a narrow zone. The strong reorientation and breaking of the particles causes material inhomogeneity. Shear band propagation also leads to induced anisotropy. The inhomogeneity and anisotropy have not been considered in all the existing algorithms for shear band simulation. Furthermore, the whole process beyond the onset of shear band localization cannot be effectively modeled. As a result, such analyses can only make a crude approximations of the actual physical behavior (Ingraffea, 1977).

Once a narrow localized shear band is introduced in the finite element scheme with special constitutive properties, the evolution of shear band localization may be tracked with the help of the contact band element proposed in chapter 6 (Wang et al., 1995). This contact band element approach can closely simulate the actual behavior of a

shear zone.

In this chapter, an efficient method to simulate the propagating of a shear band through a general finite element mesh is presented. The shear band elements are generated once localization is detected based on the bifurcation criterion. Soil elements through which shear bands propagate are split up and re-shaped into new elements by adding new nodes without regenerating the whole mesh. This leads to the additional degrees of freedom. The shear band elements are furnished with band material properties. The process of generating shear band elements and reshaping the soil elements will be discussed in detail in this chapter. A special empirical criterion is proposed for the initiation of band localization for elastic-perfectly plastic material. A scheme called "location criterion" is developed for generating new band elements.

The proposed finite element strategy has been successfully used in simulating the localization process in a biaxial test and a passive earth pressure problem. The results show that the effectiveness of the discrete shear band approach in analyzing this class of problem. Once large shear deformations develop along the shear band channels owing to their propagation, the contact band element approach will also be used.

8.2 The empirical criterion for shear band localization

In chapter 4, a general localization criterion has been presented. Mathematically, the presence of fissures and discontinuities coincides with the occurrence of a zero eigenvalue of the symmetric part of the constitutive matrix [D] for a diffuse bifurcation or general bifurcation. Shear band localization (macro shear banding) may occur when there

is a zero eigenvalue of the acoustic tensor, det(Q)=0, which is consistent with the loss of ellipticity of equations governing incremental equilibrium. Therefore, a soil structure would undergo plastic deformation, diffuse bifurcation and shear band localization before failure, as shown in figure 8.1. The critical hardening moduli could be given for the three critical points provided general plasticity with a hardening model is adopted. The detailed discussion can been seen in chapter 4

In the analyses of practical engineering problems, elastic-perfectly plastic models are still commonly used because of its simplicity. Derived from the general localization criterion, the diffuse bifurcation and localization may occur simultaneously only on condition that the hardening modulus H is equal to 0. In figure 8.2, on the horizontal line, the values at any point is equal to zero. However, physically, they occur at different magnitudes of plastic shear strains as shown in figure 8.2. Mathematically, the plastic shear strain for plane problems (plane stress and plane strain) is given by:

$$\varepsilon_p = \frac{2}{3}\sqrt{\frac{1}{2}\left[\left(\varepsilon_x-\varepsilon_y\right)^2+\left(\varepsilon_y-\varepsilon_z\right)^2+\left(\varepsilon_z-\varepsilon_x\right)^2\right]+\frac{3}{4}\varepsilon_{xy}^2}\,. \qquad (8\text{-}0)$$

Well documented laboratory tests can assist us in determining the initial point of severe macro shear banding, namely shear band localization. Researchers have proven that shear band localization emerges shortly before or after the peak point on the stress-strain curve (Morgenstern and Tchalenko, 1967), at which the accumulated plastic shear strains around the band tip are assumed to be 10 to 40%. Accordingly, the critical value of plastic shear strain for the onset of macro shear band localization is assumed to range from 10% to 40%, as shown in figure 8.2. In this case, the shear band localization can be identified based on the accumulated plastic shear strains. So far, researchers can hardly

provide from experiments the critical values of the plastic shear strain. More endeavors should be made to determine this critical plastic shear strain for the initiation of shear band localization for different materials. It is noted that there is no need to give the empirical criterion if a constitutive hardening model is employed. In this case, the discontinuous bifurcation point indicating the inception of a shear band can be automatically detected using the bifurcation theories. The diffuse bifurcation and discontinuous bifurcation will occur at different hardening moduli which are calculated using bifurcation theory.

8.3 Framework of formation of shear band elements

The formation of discrete shear band elements requires additional nodes and degrees of freedom to the finite element mesh. The addition of new nodes at arbitrary points within a mesh may increase the bandwidth of the stiffness matrix significantly. The stiffness matrix will take a lot of space. But this space problem would not be serious with the current development of computers.

The incorporation of new band elements and new nodes will be discussed in this section. For the sake of simplicity, only 4-node quadrilaterals and 3-node triangular elements are used. In order not to reduce stress concentrations near the shear band tip, triangular elements are used for the tip which can be evolved into quadrilateral elements during propagation of the shear band. The thickness of the shear band elements is chosen based on experimental data (Muhlhaus, 1986).

8.3.1 Techniques to generate shear band elements

As usual, the detection of localized bifurcation in an element is based on the stresses and strains at its Gaussian integration points. At each loading step, immediately after the analysis has converged, the empirical bifurcation criterion is checked at each Gaussian point to detect the initiation of macro shear banding. Once the criterion is satisfied at one or more Gaussian points, a further check is made to see if the formation of the band across the Gaussian point is geometrically feasible, which implies that the potential shear band will still go through the element after it is reshaped.

8.3.1.1 Geometric check of potential band in one element

Based on the empirical bifurcation criterion only, it cannot be concluded whether a band would actually exist in an element. The location and alignment of the potential band should be examined to make sure that it will be compatible with the existing configuration of the element. If compatibility is satisfied, it implies that either an old shear band will propagate through the current element or a new shear band will form in the current element. With the application of the bifurcation theory to an elastic-perfectly plastic model with associative flow rule, the orientation of the potential band can be determined in terms of the friction angle ϕ:

$$\theta = \frac{\pi}{4} - \frac{\phi}{2}, \tag{8-1}$$

where θ is the angle between the length of the shear band and the major principal stress direction. If the direction of the shear band is measured with respect to a horizontal line, the corresponding angle is expressed as:

$$\alpha = \frac{\pi}{4} - \frac{\phi}{2} + \gamma, \qquad (8\text{-}2)$$

in which γ is the angle between the major principal stress direction and the horizontal line.

With the global coordinates of the Gaussian point and the alignment of the potential shear band, the intersection between the shear band and element boundaries could be determined. If there is no intersecting point found on one boundary, the search will proceed to the next boundary until an intersecting point is formed. As shown in figure 8.3 (a), K is the intersecting point for boundary KK_1.

Further checking for the existence of a real shear band in the element is still necessary. Element $e_{k_0k_1k_2k_3}$ is reshaped by moving temporarily nodal point K_o on the boundary which is closest to point K to overlap nodal point K. Take node K_o on the boundary which is closest to point K as the initial point, and K_3 as the ending point. Then, calculate global orientations for boundaries K_oK_1 and K_oK_3, which are represented by θ_1 and θ_2, respectively, as sketched in figure 8.3 (a). If $\theta_1 \le \theta \le \theta_2$, shear band is created for this element, and reshaping of the element will be kept permanent. If $\theta < \theta_1$ or $\theta > \theta_2$, shear banding is not geometrically feasible, and the temporary reshaping will be ignored, as shown in figure 8.3 (b), (c). Sometimes, the bifurcation criterion is satisfied at more than one Gaussian point, and the geometrical requirements mentioned above are also met for the existence of shear bands. Then, the point with the largest value of plastic shear strain is selected for the shear band.

8.3.1.2 Location criterion

Once the existence of a shear band in a normal element is established, it is

necessary to make certain whether the shear band is the consequence of the propagation of an existing shear band, or is the emergence of a new band. Strictly speaking, shear band KK′ is usually not consistent with all the existing shear bands in terms of alignments and locations, as seen in figure 8.4. However, from a practical point of view, the shear bands are considered to be connected if they are close enough to each other. A geometric criterion would be helpful in making a judgment. The location criterion is literally written as:

$$\left|\mathbf{X}-\mathbf{X}_i^{tip}\right| \le \varepsilon_L, \tag{8-3}$$

$$\left|\theta-\theta_i\right| \le \varepsilon_\theta, \tag{8-4}$$

in which $\mathbf{X}$, $\mathbf{X}_i^{tip}$ and θ, θ_i are shown in figure 8.4. $\mathbf{X}$ and $\mathbf{X}_i^{tip}$ are the location vectors for the end of the new shear band and the tip of the existing shear band number i, respectively. θ, θ_i are used to indicate the orientations of the new band and the ith band. ε_L, ε_θ are tolerances for location and orientation. If equations (8-3) and (8-4) are satisfied, the shear band in the current element would be moved to connect to the existing ith shear band, and it is viewed as the extension of the ith shear band with the same orientation. If only equation (8-3) is satisfied, it is looked upon as the elongation of the ith shear band, but with an alteration of orientation, as shown in figure 8.5 (b). If neither (8-3) nor (8-4) is satisfied, the shear band must be a new band. In order to avoid tedious description, in this section and the next, we just take a rectangular element as an example to describe the generation of band elements and the remesh for the regular soil elements.

8.3.1.3 The propagation of old shear bands and the generation of new band elements

Figure 8.5 (b) and (c) show that the propagation of a shear band could be classified in two categories by Zhau and Lin (1989).

As shown in figure 8.5 (a), points M and N are mid points of element boundaries ij and jk, respectively. If the new band element falls in region I, node i or k will be moved to the band tip. The affected soil elements will be reshaped. Soil elements will not be broken up. In this case, a new nodal point l' should be placed around node l and its coordinates are calculated based on the shear band thickness. The new triangular band element $e_{l'il}$ is created along the realigned boundary il. The last tip band element, e_{glh}, is updated into a rectangular element, $e_{gl'lh}$.

If the shear band extends to region II, then, firstly, move node j to the place of the new band tip. Secondly, breakup current rectangular element e_{lkji} into triangular elements e_{lkj} and e_{lji}. Element e_{lkj} will be renumbered as $e_{l'kj}$. The technique will be stated later. The new tip band element is $e_{l'jl}$ along the new boundary lj. In the same way, the previous tip band element e_{glh} is updated into element $e_{gl'lh}$. The technique to renumber soil element e_{lkj} will be given in section 8.3.3.

Occasionally, shear bands are created in some isolated soil elements, but there are no shear band elements formed for these shear bands. More details will be given in the next sub-section. As illustrated in figure 8.6 (a), band b_{lh} had no band element with it before it extends, and was isolated in one soil element. With its extension to neighboring soil element e_{jilk}, two triangular tip elements $e_{lhl'}$ and $e_{l'jl}$ have formed along this band (figure 8.6 (b)) at the same time.

8.3.1.4 The creation of new shear band

If the geometric criterion is violated, the shear band which emerges in the current element would not be considered as an extension of the old band, but would be considered as a new shear band. Figures 8.7 (a) and (c) show the two cases. As mentioned at the beginning of this chapter, only one node is placed at the tip of a shear band to avoid the reduction of the stress concentration around the tip because of the width of the shear zone. If two tips of the shear band lie on two boundaries of one soil element (figure 8.7 (a)), geometrically, it is impossible to create a discrete band element for the band. An effective way is to modify the stiffness matrix to simulate the strain discontinuity across the shear band in such a way as proposed by Pietruszczak and Mroz. (1981). A detailed discussion is out of the scope of this thesis. If one or two tips lie on the boundaries of a soil structure, new nodes should be created around the tips. As a result, the triangular element (one tip on structure boundary) or quadrilateral element (two tips on the structure boundaries) is used to model the new shear band, as shown in figure 8.7 (c).

With the presence of the shear band in the element as illustrated in figure 8.7 (a), it is necessary to break up current quadrilateral element e_{1234} into triangular elements e_{i2j} and $e_{j4i,}$ and to move nodes l and 3 to the two tip points i and j respectively. The relevant elements are automatically reshaped. Figure 8.7 (b) shows another case. The tip of new shear band (node k) is not close enough to the tip of the other existing shear band which is connected to one node of this soil element. At the first step, the original element e_{1234} is divided into triangular element e_{1k4} and rectangular element e_{k2j4} that contains the new shear band. Subsequently, element e_{k2j4} is broken up into two triangular elements e_{k2j} and e_{j4k}. Before the element is broken up, nodal point 3 is moved to point j.

8.3.2 The recalculation of stresses for shear band elements and reshaping of regular soil elements

Without losing generality, the stress distribution in element e_{1234} with 4 Gaussian interpolation points (figure 8.7 (a)) can be assumed as:

$$\sigma_{ij} = A + Br + Cs + Drs, \qquad (i=1,2; j=1,2) \qquad (8\text{-}5)$$

where A, B, C and D are constants in the element, and r, s are local coordinates for any point in the element. With the stress values at the original Gaussian points, the four constants are obtained. For any triangular element with 4 Gaussian points, this is also true. In some cases with triangular elements, the stresses at Gaussian points need to be interpolated from the stresses at nodal points. Then, constant D is always equal to zero. Subsequently, at any point in this element, stresses can be determined. After the element is reshaped or broken up into two elements, as shown in 8.7(b), the stresses at the nodal points can be calculated based on the new local coordinates. Once the elements are reshaped or new elements are created, the four constants of the equation (8-5) are then re-evaluated for the relevant elements based on the nodal stresses. Finally, stresses at new Gaussian points for these elements can be obtained based on the new constants.

The same strategy is applied to shear band elements. In figure 8.7 (c), node j' is created. Thickness of the shear band is obviously much smaller than the length of the element boundary. Therefore, stresses at node j' approximately take the same magnitudes of stresses at node j. Knowing the stresses at the nodal points, the above steps can be used for the reshaped soil elements. The stresses at Gaussian points in the band element may be calculated.

In the above, the evaluation of stresses in reshaped soil elements and new shear band elements have been discussed. The same scheme should be applied to strains and mechanical parameters (hardening modulus, mobilized dilation angles, frictional angles, etc.) for the elements. In the reshaped soil elements, the load matrices should also be re-evaluated because of the changes in geometry.

8.3.3 Numbering of new band elements and remeshed soil elements

The numbering of new band elements requires a considerable amount of programming work. Here, only a simple case is briefly illustrated to show the scheme. A number of more sophisticated cases are involved in programming work. Frequently, the problem of a negative value of the determinant of the Jacobian of the transformation matrix arises for a new shear band element if incorrect numbering of the band element is used. For tip band elements (triangles), which are shown in figure 8.8 (a), the element is numbered as k→i→j. To validate the sequence of nodal numbers, simply calculate determinant value of the following matrix:

$$S = \begin{vmatrix} x_k & y_k & 1 \\ x_i & y_i & 1 \\ x_j & y_j & 1 \end{vmatrix}, \qquad (8\text{-}6)$$

where x, y are coordinates for each nodal point. If S>0, the current numbering is correct. Otherwise, change the sequence into j→i→k, and provide new numbering. A rectangular element is examined based on three triangular elements. In figure 8.8 (b), positive values of S in equation (8-6) for e_{ijk}, e_{ikl} and e_{ijl} imply the correct numbering for the rectangular element. If this is not true, switch nodes j and k, or nodes i and l, or nodes j and i depending on the signs of the three S values.

With the addition of new nodes, some soil elements should be renumbered. In figure 8.8 (c), new node j is created around node k. Subsequently, node k should be replaced by node j in some elements around nodal point i. Briefly, the scheme is as follows:

First, it is necessary to evaluate the orientations of the two boundaries of ij and ik of the band element, which are represented by θ_{ji}, θ_{ki}, respectively. Then find θ_{pi} and θ_{qi} for the orientation of lines pi and qi respectively. Points p and q are the centre points of elements E_1 and E_2 which are connected at point i. Before a shear band element is generated, the following criteria are checked. If $\theta_{pi}<\theta_{ji}$, node k in element E_1 is replaced by node j. If $\theta_{qi}>\theta_{ki}$, node k is kept in element E_2. Carry out the above check for all the soil elements around node i.

8.4 Numerical Examples

8.4.1 Plane strain biaxial test

In this section, the proposed finite-element method is used to simulate shear band initiation and propagation in a plane strain biaxial test of soil. The analyses were carried out using the elastic-perfectly plastic model with Mohr-Coulomb criterion in which the associated flow rule is followed for all the soil elements. In order to trigger shear banding, a weak element is placed with smaller ϕ and c values at the right boundary in the middle of the specimen, as shown in figure 8.9. The cross-isotropic elastic model with special Mohr-Coulomb yielding criterion was used for the shear band material. It is noted that the stress state is not constant throughout the specimen before the onset of

localization because of the presence of the weak element. The original mesh is drawn using Sigma/W (GEO-SLOPE International, 1992). The size of all the elements are exactly the same. Geometrically, there will be equal opportunity for each soil element regarding the initiation and propagation of the shear band. No shear band orientation is specified. A shear band thickness is assumed to be 1 mm in the analysis.

8.4.1.1 Brief description of the biaxial test

The specimen tested is 40 mm wide and 140 mm high. It is originally discretized with a total of 150 elements and 182 nodal points. The material data are taken as follows: E=100 N/mm^2 and ν=0.30 for elastic behavior for all the elements except the weak one before the initiation of shear bands; E=100 N/mm^2 and ν=0.35 for the weak element. After the initiation of the first band, the band material will take E_t= 10 N/mm^2, ν_t= 0.35, E_v= 70 N/mm^2, ν_n=0.35, for its tangential and normal directions, respectively. Shear modulus along the shear orientation G=3.846 N/mm^2, ϕ, c values for the soil elements, and the weak element and shear band elements are listed in the table 8.1. The loading conditions are given in table 8.2.

Table 8.1 Strength parameters used for the biaxial test

Parameters	Soil element	weak element	shear band element
ϕ(°)	25	20	15
c(N/mm^2)	0	0	0

Table 8.2 Loading procedures for the biaxial test

Load step	1	2	3	4
Conditions	Apply confining pressure p	Apply vertical displacement on the top		
Value	5.0 N/mm^2	2.0 mm	2.0 mm	2.0 mm

Table 8.2 Loading procedures for the biaxial test(Continued)

Load step	5	6	7	8	9	10	11	12	13	14	15	16
Conditions	Apply the vertical displacement on the top											
Value (mm)	2	2	2	2	1	0	1	0.0	.5	0.0	.5	0.0
Load step	17	18	19									
Value (mm)	0.5	0.0	0.0									

8.4.1.2 Shear band initiation and development

A shear band was initiated at the corner of the weak element when the axial strain was equal to about 13%. Then, propagation and initiation of new bands were detected during subsequent loading. The whole procedure, including the initiation and the propagation of shear bands is shown in figures 8.9 through 8.16. It is important to note that, the shear band patterns are seen explicitly, whereas those previously developed by some other researchers were usually too diffuse to adequately describe the physical reality. Almost all the shear bands form an angle of around $\frac{\pi}{4}+\frac{\phi}{2}$ with respect to horizontal direction at the moment of their occurrences. Subsequently, some of shear band orientations will alter slightly because of the deformation of the structure. It is noteworthy that shear bands still propagate even without applying any load at "steps" 18 and 19, which are shown in figures 8.14 through 8.16. The number of new nodes and shear band elements kept increasing as shown in table 8.3. A total of 14 new nodes and 16 new shear band elements are created 20 steps.

From the load-axial strain curve shown in figure 8.17, it is clearly seen that shear band propagation was stable at the initial stage. At the stable stage, shear bands will stop propagating if no further vertical displacement applies on the top. Then, even the vertical displacement was increasing, the equivalent load applied on top of the specimen was

constant. Unstable propagation of shear bands took place on the other side of the specimen without any addition of displacement immediately before the structure collapses. No convergent results can be obtained in the final stage. The strength of the shear band materials gradually mobilized to residual strength. However, it actually went down slightly and the structure was seriously damaged to the extent that no converged results were obtained in step 20. In the intermediate load steps, the convergence is still easily obtained despite of the reshaping of soil elements and recalculation of the stresses and strains. All the results have verified that the proposed finite element method could successfully simulate initiation and propagation of shear bands. The induced inhomogeneities due to the propagation of shear bands are modeled using independent shear band elements. The shear band patterns are quite realistic compared with the diffuse patterns obtained by other researchers (de Borst et al., 1993; Larsson, et al.,1996). Especially, the multi-band pattern, which is very close to the realistic situations that take place in laboratory experiments.

If the imperfection at the right middle side of the specimen is ignored, and the specimen is viewed as homogeneous, the limit loads valued at 12.33 N/mm^2 and 8.49 N/mm^2 are calculated using peak frictional angle ϕ_p=25°, and residual frictional angle ϕ_r=15°, respectively. However, a limit load of 11 N/mm^2 is obtained from the load-axial strain curve (figure 8.17 (a)) for the shear band analysis.

Table 8.3 The automatic creation of nodal points and shear band elements

Load step	New nodes	New shear band elements
10	183	98 90 183
15	184	98 90 184 183 90 82 184
17	185 186	90 82 186 184 75 68 185 185 83 75 82 74 186
18	187	68 60 187
19	188 189 190 191 192	29 189 37 188 189 191 45 37 52 44 190 190 60 52 191 190 45 67 59 192 192 74 67
20	193 194	53 46 193 193 61 53 194 83 76 76 69 194

The differences in limit load illustrate that shear band initiation and propagation in the specimen is a progressive failure process. The final rupture of the soil sample occurs before a shear band channel forms through the sample along which shear strength is mobilized fully at residual strength. This has shown again that the average strength of a soil mass at failure must be greater than the residual strength (Potts et al., 1990). It must be admitted that neglecting connections between independent shear bands in the scheme

artificially increases the limit load, as shown in figure 8.15 to illustrate the ill conditioning of the propagation of the shear bands. Some "locking" occurs along the shear band channel which prevents sliding.

If the imperfection is moved to left middle boundary of the specimen, and the material properties and discretization are kept unchanged, the critical load is almost the same as before as shown in figure 8.22 (a). The shear band patterns are more or less the same, but the shapes and locations of the shear bands are different, which may result from the change of the relative location of the weak element to the left corner of the specimen. The left corner is different from the right one in that it is simply supported. Many experimental observations have suggested that slight alterations in specimen geometry, loading conditions, material properties or imperfections will bring about different localization patterns. Exactly the same localization patterns can never be repeated in experiments because of the differences mentioned above among the specimens.

8.4.2 A passive earth pressure problem

8.4.2.1 Description of the problem

As a further test, the analysis of the passive resistance of a frictional soil supported by retaining wall is another example that can be used to verify the efficiency of the proposed framework. Its success will exhibit the possibility of practical use of contact band element to realistic geotechnical problems. In this analysis, the wall is considered to be elastic. The cohesion of the soil is assumed to be zero. Associated Mohr-Coulomb criterion with elastic-perfectly plastic constitutive model is employed for the originally non-localized soils. The soil parameters are: $E=5x10^4$ kPa, $\nu=0.35$,

frictional angle ϕ=25°. After the emergence of shear bands, the proposed cross-isotropic elastic model with special Mohr-Coulomb yielding criterion is used for the shear band materials. Along the shear band, E_t=100.0 kPa, ν_t=0.35, the shear modulus G=384.6 kPa. Across the shear band, E_n=1000.0 kPa, ν_n=0.35. For the shear band material, ϕ is set to be 10°, which corresponds to the residual strength of the soil mass. For the normal operation of the numerical analysis, the critical plastic strain for the onset of shear bands is assumed to be equal to 1%. This example differs from the biaxial test in that there were no weak elements introduced to trigger shear band localization.

In case I, the wall is taken as elastic as the soil mass, E_{wall}=5x10^4 kPa, ν_{wall}=0.25. The wall is around 1 m deep and 0.11 m thick, with an embedment depth of 0.34 m. In case II, the embedment depth of the wall is equal to zero in order to compare with the results from classical earth pressure theories. The total number of elements and nodal points are kept unchanged, as shown in figure 8.23 (b). The elastic modulus of the wall was highly increased to 800 MPa, which is almost rigid compared to the soil mass. All the other material properties remained unchanged. The soil domain selected and the wall for the analysis are shown in figure 8.23 (a) and (b). In both cases, the soil and wall were initially discretized with a total of 216 elements, and 249 nodal points. For the sake of simplicity, switch-on-gravity was applied for both the wall and the soil in step 1 with unit weight equal to 25 kN/m^3 and 20 kN/m^3, respectively. In step 2, a horizontal displacement of 0.5 mm was applied to the left side of the wall toward the soil. For case I, steps 3 to 12, an increment of horizontal displacement of 0.2 mm applies at the same place each step. For case II, steps 2 to 6, an increment of horizontal displacement of 0.2

mm was applied in each step. From step 7 to step 9, the increment was decreased to 0.1 mm.

8.4.2.2 Analyses of results and discussions

In case I, with the increase of horizontal displacement acting on the wall, soil elements Nos 67 and 70 near the toe of the pit yielded. When horizontal displacement U_h was increased to 1.1 mm, two shear bands were initiated around the toe, but no shear band elements were created because the two bands were isolated in single elements. From then on, new bands and old bands would continuously form and propagate. The shear bands elements were always surrounded by yielding soil elements. Eventually, when U_h was equal to 2.5 mm, multiple shear band channels (slip surfaces) occurred in the soil behind the wall. The evolving process of shear band channels can be seen in the figures from figure 8.24 to 8.31. It is necessary to indicate that the overall slipping of the soil mass over a slip surface still cannot be properly simulated due to the failure to consider connections between different shear bands. This is also one of the reasons which causes high passive earth pressure which will be discussed later. If the shear bands were connected, a portion of energy would have not been absorbed by the soils to create more shear bands but, instead, would have been dissipated through friction between the soil masses above and below the slip surfaces. Consequently, fewer shear band channels would have formed. It is seen that the slip surfaces lying at shallow level took the form of a straight line, and that those lying at relatively deep level were consistent with the closed form solution using plasticity theory which compared most favorably with the realistic cases.

The lateral soil resistance on the wall versus the applied horizontal displacement is plotted in figure 8.32 (a). The minimal resistant force P_{p1}=14.9 kN is obtained directly from the plot. If the passive earth pressure is defined by the Mohr rupture envelope without considering the effect of the wall, a value of P_{p2}=6.57 kN is calculated based on the residual frictional angle. Rosenfarb and Chen (1972) proposed the 'log-sandwich' mechanism using theory of plasticity and developed a closed form solution. For vertical walls with horizontal backfills, the closed form solution is exactly as same as that from the Coulomb earth pressure theory. In this test, the interaction between the soil and pile wall is simply taken into account by assuming a rough friction angle of 30° between them (Bowles, J. E., 1988), the corresponding passive earth pressure is P_{p3}=12.8 kN, corresponding to the residual shear strength of the soil.

The main results for case II are shown from figures 8.33 to 8.37, it can be seen that the initiation and the evolution of shear bands differ from those in case I because of the influences of the stiffness and the embedment of the wall. When the accumulated horizontal displacement applied on the wall reached 1.5 mm, the critical resistance P_{p3} from the soil was equal to 18.32 kN, which, here, is assumed to be the passive earth resistant force, with a rupture surface channel which passed through the soil mass. The magnitudes of passive resistant forces from different sources are listed table 8.4. The analytical results are obtained based on the soil residual strength. The resistant force obtained from the finite element analysis is much higher than that from the Mohr rupture surface because the wall effect is neglected in the calculation of lateral earth pressure. However, it is still higher than the one from theory of plasticity. It can be readily explained as follows.

Table 8.4 The comparison of passive resistant forces using different ways

Methods of calculating passive earth pressure	Passive resistant forces
Mohr rupture surface	6.57 kN
Plasticity theory (equivalent to Coulomb theory)	12.8 kN
Finite element method (elastic sheet pile wall)	14.9 kN
Finite element method ('rigid' sheet pile wall)	18.3 kN

In this example, the frictional interaction between the wall and the soil has not been properly considered. The soil elements were rigidly connected to the pile wall. On the other hand, the unreasonable connections between the shear bands do not allow soils in some areas to mobilize residual shear strength. These two effects lead to higher passive earth pressure. Interaction between the wall and the soil can be better modeled by using a continuous interface element. Then, sliding can be accounted for in the analysis. In this example, the passive resistance force calculated from the plasticity theory based on the residual strength should be lower than the limit load. Often final rupture of the soil mass occurred before the failure surface has been developed fully. Thus the average strength of the soil mass must be less than the peak strength of the soils and greater than the residual strength (Potts et al., 1990). Subsequently, the actual resistance should be greater than the closed form solution based on residual strength. The passive resistance force for the elastic wall is lower than that for the rigid wall because the elastic wall restricts the soil mass in the backfill less than the 'rigid' sheet pile wall.

This numerical example is of groundbreaking significance for analyses of the critical earth pressure. First of all, a number of assumptions made for the classical theories do not apply to this finite element method anymore. Rupture surfaces are never specified before the analysis. The deformation properties of soils and retaining walls are considered. The most striking point in this analysis is that progressive failure of the soil mass accompanied by the emergence and propagation of shear bands has been simulated, which cannot be recovered from conventional limit equilibrium theory or any other conventional numerical methods. Shear banding was initiated first in the mass around the toe of wall. Then, the band propagated, and new shear bands formed continuously. The inception and propagation of the band were both strain dependent. The post-peak strains within the shear zone increased, and strength reduced from peak towards residual gradually.

8.5 Concluding remarks

In this chapter, a framework to generate automatically discrete shear bands is developed. The propagating shear band is modeled with the discrete shear band elements going through the original finite element mesh, which are 3-node triangular elements and 4-node quadrilateral elements. The orientations are determined using bifurcation theories. No prescription is necessary for the alignments of shear bands. No shear band elements are predetermined in the original mesh. In order to make the simulation more realistic, the proposed empirical bifurcation criterion and location criterion are applied. Preliminary numerical results from the simulation of biaxial tests have shown that the

imperfections at sides of the specimen trigger shear bands that originate from the imperfections and then propagate to other sides. The localization patterns with multiple shear bands are quite realistic. On the contrary, the diffuse patterns obtained by other researchers usually don't give the exact shear band zone. The method is also successfully applied to a passive earth pressure problem, which indicates that the method is promising in solving engineering problems. It has given realistic multiple rupture surfaces in the backfill. Progressive failure can be reflected in the analyses. The differences of limit loads calculated from different sources demonstrate that more endeavors should be made to improve the proposed scheme for shear band analyses.

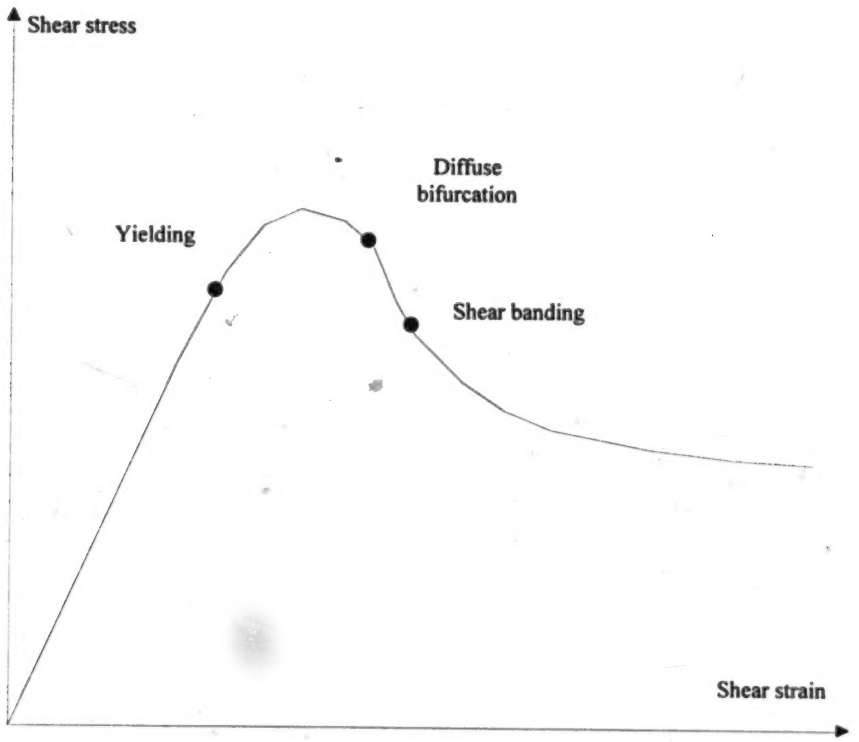

Figure 8.1 An illustration of relationships among yielding, diffuse bifurcation, and shear banding

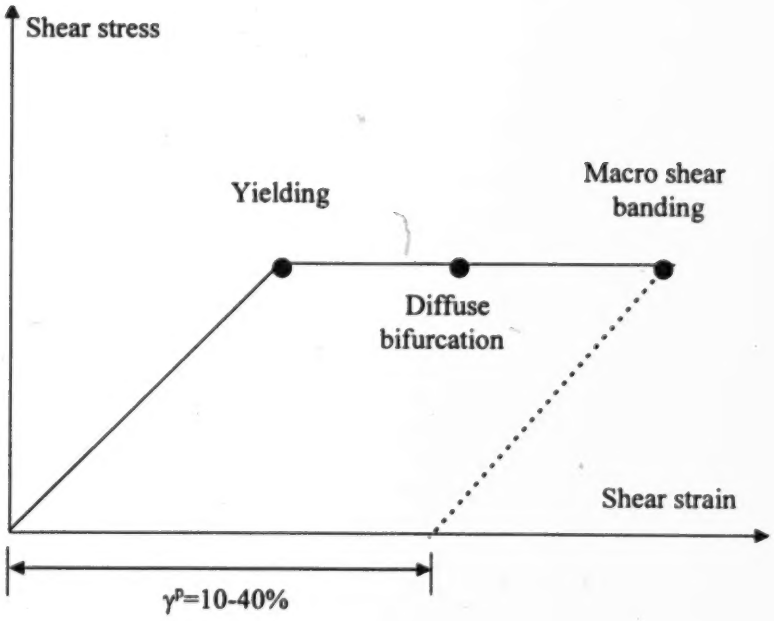

Figure 8.2 Plastic shear strain at the onset of shear band localization under elastic-perfectly plastic model

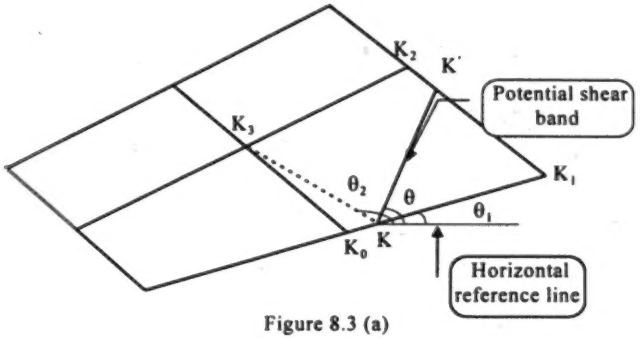

Figure 8.3 (a)

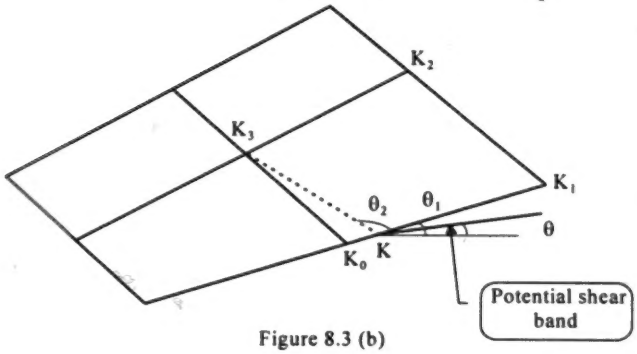

Figure 8.3 (b)

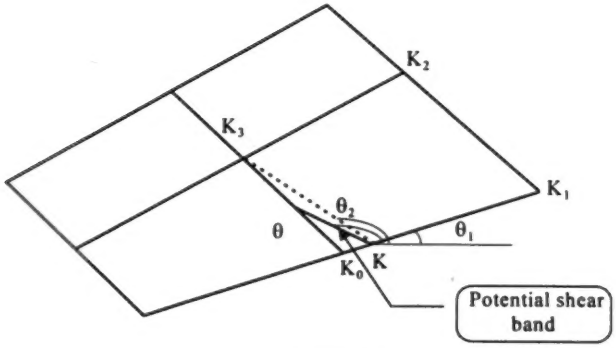

Figure 8.3 (c)

Figure 8.3 The geometric check of the potential shear band line, (a) $\theta_1<\theta<\theta_2$, (b) $\theta<\theta_1$, (c) $\theta<\theta_2$

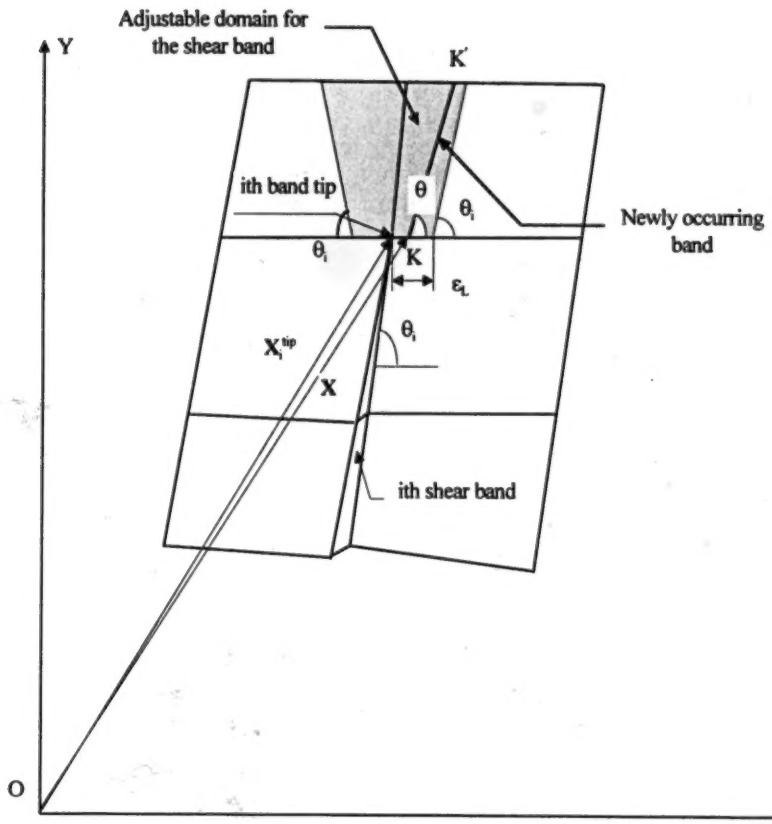

Figure 8.4 Location and orientation check for the newly occurring shear band

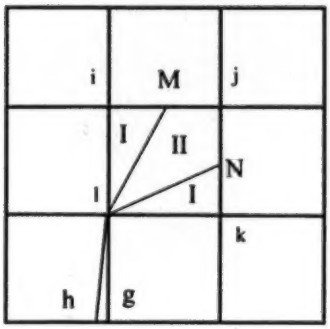

Figure 8.5 (a)

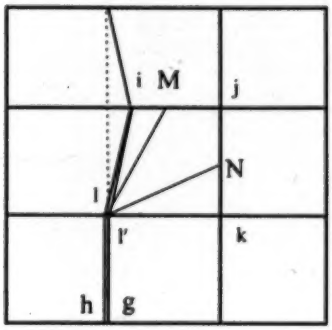

Figure 8.5 (b)

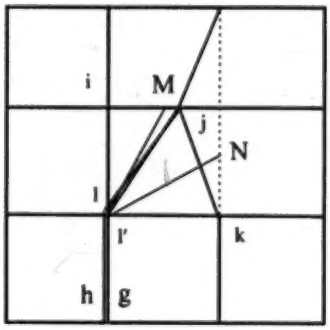

Figure 8.5 (c)

Figure 8.5 Two categories of shear band propagation, (a) the definitions of three domains in an element, (b) reshape of soil element, (c) breakup of soil element (after Zhau and Lin, 1989)

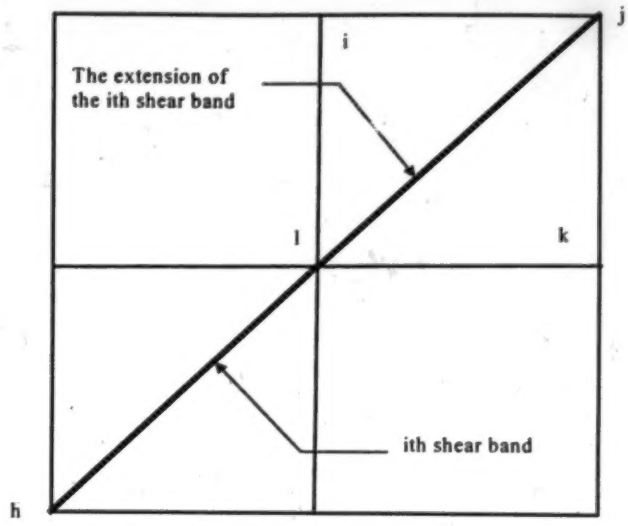

Figure 8.6 (a)

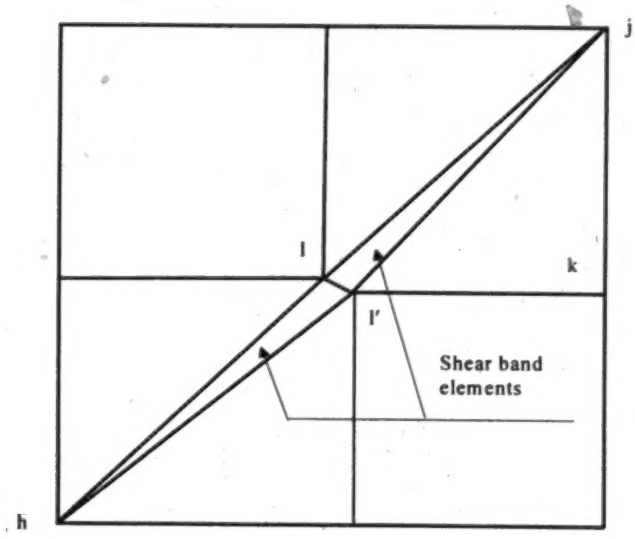

Figure (b)

Figure 8.6 The creation of double shear band elements, (a) extension of an isolated band, (b) creation of two band elements

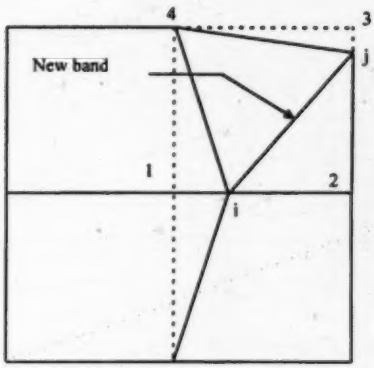

Figure 8.7 (a)

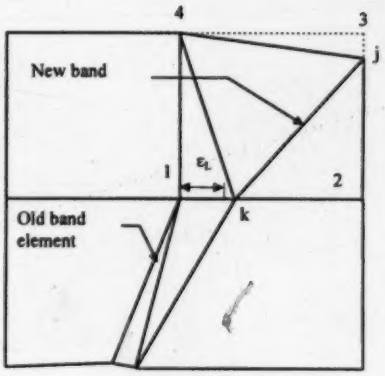

Figure 8.7 (b)

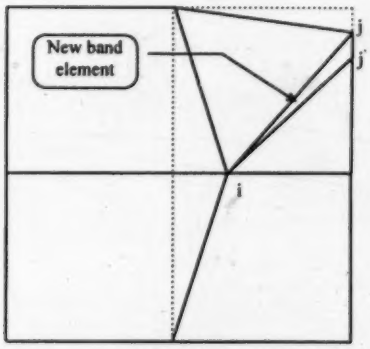

Figure 8.7 (c)

Figure 8.7 Different cases for the creation of new bands (a) isolated band, (b) violation of location criterion, (c) band tip on soil structures

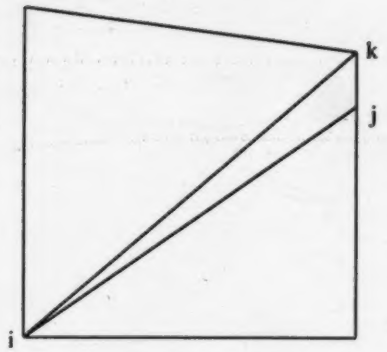

Figure 8.8 (a)

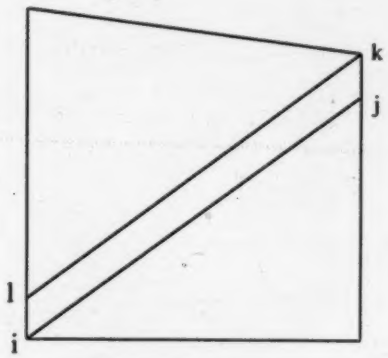

Figure 8.8 (b)

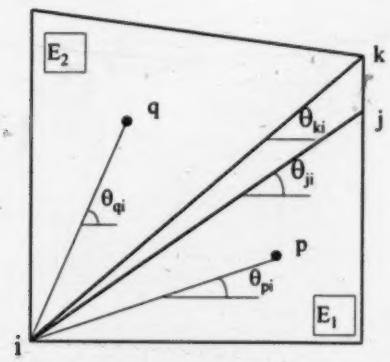

Figure 8.8 (c)

Figure 8.8 Renumbering of regular soil elements and band elements, (a) triangular band element, (b) regular soil element

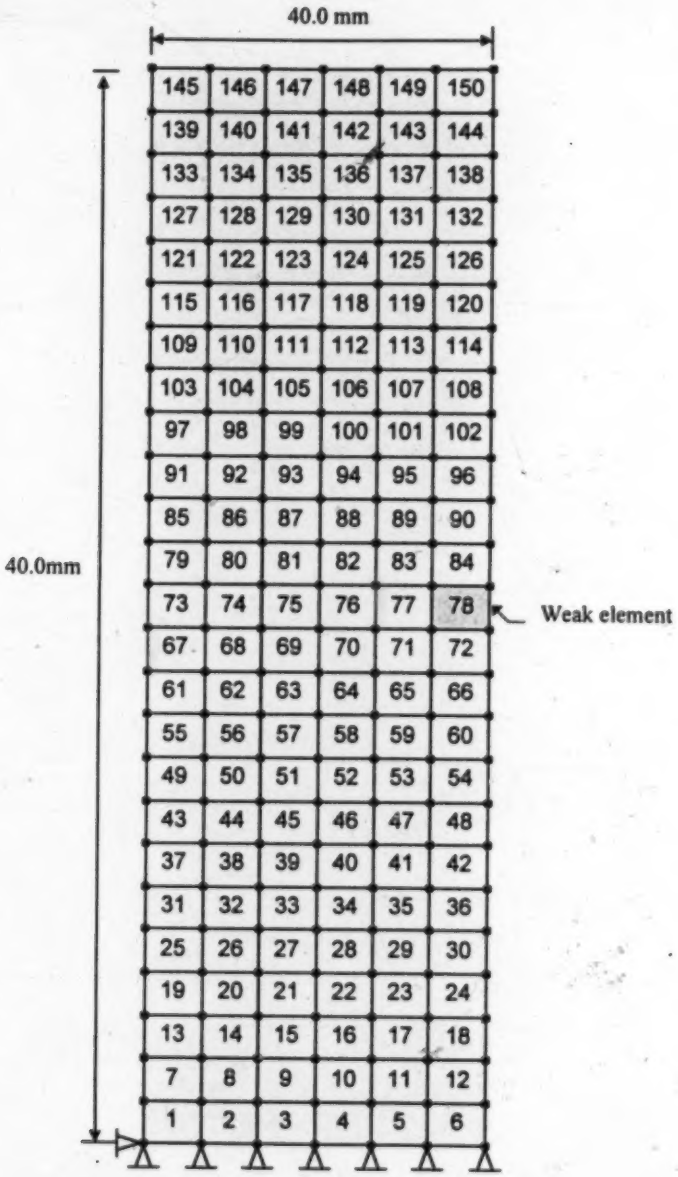

Figure 8.9 Original mesh for the biaxial test

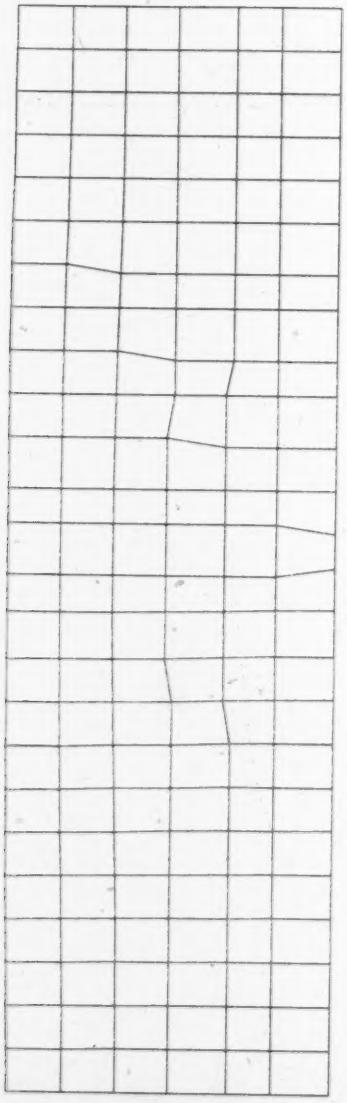

Figure 8.10 The structure configuration at axial strain equal to 13.3 %

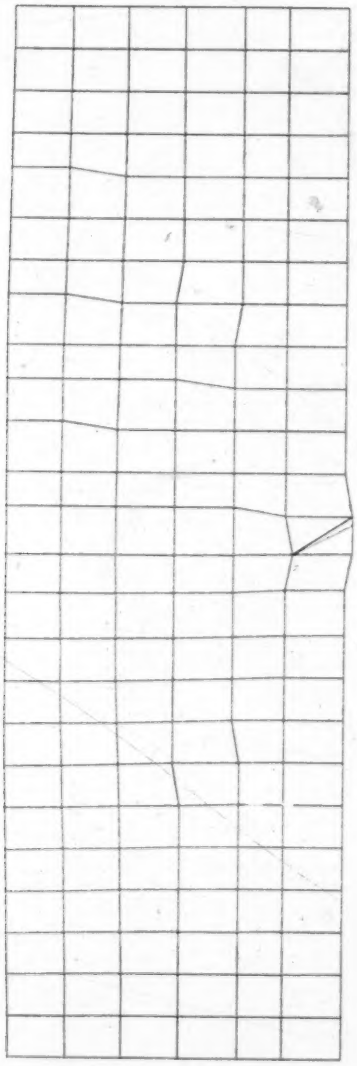

Figure 8.11 The structure configuration at axial strain equal to 14.0 %

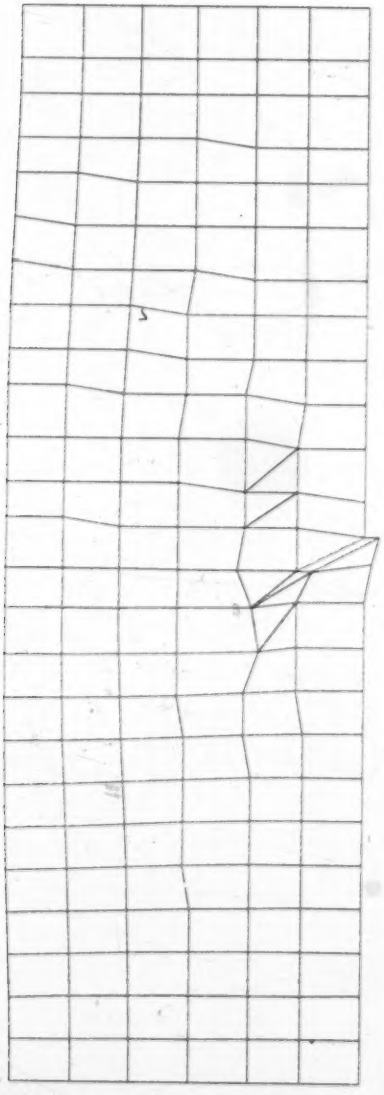

Figure 8.12 The structure configuration at axial strain equal to 14.7 % (stage 1)

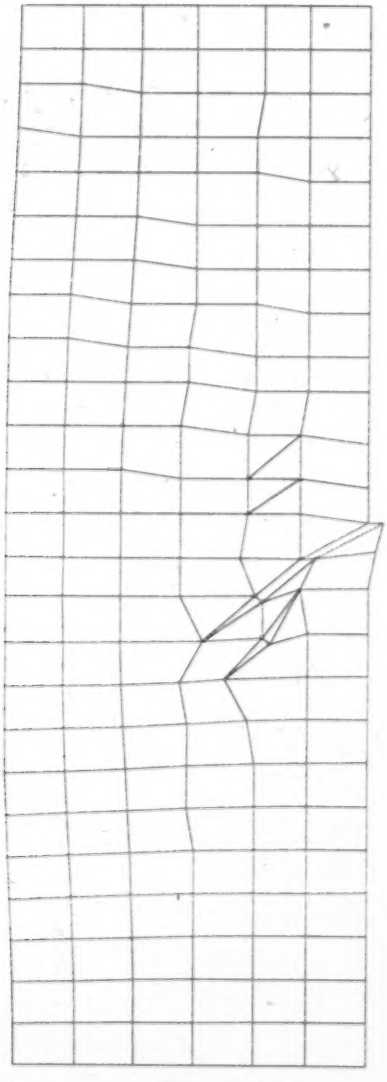

Figure 8.13 The structure configuration at axial strain equal to 14.7 % (stage 2)

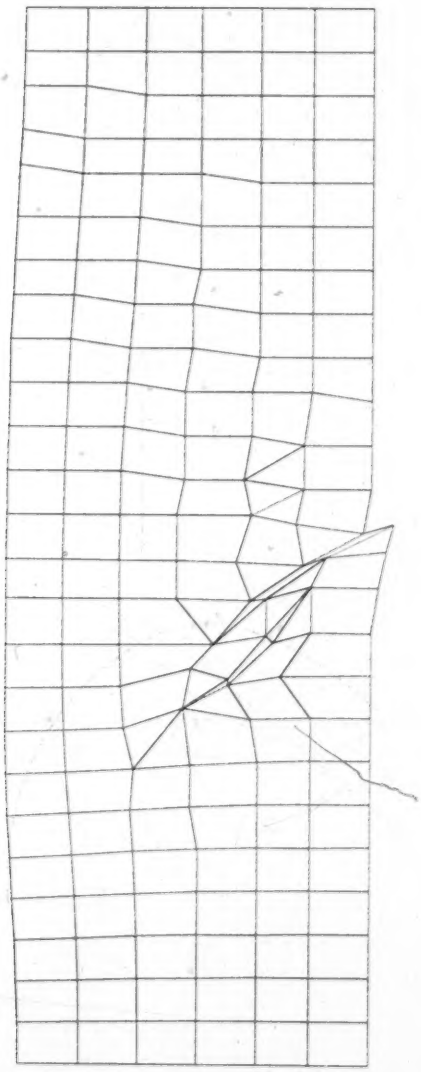

Figure 8.14 The structure configuration at axial strain equal to 15.1 % (stage 1)

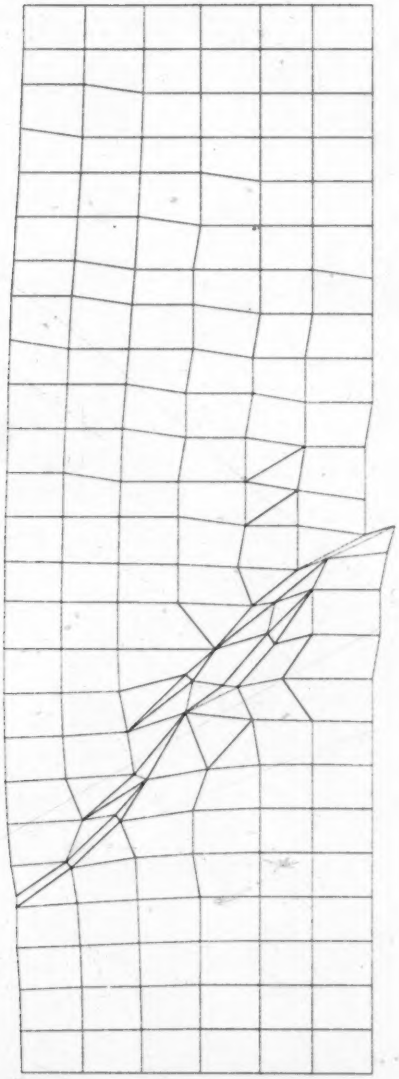

Figure 8.15 The structure configuration at axial strain equal to 15.1 % (stage 2)

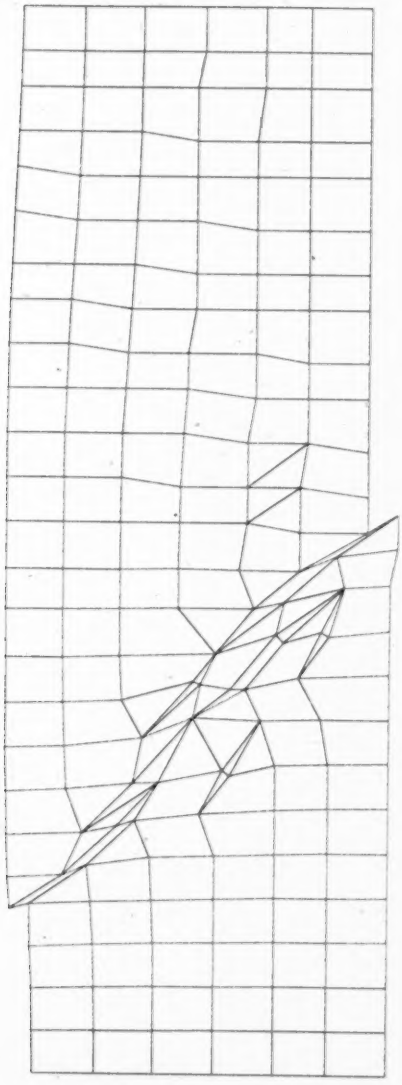

Figure 8.16 The structure configuration at axial strain equal to 15.1 % (stage 3)

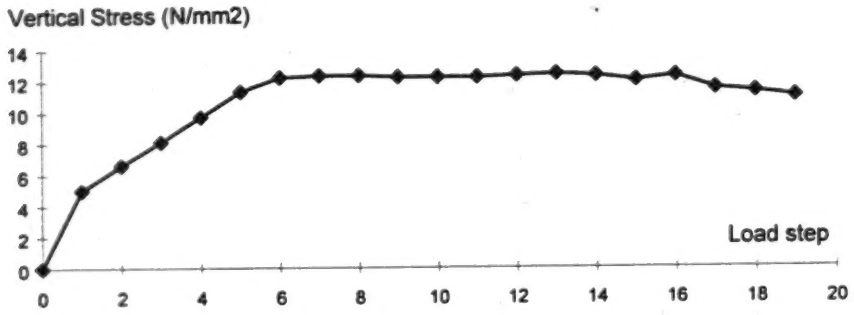

Figure 8.17 (a)

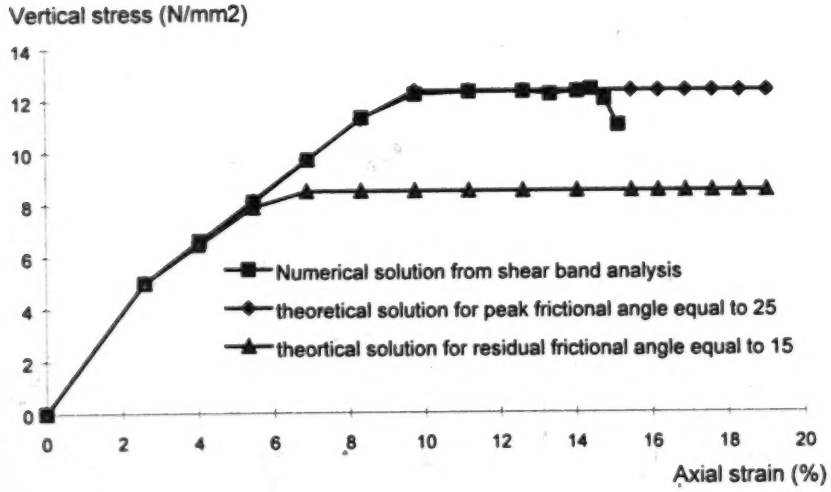

Figure 8.17 (b)

Figure 8.17 The relationship between the equivalent vertical pressure and axial load, (a) the change in equivalent pressure on the specimen top versus load steps, (b) the relationship between vertical stress and axial strain

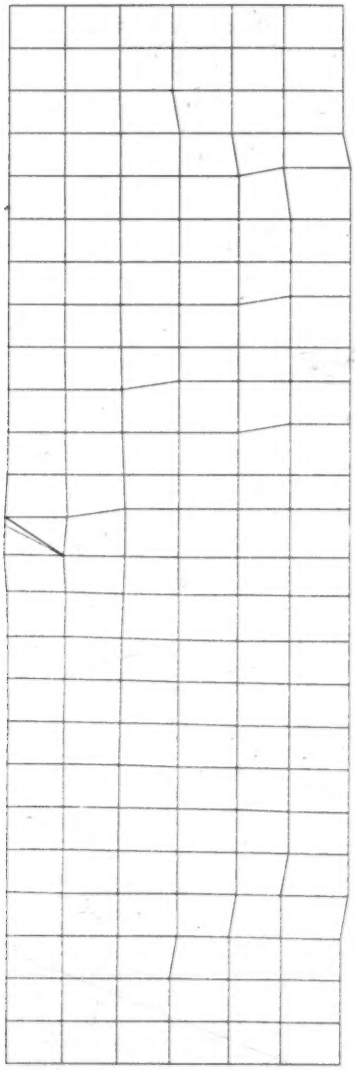

Figure 8.18 The structure configuration at axial strain equal to 14.7 % (the weak element placed at left side)

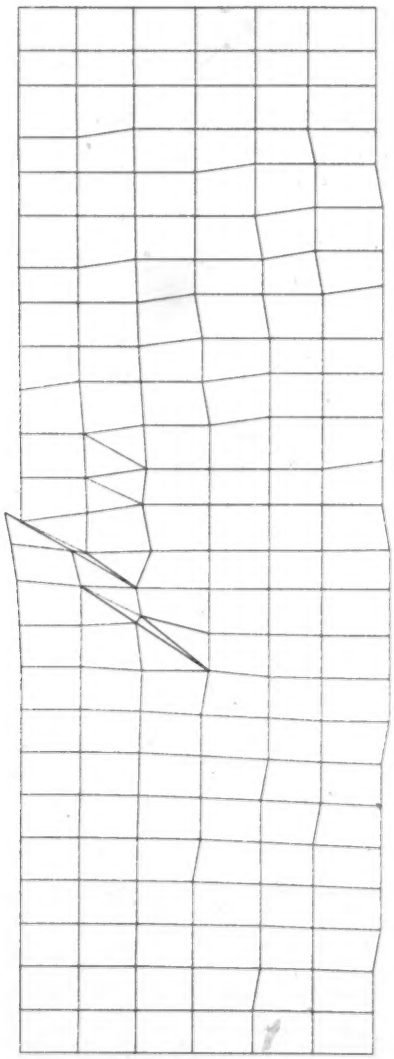

Figure 8.19 The structure configuration at axial strain equal to 16.5 % (stage 1, weak element placed at left side)

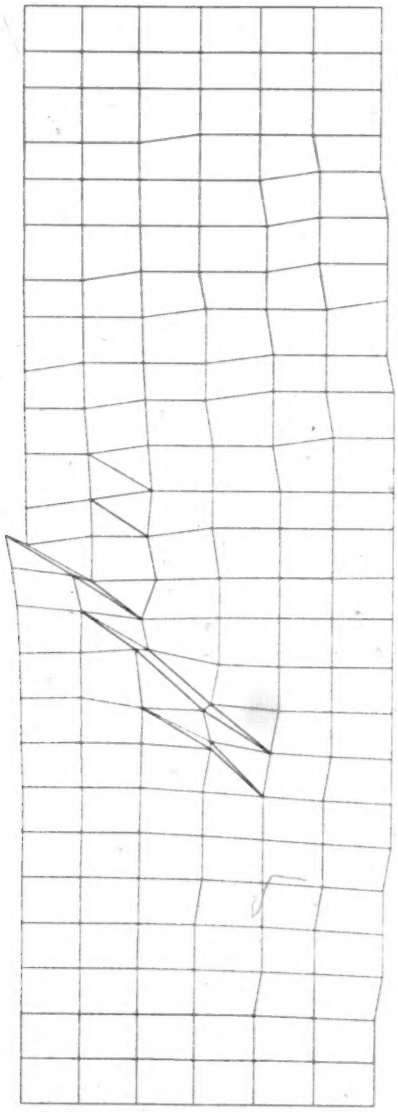

Figure 8.20 The structure configuration at axial strain equal to 16.5 % (stage 2, weak element placed at left side)

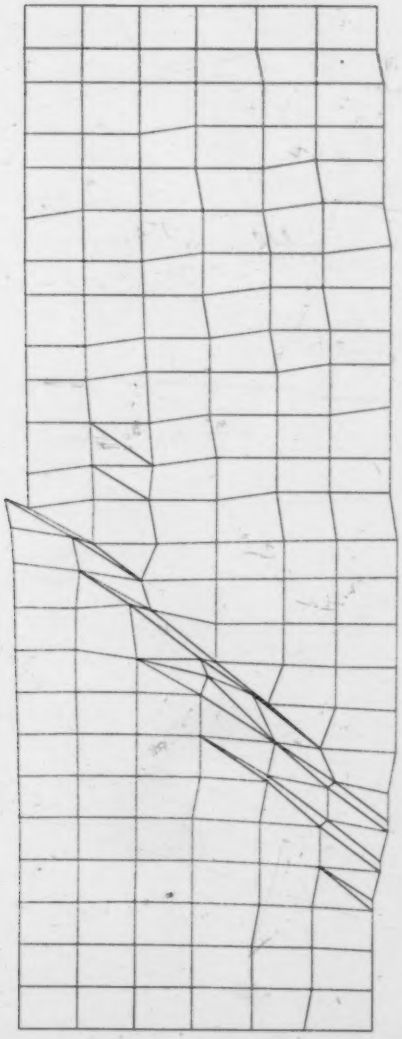

Figure 8.21 The structure configuration at axial strain equal to 16.5 % (stage 3, weak element placed at left side)

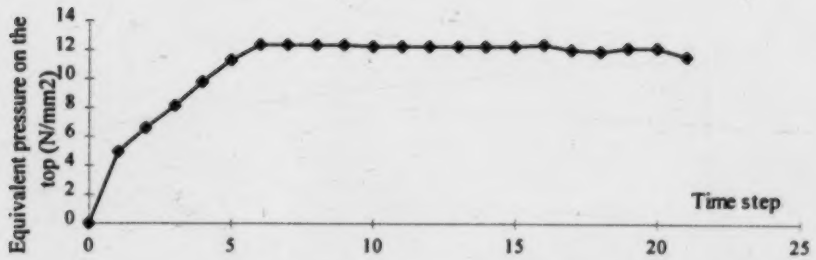

Figure 8.22 (a)

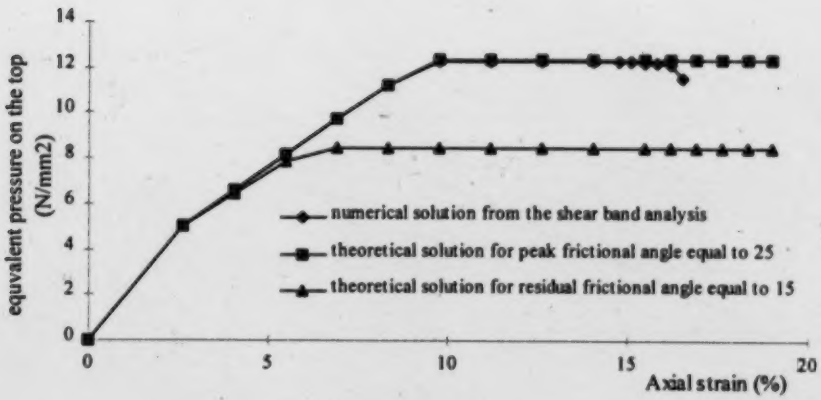

Figure 8.22 (b)

Figure 8.22 The relationship between the equivalent vertical pressure and axial load, (a) the change in equivalent pressure on the specimen top versus load steps, (b) the relationship between vertical stress and axial strain (the imperfection for the numerical analysis is placed on the left side of the specimen for the numerical analysis)

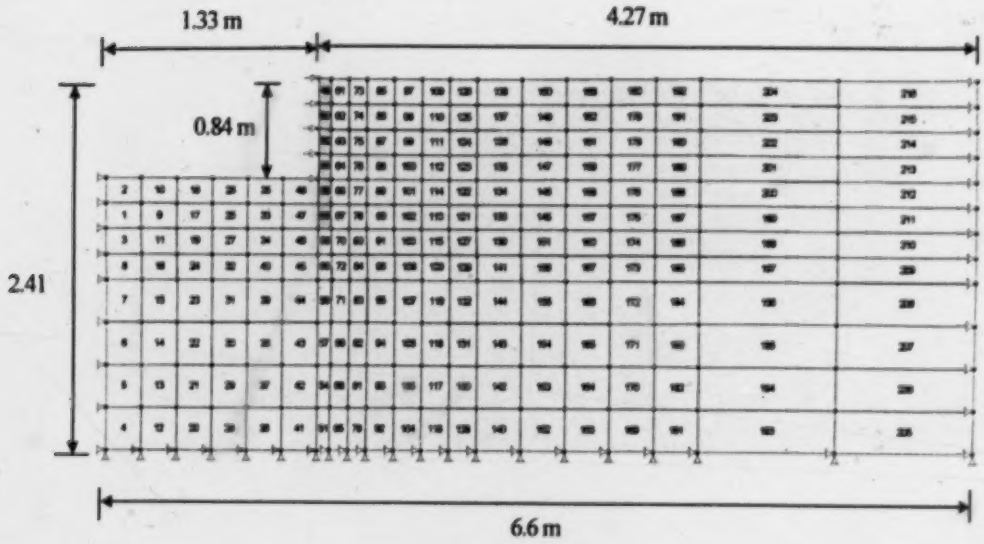

Figure 8.23 (a)

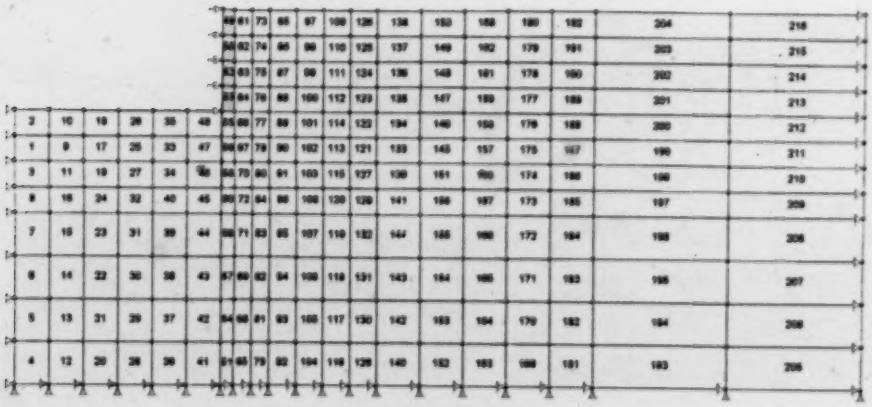

Figure 8.24 (b)

Figure 8.23 (a) A passive earth pressure problem for the elastic sheet pile wall with a finite embedment depth, (b) A passive earth pressure problem for the 'rigid' sheet pile wall with a zero embedment depth

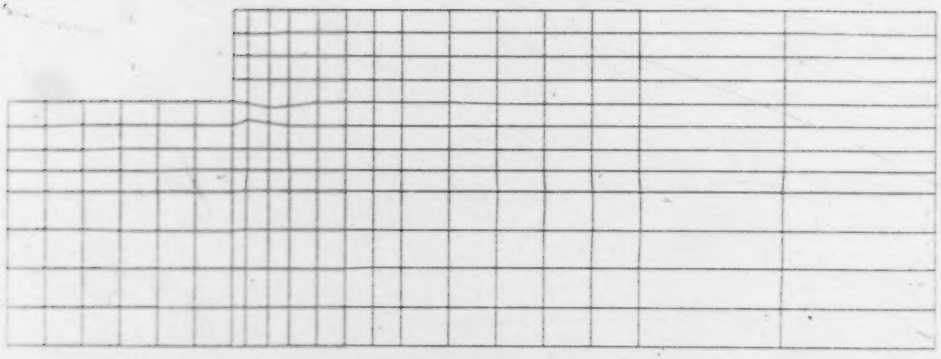

Figure 8.24 Deformed mesh when horizontal displacement equal to 1.1 mm

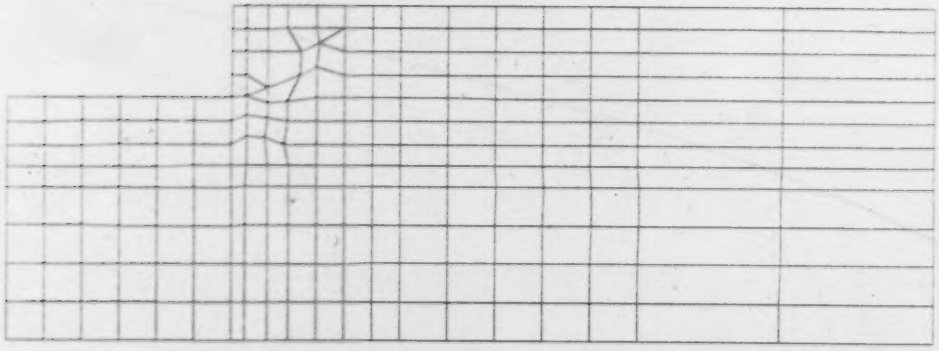

Figure 8.25 Deformed mesh when horizontal displacement equal to 1.3 mm

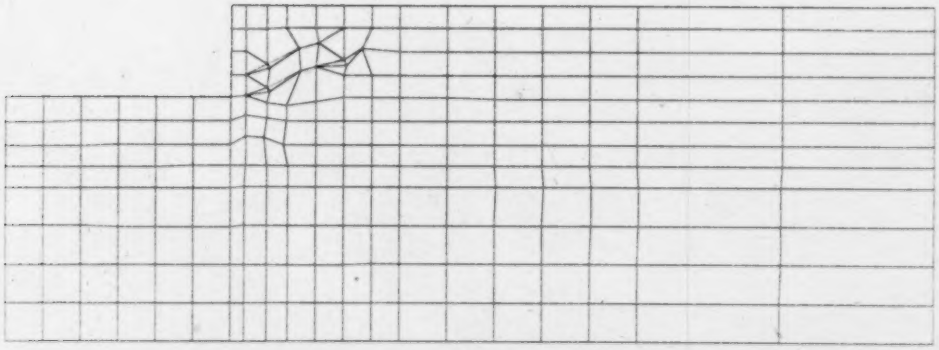

Figure 8.26 Deformed mesh when horizontal displacement equal to 1.5 mm

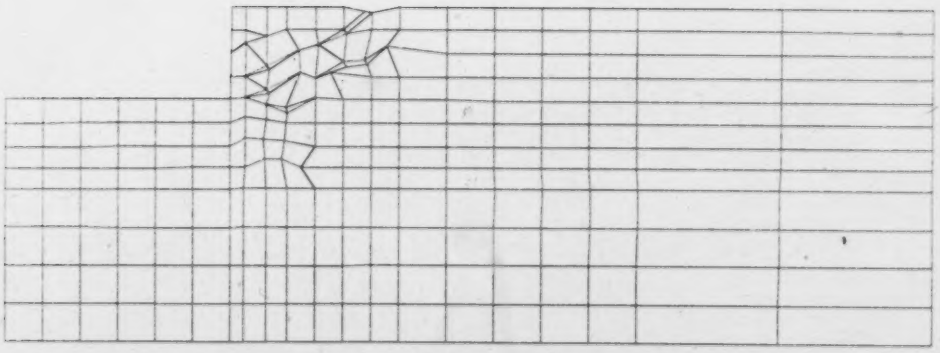

Figure 8.27 Deformed mesh when horizontal displacement equal to 1.7 mm

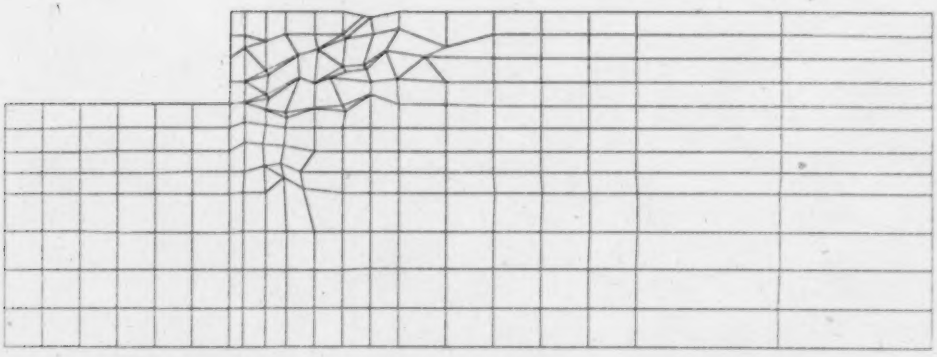

Figure 8.28 Deformed mesh when horizontal displacement equal to 1.9 mm

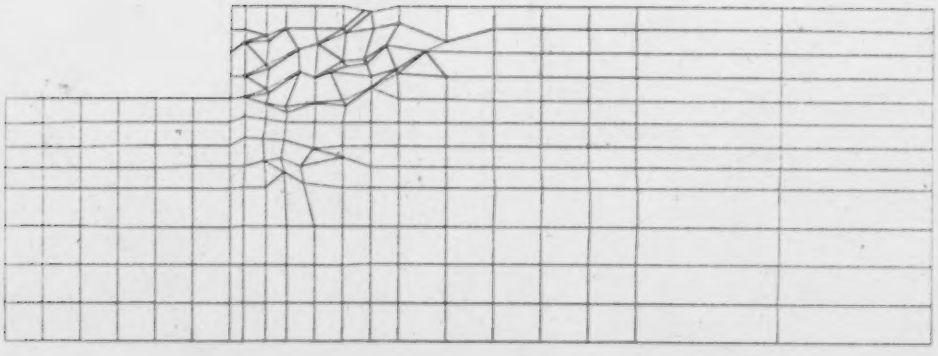

Figure 8.29 Deformed mesh when horizontal displacement equal to 2.1 mm

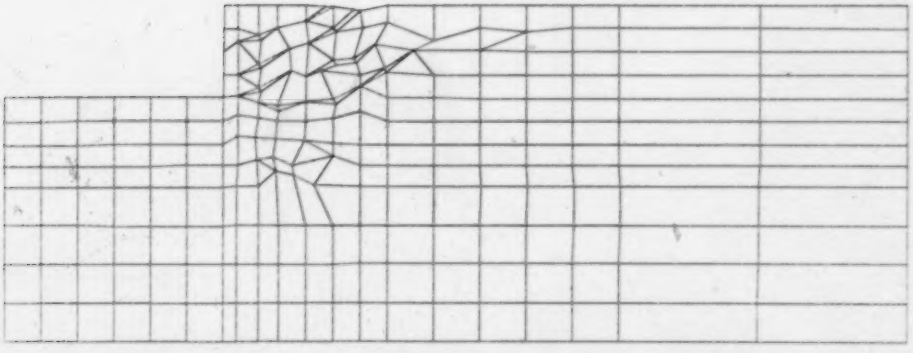

Figure 8.30 Deformed mesh when horizontal displacement equal to 2.3 mm

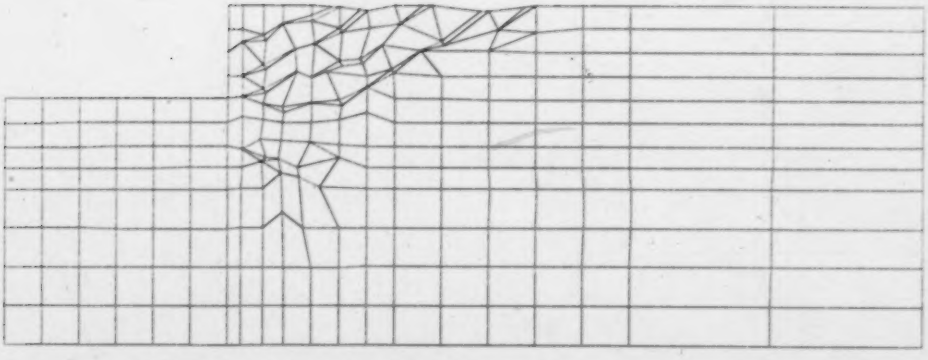

Figure 8.31 Deformed mesh when horizontal displacement equal to 2.5 mm

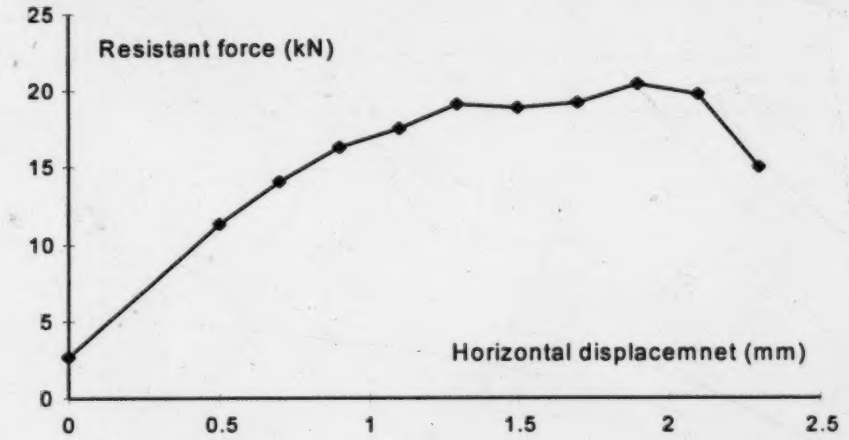

Figure 8.32 (a)

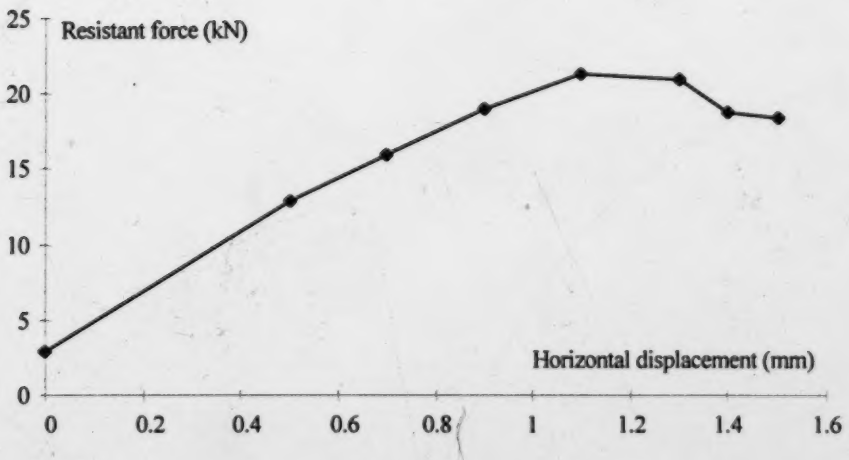

Figure 8.32 (b)

Figure 8.32 (a) Lateral earth resistant force versus horizontal displacement for the elastic sheet pile wall with a finite embedment depth, (b) Lateral earth resistant force versus horizontal displacement for the 'rigid' sheet pile wall with embedment depth set to zero

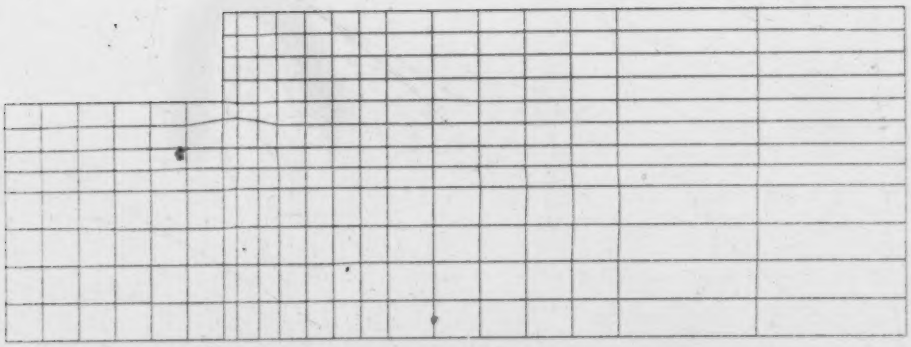

Figure 8.33 Deformed mesh when horizontal displacement equal to 1.1 mm for the 'rigid' sheet pile wall

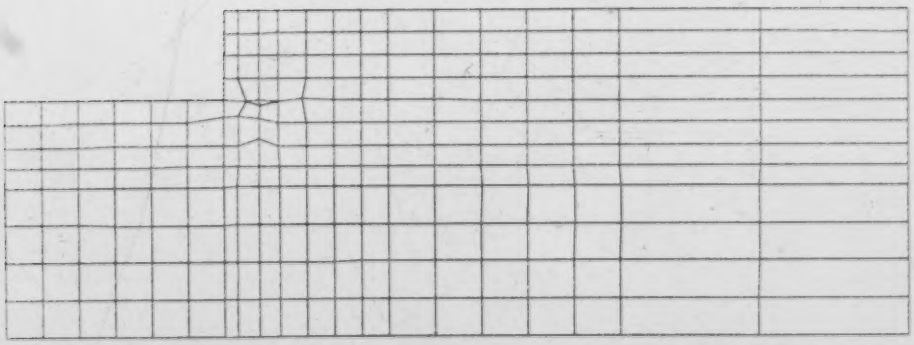

Figure 8.34 Deformed mesh when horizontal displacement equal to 1.3 mm for the 'rigid' sheet pile wall

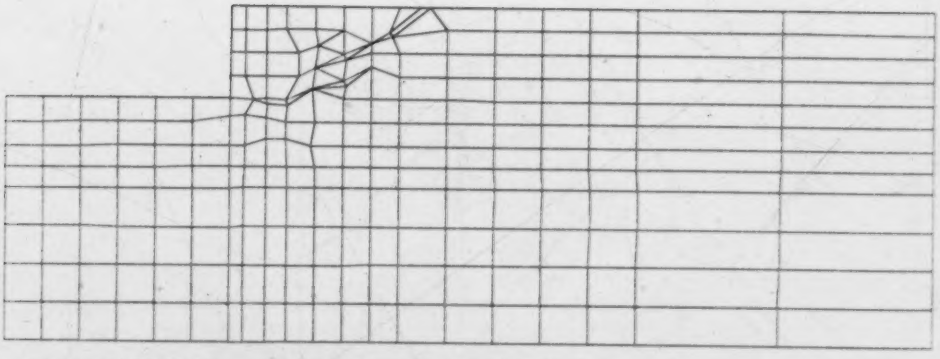

Figure 8.35 Deformed mesh when horizontal displacement equal to 1.4 mm for the 'rigid' sheet pile wall

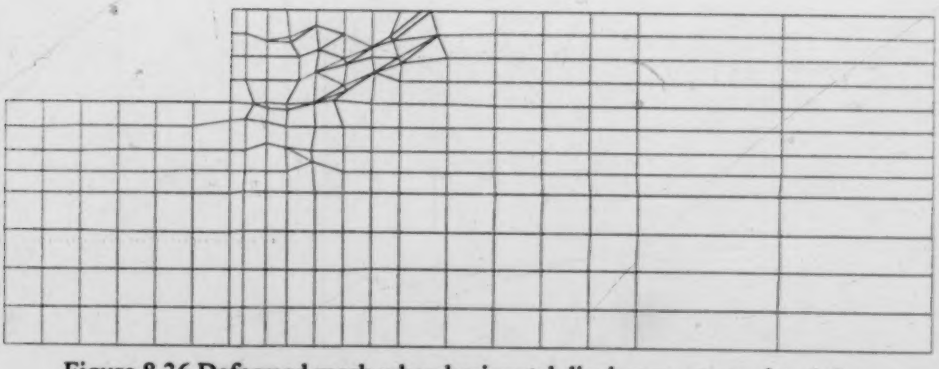

Figure 8.36 Deformed mesh when horizontal displacement equal to 1.5 mm for the 'rigid' sheet pile wall

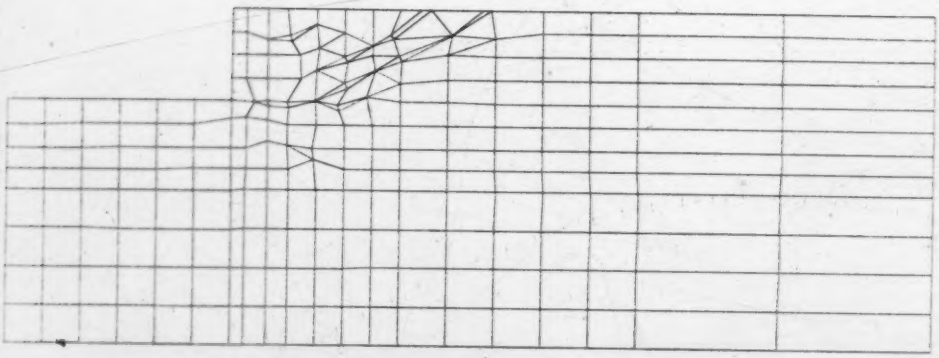

Figure 8.37 Deformed mesh when horizontal displacement equal to 1.6 mm for the 'rigid' sheet pile wall

Chapter 9

Conclusions and recommendations

9.1 Introduction

Numerical simulation of the kinematic propagation of shear bands is systematically investigated. Discrete shear band elements are used to model the generation and development of material inhomogeneities in the shear band zones. The contact band element approach is proposed. The alteration of mechanical properties and anisotropy of the shear band materials are reflected using different constitutive models. Some numerical problems such as large local distortion of shear band elements, overlapping, and band kinking are discerned, which result in numerical ill-conditioning, kinematic incompatibility problems, etc. New algorithms and constitutive descriptions have been developed to eliminate and alleviate these problems.

Secondly, a framework to generate automatically the discrete shear band element is also developed. The computing work to perform the localization analysis can start without prescribing any shear band elements in the original mesh. No prescription is necessary for alignments of shear bands. With the application of load increments, discrete shear band elements would form in the interior of the normal soil elements, then become deformed and extended. As such, the initiation and propagation of shear bands are simulated.

9.2 Conclusions

9.2.1 Contact band element approach

For the simulation of the propagation of shear bands with a definite thickness subject to large shear deformation, a methodology called the "contact band element approach" is developed. The shear band elements are formed and updated by referring to the relative locations of nodal points on the upper and lower surfaces of the shear bands. Band elements are updated step by step, which keeps the aspect ratio of 3-node triangular elements, and 4-node quadrilateral elements within acceptable ranges. A special band element with more than 4-nodes is presented, and its stiffness is derived. In this framework, distortions of the band elements are eliminated. The re-arrangement of nodal points of new band elements on different shear band boundaries greatly alleviate the shear band kinking problem. Unifying the concepts of shear band localization with tensile fracture makes it possible to model opening of shear band elements during shear band propagation.

9.2.2 Cross-isotropic elastic model with specail Mohr-Coulomb yielding criterion

A cross isotropic elastic model with special Mohr-Coulomb yielding criterion is developed. In this model, the anisotropy of the shear band material along and normal to shear band directions is taken into account. Yielding and failure can only occur along a prescribed direction. In shear band analysis, tangential shearing along the shear band direction is the preferred direction of yielding. No yielding occurs in other directions.

Strictly speaking, this implies that all the yielding criteria, including the general Mohr-Coulomb criterion, are not applicable to shear band modeling.

9.2.3 The application of contact band element approach to interfaces and joints using special strain description

The contact band element approach is successfully used to simulate large slipping of interfaces. The conventional 4-node or 8-node rectangular thin elements are replaced by 3-node and 4-node band elements to maintain geometric compatibility, even under larger shear deformation. The particular strain expressions are derived to reflect the characteristics of shear strain along an interface. The shear strain is only composed of tangent deformation based on the difference between the upper and lower surfaces of the interface. No changes in the thickness of interfaces are taken into account. To be consistent with the method of analysis of laboratory data, shear stresses along the interface and normal stresses across the interface are related to tangent and normal displacements. Pull-out tests have shown that the largest pull-out deformation has always been developed on the top and bottom of the interfaces well after the real ultimate load is reached. There are no oscillations in the distributions of mobilized shear stress and axial forces. They are smoothly and consistently distributed along the reinforcement.

9.2.4 Kinematics remedy of overlapping problem

With the application of some constitutive model such as the Modified Cam-Clay or the cross-isotropic elastic model with special Mohr-Coulomb yielding criterion, the overlapping problem can be greatly alleviated. In addition, a scheme to revise displacements to eliminate the overlapping is proposed. The displacements or corresponding forces on relevant nodal points are applied whenever penetration is

detected in some band elements. The stiffness of the elements would be updated with the new stress state. As a result, equilibrium iterations are required to reduce unbalanced forces caused by unrealistic nodal displacements. With the combination of proper constitutive relations and the above mentioned kinematics scheme, the overlapping problem can be effectively solved.

9.2.5 Automatic creation of discrete shear band elements

A scheme to automatically generate shear band elements is developed. The propagating shear band is modeled with the discrete shear band elements going through the original finite element mesh. The orientations are determined using bifurcation theories. The relevant soil elements are broken up or/and are reshaped to fit new shear band elements. The shear band elements have their own constitutive relations, stiffness, etc. As independent elements, the shear band tip is modeled with a 3-node triangular element in order not to reduce the stress concentration around the tip. A 4-node quadrilatera

l element is used for all the other shear band domains. The use of an empirical discontinuous bifurcation criterion, and of a location and orientation check of newly created band elements, ensure that the initiation and the propagation is as realistic as possible. The preliminary numerical results from the simulation of biaxial tests have shown that the imperfections at the sides of the specimen trigger shear bands. Shear bands initiate from the weak elements. They keep propagating with the increase of load on the top the specimen. Finally, they reach the other side of the specimen. In the process of propagation, approximately parallel bands have formed with reasonable

alignments. Discrete shear band elements model much more closely the actual patterns of shear bands. The application of the proposed scheme to the passive earth pressure problem has enhanced its availability to practical uses. The rupture surfaces generated in the backfill are successfully tracked. The different limited load values from classical closed form solution and numerical results have demonstrated that further investigations should be undertaken for the proposed approach.

9.3 Recommendations

All the approaches and techniques developed in this research present a basis for the analysis of shear band initiation and propagation. Much more research effort should be made to realize their potential applications to practical engineering problems. Some major problems have arisen and require more attentions.

9.3.1 The study of constitutive response of shear band materials

Obviously, more attention should be focused on the study of constitutive response in the interior of shear band zones. After shear band localization forms, most of the fissures and discontinuities join together. A strong reorientation and breaking up of the particles take place, creating a maximum of anisotropy and non-homogeneity along the shear band. The shear band materials will dilate or contract, and then keep a constant volume. All these events must be reflected in a stress-strain response, one that should be further investigated using some special graphic techniques, such as radiographs, X-ray scanning, Sterero-photogrammetry or computed tomography or image analysis. In view of labortory test results, the back analysis techniques might play an important role.

9.3.2 The further study of contact band element approach

In order to fulfill the potential use of the contact band element approach in relation to practical analysis of shear band localization and interfaces or joints to large shear deformation analyses, it is necessary to accomplish the following tasks:

9.3.2.1 Mesh independence check

Theoretically, the introduction of the shear band thickness in the displacement-based finite element analysis corresponds to the internal length scale like diameters of soil particles in the Cosserat medium. The numerical solutions will be approximately no longer mesh dependent. However, due to the complexity of engineering issues, a number of numerical examples still should be conducted for various engineering projects. In each analysis, mesh density and the aspect ratio of elements are varied to see their effects on shear band propagation, stress distribution, ultimate load, etc. Numerical experience with the contact band element approach is indispensable to get reasonable solutions for shear band analyses.

9.3.2.2 The simulation of closing -opening-reclosing procedures

Shear band openings may occur in some band elements when tensile stress exceeds the tensile strengths. With further propagation, some of them may reclose again. Strictly speaking, shear band elements keep evolving. The checking of the element state is only performed at certain global places along shear bands. The effective way might be to examine the current positions of nodes on the upper and lower surfaces of new elements placed at the old opening elements, if the thickness of the current element is

smaller than the previous one at this place for the opening element. The existence of the new element should be considered. In other words, the opening element is re-closed.

9.3.3 The automatic creation of shear band elements

Some preliminary results have been achieved to model the shear band propagation through the ordinary soil element. The shear band propagation can be automatically tracked. However, there are still some important issues which worth examining.

9.3.3.1 An independent shear band isolated in one element

Very frequently, an isolated shear band is created in the interior of an ordinary finite element. If the element is not placed at the boundaries of a soil structure, two tips of the shear band are just located on the soil element boundaries. Accordingly, no independent shear band elements form for the new shear band. The strain discontinuity may be approximately considered by using the smeared approach , in which the stiffness of the whole element stiffness is modified. The new shear band element and remeshed soil elements would replace the old modified soil element as soon as one or two of the shear band tips extend to other soil elements.

9.3.3.2 The improvement of remeshing techniques

With the extension of shear band tips, some soil elements around them should be reshaped by adjusting a few of the nodal points to give a correct band orientation. The severe distortion of some soil elements might be caused by the adjustment of nodal points, which lead to imprecise stress calculations nearby band tips. Consequently, a robust remeshing technique should be developed to maintain good shapes for the soil elements close to the tips. It might be necessary to densify the local mesh around the tips.

9.3.3.3 The treatment of shear band conjugate directions

In the current research effort, problems will very often arise in the determination of the orientation of new shear bands where there are potential conjugate directions. In such simple examples as biaxial tests, real orientation could be chosen in accordance with physical factors. It is imperative to develop a practical criterion to choose shear band orientation.

9.3.3.4 The improvement of the empirical bifurcation criterion and location criterion

For the soils yielding to elastic-perfect plastic model, it is necessary to determine the critical value of plastic shear strain for the onset of shear banding. So far, there is a lack of any large amount of experimental data to verify the selection of critical values. With the special techniques developed, there is a possibility of acquiring the data in laboratory tests. These data about the axial strain values critical values may also be back analyzed according to the axial strain values measured at the onset of shear banding. These are well documented. The establishing of geometry criterion (location and orientation) is important to give a realistic shear band propagation. The location criterion must be based on a lot of lab or field measurements. Empirical judgment is equally important.

9.3.3.5 Renumbering of all the elements

When shear bands propagate forward, new nodal points should be added continuously at arbitrary points where shear bands go through. Therefore, additional degrees-of-freedom must be supplied, and new nodal points will then significantly increase the bandwidth of the structural stiffness matrix. If the structure is discretized

using a lot of elements, the localization analysis may not be performed completely due to the limit of computer capacity. The traditional remedy should be employed to this problem. The one which is very sensitive to the reduction of bandwidth is to automatically renumber the elements throughout. Alternatively, the matrix sparsity or frontal solution techniques are also applicable.

References

Alencar, J., Chan, D. and Morgenstern, N., 1988, 'Progressive failure in the vane test', ASTM Special Technical Publication 1014, pp. 150-165.

Alsiny, A., Vardoulakis, I. and Drescher, A.,1992, 'Deformation localization in cavity inflation experiment on dry sand', Geotechnique, Vol. 42, pp. 395-410.

Arthur, J. F. R., Dunstan, T., 1977, 'Plastic deformation and failure in granular materials', Geotechnique, Vol. 27, pp. 53-74.

Arthur, J. R. F. and Dunstan, T., 1982, 'Rupture layers in granular media', Proc. IUTAM Conf. Deformation and Failure of Granular Materials. Delft, pp. 453-459.

Balasubramaniam, A. S., 1976, 'Local strains and displacement patterns in triaxial specimens of a saturated calys', Soils and Foundations, Vol. 16, pp. 101-114.

Bardet, J. P., 1990, 'A Comprehensive review of strain localization in elastoplastic soils', Computers and Geotechnics. Vol. 10, pp.163-188.

Bathe, K., 1982, 'Finite element procedures in engineering analysis', Preentice-Hall Inc., pp. 165-177.

Bathe, K. and Chaudhary, A., 1985, 'A solution method for planar and axisymmetric contact problems'. Int. J. Num. Meth. in Eng. Vol. 21, pp. 65-88.

Bazant, Z.P., 1992, 'Nonlocal damage theory based on micromechanics of crack interactions', Journal of Engineering Mechanics. Vol. 120, pp. 593-617.

Bazant, Z. P., Belytschko, T. B. and Chang, T. P., 1984, 'Continuum theory for strain softening', J. Engrg. Mech., ASCE, Vol. 110, pp. 1666-1692.

Bazant, Z. P. and Lin, F-B., 1988, 'Nonlocal yield limit degradation', Int. J. Num. Mech. Eng. Vol. 26, pp.1805-1823.

Beer, G., 1985, 'An isoparametric joint/interface element for finite element analysis', Int. J. Num. Meth. Engrg. Vol. 21, pp. 585-600.

Belytschko, J., Fish and Bayliss, A., 1990, 'The spectral overlay on finite Elements for Problems with High Gradients', Comp. Meth. App. Mech. Eng. Vol. 81, pp.71-89.

Belytschko, T., Fish, J. and Englemann, B. E., 1988, 'A Finite element with embedded localization zones', Comp. Meth. in Appl. Mech. and Eng. Vol. 70, pp. 59-89.

Bergado, D.T., Chai, J.C. and Miura, N., 1995, ' FE analysis of grid reinforcement embankment system on soft bangkok clay', Computers and Geotechnics, Vol. 17, No. 4, pp. 447-471.

Bjerrum, L., 1967, 'Progressive failure in slopes of overconsolidated plastic clay and clay shales', Journal of Soil Mechanics and Foundation Division, ASCE, Vol. 93, pp. 139-187.

Bigoni, D. and Hueckel T., 1991, 'Uniqueness and localization-I. associative and non-associative elasto-plasticity', Int. J. Solids Structures, Vol. 28, pp. 197-213.

Boganova-Bontcheva, N. and Lippmann, H., 1975, 'Rotationnssymmetrisches fliessen eines granularen modellmaterials', Acta Mech. Vol. 21, pp. 93-113.

de Borst, R., 1988, 'Bifurcation in finite element models with a non-associated flow law', Int. J. Num. Anal. Meth. Geom., Vol. 12, pp. 99-116.

de Borst, R., 1989, 'Numerical methods for bifurcation analysis in geomechanics', Ingenieur-Archiv, Vol. 59, pp. 160-174.

de Borst, R., 1991, 'Simulation of strain localization: a reappraisal of Cosserat continuum', Engineering Computations, Vol. 8, pp. 317-332.

de Borst, R. and Muhlhaus, H.-B, 1992, 'Gradient-dependent plasticity:formation and algorithmic aspects', Int. J. Num. Meth. Eng., Vol. 35, pp. 521-539.

de Borst, R. and Sluys, L.J., 1991, 'Localization in a Cosserat conditions', Comp. Meth. Eng. Vol. 82, pp. 805-827.

de Borst, R., Sluys, L. J., Muhlhaus, H.-B. and Pamin, J., 1993, 'Fundamental issues in finite element analysis of localization of deformation', Engineering Computations, Vol. 10, pp. 99-121.

Bowles, J., 1988, 'Foundation analysis and design', 4th edition, McGraw-Hill, pp. 471-521.

Brown, C. B. and Evans, R. J., 1972, 'On the application of couple-stress theories to granular media' , Geotechnique. Vol. 22, No. 2. pp. 356-361.

Carol, I., Gens, A., and Alonso, E. E., 1986, 'Three dimensional model for rock joints', Proceedings of 2nd International Symposium on Numerical Models in Geotechnics, pp. 179-189.

Chan, D., 1986, 'Finite element analysis of strain softening material', Ph. D. Thesis, The University of Alberta.

Chan, D., Wang, X., and Morgenstern, N., 1997, 'Kinematic modeling of shear zone deformation', Deformation and Progressive Failure in Geomechanics, IS-Nagoya'97, Akira Asaoka, Toshihisa Adachi, and Fusao Oka (eds.), Japan, pp.389-394.

Charlier, R., 1992a, 'Modeling of shear band localisation using interface finite elements', In Pande and Pietruszczak (eds.), Numerical Model in Geomechanics, Rotterdam: Balkema, pp. 357-365.

Charlier, R. and Wang, X. C., 1992b, 'Finite element computation of localisation using strain field refinement', In Owen, Onate and Hinton (eds.), Proc. of the Third Int. Conf. on Comp. Plasticity-COMPLAS III,. Pineridge Press, pp. 617-629.

Colemn, B. D., Hodgdon and M. L., 1985, 'On shear bands in ductile materials', Archs Ration, Mech. Analysis, Vol. 90, pp.219-247.

Chen, Z., Morgenstern, N. R. and Chan, D. H., 1990, 'Progressive failure of the Carsington dam - a numerical study', Canadian Geotechnical Journal, Vol. 29 pp. 971-988.

Chu, J., Lo, S-C. R. and Lee, I. K., 1992, 'Strain softening of a granular soil in triaxial and multi-axial testing', J. Geotech. Engrg. Div. Vol. 118, pp. 191-208.

Chu, J., Lo, S.-C. R. and Lee, I. K., 1996, 'Strain softening and shear band formation of sand in multiaxial testing', Geotechnique, Vol. 46, pp. 63-82.

Day, R. A. and Potts, D. M., 1994, 'Zero thickness interface element—numerical stability and application', Int. J. Num. Anal. Meth. Geom., Vol. 18, pp. 689-708.

Desai, C. S., Christian, J. T., 1977, 'Constitutive laws for geologic media' , Numerical Methods in Geotechnical Engineering, pp. 73-79.

Desai, C. S., Zaman, M. M., Lightner, J. G., and Sirzwardane, H. J., 1984, 'Thin-layer element for interfaces and joints', Int. J. Num. Anal. Meth. Geom., Vol. 8, pp.19-43.

Descher, A., Vardoulakis, I. and Han, C., 1990, 'A biaxial apparatus for testing soils', Geotechnical Test Journal, Vol. 13, pp. 226-234.

Desrus, J. and Chambon, R., 1989, 'Shear band analysis for granular materials : The questions of incremental non-linearity ', Ingenieur Archiv, Vol. 59, pp. 187-196.

Desrues, J., Chambon, R., Mokni, M., and Mazerolle, F., 1996, 'Void ratio evolution inside shear bands in triaxial sand specimens stridden by computed tomography', Geotechnique, Vol. 46, pp. 529-546.

Drucker, D. C., 1950, 'Some implication of work hardening and ideal plasticity', Q. Appl. Math. , Vol. 7, pp. 411-418.

Drucker, D. C., 1956, 'On uniqueness in the theory of plasticity', Q. Appl. Math. , Vol. 14, pp. 35-42.

Drucker, D. C., 1959, 'A deformation of stable inelastic materials', J. Appl. Mech. , Vol. 26, pp. 101-106.

Frantziskonis, G. and Desai, C.S., 1987, 'Constitutive model with strain softening', Int. J. Solids Structures. Vol. 23, pp. 733-750.

Fumio, Talsuoka, Shinya, Nakamura, Ching-Chuang Huang and Kazuo Tani, 1990, 'Strength anisotropy and shear band direction in plane strain tests of sand', Soils and Foundations. Vol. 30, pp.35-54.

Goodman, R. E. and St. John, C., 1977, 'Finite element analysis for discontinuous rock', Numerical Methods in Geotechnical Engineering, pp. 148-175.

Goodman, R. E., Taylor, R. L. and Brekke, T. L., 1968, 'A model for the mechanics of jointed rock', ASCE J. Solid Mech. Found. Div. Vol. 94, pp. 637-659.

Han, C. and Vardoulakis, I., 1991, 'Plane strain compression experiments on water-saturated fine-grained sand', Geotechnique, Vol. 41, pp. 49-78.

Harris, W. W., Viggiani, G., Mooney, M. A. and Finno, R. J., 1995, 'Use of stereophotogrammetry to analyze the development of shear bands in sand', Geotech. Test. J. , Vol. 18, pp. 405-420.

Hicher, P. Y., Wahyudi, and H. Tessier, D, 1994, 'Microstructural analysis of stress localization in clay', Computers and Geotechnics, Vol. 16, pp. 205-221.

Hadmard, J., 1903, 'Lecons sur la propagation des on des et les equations de L'hydrodynamique, Hermann, Paris.

Hill, R., 1958, 'A general theory of uniqueness and stability in elastic-plastic solids', Journal of the Mechanics and Physics of Solids', Vol. 6, pp. 236-249.

Hill, R. and Hutchinson, J. W., 1959, 'Bifurcation phenomenon in the plane tension tests', J. Mech. Phys. Solids, Vol. 7, pp. 209-225.

Hill, R., 1962, 'Acceleration waves in solids', J. Mech. Phys. Solids, Vol. 10, pp. 1-6.

Hughes, T. J. R., Taylor, R. L. and Kanoknukulchai, W., 1976, 'A finite element method for large displacement contact and impact problems', In K. Bathe, J. Oden and W. Walter (eds.), Formulations and Computational Algorithms in Finite Element Analysis, M. I. T. Press, pp. 468-494.

Ingraffea, A. R., 1977, 'Nodal grafting for crack propagation studies', Int. J. Num. Method. Engrg. , Vol. 11, pp. 1185-1187.

Juran, I. and Chen, C. L., 1989, ' Strain compatibility design method for reinforced earth walls', J. Geotech. Div., ASCE, Vol. 115, pp. 435-456.

Kroner, E., 1967, 'Elasticity theory of materials with long-range cohesive forces', Int. J. Solids Struct., Vol. 3, pp. 731-742.

Krumhansl, J. A., 1968, 'Some considerations of the relations between solid state physics and generalized continuum mechanics', in E. Kroner (ed.), Mechanics of Generalized Continua, Springer-Verlag, Berlin, pp. 298-331.

Kubin, L.P. and Lepinnoux, J., 1988, 'The dynamic organization of dislocation structures', in Proc. Eigth Int. Conf. On strength of metals and alloys, Tampere, pp. 35-59.

Lade, P. V., 1989, 'Experimental observations of stability, instability, and shear planes in granular materials', Ingenieur-Archiv, Vol. 59, pp. 114-123.

Lade, P. V. and Tsai, J., 1985, 'Effect of localization in triaxial tests on clays', Proc. XXI Int. Conf. Soil Mech. Found. Eng., San Fransisco, pp. 549-552.

Larsson, R. and Runesson, K., 1996b, 'Element-embedded localization band based on regularized displacement discontinuity ', Journal of Engineering Mechanics, ASCE, Vol., 122, pp. 402-411.

Larsson, R., Runesson, K. and Axellson, K., 1996a, 'Localization properties of a frictional model based on regularized strong discontinuity', Int. J. Num. Anal. Meth. Geom., Vol. 20, pp. 771-783.

Larsson, R., Runesson, K. and Ottosen, N. S., 1993, 'Discontinuous displacement approximation for capturing plastic localization', Int. J. Num. Meth. Engrg. , Vol. 36, pp. 2087-2105.

Leroy, Y. and Ortiz, M., 1989, 'Finite element analysis of strain localization in frictional materials', Int. J. Num. Anal. Meth. Geomech. Vol. 13, pp. 53-74.

Lo, K. Y., 1972, 'An approach to the problem of progressive failure', Canadian Geotechnical Journal, Vol. 9, pp. 407-429.

Mokni, M., 1992, 'Relations entre deformations en masse et deformations localisees dans les materianx quanulaires', These de Doctorat de l'Universite J. Fourier de Grenoble, France.

Molenkamp, F., 1985, 'Comparison of frictional material models with respect to shear band initiation ', Geotechnique, Vol. 35, pp. 127-143.

Morgenstern, N. R. and Tchalenko, J. S., 1967, 'Microscopic structures in kaolin subjected to direct shear', Geotechnique. Vol. 17, pp. 309-328.

Mroz, Z., 1963, 'Non-associated flow laws in plasticity', J. Mechanique, Vol. 2, pp. 21-42.

Muhlhaus, H. B., 1986, 'Shear band analysis in granular material by Cosserat theory', Ing. Archiv. Vol. 56, pp.389-399.

Muhlhaus, H. B. and Aifantis, E. C., 1991, 'A variational pricinple for gradient plasticity', Int. J. Solids Structures, Vol. 28, pp. 845-858.

Mühlhaus, H. B. and Vardoulakis, I., 1987, ' The thickness of shear bands in granular materials', Geotechnique, Vol. 37, pp. 271-283.

Nacar, A. and Needleman, A. and Ortiz, M., 1989, 'A finite element method for analyzing localization in rate dependent solids at finite strains', Comp. Meth. in Appl. Mech. and Eng., Vol. 73, pp. 235-258.

Nagtegaal, J. C., Parks, D. M. And Rice, J. R., 1974, 'On numerically accurate finite element solutions in the fully plastic range', Computer methods in applied mechanics and engineering, Vol. 4, pp. 153-177.

Needleman, A., 1979, 'Non-normality and bifurcation in plane strain tension and compression', J. Mech. Phys. Solids, Vol. 27, pp. 231-254.

Needleman, A. 1988, 'Material rate dependence and mesh sensitivity in localization problems', Comp. Meth. in Appl. Mech. and Eng., Vol. 67, pp. 69-85.

Needleman, A. and Trergaard, V., 1983, 'On the finite element analysis of localized plastic deformation', in: J. T. Oden and G. F. Carey, eds., Finite Elements-Special Problems in Solids Mechanics, 94-157.

Neilsen, M. K., Schreyer, H. L., 1993, 'Bifurcation in elastic-plastic materials ', J. Solids Structures, Vol. 30, pp. 521-544.

Ortiz, M,. Leroy, Y. and Needleman, A., 1987, 'A finite method for localized failure analysis', Comp. Meth. in Appl. Mech and Eng., Vol. 61, pp. 189-214.

Ottosen, N. S. and Runesson, K., 1991, 'Properties of discontinuous bifurcation solutions in Elasto-plasticity', Int. J. Solids Structures. Vol. 27, pp. 401-421.

Palmer, A. C. and Rice, J. R., 1973, 'The growth of slip surface in the progressive failure of overconsolidated clay', Proc. Roy. Soc. London, Vol. 332, pp.527-548.

Pande, G. N. and Shama, K. G., 1979, 'On joint/interface elements and associated problems of numerical ill-conditioning', Int. J. num. Anal. Meth. Geom., Vol. 3, pp. 293-300.

Pastor, M., Peraire, J. and Zinkiewicz, O. C., 1991, 'Adaptive remeshing for shear band localization problems', Archive of Applied Mechanics, Vol. 61, pp. 30-39.

Pastor, M., Rubio, C. and Mira, P., 1992, 'Numerical analysis of localization', Numerical Models in Geomechanics, Pande, & Pietruszczak (eds.), pp. 339-365.

Peters, J. F., Lade, P. V. and Bro. A., 1988, 'Shear band formation on triaxial and plane strain tests ', Advanced triaxial testing of soil and rock, ASTM STP 977, American Society for Testing and Materials, pp. 604-627.

Pietruszczak, S. T. Mroz, and Z., 1981, 'Finite Element Analysis of Deformation of Strain Softening Materials', Int. J. Num. Meth. Eng., Vol. pp. 327-334.

Pietruszczak, S. T. and Stolle, D., 1987, 'Deformation of strain-softening materials, Part II: Modeling of Strain Softening Response', Computers and Geotechnics, Vol. 4, pp.109-123.

Potts, D. M., Dounias, G. T., Vaughan, P., R., 1990, 'Finite element analysis of progressive failure of Carsington embankment', Geotechnique, Vol., 40, pp. 79-101.

Read, H. E. and Hegemier, G. A., 1984, 'Strain softening of rocks, soil and concrete- a review article', Mechanics of Materials, Vol. 3, pp. 271-294.

Rice, J., 1976, 'The Localization of plastic deformation', Theoretical and Applied Mechanics, pp. 207-220.

Roscoe, K. H., 1970, 'The influence of strains in soil mechanics', Tenth Rankine lecture, Geotechnique, Vol. 20, pp. 129-170.

Rosenfarb, J. L. and Chen, W. F., 1972, 'Limit analysis solutions of earth pressure problems', Fritz Eng. Laboratory Report 355.14, Lehigh University, 53 pp..

Rowe, P. W., 1962, 'The Stress-dilatancy relation for static equilibrium of an assembly of particles in contact', Proc. Roy. Soc. Series A, Vol. 269, pp. 500-527.

Rudnicki, J. W. and Rice, J. R., 1975, 'Conditions for the Localization of Deformation in Pressure-Sensitive Dilatant Materials', J. Mech. Phys. Solids, Vol. 23, pp. 371-394.

Runesson, K. and Mroz, Z., 1989, 'A note on non-associated plastic flow rules', Int. J. Plasticity, Vol. 5, pp. 639-658.

Runesson, K., Ottosen, N. S. And Peric, D., 1991, 'Discontinuous bifurcation of elastic-plastic solutions at plane stress and plane strain ', Int. J. Plasticity, Vol. 7, pp. 99-121.

Saada, A. S., Bianchini, G.F. and Liang, Liqun, 1994, 'Cracks, bifurcation and shear bands propagation in saturated clays', Geotechnique. Vol. 44, pp. 35-64.

Scarpelli, G . and Wood, D. M., 1982, 'Experimental observations of shear band patterns in direct shear tests', Proc. IUTAM Conf. Deformation and Failure of Granular Materials, pp. 473-484.

Sharma, K. G. and Desai, C. S., 1992, 'Analysis and implementation of thin-layer element for interfaces and joints', ASCE J. Engrg. Mech. Vol. 118, pp. 2442-2462.

Shewbridge, S. E. and Sitar, N., 1996, 'Formation of shear zones in reinforced sand', J. Geotech. Div. , ASCE, Vol. 122, pp. 872-885.

Shewbridge, S. E. and Sitar, N., 1989, 'Deformation characteristics of reinforced sand in direct shear', J. Geotech, Div. , ASCE, Vol. 115, pp. 1134-1147.

Simo, J. C., 1989, 'Strain softening and dissipation: a unification of approaches', in cracking and damage: strain localization and size effect (Eds. J. Mazars and Z.P. Bazant), New York, pp. 440-461.

Skempton, A. W., 1964, 'Long term stability of clays slopes', Geotechnique, Vol. 14, pp. 77-101.

Sluys, L.J., 1992, 'Wave propagation, localization and dispersion in softening solids', Dissertation, Delft University of Technology.

Thomas, T. Y., 1961, Plastic flow and fracture in solids, Academic Press, New York.

Triantafyllidis, N. and Aifantis, E. C., 1986, 'A gradient approach to localization of deformation: I, hype-elastic materials', J. of Elasticity, Vol. 16, pp. 225-237.

Uchida, K. and Vaid, Y. P., 1994, 'Sand behavior under strain path control', XIII CSMFE, New Delhi, pp. 17-20.

Valanis, K. C., 1989, 'Banding and stability in plastic materials', Acta Mech. 79, pp. 113-141.

Vardoulakis, I., 1979, 'Bifurcation analysis of the triaxial test on sand samples', Acta Mech., Vol. 38, pp. 219-239.

Vardoulakis, I., 1980, 'shear modulus of sand in biaxial test', Int. J. Num. Anal. Meth. in Geomechanics. Vol. 4, pp.113-119.

Vardoulakis, I., 1983, 'Rigid granular plasticity model and bifurcation in the triaxial test', Acta. Mech. , Vol. 49, pp. 57-79.

Vardoulakis, I. and Aifantis, E. C., 1989, 'Gradient dependent dilatancy and implications in shear banding and liquefaction', Ingen-Arch, Vol. 59, No. 3, pp. 197-208.

Vardoulakis, I., Goldscheider, M. and Gudehus, G., 1978, 'Formation of shear bands in sand bodies as a bifurcation problem'., Int. j. Num. Anal. Meth. Geomech., Vol. 2, pp. 99-128.

Vardoulakis, I. and Graf, B., 1985, 'Calibration of constitutive models for granular materials using data from biaxial experiments', Geotechnique, Vol.35, pp. 299-319.

Vermeer, P. A., 1982, 'A Simple shear-band analysis using compliances', Proc. IUTAM Symp. Deformation and Failure of Granular Materials, pp. 493-499.

Waldron, L. J., 1977, 'The shear resistance of root-permeated homogeneous and stratified soil', Soil Sci. Soc. of Am. J., Vol. 41, pp. 843-849.

Wan, R. G., 1990, 'The numerical modeling of shear bands in geological materials', Ph.D Thesis, University of Alberta, pp. 23-58.

Wan, R. G., Chan, D. H. and Morgenstern, N. R., 1992, 'Modeling discontinuous behaviour and fault formation in geomaterials', Fractured and Rock Masses Conference, pp. 1-8.

Wang, X. R. and Chan, D. H. and Morgenstern, N. R., 1995, 'A numerical scheme for modeling kinematic propagation of shear bands', in Numerical Models in Geomechanics. NUMOG V, Davos, Switzerland, pp. 215-222.

Wilson, E.L., 1977, 'Finite elements for foundations, joints and fluids ', in A. G. Gudefius (ed.), Finite Elements in Geomechanics, Chap. 10, Wiley, New York.

Wood, D. M., 1990, Soil behavior and critical state soil mechanics, Cambridge University Press, pp. 85-137.

Xu, Zhilun., 1977, 'Finite element method in elasticity' (in Chinese), Editorial Board of Water Conservancy, Beijing, China, pp. 38-42.

Yamamuro, A. and Lade, P. V., 1995, 'strain localization in extension tests on granular materials', J. of Engrg. Mech., Vol. 121, pp. 828-836.

Yi, C. T., Chan, D. H. and Scott, J. D., 1995, 'A large slipping finite element model for geosynthetics interface modeling', Geosyntics, Vol. 1, pp. 93-104.

Yin, Zongze and Zhu, Hong, 1995, 'A study of deformation in the interface between soil and concrete', Computers and Geotechnics, Vol. 17, pp. 75-92.

Yu, J., Peric, D. and Owen, D. R. J., 1991, 'An assessment of cosserat continuum through the finite element simulation of a strain localization problem', Finite Element in the 90's. Spring-Verlag, pp. 321-332.

Zhau, Guofan and Lin, Gao, 1989, 'A framework to judge the development of fractures in concrete' (in Chinese), research report No. 17-2-1-3 FL/$C_{1,2}$, Dalian University of Technology, pp. 298-322.

Zienkiewicz, O.C. et al., 1970, 'Analysis of nonlinear problem with particular reference to jointed rock systems', Proc. 2nd Int. Conf. Soc. of Rock Mech., Belgrade, Vol. 3, pp. 501-509.

Zienkiewicz, O. C., Huang, M., and Pastor, M., 1995, 'Localization problems in plasticity using finite element with adaptive remeshing', Int. J. Num. Anal. Meth. Geom. , Vol. 19, pp. 127-148.

Zienkiewicz, O. C. and Taylor, R. L., 1989, 'The finite element method', Vol. 1, McGraw-Hill book company, pp. 35-44.